TU WIEN Informatics

BrainGait

Ganganalyse und Visualisierung in durch Robotik gestützter Rehabilitation

DIPLOMARBEIT

zur Erlangung des akademischen Grades

Diplom-Ingenieur

im Rahmen des Studiums

Visual Computing

eingereicht von

Stefan Spelitz, BSc
Matrikelnummer 0925601

an der Fakultät für Informatik

der Technischen Universität Wien

Betreuung: Ao.Univ.Prof. Dipl.-Ing. Dr.techn. Eduard Gröller
Mitwirkung: Dipl.-Ing. Dr.techn. Armin Kanitsar

Wien, 21. April 2020

Stefan Spelitz	Eduard Gröller

Technische Universität Wien
A-1040 Wien ▪ Karlsplatz 13 ▪ Tel. +43-1-58801-0 ▪ www.tuwien.at

Die approbierte gedruckte Originalversion dieser Diplomarbeit ist an der TU Wien Bibliothek verfügbar.
The approved original version of this thesis is available in print at TU Wien Bibliothek.

TU Bibliothek Your knowledge hub WIEN

Die approbierte gedruckte Originalversion dieser Diplomarbeit ist an der TU Wien Bibliothek verfügbar.
The approved original version of this thesis is available in print at TU Wien Bibliothek.

TU WIEN Informatics

BrainGait

Gait Event Detection and Visualization for Robotic Rehabilitation

DIPLOMA THESIS

submitted in partial fulfillment of the requirements for the degree of

Diplom-Ingenieur

in

Visual Computing

by

Stefan Spelitz, BSc
Registration Number 0925601

to the Faculty of Informatics

at the TU Wien

Advisor: Ao.Univ.Prof. Dipl.-Ing. Dr.techn. Eduard Gröller
Assistance: Dipl.-Ing. Dr.techn. Armin Kanitsar

Vienna, 21st April, 2020

Stefan Spelitz	Eduard Gröller

Technische Universität Wien
A-1040 Wien ▪ Karlsplatz 13 ▪ Tel. +43-1-58801-0 ▪ www.tuwien.at

Die approbierte gedruckte Originalversion dieser Diplomarbeit ist an der TU Wien Bibliothek verfügbar.
The approved original version of this thesis is available in print at TU Wien Bibliothek.
TU Bibliothek Your knowledge hub WIEN

Die approbierte gedruckte Originalversion dieser Diplomarbeit ist an der TU Wien Bibliothek verfügbar.
The approved original version of this thesis is available in print at TU Wien Bibliothek.

Erklärung zur Verfassung der Arbeit

Stefan Spelitz, BSc

Hiermit erkläre ich, dass ich diese Arbeit selbständig verfasst habe, dass ich die verwendeten Quellen und Hilfsmittel vollständig angegeben habe und dass ich die Stellen der Arbeit – einschließlich Tabellen, Karten und Abbildungen –, die anderen Werken oder dem Internet im Wortlaut oder dem Sinn nach entnommen sind, auf jeden Fall unter Angabe der Quelle als Entlehnung kenntlich gemacht habe.

Wien, 21. April 2020

Stefan Spelitz

Die approbierte gedruckte Originalversion dieser Diplomarbeit ist an der TU Wien Bibliothek verfügbar.
The approved original version of this thesis is available in print at TU Wien Bibliothek.
TU Bibliothek Your knowledge hub WIEN

Die approbierte gedruckte Originalversion dieser Diplomarbeit ist an der TU Wien Bibliothek verfügbar.
The approved original version of this thesis is available in print at TU Wien Bibliothek.

Kurzfassung

Beeinträchtigungen in der Beweglichkeit von Erwachsenen sind eine der meistverbreiteten Behinderungen in Industriestaaten. Gangtraining und Physiotherapie werden angewandt und können dabei helfen, die Beweglichkeit wiederherzustellen, insbesondere nach einem Schlaganfall. In den letzten Jahren gab es ein reges Interesse an robotergestützter Therapie, sowohl in Rehazentren, als auch in der wissenschaftlichen Forschung. Mit dem Aufkommen von Robotik in der Physiotherapie kommt auch die Notwendigkeit, die Patientenleistung objektiv messen zu können. Therapeuten brauchen kompakt dargestellte Informationen bezüglich des aktuellen Status des Patienten in der Maschine, sowie praktische Vorschläge, wie das Gangbild verbessert werden könnte. Mediziner hingegen verlassen sich auf statistische Messwerte, um den Fortschritt des Patienten im Verlauf der Therapie beurteilen zu können.

Im Folgenden beschäftigt sich diese Arbeit mit häufig eingesetzten Visualisierungen, sowie statistischen Kenngrößen in der Ganganalyse. Gleichzeitig werden Verbesserungen und Anpassungen vorgeschlagen, welche im Rahmen von *PerPedes*, einem neuartigen Gangroboter, umgesetzt wurden. Um die Leistung des Patienten in der Maschine beurteilen zu können, wurde ein neuer Algorithmus zur Ganganalyse entwickelt, basierend auf der Auswertung von Kraftdaten. Die nachfolgende Arbeit demonstriert, dass Standardansätze zur Ganganalyse in PerPedes scheitern, während der entwickelte Vorschlag auch mit stark verzerrten Gangbildern, wie Halbseitenlähmung, Fußhebeschwäche oder Rückwärtsgehen umgehen kann. Die während dieser Arbeit entwickelte Software bietet dem Therapeuten Rückschluss auf die Leistung des Patienten. Die vom System generierten Anweisungen können benutzt werden, um das Gangbild zu verbessern. Zusätzlich werden von jeder Therapiesitzung Kennzahlen ermittelt, welche anschließend für die weitere Analyse und den Vergleich zwischen Patienten genutzt werden können.

Die approbierte gedruckte Originalversion dieser Diplomarbeit ist an der TU Wien Bibliothek verfügbar.
The approved original version of this thesis is available in print at TU Wien Bibliothek.
TU Bibliothek Your knowledge hub WIEN

Die approbierte gedruckte Originalversion dieser Diplomarbeit ist an der TU Wien Bibliothek verfügbar.
The approved original version of this thesis is available in print at TU Wien Bibliothek.

Abstract

Mobility impairment in adults is one of most prevalent types of disabilities in developed countries. Gait rehabilitation can be used to regain some or all motor functions, especially after a stroke. In recent years, robot-assisted gait training attracted increasing interest in rehabilitation facilities and scientific research. With this advent of robotic recovery comes the need to objectively measure the patient's performance. Physiotherapists need essential information about the current status during training and how to improve the patient's gait, presented in an easy to grasp and compact form. On the other hand, physicians rely on statistical measures in order to evaluate the patient's progress throughout the therapy.

This thesis discusses commonly used visualizations and statistics while proposing improvements and adaptations in the context of *PerPedes*, a novel robotic gait rehabilitation device. In order to measure the patient's performance, a new algorithm for gait event detection was developed, based on force data from pressure plates. The following work demonstrates that standard algorithms fail with PerPedes, while the proposed solution can robustly handle highly distorted gait patterns, such as hemiplegic gait, foot drop, or walking backwards. The software application developed during this thesis provides feedback to the therapist and generates suggestions for gait improvement. Furthermore, gait statistics are inferred from each therapy session and collected in order to be used for future analysis and inter-patient comparison.

Die approbierte gedruckte Originalversion dieser Diplomarbeit ist an der TU Wien Bibliothek verfügbar.
The approved original version of this thesis is available in print at TU Wien Bibliothek.
TU Bibliothek Your knowledge hub WIEN

Die approbierte gedruckte Originalversion dieser Diplomarbeit ist an der TU Wien Bibliothek verfügbar.
The approved original version of this thesis is available in print at TU Wien Bibliothek.

Contents

Die approbierte gedruckte Originalversion dieser Diplomarbeit ist an der TU Wien Bibliothek verfügbar.
The approved original version of this thesis is available in print at TU Wien Bibliothek.
TU Bibliothek Your knowledge hub WIEN

Die approbierte gedruckte Originalversion dieser Diplomarbeit ist an der TU Wien Bibliothek verfügbar.
The approved original version of this thesis is available in print at TU Wien Bibliothek.
TU Bibliothek Your knowledge hub WIEN

Die approbierte gedruckte Originalversion dieser Diplomarbeit ist an der TU Wien Bibliothek verfügbar.
The approved original version of this thesis is available in print at TU Wien Bibliothek.
TU Bibliothek Your knowledge hub WIEN

TU Bibliothek Your knowledge hub WIEN
Die approbierte gedruckte Originalversion dieser Diplomarbeit ist an der TU Wien Bibliothek verfügbar.
The approved original version of this thesis is available in print at TU Wien Bibliothek.

CHAPTER 1

Introduction

It is estimated that about 15% of the world's population - this is more than a billion people - live with some form of disability [Wor11]. In the US alone, mobility impairment is the most prevalent type of disability, with 13.7% of adults being seriously affected while walking or climbing stairs [OHCGB18]. In the EU, 14% of people among the working age population report difficulty in basic activities (such as difficulty in seeing, hearing, walking or communicating). With walking being the second most reported difficulty after lifting and carrying [Eur11].

This thesis covers gait rehabilitation with a novel robotic gait training device. Special focus is put on the analysis of gait as well as visualization as a tool for therapists and physicians to measure the patient's activity and progress. The target group is people with motor impairments in their lower limbs, such as stroke survivors.

1.1 Stroke

Stroke is a cerebrovascular disease that is caused by a restriction in blood flow to parts of the brain, leading to sudden cell death. Main types are either an *ischaemic* stroke, which occurs due to an insufficient blood flow leading to poor oxygen supply, or a *hemorrhagic* stroke due to bleeding within the skull. In an analysis for the global burden of disease (GBD) study 2015, Wang et al. [WNA+16] determined stroke to be the second leading cause of years of life lost (YLL) due to early dying. According to an analysis for the GBD study 2016 [VAA+17], ischaemic stroke is ranked seventeenth in the leading causes for years lived with disability (YLD). This means that stroke is not only one of the diseases with the highest incidents of death, but also incorporates a high burden in living with resulting disabilities. Most prevalent post-stroke impairments are paralysis, often on one side of the body (hemiplegia) and problems related to motor control.

Die approbierte gedruckte Originalversion dieser Diplomarbeit ist an der TU Wien Bibliothek verfügbar.
The approved original version of this thesis is available in print at TU Wien Bibliothek.
TU Bibliothek Your knowledge hub WIEN

Gait post-stroke is characterized by slower gait velocity and gait asymmetry [HB12]. We focus on gait symmetry throughout this thesis, notably in Sections 2.6, 3.3, and 7.2.

1.2 Gait Rehabilitation

The possibilities for physical therapy poststroke are manifold. Depending on the abilities of the patient, different therapies can be applied. Balance training, either while sitting or standing, can be applied. Treadmill training with or without body weight support, muscle stimulating devices (e.g. transcutaneous electrical nerve stimulation (TENS), functional electrical stimulation (FES)), water-based exercise, virtual reality mobility training, or training in groups can be performed to recover mobility loss [VvWvP+14].

However, limitations to conventional therapy apply. Physiotherapists are exposed to physical strain, lifting the patients, stabilizing their gait, or manually moving their limbs. There might be more than one therapist required, while training itself is limited both in duration and intensity. During therapy, the gait pattern cannot be exactly reproduced or repeated. Robotic mobility rehabilitation could be used to relieve the therapist of some burden, but also to precisely repeat an optimal motion sequence with the patient.

A possible drawback of automatic rehabilitation devices is the missing feedback for the therapist of how actively the patient is participating during the training. The patient might be moved passively by the device while the lack of participation goes unnoticed. Wagner et al. [WSEG+12] investigated the spectral patterns of electroencephalography (EEG) to distinguish between active and passive participation in robotic gait trainers. This could be used to objectively measure the patient's involvement and help the therapist intervene accordingly.

1.3 The BrainGait[1] Project

In the context of the BrainGait project [For20], a novel rehabilitation system used for motor recovery is being developed. It is targeted at stroke survivors, patients with spinal cord injuries, or more generally at people with motor impairments in their lower limbs. The novelty of the project stems from the combination of a multitude of sensory interfaces in the context of a gait training robotic device. The project's main goal is to objectively measure the patient's level of participation via EEG and provide visual information to the therapist or medical practitioner. Further objectives are the measurement of muscle activities via electromyography (EMG) for automatic detection of spasms, exploration of FES in the context of robotic training, and the connection to the hospital information system (HIS) for data exchange.

[1] BrainGait wird vom Bundesministerium für Verkehr, Innovation und Technologie (bmvit) im Rahmen des Programms COIN-Netzwerke gefördert. ©2018 SAP SE. Alle Rechte vorbehalten. ©2016. Cerner Corporation, 2800 Rockcreek Parkway, North Kansas City, Missouri 64117-2551 U.S.A. All rights reserved.

Die approbierte gedruckte Originalversion dieser Diplomarbeit ist an der TU Wien Bibliothek verfügbar.
The approved original version of this thesis is available in print at TU Wien Bibliothek.
TU Bibliothek Your knowledge hub WIEN

The project's partners and their responsibilities are as follows. Project coordinator is the *AIT (Austrian Institute of Technology) GmbH*, also responsible for EEG feature extraction and EMG analysis in corporation with *g.tec medical engineering GmbH*. The g.tec company provides EMG and EEG equipment, the software interface to these devices, and additional expertise. *Schepp medtech GmbH* develops and provides PerPedes, the robotic gait rehabilitation device. *INFORMATICS Healthcare GmbH* with their know-how in SAP-based systems, provides the interface to the HIS. The company *VISUAPPS GmbH* is responsible for visualizations and statistics targeted at the therapist, a visual feedback system for the patient, and additionally storing patient data to the HIS via the interface provided by INFORMATICS.

1.4 Thesis Goals

This thesis was created in the course of an employment at the company VISUAPPS. Initially, the goal was to create visualizations for the therapist, using the available force data, EMG, and EEG signals. During the progression of the project it became clear that the EMG does not provide a clear image of the patient's activity. This is due to the fact that the muscle activity while training in the robotic gait trainer appears to be different to gait, as reported in the literature. Furthermore, the application of sensors for both EMG and EEG is tedious, especially when using gel based EEG electrodes. During an actual therapy session with the patient, which might only last thirty minutes, there would be additional time necessary to apply the sensors. Since the EMG signals were not as clearly interpretable as we hoped for and the setup of the peripheral equipment would consume too much time in real-life settings, the focus of this thesis shifted to force data analysis.

The main goal of this thesis is to present status information to the therapist while the patient is training. This presentation should be concise, use existing visualizations from standard literature, and help the therapist evaluate the current performance of the patient. As a secondary objective, the patient's gait should be analyzed, creating measures proposed in scientific research in order to document each therapy session and the patient's progress.

Since PerPedes is a novel robotic rehabilitation system, at the time of writing, scientific research for this platform was not yet available. Our experiences with this system lead to new developments not only in gait analysis, but also in visualization. In this thesis we provide a novel gait event detection (GED) algorithm, suitable measures, and visualizations developed for the PerPedes platform. All of which are based on force data. Our discoveries have potential use outside the PerPedes ecosystem, allowing the study of severe gait disabilities.

Die approbierte gedruckte Originalversion dieser Diplomarbeit ist an der TU Wien Bibliothek verfügbar.
The approved original version of this thesis is available in print at TU Wien Bibliothek.
TU Bibliothek Your knowledge hub WIEN

1.5 Development & Implementation

The development framework was already predefined and given. Prototypes, especially with regards to signal processing (e.g. for GED) have been developed in Matlab R2018a [The18]. Implementation was then realized as a client/server web application.

The server application is developed with Eclipse Equinox [Ecl20a], an implementation of the OSGi core framework specifications. The existing server side codebase is structured into Eclipse plugins, developed in Java and deployed as a web application. It is embedded in a servlet container, for example Eclipse Jetty [Ecl20b] or Wildfly [Red20] (formerly known as JBoss application server). Contrarily, the client side is developed in Java and successively compiled to highly optimized JavaScript using the Google Web Toolkit (GWT) [Goo20]. The result is cross-browser compatible, including mobile browsers.

Visualizations are created using the HTML5 canvas. This allowed us to create flexible, fast, and responsive UI elements. Initial attempts of implementing elements based on scalable vector graphics (SVG) turned out to utilize more of the CPU and were slower to develop. 3D visualizations were created using the Babylon.js 4.0 framework [CRR20], since it provides out-of-the-box skeletal animation and is distributed with the permissive Apache software license. The 3D character (Section 8.5) is based on Adobe's Mixamo [Ado20] virtual character and animation service.

Die approbierte gedruckte Originalversion dieser Diplomarbeit ist an der TU Wien Bibliothek verfügbar.
The approved original version of this thesis is available in print at TU Wien Bibliothek.
TU Bibliothek Your knowledge hub WIEN

CHAPTER 2

Gait Terminology

2.1 The Gait Cycle

In the following, we describe the human gait cycle during normal walking. The gait cycle describes a sequence of movements; it starts and ends with two successive events of the same leg, spanning 100%. In Figure 2.1, the gait cycle starts with the initial contact of the right leg and ends with the next successive initial contact of the same leg. In the context of this thesis, we define the gait cycle to start and end with the left initial contact. This represents the same information as in Figure 2.1, but it is shifted by 50% of the gait cycle. Since perfect gait is symmetrical, the same movement can be expected to happen on the left side as on the right side, but offset by half the gait cycle.

Each limb undergoes two major phases; a stance phase, when the limb has contact to the ground, and a swing phase, when the limb has not. Each stance phase lasts around 60% of the gait cycle, while each swing phase lasts around 40%. During normal walking, at every point in the gait cycle, at least one side has contact to the ground. Contrarily, during running this is not the case, since both feet can be in the air at the same time. The left foot's stance phase and the right foot's stance phase are overlapping twice during the gait cycle. These overlapping phases are called double support, with both feet touching the ground. Each double support phase is typically approximated to make up 10% of the gait cycle. During double support, weight is transferred from left to right and vice versa.

Die approbierte gedruckte Originalversion dieser Diplomarbeit ist an der TU Wien Bibliothek verfügbar.
The approved original version of this thesis is available in print at TU Wien Bibliothek.
TU Bibliothek Your knowledge hub WIEN

Dividing the major phases even further is done either according to traditional (T) or Rancho Los Amigos (RLA)[1] terminology [LN05]. The following RLA subphases are defined:

1. **Loading response** - The first double support phase. From initial contact until the contralateral limb leaves the ground.
2. **Midstance** - The first portion of single support until the body is directly over the supporting limb.
3. **Terminal stance** - The last portion of single support until the contralateral limb touches the ground.
4. **Preswing** - The second double support phase until the ipsilateral limb leaves the ground.
5. **Initial swing** - The portion of the swing phase until maximum knee flexion of the swinging leg occurs.
6. **Midswing** - The next following portion of the swing phase until the tibia of the swinging leg is in a vertical position.
7. **Terminal swing** - The last portion of the swing phase before the next initial contact.

[1] Rancho Los Amigos National Rehabilitation Center, California, United States

Die approbierte gedruckte Originalversion dieser Diplomarbeit ist an der TU Wien Bibliothek verfügbar.
The approved original version of this thesis is available in print at TU Wien Bibliothek.
TU Bibliothek Your knowledge hub WIEN

Die approbierte gedruckte Originalversion dieser Diplomarbeit ist an der TU Wien Bibliothek verfügbar.
The approved original version of this thesis is available in print at TU Wien Bibliothek.

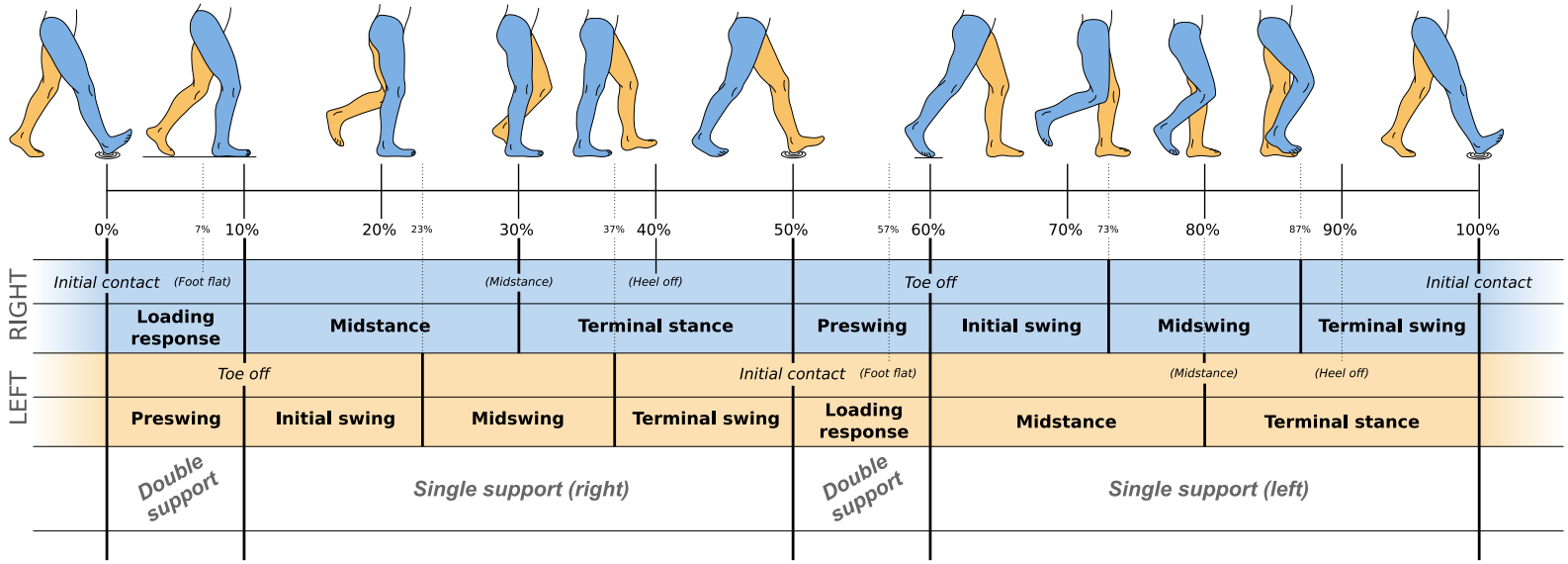

Figure 2.1: The gait cycle, illustrated. Depicted are the gait cycle's subphases according to RLA terminologies for the left and right foot respectively. The right foot's heel strike starts the right leg's stance phase ($0\% - 60\%$). After the toe off event, the swing phase ($60\% - 100\%$) completes the cycle. All events and phases for the left leg are offset by half a gait cycle (i.e. 50%). Events, according to RLA are displayed in *italic*, traditionally defined events as *(italic in parentheses)*, and RLA subphases are displayed in **bold**. Image adapted from Levangie and Norkin [LN05].

2.2 Gait Events

Gait events refer to specific points in the gait cycle. As with gait cycle subphases, events are defined either traditionally (T) or according to RLA:

- **Initial contact** (RLA) or **Heel strike** (T) - The instant when the foot strikes the ground.
- **Foot flat** (T) - Around 7% after initial contact. The first instant when the sole of the foot contacts the ground.
- **Midstance** (T) - The instant when the body is directly over the supporting limb.
- **Heel off** (T) - The instant when the heel leaves the ground.
- **Toe off** (RLA, T) - The instant when the foot leaves the ground.

The terms heel strike and toe off are somehow misleading, since initial contacts do not need to happen with the heel nor do last contacts need to happen at the toes. In subjects with pathological gait, the entire foot or even only the toes may have initial contact with the ground.

The most important events are initial contact and toe off. These events define the beginning of the gait cycle, swing, stance, and double support phases. In the literature these events are named inconsistently. Initial contact (IC) [SFB+05], foot strike (FS) [BR14], or heel strike (HS) [ZJRH08] all refer to the same event in the gait cycle. Likewise, foot off (FO) [RCC+08], terminal contact (TC) [SFB+05], final contact (FC) [SBM16], or toe off (TO) [ZJRH08] identify the instant in the gait cycle where the foot leaves the ground.

In this thesis we use the terms heel strike (HS) and toe off (TO) to refer to these important events of the gait cycle. Specifically, events for the left side are referred to as heel strike, left (HSL) and toe off, left (TOL), while events on the right are heel strike, right (HSR) and toe off, right (TOR).

2.3 Ground Reaction Force

Whenever a body touches the ground, it exerts a force on the ground and the ground itself exerts an equal and opposite force on the body (Newton's third law). While it is a matter of definition which force is acting and which force is reacting, by convention the force that the ground is exerting on the body is called the ground reaction force (GRF). The GRF is typically defined as a three component vector (Figure 2.2), reflecting the direction and the magnitude of the force. The vertical GRF represents the largest component of the GRF, with the anterior-posterior (AP) component being approximately ten times less and the mediolateral (ML) component being approximately one hundredth of the vertical force [TW10].

Die approbierte gedruckte Originalversion dieser Diplomarbeit ist an der TU Wien Bibliothek verfügbar.
The approved original version of this thesis is available in print at TU Wien Bibliothek.

This thesis deals exclusively with the vertical GRF component, since no other force can be measured in the underlying PerPedes system. Therefore, whenever the term GRF is mentioned throughout the thesis, it is safe to assume that we refer to the vertical force component.

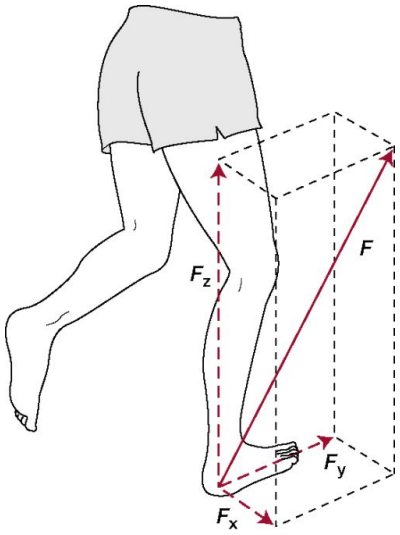

Figure 2.2: Ground Reaction Force components. F_x denotes the mediolateral, F_y the anterior-posterior, and F_z the vertical ground reaction force component. Image taken from Mooney [Moo09].

Figure 2.3a illustrates the vertical GRF throughout the gait cycle for a single leg while walking. Figure 2.3b shows the interaction of left and right forces. After the heel strike, the respective vertical GRF rises quickly until the first peak of maximum weight acceptance (MWA). Displayed force readings are normalized to the subject's body weight and might exceed 100%. This occurs because the body's center of mass (CoM) is moving downwards (Figure 2.4) before deceleration, resulting in an increased vertical GRF. During midstance at around 30% of the gait cycle after the heel strike, the CoM is maximally displaced away from the ground, decreasing the vertical GRF. The second peak is caused by pushing off the ground, increasing the acting force and therefore the vertical GRF. Successively, the GRF will fall again while the weight is transferred to the other leg until the foot's contact with the ground ends in the toe off event. Generally speaking, no GRF will occur after the foot is lifted, although Schepp's PerPedes allows the measurement of negative forces (Section 4.1). During each weight transfer, one characteristic is the weight transfer point (WTP), marking the time of equal forces (i.e. $GRF_L = GRF_R$). The WTP can be used to identify weight transfers in the gait cycle, located between each pair of heel strike and toe off event.

Die approbierte gedruckte Originalversion dieser Diplomarbeit ist an der TU Wien Bibliothek verfügbar.
The approved original version of this thesis is available in print at TU Wien Bibliothek.
TU Bibliothek Your knowledge hub WIEN

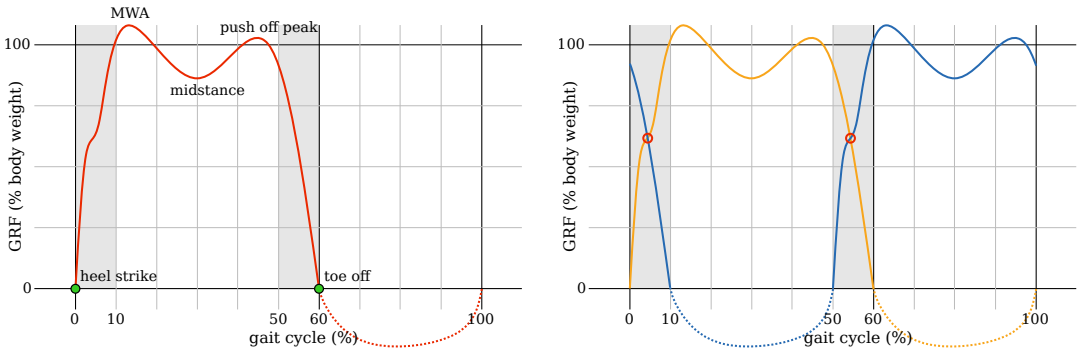

(a) One leg (b) Both legs

Figure 2.3: Illustration of vertical GRF for a single leg (a) and the interaction between both legs (b). Left leg's GRF depicted in orange, right leg's GRF in blue. Gait events marked in green, WTPs (red circles) highlight the points of equal forces. Gray areas mark the double support phases, dashed lines highlight potentially occurring negative forces.

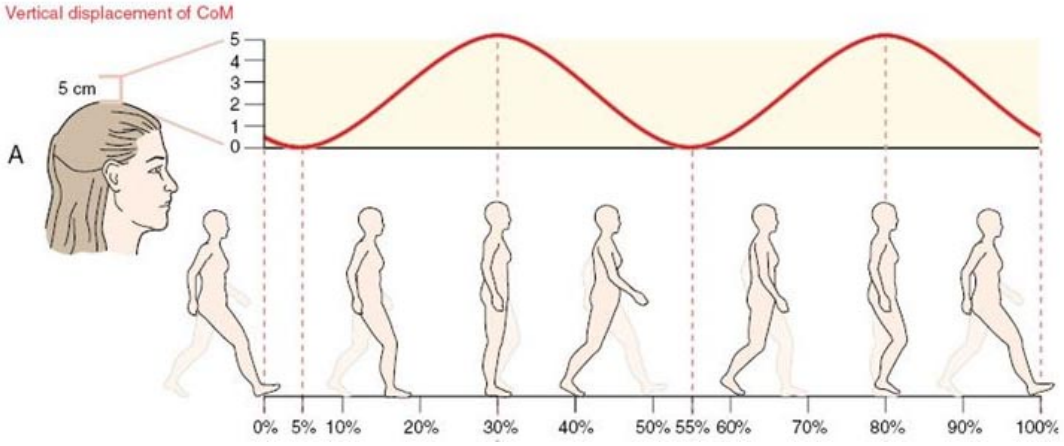

Figure 2.4: Vertical displacement of the CoM throughout the gait cycle. Image taken from Neumann [Neu10].

Die approbierte gedruckte Originalversion dieser Diplomarbeit ist an der TU Wien Bibliothek verfügbar.
The approved original version of this thesis is available in print at TU Wien Bibliothek.
TU Bibliothek Your knowledge hub WIEN

2.4 Center of Pressure

The theoretical single point of application of the GRF is called the center of pressure (CoP). This point is located somewhere on the sole of the foot if standing on one foot. It is between the feet, when both are touching the ground. The CoP is typically measured with a force plate and corresponds to a weighted average between sensor locations and measured forces.

In clinical applications, when using a pressure sensitive walkway (e.g. with a pressure sensing mat), the CoP's trajectory will look similar to Figure 2.5a, depicting one gait cycle. The gait cycle starts with a HSL, initiating the first double support phase until the right foot is lifted (TOR). Afterwards, single support on the left foot continues as long as the right foot is lifted and ends with the HSR event. This starts the second double support phase and weight shifts from left to right until the left foot is fully lifted (TOL). The right foot's single support phase will then last until the left foot contacts the ground again (HSL), completing the gait cycle.

An alternative to walkways are instrumented treadmills, which can be used in gait laboratories. These devices consist of a moving belt with force-sensing components mounted underneath. Plotting the CoP's trajectory within such a system results in a butterfly-shaped diagram, also known as gaitogram [RCS+14], or cyclogram [WCH+99] (Figure 2.5b). This characteristic shape occurs when one foot is being dragged backwards by the treadmill's belt during the single support stance phase, leading to the CoP's progression top to bottom. The contralateral foot's HS initiates the double support phase and quickly moves the CoP forward and to the other side. The weight transfer is completed with the corresponding TO event and the process continues analogously on the other side. The analysis of this form of CoP trajectory is called gaitography [RCS+14].

In the context of this thesis, we refer to a gaitogram including the movement of the feet as *dynamic gaitogram*. Contrarily, if the feet are assumed non-moving, one can analyze the CoP's trajectory between feet as if standing still. This *static gaitogram* can be created from insole pressure sensors [WCH+99] where the position of the feet is unknown or by explicitly removing the respective foot's position from the dynamic gaitogram. Using a conventional treadmill setup without the use of external cameras, the position of the feet is generally unknown and a static gaitogram cannot be inferred. In the PerPedes system, a static gaitogram can be created by excluding the movement of the pressure plates.

An example for both gaitogram types is given in Figure 2.6. The static gaitogram shows the interaction between the feet and the pressure along each foot. In healthy gait, the pressure will move from heel to toe (back to front). At the end of the stance phase, while the pressure is in the front of the foot in order to use the forefoot to push off the ground, the contralateral heel strike will occur. In the static gaitogram, this will move the CoP backwards to the heel of the striking foot. Contrarily, the dynamic gaitogram's CoP will move forward, since the striking foot is in front of the other. While the dynamic gaitogram might be used for gait symmetry analysis, the static gaitogram can provide information about specific gait patterns (e.g. toe walking).

Die approbierte gedruckte Originalversion dieser Diplomarbeit ist an der TU Wien Bibliothek verfügbar.
The approved original version of this thesis is available in print at TU Wien Bibliothek.
TU Bibliothek Your knowledge hub WIEN

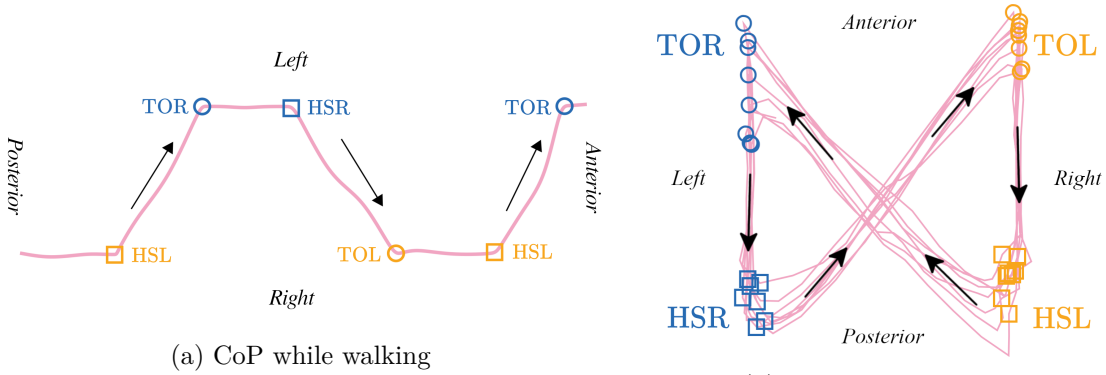

(a) CoP while walking

(b) Dynamic gaitogram

Figure 2.5: Annotated CoP trajectories during walking on flat ground (a) and within a moving system like a treadmill (b).

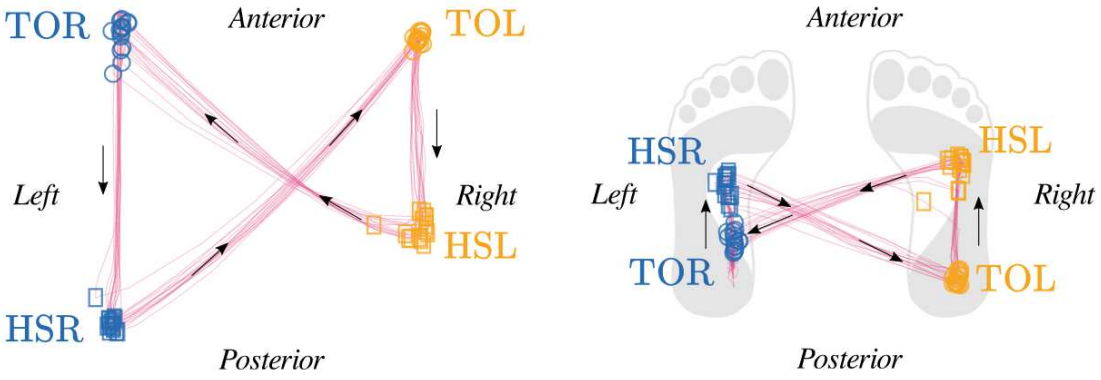

(a) Dynamic

(b) Static

Figure 2.6: Gaitogram types. Including each foot's position (a) or assuming non-moving (static) feet (b) when computing the CoP.

2.5 Spatiotemporal Gait Variables

In order to describe and measure gait, multiple types of variables have been identified in biomechanics research [LN05]. These variables can encode temporal information; for example the amount of time spent in a specific gait cycle phase (e.g. stance time, swing time). They can also represent spatial information, like distance travelled. Each variable might be affected by factors unique to an individual subject. Age, sex, body height, footwear, fitness level, and of course existing disabilities can change certain variable measurements. As discussed in Section 2.1, the double support phases during walking are commonly assumed to make up around 10% of the gait cycle, each. This ratio decreases with faster movements and disappears during running. In contrast, the ratio might

Die approbierte gedruckte Originalversion dieser Diplomarbeit ist an der TU Wien Bibliothek verfügbar.
The approved original version of this thesis is available in print at TU Wien Bibliothek.
TU Bibliothek Your knowledge hub WIEN

increase with elderly subjects or people with balance disorders, since weight transfer from one leg to the other happens more slowly.

In the following, we introduce commonly used spatiotemporal variables. Our system has been designed to extract these variables from the subject's gait and we make use of them throughout this thesis. In order to determine properties of gait, core information about the gait cycle is necessary. Most relevant data can be extracted, once gait events (HS, TO) have been identified. The reader is referred to Section 3.2 on how to identify events in current research. Chapter 6 will discuss detection of gait events in the context of our system.

Gait events (HS, TO) are temporal variables, since they occur at a specific point in time within a gait cycle. Recording their respective time of occurrence, the duration of gait cycle phases can be measured. The *stance time* is the amount of time spent in the stance phase. Since the stance phase starts with the corresponding foot's heel strike and ends with its toe off event, the stance time is the duration between HS and TO events of the same limb. Similarly, the *swing time* can be determined as the duration between TO and HS event. The time spent during weight transfer is expressed through the two *double support times*. Each weight transfer from left to right and vice versa occurs between HS of one limb and TO of the other extremity.

The gait events are also spatial variables, since they occur at a specific location. This can be used to derive the *step length* and the *stride length* as illustrated in Figure 2.7. We refer to the step lengths on each side as step length, left (SLL) and step length, right (SLR), respectively. The step length expresses how far ahead one foot moves in front of the other one, by measuring the distance between two consecutive and similar points (e.g. between heels) of both feet. The step length is usually positive, although it can be zero in case the foot is only brought up beside the other one, or negative when moving backwards or 'dragging' one foot behind the other one. Stride length as the sum of the left and right step length can be inferred by measuring the distance between two successive placements of the same foot. We talk about spatiotemporal variables in the context of our system in Chapter 7.

Die approbierte gedruckte Originalversion dieser Diplomarbeit ist an der TU Wien Bibliothek verfügbar.
The approved original version of this thesis is available in print at TU Wien Bibliothek.
TU Bibliothek Your knowledge hub WIEN

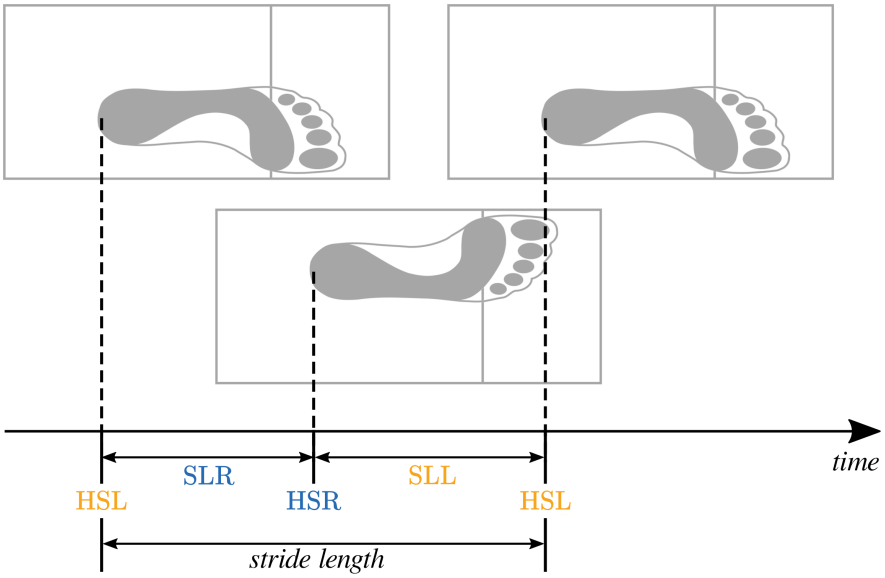

Figure 2.7: Illustration of step length and stride length. Step length is measured between two successive and similar contact points (e.g. the heel) of opposing feet. The right step length SLR can be measured between the contact point of the right heel strike event HSR and the contact point of the previous left heel strike event HSL. The left step length SLL is calculated in an analogous manner. Stride length is determined through SLL + SLR.

2.6 Gait Symmetry

An important aspect in evaluating the performance of subjects with one-sided gait disabilities, as for example hemiparetic patients after stroke, is to compare left and right spatiotemporal variables. Measuring symmetry between variables allows the therapist and attending physician not only to evaluate the current patient's state, but also the progress during rehabilitation therapy. In general, symmetry in gait can also be an important tool in distinguishing healthy from impaired gait. Roerdink and Beek [RB11] state that a majority of hemiplegic stroke patients show longer paretic steps in comparison to their nonparetic side. Other studies [HRJ+97], [BBNK07] also demonstrate a longer step length, longer swing phase, and shorter stance phase with paretic legs in patients with hemiparesis. Furthermore, Roerdink et al. [RCS+14] examined amputees and showed the same effect for prosthetic legs. Extracting parameters, like step length and duration of gait phases, and determining symmetry parameters could therefore be used to measure existing disabilities and document therapy progress. We talk more about symmetry measures in the literature in Section 3.3 and in the context of our system in Section 7.2.

Die approbierte gedruckte Originalversion dieser Diplomarbeit ist an der TU Wien Bibliothek verfügbar.
The approved original version of this thesis is available in print at TU Wien Bibliothek.
TU Bibliothek Your knowledge hub WIEN

CHAPTER 3

Related Work

3.1 Commercial Solutions for Gait Training/Analysis

Gait analysis in the commercial sector is done with pressure sensing systems, cameras and markers, inertial motion trackers, or a combination of these. The company CIR Systems Inc. [CIR20] provides portable, pressure sensitive walkways using pressure sensing mats within their *GAITRite* product palette. They state that their products have been cited more than 5000 times in research publications since 2005. Additionally, they provide proprietary software to obtain spatiotemporal gait measures, for both clinical and research applications.

Gait rehabilitation is often done with treadmills or robotic trainers in order to reduce the workload of the therapist and provide repetitive training scenarios. The complexity of these systems varies, but typically includes fall protection via support harness. Solutions, like the Hocoma Andago [Hoc20a] provide a mobile platform for overground gait training. It follows the patient with two electrically driven wheels while providing stabilization and fall protection. Contrarily, most offered gait training solutions are stationary and can range from treadmills (Zebris Rehawalk [Zeb20b], Motek GRAIL [Lin20]) to orthosis-based (Hocoma Lokomat [Hoc20b]) robotic devices. The company Reha Technology AG provides the robotic gait trainer $G-EO_1$ [Reh20] to simulate the climbing of stairs. Some examples of the mentioned gait rehabilitation systems are shown in Figure 3.1. The interested reader is referred to Morone et al. [MPC+17] for an overview of gait training on recent robotic platforms.

Die approbierte gedruckte Originalversion dieser Diplomarbeit ist an der TU Wien Bibliothek verfügbar.
The approved original version of this thesis is available in print at TU Wien Bibliothek.
TU Bibliothek Your knowledge hub WIEN

(a) Hocoma Lokomat [Hoc20b]

(b) Zebris Rehawalk [Zeb20b]

(c) Reha Technology $G-EO_1$ [Reh20]

Figure 3.1: Gait Rehabilitation - Commercial Solutions.

3.2 Gait Event Detection

Gait events (HS, TO) are important points in the gait cycle, which are used to derive parameters (e.g. step length). The possibilities to detect events are manifold and depend not only on the used equipment but also on the processing of the recorded data. We distinguish between two physical ways to analyze gait events, i.e. kinematic and kinetic approaches. Kinetics, as part of classical mechanics, is concerned with the study of motion and its causing forces or moments (torques). Kinematics on the other hand describes motion without taking the causing forces into account. In biomechanics, this is done by analyzing the motion of the human skeleton or parts of the body (e.g. limbs, joints). This motion, expressed through displacement, accelerations, velocities, or angular

Die approbierte gedruckte Originalversion dieser Diplomarbeit ist an der TU Wien Bibliothek verfügbar.
The approved original version of this thesis is available in print at TU Wien Bibliothek.
TU Bibliothek Your knowledge hub WIEN

quantities, can be measured directly (e.g. with an inertial measurement unit (IMU)) or indirectly (e.g. with camera tracking and reflective markers).

Roerdink et al. [RCS+14] detect gait events from the CoP's trajectory by identifying minima and maxima in the gaitogram's AP component as HS and TO, respectively. Van der Veen et al. [vdVHBH18] compares two marker-based kinematic methods to the previously mentioned CoP-based kinetic method [RCS+14] used as a gold standard. The first marker-based method M_1, as defined in previous studies [RCC+08], [PBvD04] detects HS as a minimum in the vertical displacement and TO as a local maximum in the vertical velocity, both referring to a heel marker. The second method M_2 [ZJRH08] defines HS as the maximum anterior displacement of the heel marker and TO as the instant when the forward velocity of the toe marker crosses zero. They compare data from both stroke patients and healthy subjects and determined method M_1 might not be considered reliable for stroke patients, while M_2 might detect events too early. They conclude that GED, based on the CoP's trajectory may be more appropriate with stroke patients. At the same time, it is pointed out that CoP-based methods might not work with severely affected gait and non-butterfly shaped gaitograms.

Mansfield and Lyons [ML03] compare GED with a footswitch to accelerometer-based detection, attached to the lower spine. They argue that for people with an initial contact not performed with the heel, such as hemiplegic patients with foot drop, the accelerometer-based method might be a favorable choice. On the other hand, Hanlon and Anderson [HA09] demonstrate in their study of healthy participants that footswitch-based GED show significantly lower errors than their accelerometer-based method.

Pappas et al. [PPK+01] combine a gyroscope attached to the heel with force sensitive resistors in the shoe sole for GED. While the HS event is detected when any of the resistors is pressed, the TO event is based on the heel being lifted and simultaneously exceeding an angular threshold, measured through the gyroscope. Another approach [HHH+13] uses a shank-mounted gyroscope to determine initiation and termination of a forward swing. These instants indicate the shank's change in angular direction and are closely related to gait events. Recent work in GED investigates the use of smartphones [PVS17] instead of dedicated IMUs, as well as neural networks [Mil09], [KDS19] as an alternative to signal processing.

3.2.1 Threshold-based Methods

In their recent work, Benson et al. [BCW+19] state that the use of thresholds with GRF data from force plates is considered the *gold standard* for GED. Rueterbories et al. [RSLA10] also highlight that force-based event detection, either with force plates or sensors attached to the feet, is still used as a reference to validate against.

While threshold-based methods are very common in event detection, there appears to be no agreement on the choice of threshold or on the force component to use. The literature describes thresholds on the vertical GRF of 10 N [GSDE04], [HM00] and 20 N [SFB+05]. Alternatively, thresholds on the total amount of GRF of 2.5 N [WC96], 5 N [HA09], or

Die approbierte gedruckte Originalversion dieser Diplomarbeit ist an der TU Wien Bibliothek verfügbar.
The approved original version of this thesis is available in print at TU Wien Bibliothek.
TU Bibliothek Your knowledge hub WIEN

6.5% of the body weight [ZH03] are reported. Furthermore, Hesse et al. [HRJ+97] detect HS events when the AP force component exceeds 5 N.

In general, threshold-based GED are not applicable in scenarios where early contacts are not indicating a heel strike event. This is the case with gait abnormalities such as shuffling gait, where subjects are dragging their feet as they walk (e.g. with Parkinson's disease). Similarly, these methods are not applicable in our system, since exceeding a force threshold does not indicate a weight transfer. This is discussed in Section 6.4.

3.2.2 Total Vertical Ground Reaction Force

Mawase et al. [MHBHK13] demonstrate in their work the relation between the total amount of vertical ground reaction forces (sum of left and right forces) and gait events (Figure 3.2). They observe maxima in the double support phases and minima during single support. Heel strikes are located at a local minimum, preceding strong peaks in the total vertical force. Following this maximum peak, toe off events are located immediately after the next local minimum. Controversially, Roerdink et al. [RCC+08] locate toe off events exactly at this local minimum. We examine the possibility of using the total vertical GRF in our system in Section 6.4.3.

Die approbierte gedruckte Originalversion dieser Diplomarbeit ist an der TU Wien Bibliothek verfügbar.
The approved original version of this thesis is available in print at TU Wien Bibliothek.

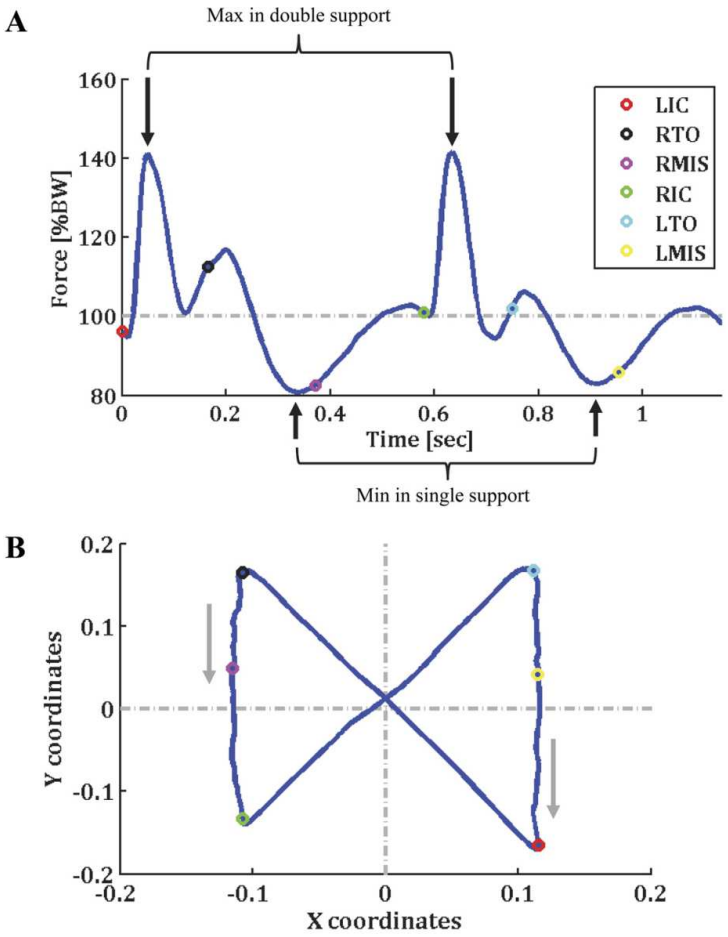

(a) Images taken from Mawase et al. [MHBHK13].

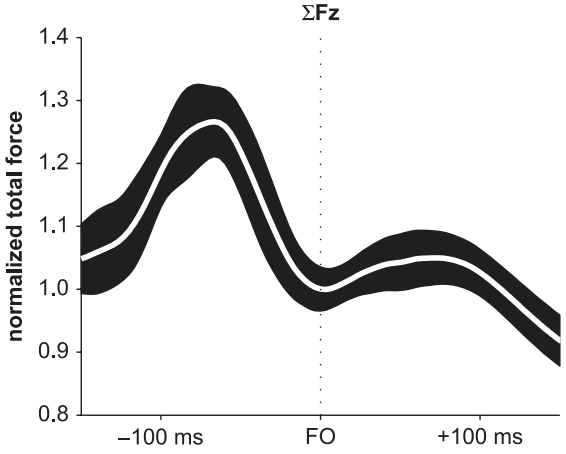

(b) Image taken from Roerdink et al. [RCC+08].

Figure 3.2: Total vertical ground reaction forces and gait events. This example shows important points in the gait cycle and in the (dynamic) gaitogram. Abbreviations: LIC (left initial contact), RTO (right toe off), RMIS (right midstance), RIC (right initial contact), LTO (left toe off), LMIS (left midstance), and FO (foot off).

Die approbierte gedruckte Originalversion dieser Diplomarbeit ist an der TU Wien Bibliothek verfügbar.
The approved original version of this thesis is available in print at TU Wien Bibliothek.
TU Bibliothek Your knowledge hub WIEN

3.2.3 Continuous Wavelet Transform

In recent years, the continuous wavelet transform (CWT) has seen an increased application in biosignal processing [AWG09] and in gait analysis to explore the time-frequency relationship between gait event and gait cycle [KW16]. In contrast to the Fourier transform (FT), the CWT offers a time-frequency representation of a signal that is both very well localized in frequency **and** time. Another distinctive feature of the CWT over the FT is the use of basis functions other than sinusoidal (sine, cosine) curves. The CWT's basis functions are scaled and shifted versions of one *mother wavelet*. Different mother wavelets are commonly used in gait analysis, among them the Morlet [KW16] and the derivative of Gaussian (DoG) [MDGM12] wavelets.

As an example, the Gaussian function, centered at zero with standard deviation σ and its corresponding first order derivative can be written as:

$$G(x) = \frac{1}{\sigma\sqrt{2\pi}} \exp(-\frac{x^2}{2\sigma^2}) \tag{3.1}$$

$$\frac{\mathrm{d}G(x)}{\mathrm{d}x} = -\frac{x}{\sigma^2} \cdot G(x) \tag{3.2}$$

Illustrations of both functions can be seen in Figure 3.3.

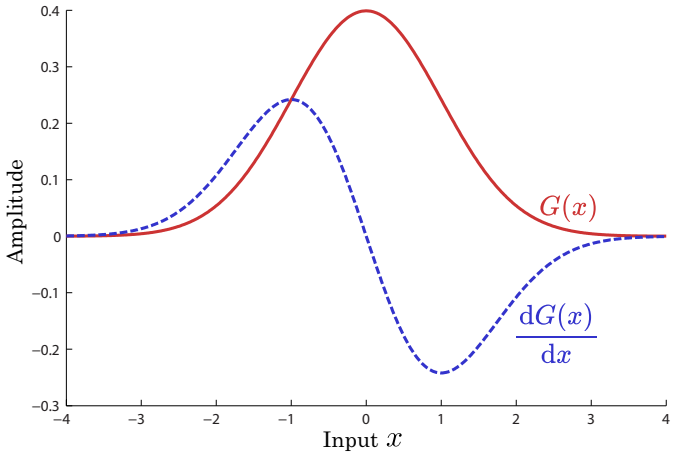

Figure 3.3: Gaussian (solid red line) and its first order derivative (dashed blue line) with $\sigma = 1$. The corresponding Matlab code can be found in Appendix A.2.

Die approbierte gedruckte Originalversion dieser Diplomarbeit ist an der TU Wien Bibliothek verfügbar.
The approved original version of this thesis is available in print at TU Wien Bibliothek.
TU Bibliothek Your knowledge hub WIEN

CWT - A Buzzword?

> **Definition** of *buzzword*: An important-sounding usually technical word or phrase often of little meaning used chiefly to impress laymen.
>
> Merriam Webster dictionary [Mer19]

The goal of the CWT is to provide a tool for time-frequency analysis in the context of gait event detection. While promising, current publications suggest that the method can be misunderstood and its applicability might be overrated. The following section demonstrates that a simple Gaussian smoothing operation can replace a complex arrangement of steps incorporating the CWT.

The influential paper *"An enhanced estimate of initial contact and final contact instants of time using lower trunk inertial sensor data"* by McCamley et al. [MDGM12] uses CWT in the context of GED. As of April 2020, it has been cited more than 100 times, as well as re-implemented and evaluated repeatedly [TRHC15], [SBM16], [DDGR15], [FOL19]. Their method (M_{CWT}) analyzes a vertical acceleration signal, acquired from a single IMU, positioned at the lower spine. They propose to integrate the acceleration signal, followed by a differentiation step using a CWT with a first order DoG wavelet. HS events are then located at the minima of the resulting signal, while TO events are to be found at the maxima of the signal obtained after another CWT differentiation step.

Remarkably, three different publications, Storm et al. [SBM16], Trojaniello et al. [TRHC15], and Trojaniello et al. [TCDC14] allegedly evaluate the M_{CWT} method, but make no mention of the first integration step. Din et al. [DDGR15] and Flood et al. [FOL19] report the necessary integration step before applying the CWT.

In order to evaluate the M_{CWT} method, the first step was to reproduce the results reported by McCamley et al. Since the authors did not provide the underlying acceleration data, we decided on manually sampling their result figure's acceleration graph. The vertical acceleration function was then reconstructed from the sample points with a cubic spline interpolation (Matlab: `spline`) at a 5 ms resolution in time, since the original function had a 10 ms temporal resolution. Subsequently, the vertical acceleration was integrated (Matlab: `cumsum`) and differentiated with the CWT (Matlab: `derivative_cwt` [Luo07]). The minima of this signal correspond to heel strikes, while another CWT differentiation reveals a signal whose maxima correspond to the TO events.

Both signals resembled the reported results (Figure 3.4), although they could not be accurately reproduced, since the scaling parameter for the CWT was not reported by McCamley et al., nor by any other publication. Additionally, since the acceleration signal was sampled from an image, the data beyond the image's boundaries is unknown,

Die approbierte gedruckte Originalversion dieser Diplomarbeit ist an der TU Wien Bibliothek verfügbar.
The approved original version of this thesis is available in print at TU Wien Bibliothek.
TU Bibliothek Your knowledge hub WIEN

resulting in discrepancies near the border. Experimentally, we could establish a scaling parameter of around 15, used for the acceleration data with a sampling rate of 10 ms.

Since it is now established that an integration step is indeed necessary, we evaluate why the authors suggest to integrate and then differentiate again and for which purpose the CWT is used. Nie et al. [NWL+02] demonstrate that the CWT can be used to calculate the approximate derivative of a signal. They use the n^{th} order derivative of Gaussian function as a wavelet with a CWT to calculate the n^{th} order derivative of the signal, smoothed by a (scaled) Gaussian function. This possibility to approximate a derivative using the CWT is also reported by Luo et al. [LBS06], who provide the `derivative_cwt` Matlab function, as well as by Shao and Ma [SM03]. Both are cited in the work of McCamley et al. [MDGM12].

The CWT with a first order DoG wavelet is an approximate derivative with additional smoothing. Since the M_{CWT} method integrates the acceleration signal and subsequently uses the CWT, the result is a smoothed version of the original signal. The process can therefore be substituted by merely using an appropriately sized Gaussian to smooth the acceleration data. We provide a visual comparison between integration, followed by a CWT in contrast to a simple smoothing in Figure 3.5. The signal beyond the boundaries at times $t = 0$ and $t = 2$ is assumed constant and equal to the mean signal value. The normalized Gaussian kernel used for smoothing is appropriately scaled in time to the signal's domain $t \in [0, 2]$. Note that the Gaussian kernel in Figure 3.5 is for illustrative purposes, correctly showing the extent in the time domain, but its amplitude does not match the acceleration signal's domain. The corresponding Matlab code used to generate Figures 3.4 and 3.5 can be found in Appendix A.1.

In summary, our findings show that McCamley et al.'s method can be simplified to using a Gaussian smoothing kernel on the acceleration signal A to create a smoothed version A_s. Followed by a conventional numerical differentiation step and an additional Gaussian smoothing, we arrive at signal D_s. HS events are then located at the minima of A_s, while TO events are located at the maxima of D_s. These maxima approximately correspond to the inflection points of A_s and are positioned roughly halfway between minima and maxima of A_s. The publication [MDGM12] does not mention why those inflection points should represent TO events.

Trojaniello et al. [TRHC15] report significantly larger errors when applying the M_{CWT} method to subjects with pathological gait. Din et al. [DDGR15] initially find that the M_{CWT} method generates spurious HS events in 37% of healthy participants and 58% of patients with Parkinson's disease. As a consequence, they decide to refine the method before comparing it to other selected algorithms. Storm et al. [SBM16] evaluate M_{CWT} and another method. They conclude that event timings cannot be reproduced as accurately as reported in the M_{CWT} method's original paper. For outdoor free walking M_{CWT} performs worse than the compared method with a shank-mounted IMU. In conclusion, even results from well-received and cited papers have to be reflected on and checked for applicability and reproducibility in a given situation.

Die approbierte gedruckte Originalversion dieser Diplomarbeit ist an der TU Wien Bibliothek verfügbar.
The approved original version of this thesis is available in print at TU Wien Bibliothek.
TU Bibliothek Your knowledge hub WIEN

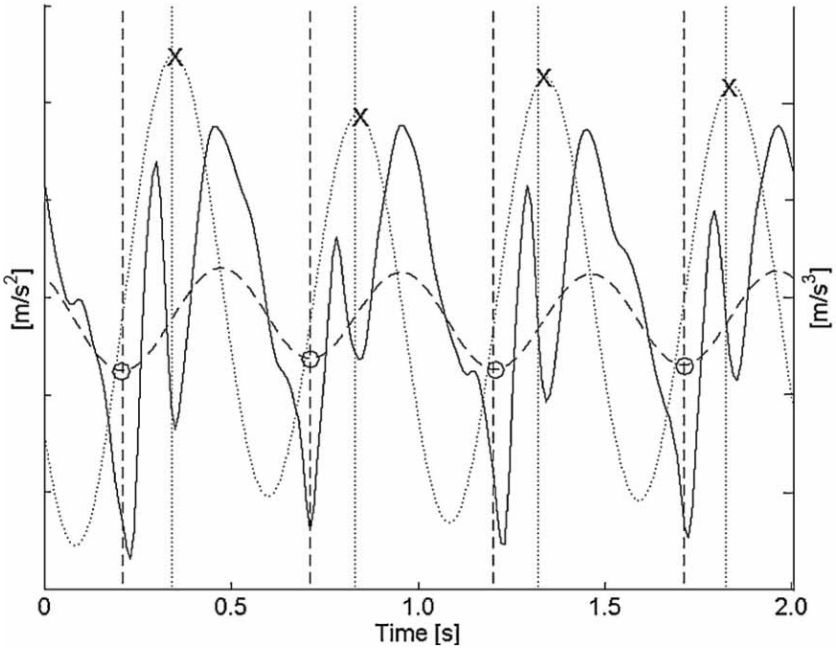

(a) Image taken from McCamley et al. [MDGM12], Fig. 1.

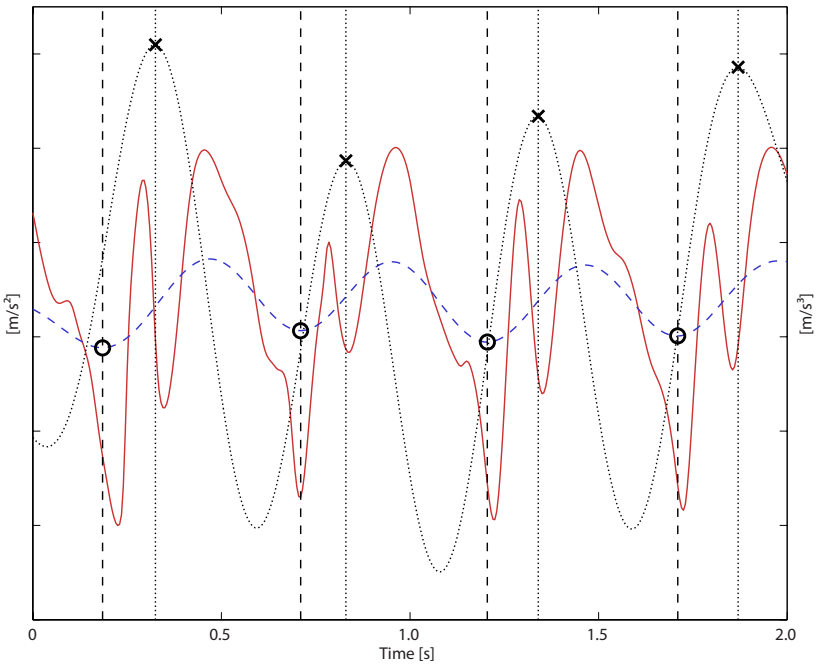

(b) Our reproduction of the results.

Figure 3.4: Verification of the M_{CWT} method. The measured vertical acceleration (solid line) is first integrated and subsequently a CWT is applied, resulting in a smoothed acceleration (dashed line). Applying another CWT results in a smoothed jerk (dotted line). The minima of the smoothed acceleration correspond to HS (∘) events, while the maxima of the smoothed jerk represent TO (×) events.

Die approbierte gedruckte Originalversion dieser Diplomarbeit ist an der TU Wien Bibliothek verfügbar.
The approved original version of this thesis is available in print at TU Wien Bibliothek.
TU Bibliothek Your knowledge hub WIEN

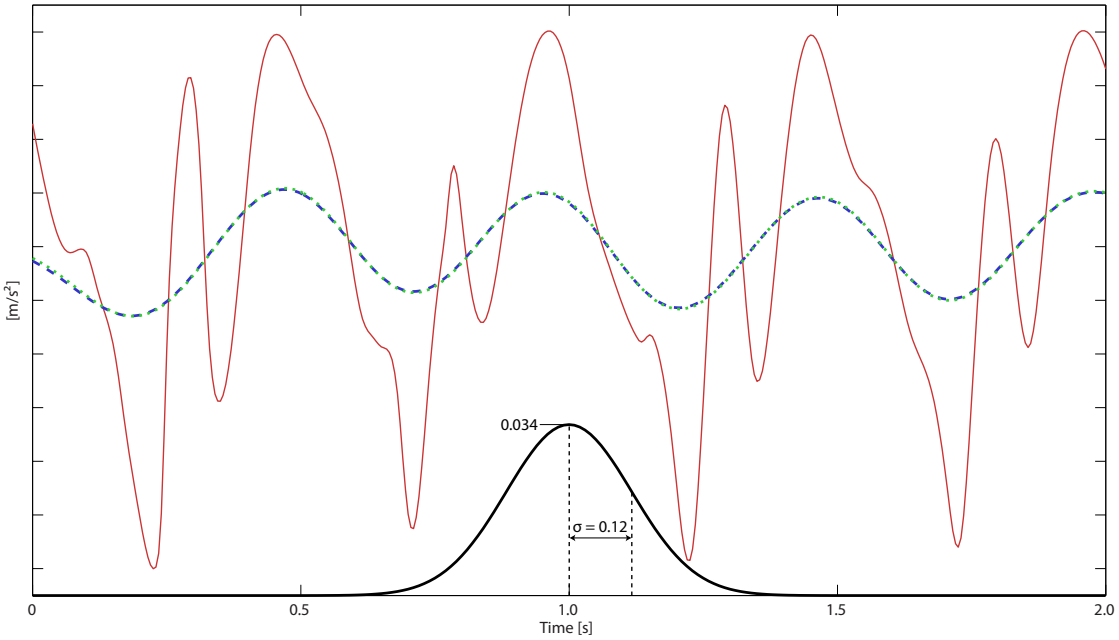

Figure 3.5: Comparing the M_{CWT} method to smoothing. The vertical acceleration (solid red line) is integrated and transformed through a CWT, resulting in a smoothed acceleration (dashed blue line). Smoothing the acceleration with an appropriately sized Gaussian kernel (solid black line) results in a nearly identical signal (dotted green line).

3.2.4 Correlation between GRF and Acceleration

Multiple studies analyze the relation between ground reaction forces and accelerometer data. Elvin et al. [EEA07] show a strong and significant correlation between peak GRF and peak tibial accelerations during jumping. Neugebauer et al. [NHB12] estimate peak vertical GRF from hip accelerations and provided a mixed model regression equation. Fortune et al. [FMK14] use ankle, waist, tibia, and thigh positioned accelerometers to estimate peak (vertical) GRF and peak (vertical) loading rate. They provide linear regression equations from which those quantities can be inferred. Ankle and waist worn accelerometers show the most accurate estimates. Rowland and Stiles [RS12] demonstrate that acceleration correlates with GRF in accelerometers worn at the wrist and the hip. Pouliot-Laforte et al. [PLVRL14] show that accelerometry could be a valid tool to estimate the vertical GRF for healthy children as well as children with osteogenesis imperfecta type I, a genetic disorder affecting the bones. The accelerometer was positioned at the waist and different tests were carried out to reflect everyday life settings in children.

Initially, we were investigating the possibility to apply acceleration-based GED algorithms in the context of our system, because of the correlation between GRF and acceleration. The literature suggests that there could be a correlation between tibia-based accelerations and vertical GRF of one foot, as well as waist-based accelerations and the total amount

Die approbierte gedruckte Originalversion dieser Diplomarbeit ist an der TU Wien Bibliothek verfügbar.
The approved original version of this thesis is available in print at TU Wien Bibliothek.
TU Bibliothek Your knowledge hub WIEN

of vertical GRF. Gait in PerPedes (Chapter 4) restricts free movement and there are no evaluations available if the correlation holds in this case, and if so, which regression model is valid in the context of our system. Additionally, converting GRF to acceleration data will likely introduce additional imprecision. Therefore, we decided against using acceleration-based methods for GED and use kinetic methods, based on the force data instead.

3.3 Symmetry Measures

An important aspect in evaluating the patient's performance and document the therapy's progress is the acquisition of gait symmetry indicators. According to Patterson et al. [PGB+10], there exists no accepted standard for assessing symmetry in gait. According to Blazkiewicz et al. [BWW14], the symmetry index (SI) is the most commonly used and cited measure in publications on gait symmetry. The literature commonly proposes two kinds of symmetry measures. The first kind deals with comparing spatiotemporal parameters between the patient's left and right side. The second group of symmetry measurements is inferred from the gaitogram's graphical representation.

3.3.1 Symmetry from Spatiotemporal Parameters

Publications (see caption in Table 3.1) propose multiple symmetry measures, commonly used in evaluating gait symmetry. Symmetry measures quantify the correlation between values of the left V_L and right side V_R of the body. In patients with partial paralysis, it can be used to compare the performance of the paretic side to the non-paretic side, in other words, comparing the impaired to the healthy side.

Given strictly positive spatiotemporal parameters V_L and V_R, different symmetry measures are proposed in publications on gait symmetry. The most common symmetry measures are summarized in Table 3.1. Each measure's value is zero if $V_L = V_R$, positive if $V_R > V_L$, and otherwise negative. While SR, SA, and GA just compare the ratio between both values and apply different scaling, SI compares the difference to the average of both values. GA is ambiguously defined in the literature; with and without absolute value $|\ln(\cdot)|$. For consistency, the GA's range of values is centered at zero, therefore no absolute value is used. Patterson et al. [PGB+10] provide an evaluation of all symmetry measures. They also propose the symmetry ratio SR to represent the fraction between the smaller and the larger value while indicating the direction of symmetry with a sign convention.

The given formulas are only applicable if both values V_L, V_R are positive, but can be extended as follows. If both quantities are negative, symmetry can be measured between the new parameters $V'_L = -V_R$ and $V'_R = -V_L$. This will lead to a positive value if $|V_R| > |V_L|$. Furthermore, if both quantities are zero ($V_R = V_L = 0$), a symmetry measure can be defined as zero (i.e. symmetric). If one quantity is positive and the other negative, the given measures are not applicable. The range of SR is either exceeded or its value is undefined if $\max(V_L, V_R) = 0$. Similarly, the range of SI is either exceeded or its value is

Die approbierte gedruckte Originalversion dieser Diplomarbeit ist an der TU Wien Bibliothek verfügbar.
The approved original version of this thesis is available in print at TU Wien Bibliothek.
TU Bibliothek Your knowledge hub WIEN

undefined if $V_R + V_L = 0$. For SA and GA, the symmetry cannot be determined, since $\frac{-V_R}{V_L} = \frac{V_R}{-V_L}$.

In their work, Patterson et al. [PGB+10] specified the spatiotemporal parameters step length, swing time, and stance time to be most useful in the context of gait symmetry with stroke patients. Since swing time and stance time are strictly positive values, the measures can be applied as is. Step lengths could potentially be negative (e.g. walking backwards), therefore the symmetry measures are valid with the proposed adaptations.

Symmetry Measure	**Equation**	**Range**
Symmetry Ratio (SR)	$100\% \cdot \text{sgn}(V_R - V_L) \cdot (1 - \frac{\min(V_L, V_R)}{\max(V_L, V_R)})$	$[-100\%, 100\%]$
Symmetry Index (SI)	$100\% \cdot \frac{V_R - V_L}{0.5(V_R + V_L)}$	$[-200\%, 200\%]$
Symmetry Angle (SA)	$100\% \cdot (45° - \text{atan}(\frac{V_L}{V_R}))/90°$	$[-50\%, 50\%]$
Gait Asymmetry (GA)	$100\% \cdot \ln(\frac{V_R}{V_L})$	$(-\infty\%, \infty\%)$

Table 3.1: Commonly used symmetry measures. Symmetry ratio [PGB+10], [LBAN14], symmetry index and symmetry angle [PGB+10],[Pat10],[HB12],[BWW14],[LBAN14], as well as gait asymmetry [PGB+10],[Pat10],[HB12],[BWW14].

3.3.2 Symmetry in the Gaitogram

The analysis of the CoP's trajectory throughout one or more gait cycles has been the topic of research in multiple publications. The so called gaitography is applied in different studies, dealing with gait disabilities. It is applied in gait pattern analysis for prosthetic walking [RCS+14], toe walking [KYB16], multiple sclerosis [KF15], [KDFA13], and with hemiplegic stroke patients [WPH+04].

The *Zebris FDM-T evaluation* software [Zeb20a] (Zebris Medical GmbH), a commercial solution for gait analysis, automatically creates gaitogram visualizations and derives analytic parameters from the patient's CoP trajectory. A gait report [Tol17] can then be generated per therapy session.

Gait analysis [KF15], [KDFA13] introduces three symmetry parameters, derived from the patient's gaitogram (Section 2.4). We discuss these parameters in the context of our system in Section 7.2.

Die approbierte gedruckte Originalversion dieser Diplomarbeit ist an der TU Wien Bibliothek verfügbar.
The approved original version of this thesis is available in print at TU Wien Bibliothek.
TU Bibliothek Your knowledge hub WIEN

CHAPTER 4

Schepp's PerPedes

Figure 4.1: Schepp Medtech's PerPedes [Med15]. Robotic gait rehabilitation with plantar flexion and dorsiflexion support. The system provides vertical GRF readings for both feet. Since the subject's feet are strapped in (red frame), negative forces can potentially occur. Images taken from the manufacturer [Med15] and the SFG [Ste17].

Die approbierte gedruckte Originalversion dieser Diplomarbeit ist an der TU Wien Bibliothek verfügbar.
The approved original version of this thesis is available in print at TU Wien Bibliothek.
TU Bibliothek Your knowledge hub WIEN

4.1 Overview

Schepp Medtech GmbH [Med15], as one of the partners in the BrainGait project (Section 1.3), provides the robotic gait rehabilitation device, named *PerPedes* (Figure 4.1). The device can be used to emulate a natural walking motion with plantar flexion (PF) and dorsiflexion (DF) support. PF and DF refer to the angle between foot and tibia (Figure 4.2a). Rotating the foot around the ankle downwards increases the angle between foot and leg; the ankle is in plantar flexion. Decreasing the angle and therefore bringing the toes closer to the tibia leads to dorsiflexion. Over the course of a gait cycle, this angle naturally changes (Figure 4.2b). During a heel strike, the ankle is in neutral DF. After heel strike, the fast transition to a flat foot leads to an increased PF during the loading response subphase. While the body's CoM moves in front of the weight-bearing foot during the stance phase, the dorsiflexion angle increases to around 10°. During push-off, the ankle switches to PF; it subsequently reaches an angle of around −20°. The foot's ankle then returns to neutral DF during the swing phase. The PerPedes platform supports the PF at the end of the stance phase by raising the subject's heel. Furthermore, to assure neutral DF during heel strike, the forefoot is automatically lifted.

PerPedes consists of two moving plates with each plate containing six weight (pressure) sensors (Figure 4.3). The used sensors are not multi-axis force sensors, therefore only vertical ground reaction forces can be determined. Since the subject's feet are held down with foot straps on top of the plates, it is also possible to measure negative forces if a foot is lifted and pulls on the foot straps. The small number of sensors can be used to determine the average pressure location on each plate (Section 5.4), but lacks the capabilities of a full pressure sensor matrix with hundreds or even thousands of pressure readings used in pedobarography [SMS+14].

For safety, the subject wears a harness, which allows part of the subject's weight to be carried by a weight support system. The amount of weight support, between 0% and 100% of the subject's body weight, can be adjusted via Schepp's tablet software. This weight lifting system also allows the reproduction of the subject's natural torso movement in the vertical direction during therapy. Furthermore, support of the horizontal movement of the pelvis can be activated in order to simulate natural walking. The overall sense of personal safety is increased by the provided handrails for individual stabilization.

The step length can be adjusted separately for each pressure plate, ranging from 270 to 620 mm. The step width is adjustable with two possible positions in ML direction on each plate, resulting in a 90 or 190 mm spacing between the midlines of the feet. The maximum cadence is 94 steps per minute. Using the maximum step length of 620 mm, this results in a maximum walking speed of around 3.5 km/h[1]. The machine's movements are either at a fixed speed or user-controlled by "pulling" the pressure plates.

The PerPedes platform provides data readings, configurable between 2 Hz (every 500 ms) and 50 Hz (every 20 ms). The most important data in our context are the pressure

[1] $94\ \text{steps/min} \cdot 620\ \text{mm/step} = 58,280\ \text{mm/min} = 3.4968\ \text{km/h}$

Die approbierte gedruckte Originalversion dieser Diplomarbeit ist an der TU Wien Bibliothek verfügbar.
The approved original version of this thesis is available in print at TU Wien Bibliothek.
TU Bibliothek Your knowledge hub WIEN

sensors' readings, pressure plate positions, support load, and therapy speed.

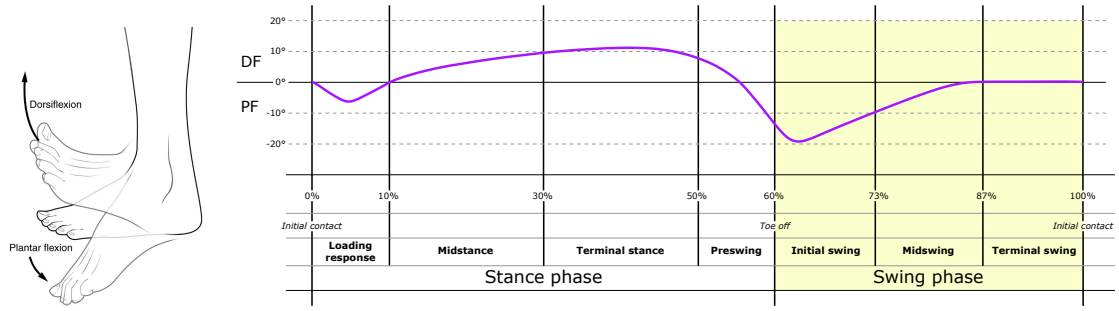

(a) (b)

Figure 4.2: PF and DF of the human foot (a) and throughout the gait cycle (b). Figure (a) taken from Connexions [Con13]. Figure (b) adapted from Perry [Per08].

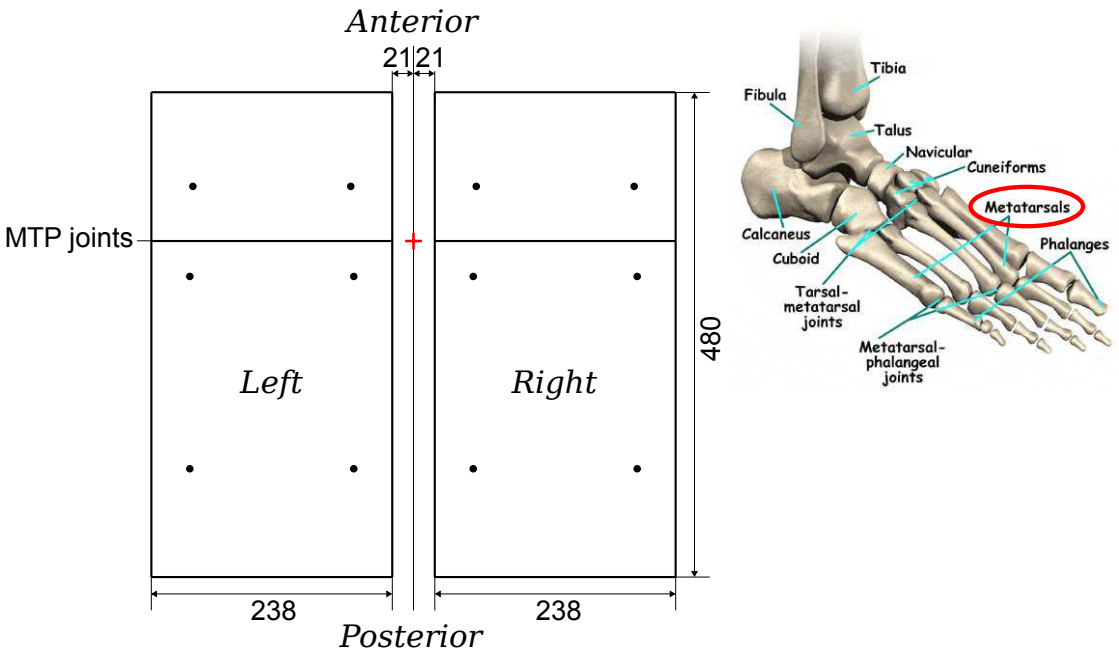

Figure 4.3: PerPedes' pressure plate setup. Each pressure plate has six pressure sensors (black dots), the coordinate origin is marked with a red cross, and dimensions are in millimeter. Each pressure plate consists of two connected sections (front and back). The subject's metatarsophalangeal (MTP) joints of each foot are placed between both sections. Right image taken from Pearl [Pea19].

Die approbierte gedruckte Originalversion dieser Diplomarbeit ist an der TU Wien Bibliothek verfügbar.
The approved original version of this thesis is available in print at TU Wien Bibliothek.
TU Bibliothek Your knowledge hub WIEN

4.2 Plate Movement

The pressure plates' movement defines the machine's gait cycle. Each plate is positioned at a maximum frontal position when reaching its preset step length, i.e. the moment of optimal heel strike. It is positioned furthest back around the optimal toe off instant. The plate's backwards movement (during stance) is slightly slower than its forward movement, reflecting the optimal 60:40 ratio of stance and swing phase in the gait cycle. This leads to an asymmetrical movement of both plates throughout the gait cycle (Figure 4.4).

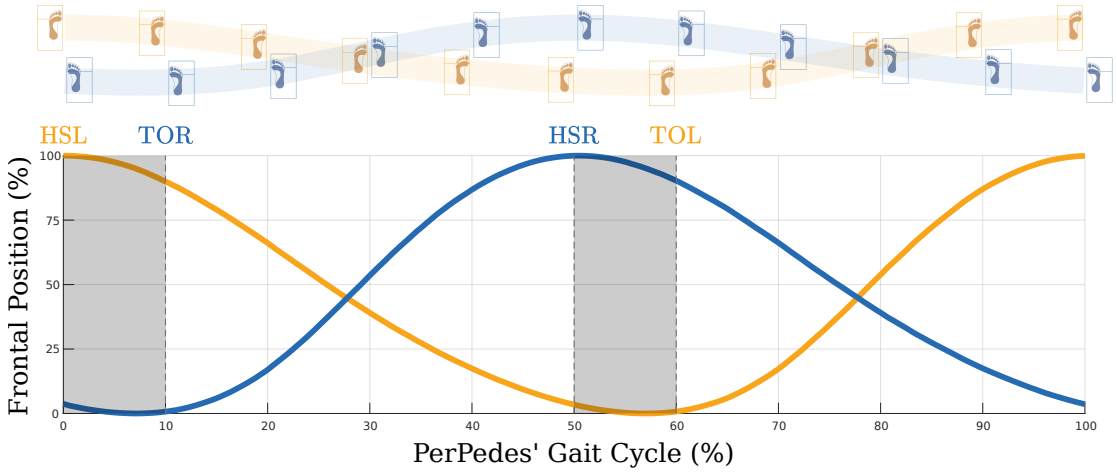

Figure 4.4: PerPedes' plate movement throughout its gait cycle. The most frontal position (i.e. 100% of the machine's step length) of the plates is reached at 0% and 50% of the gait cycle, while the plates are positioned farthest back at around 57% and 7% of the gait cycle for the left and right plate, respectively. They are positioned next to each other at around 28% and 78%.

Die approbierte gedruckte Originalversion dieser Diplomarbeit ist an der TU Wien Bibliothek verfügbar.
The approved original version of this thesis is available in print at TU Wien Bibliothek.
TU Bibliothek Your knowledge hub WIEN

CHAPTER 5

Data Recording and Preprocessing

5.1 Resampling

Force plate data readings in Schepp's PerPedes device are provided per default at a frequency of 10 Hz (every 100 ms), but could potentially be read at up to 50 Hz (every 20 ms). The number of measurements per gait cycle depends on the machine's therapy speed, expressed in steps per minute. Studies [TLR+07], [TMR97] have shown that the mean cadence of post-stroke patients can range from 50 to 63 steps per minute. Therefore, a gait cycle consisting of two steps might take between 1.9 and 2.4 seconds on average. With 10 samples per seconds, this results in 19 to 24 force plate measurements per gait cycle. Test data recorded for our analysis used a cadence of 40 steps per minute, therefore each gait cycle took 3 seconds with 30 measurements. For further data processing, our system employs a resampling strategy of the pressure plates' readings. Every gait cycle is sampled at uniformly distributed (equally spaced) sample points. According to the Nyquist-Shannon sampling theorem [Sha49], the points for resampling should be more than twice as many as the underlying original data, therefore ranging from 39 to 49 points for the average stroke patient. Since movement in our test data was even slower with 30 readings per gait cycle, the resampling needs to be done with more than 60 sample points. Our system divides each gait cycle into 59 equally sized intervals, i.e. 60 sample points, with each around 1.6% of the gait cycle apart. While an optimal sampling strategy would require one additional sample point for very slow movements, it is sufficient for the average walking speed of a post-stroke patient in combination with the default 10 Hz data transfer rate. Sampling the data of each gait cycle at the same points in time (e.g. at every 40% of each gait cycle) allows the calculation of statistical measures (e.g. mean, variance) over multiple gait cycles for these points in time. In the

Die approbierte gedruckte Originalversion dieser Diplomarbeit ist an der TU Wien Bibliothek verfügbar.
The approved original version of this thesis is available in print at TU Wien Bibliothek.
TU Bibliothek Your knowledge hub WIEN

context of force readings, this allows the visualization of mean and standard deviation over the past N gait cycles alongside the currently measured data (see Section 8.3).

5.2 Body Weight Estimation

Ground reaction force measurements are commonly normalized with respect to the subject's body weight. The PerPedes system allows the operator (e.g. therapist) to manually enter the subject's body weight. In case the weight is specified, this value is used for normalization. However, in most cases, a pre-determined body weight is not entered and therefore unavailable. Nevertheless, the PerPedes platform provides various sensory inputs, which can be used to estimate the body weight, while improving precision over time. In a typical gait training scenario, the subject is wearing a harness and is suspended from the top of the PerPedes machine. This provides stability and fall protection for the subject while simultaneously reducing load on the subject's legs. If the subject is standing still without holding onto the handrails, the body weight is equal to the sum of the measured load at both pressure plates plus the support load, carried by the suspension system. In general, if the subject is moving, the measured load will vary and underlying acceleration forces will cause the sum of loads to fluctuate above or below the actual body weight. With the assumption that acceleration and deceleration forces throughout a gait training session cancel each other out, we can calculate the body weight as the mean of the measured loads over N samples:

$$W_B = \frac{1}{N} \sum_{i=1}^{N} (W_L(i) + W_R(i) + W_S(i)) \tag{5.1}$$

With W_L and W_R denoting the weight measured at the left and right pressure plate respectively. The support load W_S measures how much weight is carried by the suspension system. The mean body weight W_B is continuously updated in an online fashion [Wel62], increasing precision over time.

If the subject is using the handrails to support part of his or her body weight, the estimate will deviate from the ground truth by this support factor. Since the utilization of handrails is an important factor for the personal feeling of safety, this deviation cannot be avoided unless subjects are explicitly instructed to avoid using them. Keeping this in mind, the body weight estimate is primarily used for visualization and scaling of ground reaction forces. A deviation of the estimate from the ground truth does not influence the system's results.

5.3 Vertical Ground Reaction Force

The vertical ground reaction force is equal to the measured weight at the respective pressure plate, normalized by the (estimated) body weight and expressed in percent:

$$GRF_{\{L,R\}} = \frac{100\%}{W_B} \cdot W_{\{L,R\}} \tag{5.2}$$

Die approbierte gedruckte Originalversion dieser Diplomarbeit ist an der TU Wien Bibliothek verfügbar.
The approved original version of this thesis is available in print at TU Wien Bibliothek.
TU Bibliothek Your knowledge hub WIEN

The vertical ground reaction force is therefore equal to the measured weight, scaled by a constant factor.

5.4 Locations of Pressure

The PerPedes system consists of two pressure plates with each plate having six pressure sensors built in (Figure 4.3). Each sensor's position $SP^{\{1,..,6\}}_{\{L,R\}}$ is known and fixed. SP is a two-component vector with its first component referring to the ML axis (left to right) with negative values to the left and positive values to the right. The second component refers to the inverted AP axis (back to front) with negative values to the back and positive values to the front.

Each pressure sensor continuously reports its measured weight $SW^{\{1,..,6\}}_{\{L,R\}}$, which is either positive (pushing down) or negative if the respective foot is lifted and pulls on the foot straps. Using the sensor locations and their respective weights, we determine the pressure point for each pressure plate and the center of pressure between both plates.

5.4.1 Pressure Point

The pressure point refers to the location of average pressure applied at each pressure plate. The pressure point $P_{\{L,R\}}$ is the weighted sum over all sensor positions of the respective pressure plate:

$$\begin{aligned} P_L &= \frac{1}{W^+_L} \sum_{i=1}^{6} \max(0, SW^i_L) \cdot SP^i_L \\ P_R &= \frac{1}{W^+_R} \sum_{i=1}^{6} \max(0, SW^i_R) \cdot SP^i_R \end{aligned} \tag{5.3}$$

With $W^+_{\{L,R\}}$ being the total amount of positive weight measured at each pressure plate. This corresponds to the sum of positive forces over the pressure plate's sensors:

$$\begin{aligned} W^+_L &= \sum_{j=1}^{6} \max(0, SW^j_L) \\ W^+_R &= \sum_{j=1}^{6} \max(0, SW^j_R) \end{aligned} \tag{5.4}$$

With $SW^j_{\{L,R\}}$ being the measured weight at sensor j for the left or right plate, respectively. In case $W^+_{\{L,R\}}$ is near zero, substitute coordinates are used for the respective pressure point $P_{\{L,R\}}$. These coordinates correspond to a fixed location, reflecting the approximate center of each foot.

Die approbierte gedruckte Originalversion dieser Diplomarbeit ist an der TU Wien Bibliothek verfügbar.
The approved original version of this thesis is available in print at TU Wien Bibliothek.
TU Bibliothek Your knowledge hub WIEN

5.4.2 Center of Pressure

The center of pressure is the weighted average between left and right pressure point. We distinguish between a *static* center of pressure CoP_s and a *dynamic* center of pressure CoP_d. The CoP_s assumes a static frame of reference with fixed non-moving pressure plates, positioned next to each other. Contrarily, the CoP_d incorporates the movement of the pressure plates. Each center of pressure can be inferred from:

$$CoP_s = \frac{P_L \cdot W_L^+ + P_R \cdot W_R^+}{W_L^+ + W_R^+} \tag{5.5}$$

$$CoP_d = \frac{(P_L + D_L) \cdot W_L^+ + (P_R + D_R) \cdot W_R^+}{W_L^+ + W_R^+} \tag{5.6}$$

With $D_{\{L,R\}} = \begin{bmatrix} 0 & d_{\mathrm{AP}} \end{bmatrix}_{\{L,R\}}$ describing the displacement in AP direction of the corresponding force plate with respect to the system's origin.

Note that only positive weights can be taken into account when dealing with locations. Incorporating negative weights would result in locations outside the convex hull of sensor positions, possibly even beyond the pressure plates' bounds. In case both weights are zero (i.e. $W_L = W_R = 0$), the mean between both pressure points is used:

$$CoP_s = 0.5P_L + 0.5P_R \tag{5.7}$$

$$CoP_d = 0.5(P_L + D_L) + 0.5(P_R + D_R) \tag{5.8}$$

Test data has demonstrated another possible case, where both legs are lifted (i.e. $W_L < 0, W_R < 0$) while the subject is being held in the support gear. In these rare cases, in order to have a meaningful center of pressure, it is calculated as follows:

$$CoP_s = \frac{P_L \cdot W_R + P_R \cdot W_L}{W_L + W_R} \tag{5.9}$$

The weights are exchanged, since the pressure point with the larger weight should have more influence in the center of pressure calculation, as is shown in the following example:

$$W_L = -20, W_R = -10, W_L + W_R = -30 \tag{5.10}$$

$$CoP_s = \frac{-10P_L - 20P_R}{-30} = \frac{1}{3}P_L + \frac{2}{3}P_R \tag{5.11}$$

Since the weights are also positive, the result will be between the points P_L and P_R and stays within the convex hull of sensor positions. The CoP_d is calculated analogously.

Die approbierte gedruckte Originalversion dieser Diplomarbeit ist an der TU Wien Bibliothek verfügbar.
The approved original version of this thesis is available in print at TU Wien Bibliothek.
TU Bibliothek Your knowledge hub WIEN

CHAPTER 6

Gait Event Detection

This chapter introduces a novel algorithm to detect gait events (heel strike, toe off) in the context of the PerPedes system and represents one of the main contributions of this thesis. Due to the distinctive features of the platform (Section 4.1), standard GED algorithms cannot be applied. We start with extending the notion of heel strike and toe off to a definition more suitable in PerPedes (Section 6.1). Section 6.2 then explains the difference between the machine's gait cycle and the subject's gait cycle and the possible offset between both. Before finding gait events, first a weight transfer is identified or rather its center (Section 6.3). Using this center as a reference point, search boundaries for gait events can be established (Section 6.4.2). Subsequently, these boundaries can be used to search for gait events. We discuss different approaches and explain why they are not applicable in PerPedes (Section 6.4.3).

With this collected knowledge about gait in PerPedes, we introduce different representations of force data (Section 6.5.1) and subsequently formulate the gait event detection algorithm (Section 6.5.2). Finally, this chapter also describes how to validate (Section 6.5.3) the newly defined gait events.

6.1 Introduction

The classic definition of heel strike (or initial contact) and toe off (or last contact) known from standard literature does not apply in the context of the PerPedes system. Here, the feet are strapped down, leading to inadvertent ground contacts and incomplete foot lifting. The initial contact does not give reasonable answers to how a subject behaves in Schepp's PerPedes. It has lost its meaning, since there might be a permanent contact with the force plates. Furthermore, the pressure plate of the striking foot might move forward after initial contact, moving the feet further apart and resembling the notion of a slippery floor. Additionally, the subject can hold onto the handrails or have a portion of the body weight carried by the support harness. All these factors combined

Die approbierte gedruckte Originalversion dieser Diplomarbeit ist an der TU Wien Bibliothek verfügbar.
The approved original version of this thesis is available in print at TU Wien Bibliothek.
TU Bibliothek Your knowledge hub WIEN

contribute to the difficulty of finding gait events. Since statistical measures (e.g. step length, stance/swing time) depend on gait events, it is necessary to find points in the gait cycle closely related to the original definition with the given restrictions in mind.

Essentially, the heel strike defines the start of a weight transfer, while toe off marks its completion. Adhering to this concept of gait events, GED in PerPedes is done by identifying the subject's *intention* of initiating and completing a weight transfer. Since the subject's intention is rather abstract, it is important to provide a characterization of a weight transfer itself. Generally speaking, a weight transfer in normal gait happens quickly, i.e. forces between left and right side are exchanged during a short time interval. The transfer should progress continuously (from left to right or vice versa) without a significant change in direction. The start of a weight transfer should be accompanied by an increase in "effort" of the subject to switch sides. This effort should be detectable through a change in the force distribution between left and right foot.

In PerPedes, weight transfers often are not complete, meaning the swinging foot is not fully lifted and exerts force during the contralateral foot's stance phase. Since the system is used as a medical platform, potentially used by patients with severe disabilities, gait events need to be detected even under severe conditions. Test data has shown that even healthy subjects show a tendency to incomplete lifting (Chapter 9). The developed GED algorithm attempts to deal with unusual gait patterns and behavior and determines when weight transfers are performed.

In general, heel strike and toe off events have very similar, but inverse characteristics. Heel strikes should correspond to a point in time before a WTP (Section 2.3), initiating a weight transfer, preferably matching an initial contact with the ground. Toe offs occur after a WTP, completing a weight transfer, preferably ending with the last contact of the foot. Heel strike and toe off are symmetrical ±5% GC [1] around a WTP in an optimal scenario (Figure 2.3b). While a HS starts a weight transfer and subsequently shows an increase in the GRF of the striking foot, the TO ends a weight transfer with a preceding decrease in the GRF of the lifting foot. Toe off events can be viewed as time-reversed heel strikes while simultaneously negating AP coordinates (switching front and back). Similarly, a heel strike on the left side can be treated exactly like a heel strike on the right side, except negating all ML coordinates (switching left and right). Treating heel strikes and toe offs equally, but opposite to each other, is done in the literature in the context of gaitography [TCvDR19], [RCC+08] and threshold-based methods [HM00]. Without loss of generality, the following sections portray GED from the (right) heel strike perspective.

6.2 The Gait Cycle (Human vs. Machine)

In the following, we distinguish between the machine's gait cycle and the human subject's gait cycle. The machine's gait cycle is defined mechanically by its moving parts. Schepp's

[1] X% GC is the short form for "X percent of the machine's gait cycle (GC)". It either refers to an absolute point in time of the gait cycle (e.g. at 5% GC) or acts as a relative time offset (e.g. 5% GC before a HS).

Die approbierte gedruckte Originalversion dieser Diplomarbeit ist an der TU Wien Bibliothek verfügbar.
The approved original version of this thesis is available in print at TU Wien Bibliothek.
TU Bibliothek Your knowledge hub WIEN

PerPedes system is built in order to simulate a complete human gait cycle, therefore gait events are clearly defined at specific positions of its moving plates. For example, the foot's initial contact should optimally coincide with the pressure plate being in its foremost position, while the TO event should occur when the plate is furthest back. These well-defined optimal points in time define the machine's gait events (Figure 4.4). The subject's gait events can deviate from the machine's optimal gait events, but in general this deviation is expected to be within certain bounds. In the following, we define these bounds, i.e. the maximum possible deviation of a subject's gait event from the corresponding machine's gait event.

First, we evaluate the consequences of deviating from the optimal gait, i.e. analyze the offset Δe between subject and machine gait events. Initially, we focus on heel strike events and then extend our reasoning to toe off events. As mentioned in Section 4.1, the step length is preset for each pressure plate. This setting determines the maximum possible displacement of each plate in AP direction. If the subject performs the heel strike at the moment of maximum displacement, 100% of the preset step length is achieved. This moment is the optimal point in time, when a heel strike should occur and is equal to the machine's HS event. In other words, there is no offset in time ($\Delta e = 0$) between the subject's gait event and the machine's gait event. Figure 4.4 shows that +28% GC after and −22% GC before each of the machine's heel strike events, the pressure plates are positioned next to each other, meaning no foot is in front of the other. Therefore, if the subject's HS event is offset by either of these time intervals (i.e. $\Delta e = -22\%$ GC or $\Delta e = 28\%$ GC), the resulting step length would be zero. In this case, the subject would not move forward, but rather walk on the spot. With an event offset of −43% GC or +57% GC, the respective pressure plate is located in its most posterior position, resulting in a maximally negative step length, essentially allowing the subject to be walking backwards. Our goal is to support and identify both, walking forward, as well as walking backwards in PerPedes.

Figure 6.1 illustrates the offset of a subject's HS event to a machine's HS event and its consequences on the achievable step length. If a subject's HS occurs within the offset range of $[-22, 28]\%$ GC to the machine's heel strike event, a positive step length and therefore forward movement is achieved. If the subject's HS occurs earlier within $[-72, -22]\%$ GC, the subject is moving backwards. All possible step lengths are achievable within the range $B = [-72, 28]\%$ GC, spanning a complete gait cycle (since $28 - (-72) = 100\%$ GC).

Associating Subject and Machine Event

For every machine's HS event, one corresponding subject's HS event shall be associated. Additionally, every subject's HS event shall be associated with at most one machine's HS event. Once the subject's gait events will have been identified, the HS event occurring within range B, relative to the machine's HS event is the corresponding one. Since each machine's HS event occurs exactly 100% GC after its predecessor, the ranges are not overlapping. This assures that no subject's HS event is associated to two different machine events.

Die approbierte gedruckte Originalversion dieser Diplomarbeit ist an der TU Wien Bibliothek verfügbar.
The approved original version of this thesis is available in print at TU Wien Bibliothek.
TU Bibliothek Your knowledge hub WIEN

It is assumed that there exists at least one corresponding subject's event in the search range. This assumption is reasonable. Since a gait cycle is cyclic and the machine's movement is periodic, we expect the subject to walk in a periodic fashion as well. Theoretically, the subject could put weight on only the left leg, while lifting the other for an indefinite amount of time. This would result in the left leg being dragged forward and back by the machine without any subject's gait events. Obviously, this is not a walking pattern and would violate this assumption. In case there exist multiple HS events in B, the one closest to the machine's gait event (smallest offset Δe) is chosen as associated event. This process is performed separately for HSL and HSR events.

Similarly, a subject's TO event is expected to be within the bounds B, relative to the machine's TO event, which occurs 10% GC after the machine's HS event. Furthermore, the same notion can be extended to WTPs, which are ideally located between HS and TO.

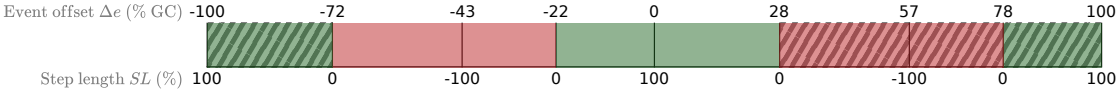

Die approbierte gedruckte Originalversion dieser Diplomarbeit ist an der TU Wien Bibliothek verfügbar.
The approved original version of this thesis is available in print at TU Wien Bibliothek.

points at each plate ($P_L = [x_L\ y_L], P_R = [x_R\ y_R]$) are opposite to each other ($x_L = -x_R$) and left and right forces are equal ($GRF_L = GRF_R$). Both, the WTP and the ML zero crossing do not necessarily exist during a weight transfer if it is incomplete. We define a weight transfer to be incomplete if the weight is not fully transferred from one side to the other (i.e. the foot is not completely lifted off the pressure plate during the swing phase). Since WTPs might not exist, we introduce an alternative point (the mediolateral midpoint), identifying the geometric center of a complete or incomplete weight transfer.

6.3.2 Mediolateral Midpoints

The mediolateral midpoint (in short: midpoint) for a weight transfer is centered halfway between the outermost left and outermost right CoP. These extrema are temporally located before and after the weight transfer, respectively. They can be identified in both static and dynamic frames of reference, since they only depend on the ML component (i.e. the left/right movement) of the CoP's trajectory CoP_{ML}.

The midpoint is equal to the ML zero crossing, if the ML component of the left and the right extremum are equally distant from the center of the machine (at ML = 0). The less symmetrical a subject's gait happens to be, the more a midpoint will diverge from the zero crossing and its nearby occurring WTP. The advantages of using midpoints over WTPs are:

1. Midpoints always exist
2. A midpoint is located at or near the geometric center of a weight transfer

Test data has shown that the midpoints closely correlate with WTPs spatially as well as temporally in standard (i.e. symmetrical) gait. Furthermore, they are preferable in strongly asymmetrical gaits, since midpoints better reflect the geometric center of a weight transfer in comparison to WTPs. Figure 6.2 gives an example of asymmetrical gait. The right foot is not fully lifted during the left stance phase, shifting the CoP's trajectory towards the right. While the midpoint identifies the geometric center of the weight transfer, the WTP and zero crossing are both situated further to the left.

Die approbierte gedruckte Originalversion dieser Diplomarbeit ist an der TU Wien Bibliothek verfügbar.
The approved original version of this thesis is available in print at TU Wien Bibliothek.
TU Bibliothek Your knowledge hub WIEN

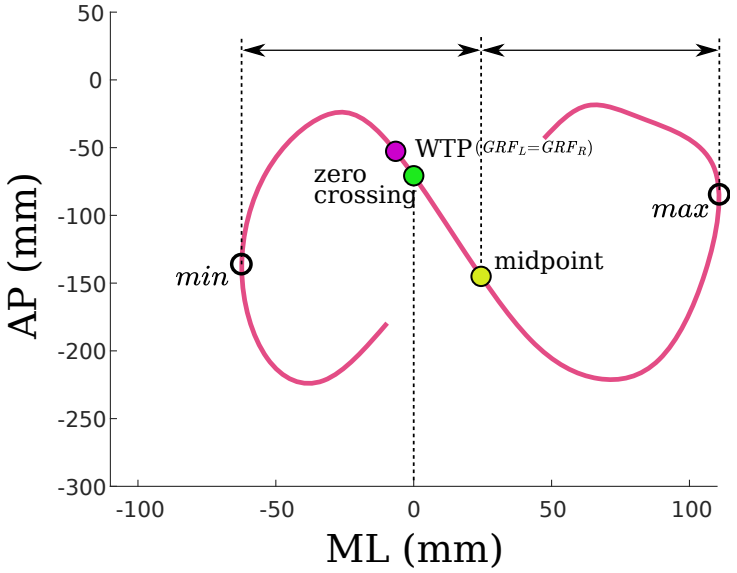

Figure 6.2: Illustrating the difference between WTP (pink marker), mediolateral midpoint (yellow) and ML zero crossing (green) in a gaitogram for one weight transfer. The midpoint is located halfway between the outermost left (min) and outermost right extrema (max) of the CoP's trajectory.

Midpoints can be determined if the left and the right extremum of CoP_{ML} can be correctly identified. For every weight transfer there should be exactly two relevant extrema (one minimum, one maximum) in CoP_{ML}. Local (spurious) extrema must be filtered out.

The Search Region for Midpoints

There are two weight transfers in a machine's gait cycle. The first weight transfer $WT_{R\to L}$ from the right side to the left side occurs between HSL at 0% GC and TOR at 10% GC. The weight transfer's center is therefore located at 5% GC. The center of the second weight transfer $WT_{L\to R}$ from left to right occurs at 55% GC.

We would like to find the corresponding subject's midpoint relative to a machine's weight transfer center. As has been established in Section 6.2, a corresponding subject's gait event is located relative to a machine's gait event within the bounds $B = [-72, 28]$% GC. This is also valid for every other point occurring between HS and TO events. Therefore, a subject's midpoint could potentially be found within bounds B, but since the CoP's extrema are necessary for its calculation, the bounds need to be extended.

The CoP's extrema occur when the majority of force is applied by only one foot, i.e. around the middle of the single support stance phases, each spanning 40% GC. Assuming the worst case, means that the first extremum before the midpoint occurs at the beginning of the stance phase, i.e. at $-(40+5)$% GC[2] relative to the midpoint. Analogously, the

[2] 5% GC, since the midpoint is in the middle of the double support phase, spanning 10% GC.

Die approbierte gedruckte Originalversion dieser Diplomarbeit ist an der TU Wien Bibliothek verfügbar.
The approved original version of this thesis is available in print at TU Wien Bibliothek.
TU Bibliothek Your knowledge hub WIEN

second extremum after the midpoint might have an offset of +45% GC.

In order to identify a midpoint relative to the center of a machine's weight transfer, one extracts the data section $S = B + [-45, +45] = [-117, 73]\%$ GC around it. This data section then contains at least the midpoint and its extrema. Note that the location of the midpoint, the weight transfer with start and end, as well as the extrema are not known as of yet.

Finding Midpoints

A simple strategy in order to identify weight transfers and the extrema is to use the center line $c = \frac{min+max}{2}$ between the global minimum min and the global maximum max of CoP_{ML} in data section S as a criterion. Every time CoP_{ML} crosses c, a weight transfer is assumed to be happening. The extrema for this weight transfer are then given by the largest/smallest CoP_{ML} value before/after crossing center c, respectively. In general, this approach will fail and either identify non-relevant weight transfers (red markers in Figure 6.3a) and local extrema (min_s in Figure 6.3a) or skip relevant ones ($min_1 \rightarrow max_1$ in Figure 6.3b).

In order to remove local extrema in CoP_{ML}, a simple smoothing operation could be sufficient. Nonetheless, smoothing will worsen the situation for valid but incomplete weight transfers. The CoP_{ML} trajectory for incomplete weight transfers might not go beyond the center line c between global minimum and maximum (Figure 6.3b). Therefore, we cannot rely on a global minimum and maximum, but need to calculate the extrema and the center line adaptively by splitting up the data section S into parts S_j and individually calculate the center lines for each subsection.

Splitting the Data for Midpoint Detection

Splitting up data section S can be done with a splitting criterion, such that no weight transfer is divided between subsections. We propose to use the maxima ξ_i of the GRFs difference function $D_{\text{GRF}} = GRF_{\text{HS}} - GRF_{\text{TO}}$ as a splitting criterion. These maxima occur during single support phases and between each pair of subsequent maxima there exist two weight transfers (Figure 6.4). For weight transfers from left to right $WT_{L\rightarrow R}$, the difference function is given by $D_{\text{GRF}}^{(R-L)} = GRF_R - GRF_L$, while for right to left weight transfers $WT_{R\rightarrow L}$, it is $D_{\text{GRF}}^{(L-R)} = GRF_L - GRF_R$. It holds that $D_{\text{GRF}}^{(L-R)} = -D_{\text{GRF}}^{(R-L)}$, therefore the maxima of one function are the minima of the other. The maxima of each difference function can be reliably found after a smoothing operation. We use a uniform smoothing kernel spanning 17% of the gait cycle (approximately 500 ms in the recorded test data). This filters out local maxima, while retaining the function's overall shape.

Die approbierte gedruckte Originalversion dieser Diplomarbeit ist an der TU Wien Bibliothek verfügbar.
The approved original version of this thesis is available in print at TU Wien Bibliothek.
TU Bibliothek Your knowledge hub WIEN

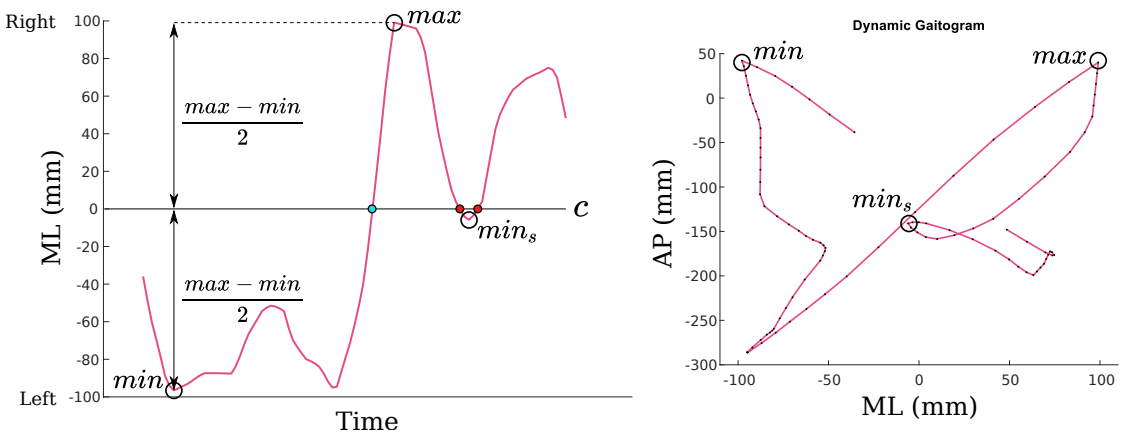

(a) Local (spurious) minimum min_s when using the center c between global minimum min and global maximum max as criterion.

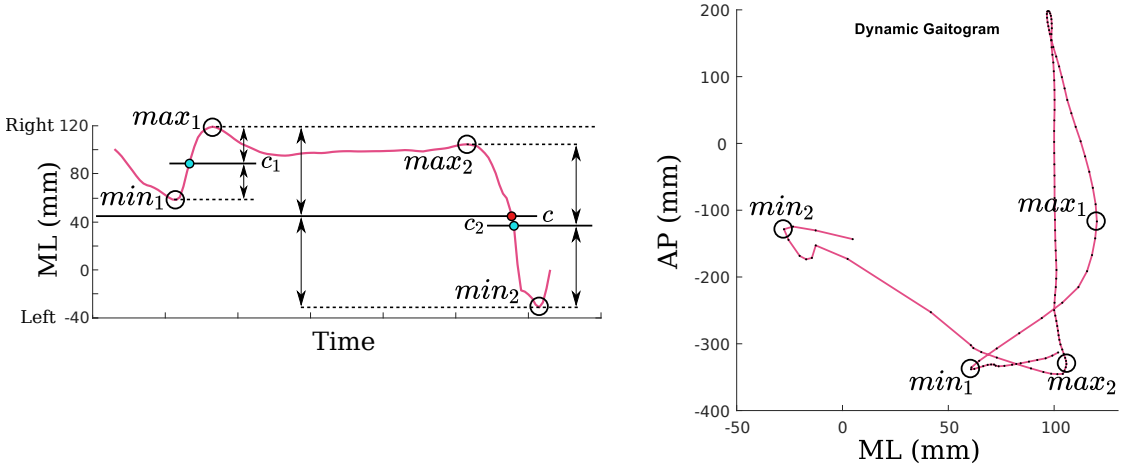

(b) Not identified minimum min_1 and maximum max_2 when using center c between global minimum min_2 and global maximum max_1. Splitting up the data into two sections could identify all extrema and their respective centers c_1, c_2.

Figure 6.3: Assuming a weight transfer every time CoP_{ML} crosses the center c between global minimum and maximum of CoP_{ML} might lead to additional non-relevant weight transfers (red markers in (a)) or might miss relevant ones (cyan markers in (b)).

Die approbierte gedruckte Originalversion dieser Diplomarbeit ist an der TU Wien Bibliothek verfügbar.
The approved original version of this thesis is available in print at TU Wien Bibliothek.
TU Bibliothek Your knowledge hub WIEN

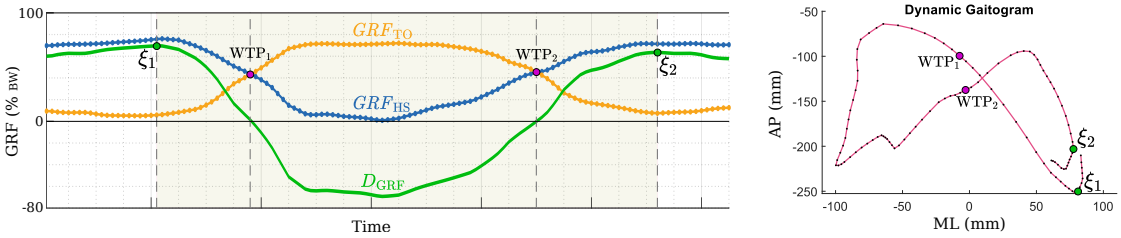

Figure 6.4: Splitting up the data into subsections according to the maxima of D_{GRF}. In the subsection (highlighted area) between the two maxima ξ_1 and ξ_2 (green markers) exist two weight transfers with their corresponding WTPs highlighted with pink markers.

The Algorithm for Midpoint Extraction

For left to right weight transfers $WT_{L\to R}$, the data S is split into subsections S_j according to the maxima in $D_{\text{GRF}}^{(R-L)}$. In each S_j the minimum min_j in CoP_{ML} and its following maximum max_j is determined. The midpoint MP_j is located at the chronologically last occurring crossing in the range $[min_j, max_j]$ between CoP_{ML} and the center line $c_j = \frac{min_j + max_j}{2}$. The data sample closest to this crossing is chosen as midpoint for subsection S_j. Of these midpoints, the one occurring (temporally) closest to the machine's weight transfer center at 55% GC is the corresponding one.

For right to left weight transfers $WT_{R\to L}$, the process is done analogously but uses the difference function $D_{\text{GRF}}^{(L-R)}$ and an inverted CoP trajectory $-CoP_{ML}$. Of the resulting midpoints, the one closest to the machine's 5% GC mark is the corresponding one. The fully formulated algorithm is available in Appendix A.4.

Midpoint Examples

Figure 6.5 shows an example of symmetrical gait where midpoints closely correlate with WTPs. The figure contains data for left and right vertical GRF, as well as the CoP's trajectory in ML direction CoP_{ML}. The maxima ξ_1, ξ_3 of $D_{\text{GRF}}^{(R-L)}$ (green) identify one subsection (yellow area) in CoP_{ML}. This subsection contains one weight transfer from left to right and its corresponding midpoint MP_2. MP_2 reflects the data sample closest to the crossing between CoP_{ML} and the center line $c_2 = \frac{min_2 + max_2}{2}$. For weight transfers from right to left, the maxima ξ_2, ξ_4 of $D_{\text{GRF}}^{(L-R)}$ (or equivalently the minima of $D_{\text{GRF}}^{(R-L)}$) define the boundaries of two subsections (pink and blue area) in $-CoP_{ML}$. Per subsection the extrema of CoP_{ML} and the resulting midpoint is determined.

Figure 6.6 illustrates three different scenarios in which midpoints differ from WTPs. The gait in Figure 6.6a shows an incomplete weight transfer from right to left. The right foot continues to exert pressure during the left stance phase, while the left force barely exceeds the right one. The dynamic gaitogram shows that the WTPs are located close to the machine's center at $\text{ML} = 0$ but are further to the left than the centrally located midpoints.

Die approbierte gedruckte Originalversion dieser Diplomarbeit ist an der TU Wien Bibliothek verfügbar.
The approved original version of this thesis is available in print at TU Wien Bibliothek.
TU Bibliothek Your knowledge hub WIEN

Figure 6.6b demonstrates an even more severe case of an incomplete weight transfer. In this example the left force never exceeds the right one. There is no point of equal forces (i.e. $GRF_L = GRF_R$) and therefore no WTP. The CoP's trajectory stays on the right side (i.e. $CoP_{ML} > 0$). Nonetheless, midpoints for the incomplete weight transfer to the left and back to the right are available.

Figure 6.6c shows that not every WTP identifies a weight transfer. The points WTP_1 and WTP_2 occur because of an intermediate step with the left foot. Test data has shown that it is not unusual for participants to drag their feet and not fully lift them during the respective swing phase. In this particular case, the participant drags the left foot so strongly that it even exceeds the right foot's force (WTP_1), immediately corrects this behavior (WTP_2) and only then starts the actual weight transfer to the left (WTP_3). Our algorithm automatically handles these cases, since the midpoint is always the chronologically last crossing of the center line between minimum and maximum. In the given case, the midpoint is equivalent to WTP_3.

Die approbierte gedruckte Originalversion dieser Diplomarbeit ist an der TU Wien Bibliothek verfügbar.
The approved original version of this thesis is available in print at TU Wien Bibliothek.

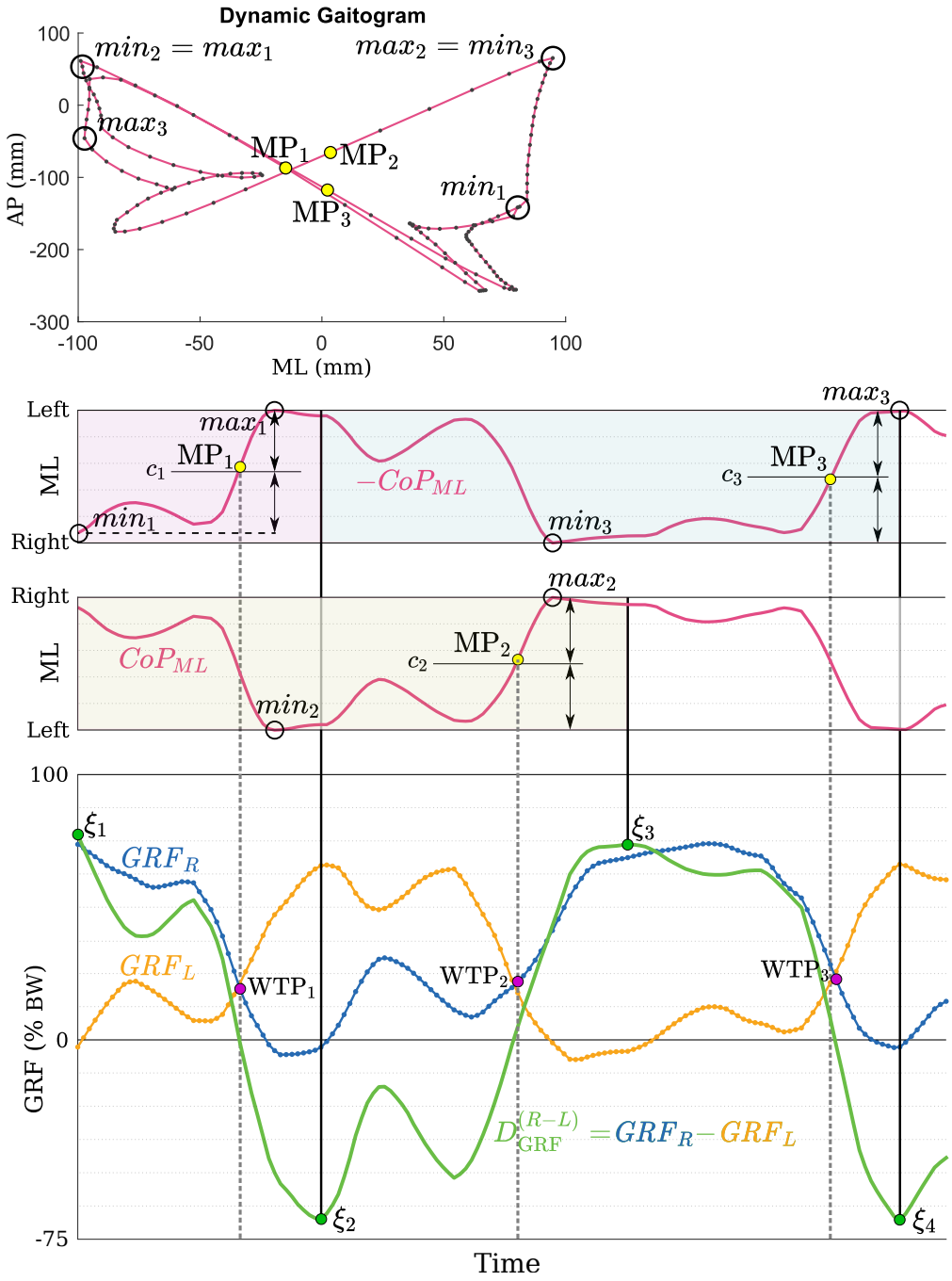

Figure 6.5: Midpoints correlate with WTPs. The data contains two weight transfers from right to left and one weight transfer from left to right. The extrema ξ_i of the difference function $D_{\mathrm{GRF}}^{(R-L)}$ between left (orange) and right (blue) vertical GRF define the boundaries of the subsections (colored area). Per subsection, the midpoint MP_j is located at the crossing between CoP_{ML} and the center line c_j.

Die approbierte gedruckte Originalversion dieser Diplomarbeit ist an der TU Wien Bibliothek verfügbar.
The approved original version of this thesis is available in print at TU Wien Bibliothek.
TU Bibliothek Your knowledge hub WIEN

Die approbierte gedruckte Originalversion dieser Diplomarbeit ist an der TU Wien Bibliothek verfügbar.
The approved original version of this thesis is available in print at TU Wien Bibliothek.

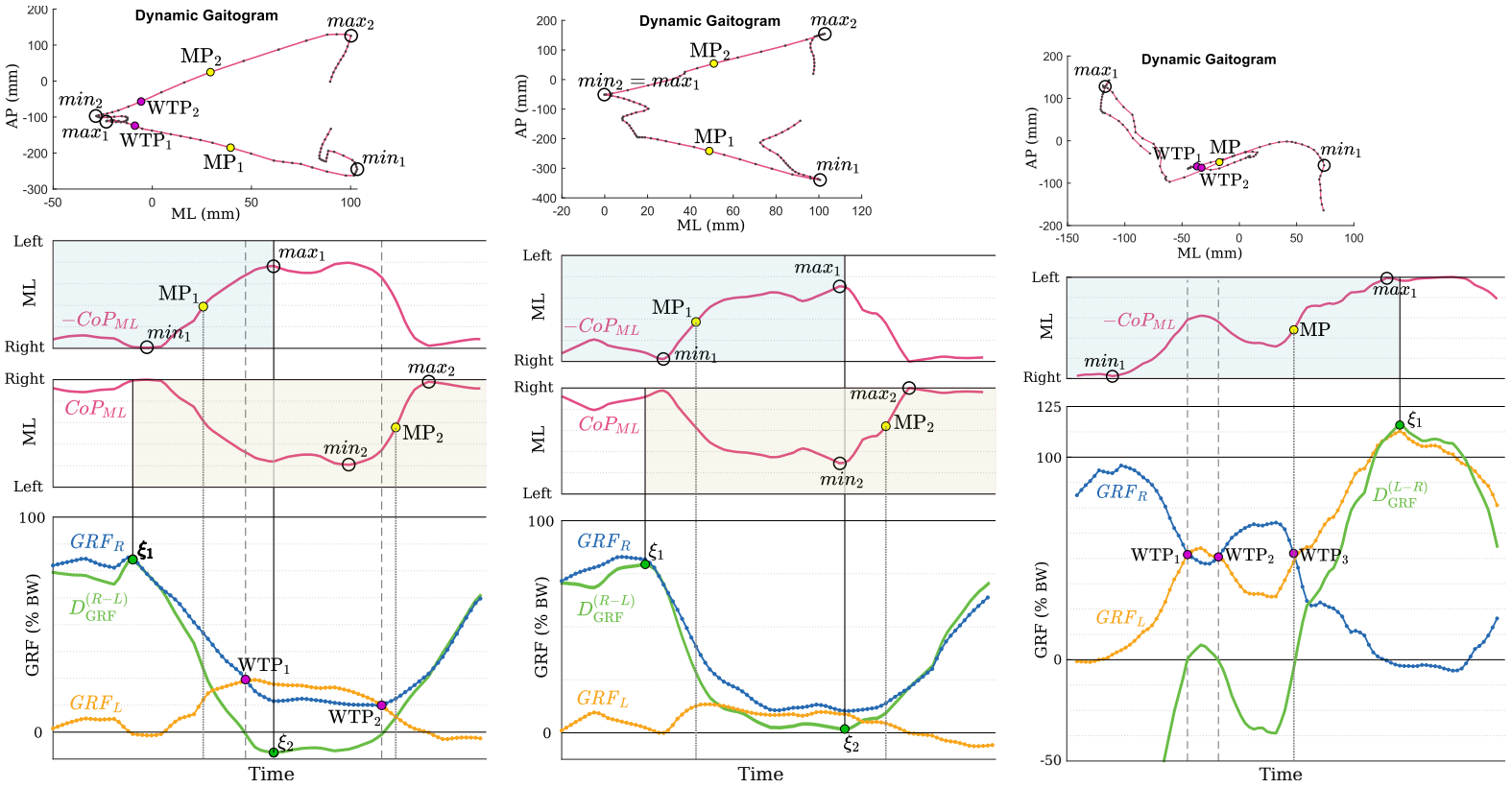

(a) Offset between midpoints and WTPs. (b) No WTPs. (c) Spurious WTPs.

Figure 6.6: Comparison of CoP midpoints and WTP. While midpoints (yellow marker) identify the geometric center of each weight transfer, WTPs (pink marker) might be offset (a), might not exist at all (b), or might occur several times (c).

6.4 O Gait Event, Where Art Thou?[3]

The midpoint identifies the geometric center of a weight transfer and is determined by using the extrema of the CoP_{ML} trajectory. However, in general, these extrema are not marking the start (HS) and the end (TO) of a weight transfer. These gait events are yet to be determined. First, this section discusses typical problems in gait event detection in PerPedes. Afterwards, the search bounds are narrowed down. Finally, we explain which approaches have been tried and are likely to fail with illustrative examples. These lessons learned can then be used to develop the final algorithm in Section 6.5.

6.4.1 Considerations

When using a typical hardware setup, based on a treadmill and a pressure sensing system, it is simple to identify the foot's initial contact (HS) and the instance of last pressure (TO). From a signal processing perspective, given continuous force measurements $GRF(t)$, HS and TO events are located exactly at the zero-crossings of function $GRF^*(t) = GRF(t) - T$, where T is a threshold, essentially ignoring small force measurements (sensor noise). Figure 6.7a gives an example of gait with existing zero-crossings in PerPedes. Since the subject's feet are held down by foot straps, a complete lifting of the feet is impossible. Nonetheless, pulling on the foot straps causes negative forces to be measured at the pressure plates.

- No WTPs, because of large one-sided pressure (Figure 6.7b).
- Additional zero crossings without event characteristics (Figure 6.7b).
- Slow force buildup (Figure 6.8a).
- Intermediate steps during swing phase (Figure 6.8b).

The most critical observation is that zero crossings in PerPedes are different to treadmill systems. Zero crossings might not exist at all, if the foot is not pulling hard enough on the foot strap in order to create negative forces. Therefore, a thresholding method for GED cannot be applied. Additional zero crossings can exist if the subject fails to lift the foot properly during the swing phase, leading to accidental contacts with the pressure plate. These contacts do not show event characteristics, since they neither start nor end a weight transfer. In case these contacts persist over a longer period of time, we might see a slow increase in forces (force buildup), until finally the forces are explosively exchanged between both sides during the moment of weight transfer.

In the following, we define a search region for gait events around the midpoint (Section 6.4.2). Within this region, different GED approaches are then discussed (Section 6.4.3). Subsequently, with a better understanding of the data, our GED algorithm is introduced in Section 6.5.

[3] A reference to the film O Brother, Where Art Thou?

Die approbierte gedruckte Originalversion dieser Diplomarbeit ist an der TU Wien Bibliothek verfügbar.
The approved original version of this thesis is available in print at TU Wien Bibliothek.
TU Bibliothek Your knowledge hub WIEN

Die approbierte gedruckte Originalversion dieser Diplomarbeit ist an der TU Wien Bibliothek verfügbar.
The approved original version of this thesis is available in print at TU Wien Bibliothek.

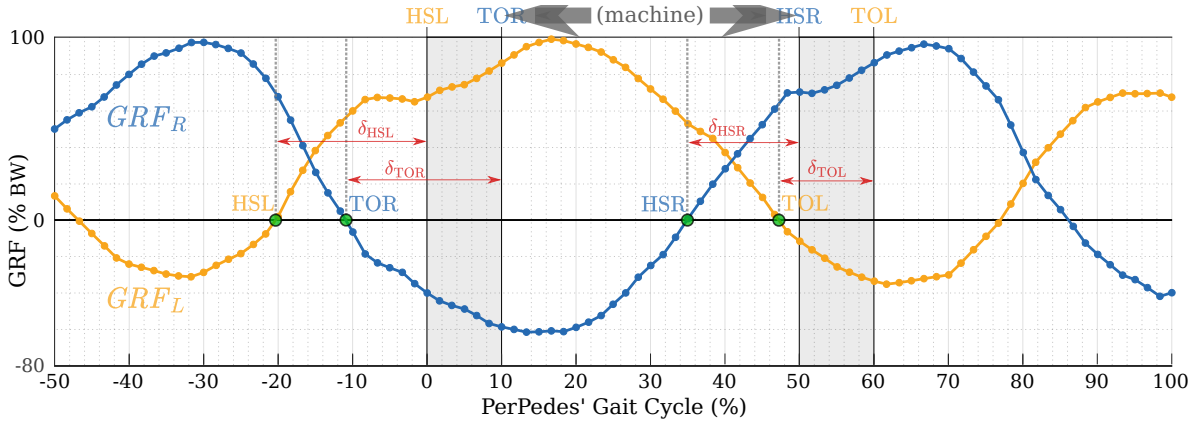

Die approbierte gedruckte Originalversion dieser Diplomarbeit ist an der TU Wien Bibliothek verfügbar.
The approved original version of this thesis is available in print at TU Wien Bibliothek.

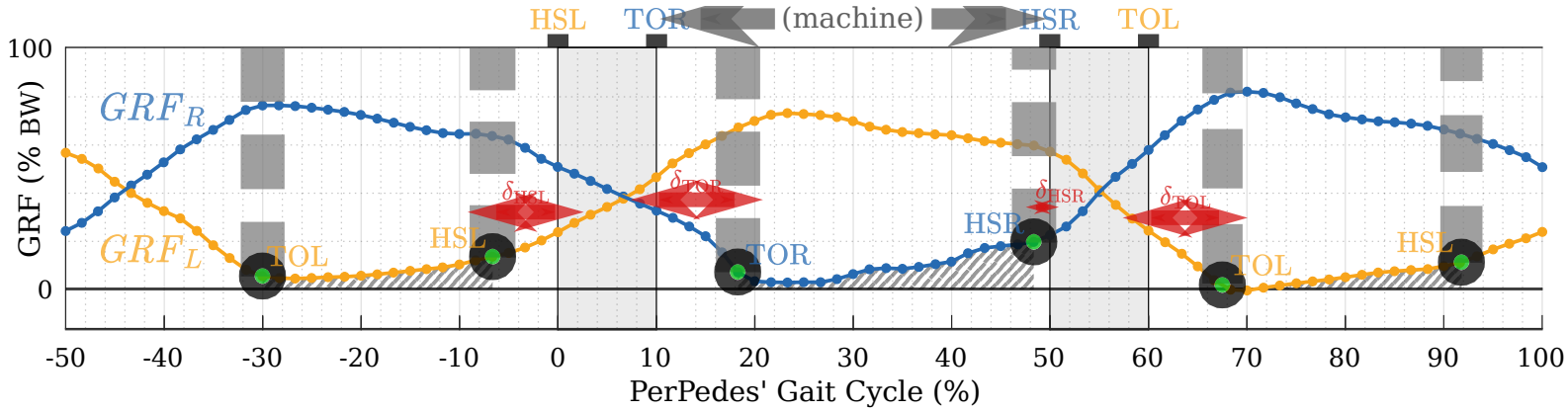

6.4.2 Fantastic Events and Where to Find Them[4]

Section 6.3.2 describes how to identify the center of a weight transfer, the mediolateral midpoint, or alternatively the WTP, if it exists. The gait events are then located before and after the midpoint, respectively. In order to find the events, the maximum possible search range around the midpoint needs to be defined.

In general we assume that the heel strike event occurs before the midpoint, while the toe off event occurs afterwards. The optimal gait cycle defines each double support phase to last 10% GC. Test data has clearly shown that this does not hold in PerPedes, leading to longer double support phases, since weight transfers happen more gradually.

As an initial conservative lower bound, we can state that the heel strike cannot be more than 50% GC away from the midpoint, since this is approximately the time of occurrence of the previous midpoint. The previous midpoint marks the location of the previous weight transfer. In the range between this lower bound and the midpoint, the HS cannot happen

① before the smallest measurement in the GRF of the striking foot,

② before the most extremal point of the CoP_{ML},

③ during or before negative GRF forces), or

④ before a "significant" turn in the CoP_{ML}

To show statement ①, we can assume that the HS occurs at location h before the smallest measurement at location m. It holds that $GRF(h) \geq GRF(m)$. This means that the foot is either raised between h and m or is not increasing pressure ($GRF(h) = GRF(m)$). It follows that there is no HS at h.

Statement ② needs some refinement. A right heel strike moves the CoP_{ML} from left to right. For a right heel strike, the most extremal point is the point furthest to the left. If the heel strike would occur before this point, then consequently the CoP would move to the left, which indicates it is not a right heel strike. For left heel strikes, the argumentation follows analogously.

Statement ③ refers to the fact that a heel strike cannot occur if the foot is lifted. Furthermore, a heel strike cannot lead to a situation where the foot is lifted.

The final statement ④ is related to ② and means that the CoP cannot move in the opposite direction after the heel strike. While we allow some tolerance (the turn must be significant), strictly speaking this does not need to be allowed. A significant turn in the CoP's mediolateral movement is defined as a point where the CoP's direction of movement changes, even after filtering is applied. We apply a uniform smoothing kernel over 5% GC to allow some inconsistency in measurements and movement.

[4] A reference to the book Fantastic Beasts and Where to Find Them

Die approbierte gedruckte Originalversion dieser Diplomarbeit ist an der TU Wien Bibliothek verfügbar.
The approved original version of this thesis is available in print at TU Wien Bibliothek.
TU Bibliothek Your knowledge hub WIEN

The search range is then limited by the closest of these four points to the midpoint. The same rules apply to TO events, although in a time-reversed manner. Figure 6.9 shows an example of these locations. The heel strike is expected to occur in the time between point ④ and the midpoint, the toe off needs to occur in the time between the midpoint and the following point marked with ②/③.

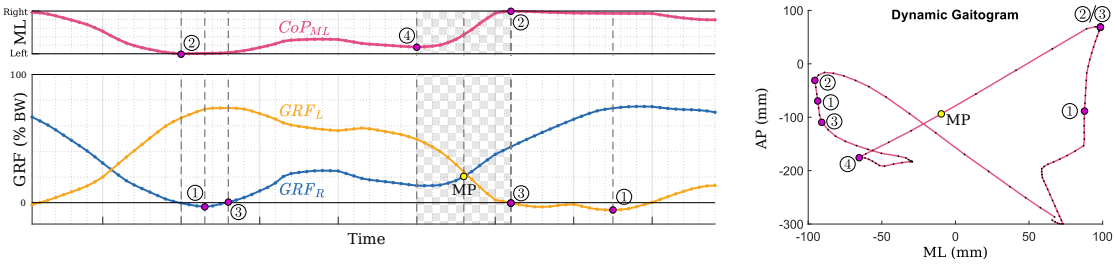

Figure 6.9: Search boundaries for GED. ① Smallest GRF measurements, ② extremal points of CoP_{ML}, ③ nearest points in time to the midpoint with negative forces, ④ significant turn in CoP_{ML}. In this example, heel strike and toe off events are expected to occur within the highlighted (checkerboard) time span.

6.4.3 (Im)possible Approaches to Find Gait Events

This section discusses approaches to find gait events with the help of illustrative examples and whether or not they are suitable in the context of our system. In nearly all cases, the usage of the midpoint and the WTP is interchangeable, but we use the midpoint in all our examples.

Earliest Contact

The earliest contact is the point with the smallest positive value in the striking foot's GRF or its first zero-crossing before the midpoint. This point typically does not show heel strike characteristics (i.e. starting the weight transfer). Most often, the earliest contact occurs while the pressure plate is still moving forward. It happens too early and indicates involuntary contact of the foot with the pressure plate in preparation of the weight transfer (Figure 6.10).

Die approbierte gedruckte Originalversion dieser Diplomarbeit ist an der TU Wien Bibliothek verfügbar.
The approved original version of this thesis is available in print at TU Wien Bibliothek.

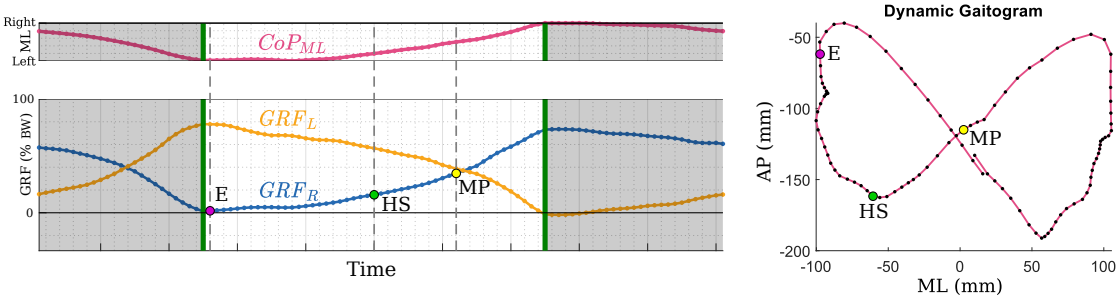

Figure 6.10: Gait event example - Earliest contact. Earliest contact (E, pink marker) with no heel strike characteristics and proposed heel strike (HS, green) before the midpoint (MP, yellow).

Relevant Change in one GRF

One could try to detect heel strikes by analyzing the change in the GRF of the striking foot. A heel strike could then correspond to a point in time preceding a significant change in the GRF. Test data shows that this is not a valid approach, since weight transfers can be started by instead "falling" into the support gear (Figure 6.11). More often, it is unclear which point of change of the GRF is triggering a weight transfer, since it is not necessarily the start of the largest nor the earliest change.

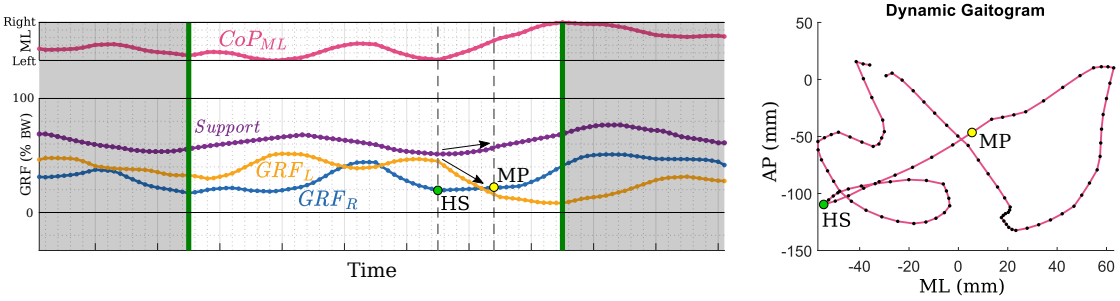

Figure 6.11: Gait event example - Weight transfer by releasing weight. Instead of increasing force on the right foot (blue), the weight transfer is performed by decreasing force on the left foot (orange) and transferring the weight to the support gear (violet).

Relevant Change in both GRFs

As we have seen, analyzing only one GRF might not be enough. Therefore, an alternative approach would be the analysis of a combination of both GRFs, i.e. the difference $D_{\mathrm{GRF}}(t) = GRF_{\mathrm{HS}}(t) - GRF_{\mathrm{TO}}(t)$ and its change $\Delta D_{\mathrm{GRF}}(t) = \frac{\mathrm{d}}{\mathrm{d}t} D_{\mathrm{GRF}}(t)$. We would expect that a heel strike triggers a change in the difference, therefore the event should be located in a (local) minimum of $\Delta D_{\mathrm{GRF}}(t)$. In Figure 6.12 the weight transfer might be starting out from a local minimum of $\Delta D_{\mathrm{GRF}}(t)$, but there is no indication which

Die approbierte gedruckte Originalversion dieser Diplomarbeit ist an der TU Wien Bibliothek verfügbar.
The approved original version of this thesis is available in print at TU Wien Bibliothek.
TU Bibliothek Your knowledge hub WIEN

minimum it could potentially be. In turn, this means that the minima of $\Delta D_{\mathrm{GRF}}(t)$ on their own are not meaningful for event detection.

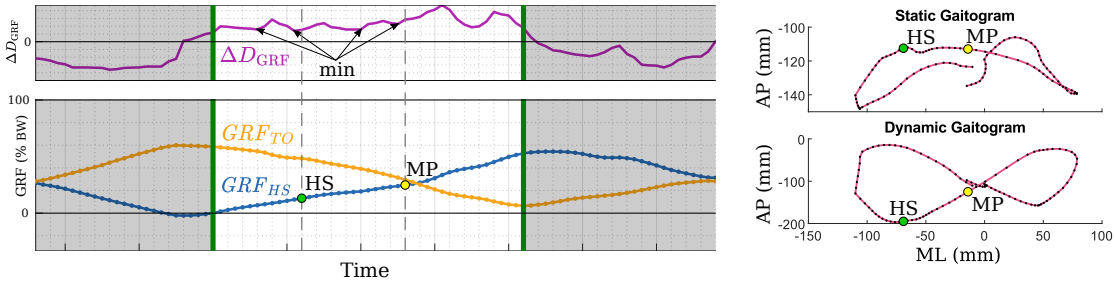

Figure 6.12: Gait event example - Change of GRF difference. The minima of the change of GRF differences ΔD_{GRF} (violet) does not reveal the start of a weight transfer.

Another combination of both GRFs, is available through the CoP_{ML} trajectory. This function represents the ML component of a weighted average between the two pressure points on each pressure plate. Therefore, it is also influenced by the pressure changes on only one plate. As an example, rocking only one foot sideways, changes the pressure point on the plate and therefore influences the CoP_{ML} trajectory. This happens even if the magnitude of forces measured at both plates stay the same. Therefore, while CoP_{ML} is similar to D_{GRF}, it incorporates more than just the force difference and might distort the analysis of forces between feet.

Upper Point of Static Gaitogram

Under perfect circumstances (Figure 6.13), one can identify gait events from a geometrical perspective as the upper corner point of the static gaitogram. Different definitions are possible to find this point. Either it is the most anterior point of the static CoP before the midpoint. Or it is the last point of the static CoP before the midpoint where the movement in AP direction is reversed (equivalently, where the velocity of the AP movement is zero). While both definitions can refer to the same point in some cases (HS in Figure 6.13 and C in Figure 6.14), in general they can be different (Points A and B in Figure 6.15).

There are several problems with this approach. Firstly, it assumes that a HS occurs while the pressure on the contralateral foot is in the front. This depends not only on a correct heel to toe motion, but also on the shoes in use. With specific gait disturbances (e.g. calcaneal gait), this might not be possible at all. Secondly, test data has shown that this corner might not exist (Figure 6.15) or is misleading (Figure 6.14) if the pressure point of the weight-bearing foot moves posterior before the start of the weight transfer.

Die approbierte gedruckte Originalversion dieser Diplomarbeit ist an der TU Wien Bibliothek verfügbar.
The approved original version of this thesis is available in print at TU Wien Bibliothek.
TU Bibliothek Your knowledge hub WIEN

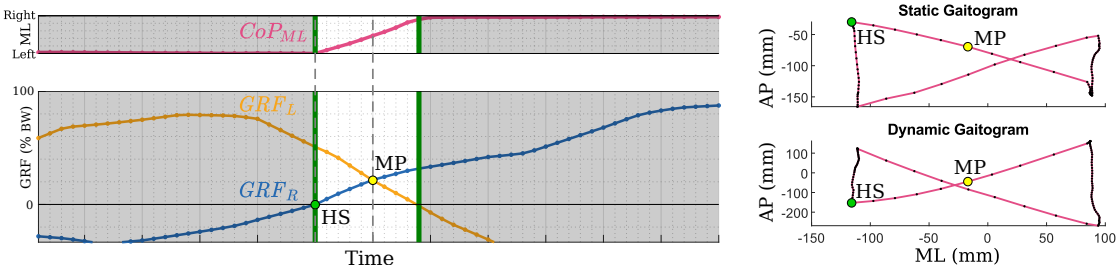

Figure 6.13: Gait event example - Geometrical approach. With rapidly changing GRFs and the foot's pressure moving from heel to toe, one can clearly identify HS events in both static and dynamic gaitograms.

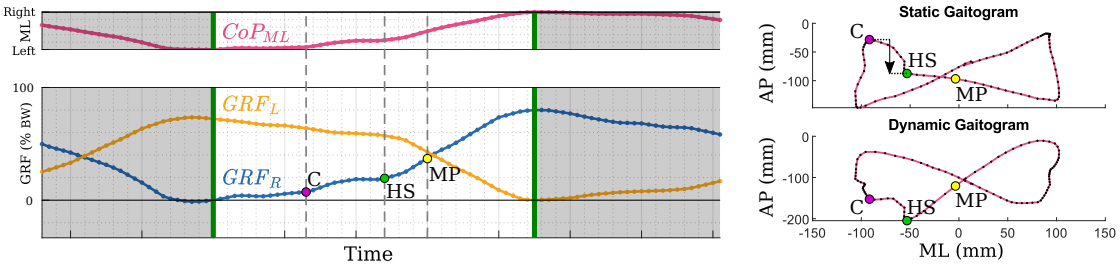

Figure 6.14: Gait event example - Static gaitogram with misleading upper corner. The corner (C, pink marker) does not represent the start of the weight transfer. After the corner, the static CoP first moves posterior (arrow), before the HS starts the weight transfer.

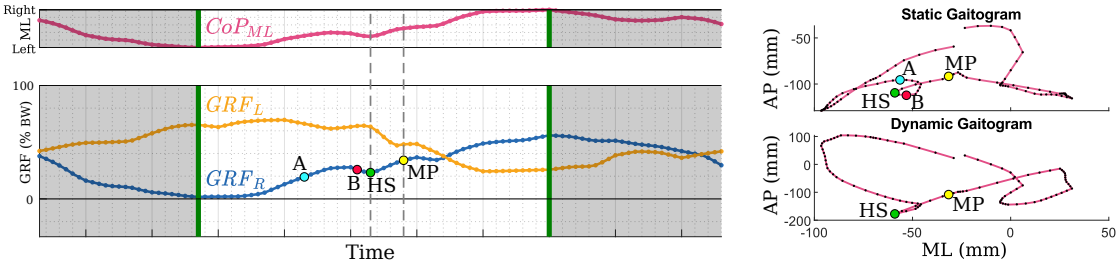

Figure 6.15: Gait event example - Static gaitogram without upper corner. Highlighted are the most anterior point (A) of the static CoP before the midpoint and the last point of the static CoP before the midpoint where movement in AP direction is reversed (B).

Lower Point of Dynamic Gaitogram

While the static gaitogram can easily be distorted by each foot's pressure point, the dynamic gaitogram is dominated by the position of each foot in the moving system, i.e. the position and movement of the pressure plates. Instead of evaluating the upper corner in the static gaitogram, one can identify the lower corner of the dynamic gaitogram as

Die approbierte gedruckte Originalversion dieser Diplomarbeit ist an der TU Wien Bibliothek verfügbar.
The approved original version of this thesis is available in print at TU Wien Bibliothek.
TU Bibliothek Your knowledge hub WIEN

gait event. This corner is either the most posterior point of the dynamic CoP before the midpoint or the last point of the dynamic CoP before the midpoint where the movement in AP direction is reversed (equivalently, where the velocity of the AP movement is zero). These definitions are not equivalent and might result in different points (HS2 vs. HS3 in Section 6.5.3).

If the subject's heel strike is optimally timed with the machine's heel strike, the pressure plates are positioned furthest apart. The pressure plate of the striking foot is then most anterior, while the weight-bearing foot's pressure plate is most posterior. Therefore, the dynamic CoP is initially posterior and the weight transfer causes it to move anterior towards the striking foot. If the weight transfer happens quickly, slowly moving pressure plates will have no significant influence on the dynamic CoP's trajectory. The dynamic gaitogram will then show weight transfers as straight lines and sharp corners as gait events (Figure 6.13). In those cases, the dynamic gaitogram's lower point clearly identifies the heel strike.

If a subject's heel strike is occurring earlier than the optimal timing, the pressure plates will not be maximally apart and are therefore still moving. If the weight-bearing foot is moving downwards with the pressure plate while the weight is simultaneously transferred to the other side, the dynamic gaitogram will become distorted (Figure 6.16). In this case, the lowest point of the dynamic gaitogram will not reflect the heel strike, but will depend on how quickly the weight is transferred and how fast the plates are moving.

The situation becomes even more pronounced when walking backwards and therefore initiating the weight transfer around half a gait cycle earlier than the optimal timing (Figure 6.17). In this case, the dynamic CoP does not move from a posterior position to an anterior position during the weight transfer, but moves front to back. The lowest point of the dynamic gaitogram becomes insignificant and does not refer to a gait event anymore.

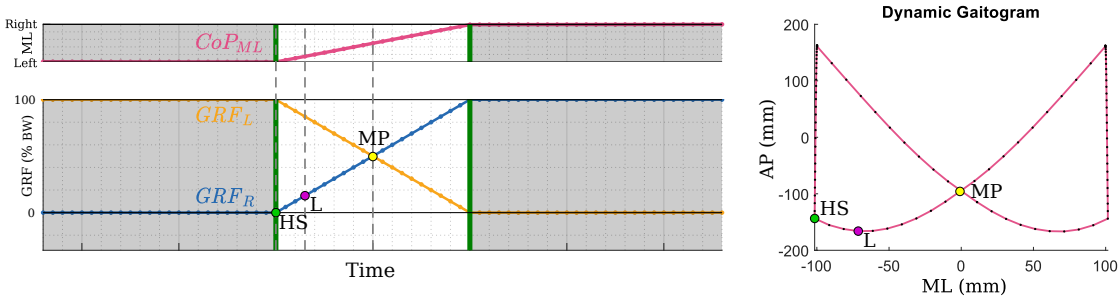

Figure 6.16: Gait event example - Dynamic gaitogram with distortions from plate movements. Synthetic data with the heel strike occurring 20% GC too early (before the optimal machine event). The lowest point (L, pink marker) of the dynamic gaitogram does not correspond to the heel strike (green).

Die approbierte gedruckte Originalversion dieser Diplomarbeit ist an der TU Wien Bibliothek verfügbar.
The approved original version of this thesis is available in print at TU Wien Bibliothek.
TU Bibliothek Your knowledge hub WIEN

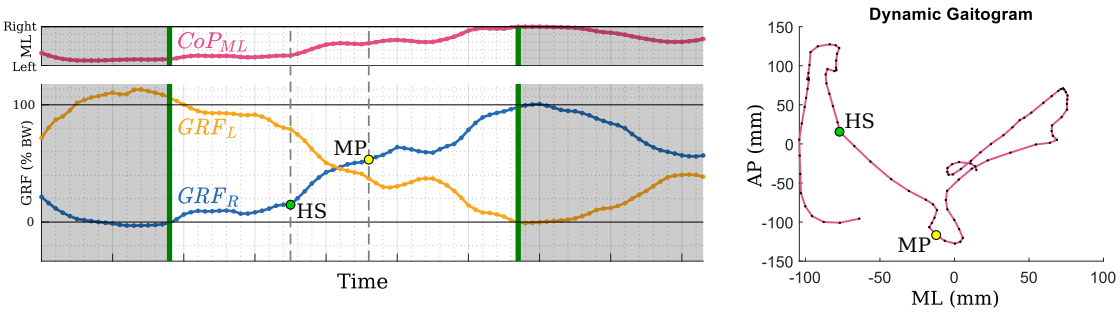

Figure 6.17: Gait event example - Dynamic gaitogram, walking backwards.

Total Vertical Forces

As Section 3.2.2 describes, the total amount of vertical ground reaction forces could be used to identify gait events. Mawase et al. [MHBHK13] describe heel strikes to coincide with a local minimum in the total vertical forces. Following a sharp peak in forces, toe off events either coincide with the next local minimum (Roerdink et al. [RCC+08]) or occur shortly afterwards (Mawase et al. [MHBHK13]).

In our system, we define the total amount of vertical ground reaction forces as:

$$\Sigma GRF = 100\% \cdot \frac{W_L^+ + W_R^+}{W_B} \tag{6.1}$$

ΣGRF is the sum of the measured positive weights at the pressure plates, in relation to the (estimated) body weight. Alternatively, the sum of total forces could include the weight W_S carried by the support system:

$$\Sigma GRF_S = 100\% \cdot \frac{W_L^+ + W_R^+ + W_S}{W_B} \tag{6.2}$$

Using these definitions and comparing the observations from the literature with our available test data, we are unable to find a reliable correlation. Local minima do not necessarily identify heel strike events, as can be seen with $\mathrm{Min}_1, \mathrm{Min}_2$, and Min_3 in Figure 6.18. In contrast, toe off events are either coinciding with (Figures 6.18, 6.19) or are located near a (local) minimum (Min_9 in Figure 6.20). Potentially, this allows the identification of toe off events, but we refrain from doing so, since the overall shape of the total vertical forces differs from the literature, as is shown next.

Mawase et al. [MHBHK13] observe maxima in the total vertical forces to occur during double support and minima during midstance. Contrarily to this, our test data shows inconsistent behavior. On the one hand, Figure 6.19 shows the maxima $\mathrm{Max}_3, \mathrm{Max}_4$ to occur during double support, toe off coincides with the next local minimum, and the global minima $\mathrm{Min}_6, \mathrm{Max}_7$ occur during single support. This is in accordance with the literature. On the other hand, Figures 6.18 and 6.20 show the maxima to occur during single support, while the global minima are close to the toe off event instead of the

Die approbierte gedruckte Originalversion dieser Diplomarbeit ist an der TU Wien Bibliothek verfügbar.
The approved original version of this thesis is available in print at TU Wien Bibliothek.
TU Bibliothek Your knowledge hub WIEN

midstance event (occurring around 20% GC later). The reasons for these discrepancies are unknown, but may be linked to the weight support system and/or the usage of the handrails.

Whether or not to include the support weight in the total amount of vertical forces remains unclear. The overall shape of both functions, ΣGRF_S and ΣGRF is very similar. However, test data has shown that including the support weight can lead to less pronounced minima in ΣGRF_S (e.g. Min_8 and Min_9 in Figure 6.20).

Our overall recommendation is not to use the total forces for GED. In case this cannot be avoided, one should rely only on the measurements at the foot plates (ΣGRF) and not include the support weight (ΣGRF_S).

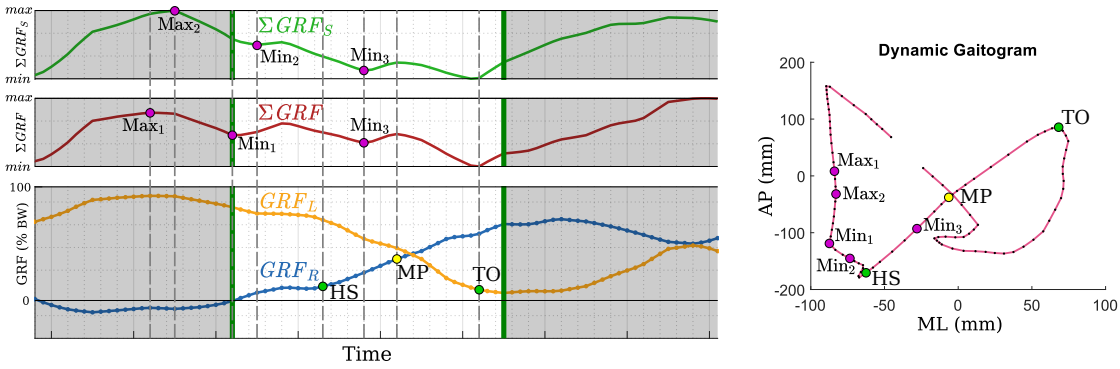

Figure 6.18: Gait event example - Total vertical GRFs (1). Analysis of extrema in the total vertical forces with (ΣGRF_S) and without support weight (ΣGRF). None of the local minima $\text{Min}_1, \text{Min}_2$, and Min_3 in either of the functions correspond to the proposed HS event. The proposed TO event can be found near the global minimum of both functions.

Die approbierte gedruckte Originalversion dieser Diplomarbeit ist an der TU Wien Bibliothek verfügbar.
The approved original version of this thesis is available in print at TU Wien Bibliothek.

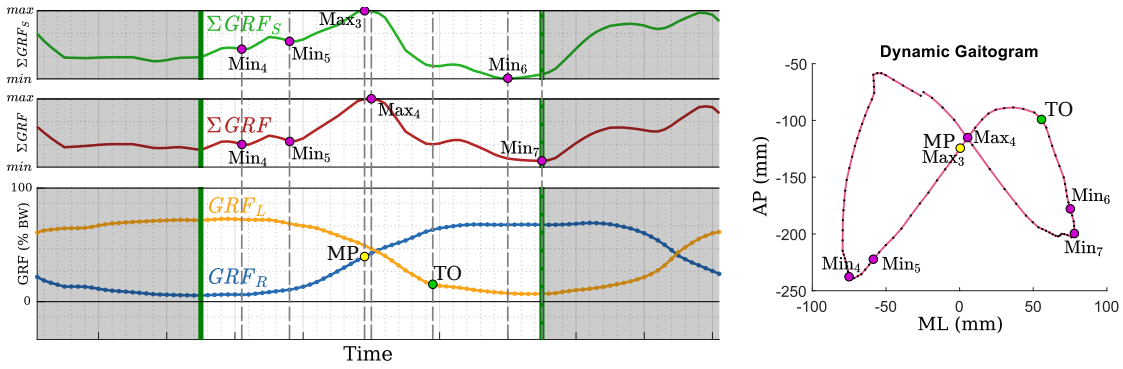

Figure 6.19: Gait event example - Total vertical GRFs (2). Analysis of extrema in the total vertical forces with (ΣGRF_S) and without support weight (ΣGRF). The precise location of the HS event is unknown but could be close to either Min_4 or Min_5. The proposed TO event can be found in a local minimum of both functions. Global minima $\text{Min}_6, \text{Min}_7$ occur during single support.

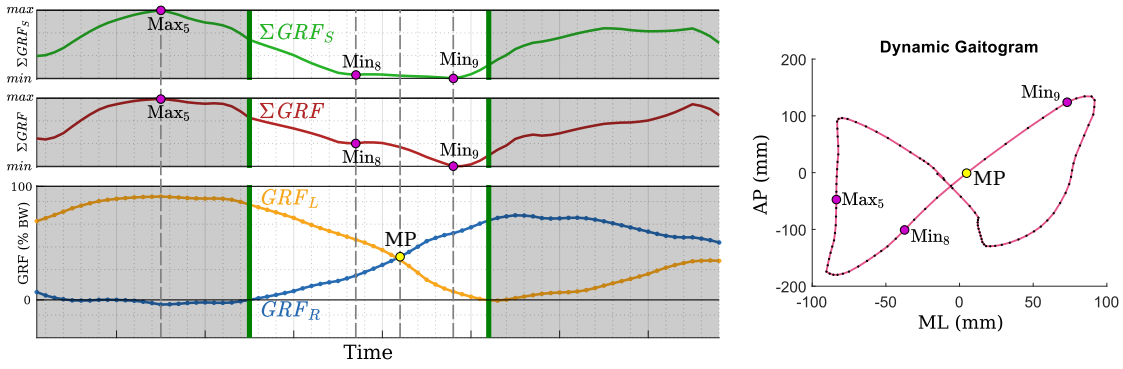

Figure 6.20: Gait event example - Total vertical GRFs (3). Analysis of extrema in the total vertical forces with (ΣGRF_S) and without support weight (ΣGRF). The minima $\text{Min}_8, \text{Min}_9$ in ΣGRF are less pronounced than in ΣGRF_S. The precise location of HS and TO is unknown, but could be close to the minima $\text{Min}_8, \text{Min}_9$, respectively.

6.5 The Gait Event Detection Algorithm

The developed gait event detection algorithm is used for both heel strike events as well as toe off events. The algorithm itself is formulated for heel strike detection. In order to detect TO events, it is sufficient to "reverse time", i.e. traverse the gait cycle's data in the opposite direction or flip the data array from left to right. Additionally, all AP coordinates need to be negated.

We propose a GED algorithm, which combines spatial information on where pressure occurs and the change in forces between left and right side. As a first step, we derive

Die approbierte gedruckte Originalversion dieser Diplomarbeit ist an der TU Wien Bibliothek verfügbar.
The approved original version of this thesis is available in print at TU Wien Bibliothek.
TU Bibliothek Your knowledge hub WIEN

functions from the force measurements and the pressure points. Afterwards, these functions are used to navigate the data and arrive at the proposed gait events.

6.5.1 Deriving Measures for Detection

In general, weight transfers happen quickly. The standard gait cycle defines a weight transfer to happen within 10% GC. During a weight transfer, the weight from the lifting foot transfers quickly to the striking foot. This means that the CoP also quickly changes position. The change in the CoP's position is its velocity.

It is assumed that it is harder (takes more effort) to transfer the same amount of weight between feet if the feet are farther apart. To reflect this assumption in the data, we need to take the distance between the feet into account. The distance between feet relates to the distance between the pressure points at the respective pressure plate:

$$D(t) = \|P_{\mathrm{HS}}(t) - P_{\mathrm{TO}}(t)\| \tag{6.3}$$

Note that P_{HS} and P_{TO} includes the displacement of the respective pressure plate in AP direction (Figure 6.21). Since the static CoP assumes that the feet are positioned next to each other, it does not correctly reflect the distance between feet. On the other hand, the dynamic CoP takes this distance into account. Because of this, the dynamic CoP's velocity will be higher when transferring weight between points farther apart.

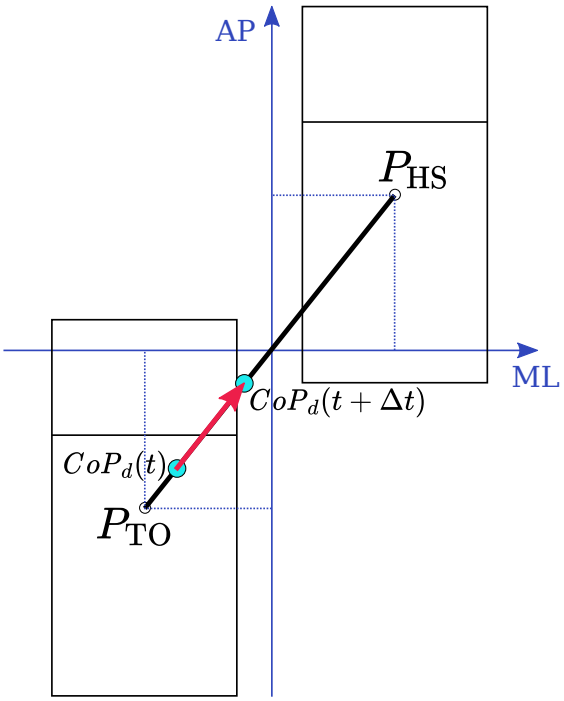

Figure 6.21: CoP movement between two fixed pressure points over the time span Δt. The CoP moves along the line $P_{\mathrm{HS}} - P_{\mathrm{TO}}$ with respect to the exchanged forces between both points.

Die approbierte gedruckte Originalversion dieser Diplomarbeit ist an der TU Wien Bibliothek verfügbar.
The approved original version of this thesis is available in print at TU Wien Bibliothek.
TU Bibliothek Your knowledge hub WIEN

Formally, we can show that the CoP's velocity is dependent on the distance between the pressure points. First, we note that the vertical GRF and the measured weight at the respective plate are equal, except for a constant factor (Section 5.3). Then we can reformulate the dynamic CoP (compare with Section 5.4.2), using vertical GRFs as:

$$CoP_d(t) = \frac{P_{\text{HS}}(t) \cdot GRF_{\text{HS}}(t) + P_{\text{TO}}(t) \cdot GRF_{\text{TO}}(t)}{GRF_{\text{HS}}(t) + GRF_{\text{TO}}(t)} \tag{6.4}$$

This represents a general case including negative forces. Again, the pressure points $P_{\text{HS}}(t), P_{\text{TO}}(t)$ include the displacement in AP direction of the respective pressure plate.

In order to understand the CoP's movement and its velocity between two pressure points, it is useful to assume that the pressure points are fixed (i.e. not changing over time). Furthermore, we assume that forces only flow between the pressure points, meaning that the total amount of forces is constant over time, i.e.

$$GRF_{\text{Total}} = GRF_{\text{HS}}(t) + GRF_{\text{TO}}(t), \forall t \tag{6.5}$$

This results in the modified version:

$$CoP^*_d(t) = \frac{P_{\text{HS}} \cdot GRF_{\text{HS}}(t) + P_{\text{TO}} \cdot (GRF_{\text{Total}} - GRF_{\text{HS}}(t))}{GRF_{\text{Total}}} \tag{6.6}$$

The velocity (i.e. its first derivative) of this idealized system is then:

$$\frac{\mathrm{d}}{\mathrm{d}t} CoP^*_d(t) = (P_{\text{HS}} - P_{\text{TO}}) \cdot \frac{GRF'_{\text{HS}}(t)}{GRF_{\text{Total}}} \tag{6.7}$$

Since the total amount of forces is constant, the change in one GRF is equal to the negative change in the other, i.e. $GRF'_{\text{HS}}(t) = -GRF'_{\text{TO}}(t)$. The velocity itself is a vector quantity and its magnitude is:

$$V^*(t) = \|\frac{\mathrm{d}}{\mathrm{d}t} CoP^*_d(t)\| = \|P_{\text{HS}} - P_{\text{TO}}\| \cdot |\frac{GRF'_{\text{HS}}(t)}{GRF_{\text{Total}}}| \tag{6.8}$$

We can see that the velocity's magnitude $V^*(t)$ increases if the distance $\|P_{\text{HS}} - P_{\text{TO}}\|$ increases or more force $|GRF'_{\text{HS}}(t)|$ is transferred between the pressure points. This shows that the distance is implicitly encoded in the CoP's velocity.

The actual velocity's magnitude

$$V(t) = \|\frac{\mathrm{d}}{\mathrm{d}t} CoP_d(t)\| = \|\frac{\mathrm{d}}{\mathrm{d}t} \frac{P_{\text{HS}}(t) \cdot GRF_{\text{HS}}(t) + P_{\text{TO}}(t) \cdot GRF_{\text{TO}}(t)}{GRF_{\text{HS}}(t) + GRF_{\text{TO}}(t)}\| \tag{6.9}$$

also depends on the change in the pressure points' location and the change in the individual forces. The total amount of forces is not constant, since forces change with the body's acceleration and can be transferred between support gear and foot plates.

If pressure is solely on one foot and constant (e.g. $GRF_{\text{TO}} = 100, GRF_{\text{HS}} = 0$), then $V(t) = \|\frac{\mathrm{d}}{\mathrm{d}t} P_{\text{TO}}(t)\|$. This means that $V(t)$ is non-zero if the pressure point $P_{\text{TO}}(t)$ changes.

Die approbierte gedruckte Originalversion dieser Diplomarbeit ist an der TU Wien Bibliothek verfügbar.
The approved original version of this thesis is available in print at TU Wien Bibliothek.
TU Bibliothek Your knowledge hub WIEN

This is true, if the pressure plate is moving during one-sided pressure. Figure 6.22 shows that $V(t)$ is high during the weight transfer (region R_2), because forces are exchanged rapidly between both sides, but also during one-sided pressure, when the pressure plates are moving quickly (regions R_1, R_3). Additionally, one can see that the start of the weight transfer (HS) is located in a local minimum before a sharp increase in $V(t)$, while TO is located in a local minimum afterwards.

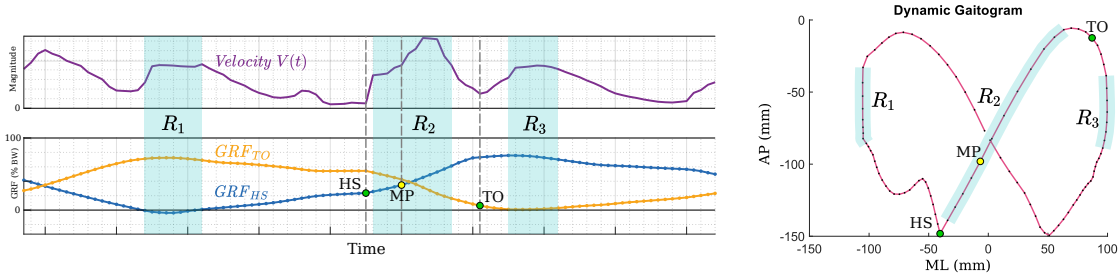

Figure 6.22: The magnitude of the dynamic CoP's velocity. Velocity is high during one-sided pressure while the pressure plates are moving quickly (regions R_1, R_3) and when the difference between left and right forces changes (region R_2).

We know from test data that local minima in $V(t)$ are ambiguous. There might be multiple minima and the last occurring minimum before the midpoint does not necessarily identify the heel strike's location. Therefore two additional measures are introduced. Those measures also identify weight transfers and can be used in combination with $V(t)$ to identify gait events.

Before a weight transfer, the force GRF_{TO} of the foot which is about to be lifted is high. After the weight transfer, the contralateral foot's force GRF_{HS} should be high. Again, assuming that a force transfer takes more effort if the feet are farther apart, we formulate our measures as:

$$M_1(t) = (GRF_{TO}(t) - GRF_{HS}(t)) \cdot D(t) \tag{6.10}$$

$$M_2(t) = GRF_{TO}(t) \cdot D(t) \tag{6.11}$$

$M_1(t)$ relates to the force necessary to transfer from $P_{\mathrm{TO}}(t)$ to $P_{\mathrm{HS}}(t)$ over distance $D(t)$ to achieve a force equilibrium between both sides. The measure $M_1(t)$ is signed, indicating the direction of forces (from striking foot to lifting foot, or vice versa). It is zero if left and right forces are equal, meaning no force needs to be exchanged to create an equilibrium.

$M_2(t)$ measures the amount of force of the lifting foot weighted by the distance between the pressure points. In other words, it measures the remaining effort to perform until the foot is lifted with respect to the distance between the pressure points. Generally, $M_2(t)$ is positive as long as the lifting foot exerts some force. It is negative if the foot is pulling on the foot straps.

Die approbierte gedruckte Originalversion dieser Diplomarbeit ist an der TU Wien Bibliothek verfügbar.
The approved original version of this thesis is available in print at TU Wien Bibliothek.
TU Bibliothek Your knowledge hub WIEN

$M_1(t)$ is at its maximum if the force $GRF_{TO}(t)$ is maximal, the force $GRF_{HS}(t)$ is minimal and the distance is maximal. $M_2(t)$ is at its maximum if both the force $GRF_{TO}(t)$ and the distance are maximal.

If the human subject walks perfectly in PerPedes, then the following conditions apply:

1. The subject's HS coincides with the moment when the pressure plates are farthest apart.
2. The subject's weight is fully on the foot to be lifted.

The moment when the pressure plates are farthest apart is the moment when the pressure plates are about to reverse direction. This means that the velocity of each pressure plate is zero and the CoP is not moving, since also no weight is exchanged. This means that the CoP's velocity is zero, i.e. $V(t) = 0$. The distance $D(t)$ is at its maximum, so is $GRF_{TO}(t)$ and $GRF_{HS}(t)$ is zero (ignoring possible negative forces in $GRF_{HS}(t)$).

In this optimal scenario, $V(t)$ is zero and at a (local) minimum, while $M_1(t)$ and $M_2(t)$ are maximal. This is exactly the point when the heel strike occurs. During the weight transfer, $V(t)$ first increases, then decreases again, while $M_1(t)$ moves to a negative minimum and $M_2(t)$ moves to zero (again, ignoring possible negative forces, this time in $GRF_{TO}(t)$).

The less optimal the subject's gait is, the less $M_1(t)$, $M_2(t)$, and $V(t)$ will agree on the same location. Figure 6.23 shows an example where the maxima of $M_1(t)$ and $M_2(t)$ coincide and pinpoint the heel strike event. Contrarily, in Figure 6.24 the maxima are at different locations but span a possible range where the heel strike is located.

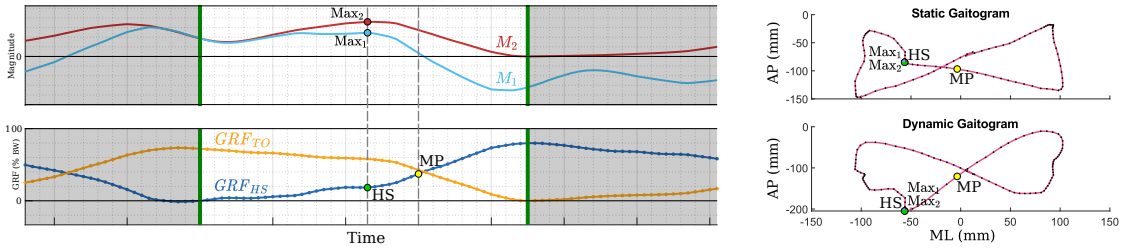

Figure 6.23: Measures M_1 and M_2 - Same location of maxima. The local maxima pinpoint the event occurrence.

Die approbierte gedruckte Originalversion dieser Diplomarbeit ist an der TU Wien Bibliothek verfügbar.
The approved original version of this thesis is available in print at TU Wien Bibliothek.
TU Bibliothek Your knowledge hub WIEN

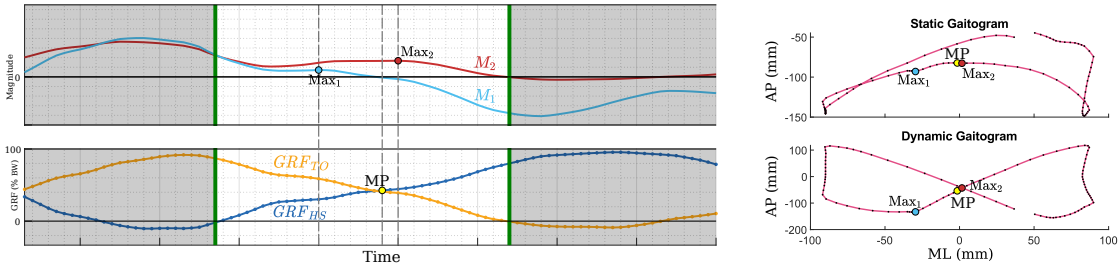

Figure 6.24: Measures M_1 and M_2 - Different locations of maxima.

6.5.2 Formulating the Algorithm

We now combine the CoP's velocity $V(t)$ and the measures $M_1(t), M_2(t)$ in order to find the heel strike. Figure 6.25 illustrates the algorithm. Our heuristic approach uses Min_2 and Max_2 of $M_2(t)$ (A) to find the maximum Max_1 of $M_1(t)$ (B) and then follow the velocity gradient $\frac{\mathrm{d}}{\mathrm{d}t}V(t)$ downwards (C) to a local minimum of $V(t)$, where we suspect the HS event.

Test data has shown that the maximum Max_1 of $M_1(t)$ generally occurs before the maximum $\text{Max}_2(t)$ of $M_2(t)$. We suspect that $\text{Max}_1(t)$ occurs before Max_2 since $M_1(t)$ includes $GRF_{HS}(t)$ and there is a tendency that changes in the GRF of the striking foot occur slightly before changes in the GRF of the lifting foot manifest. Test data also demonstrated that the maximum Max_1 is not always clearly pronounced. We therefore use the local extrema $[\text{Min}_2, \text{Max}_2]$ of $M_2(t)$ as a search region for Max_1.

With respect to the search boundaries (Section 6.4.2), the GED works as follows. The first local maximum Max_2 in $M_2(t)$ is identified before the midpoint. Searching beyond Max_2 reveals the local minimum Min_2 in $M_2(t)$. In between those limits, if it exists, the local maximum Max_1 is identified. If there is no local maximum, Max_1 corresponds to the location of the maximum value between $[\text{Min}_2, \text{Max}_2]$. We then follow the velocity gradient downwards until we reach a local minimum in $V(t)$. This point corresponds to the heel strike event. The search process is sketched in Algorithm 6.1 and the full Matlab code is given in Appendix A.5.

Die approbierte gedruckte Originalversion dieser Diplomarbeit ist an der TU Wien Bibliothek verfügbar.
The approved original version of this thesis is available in print at TU Wien Bibliothek.

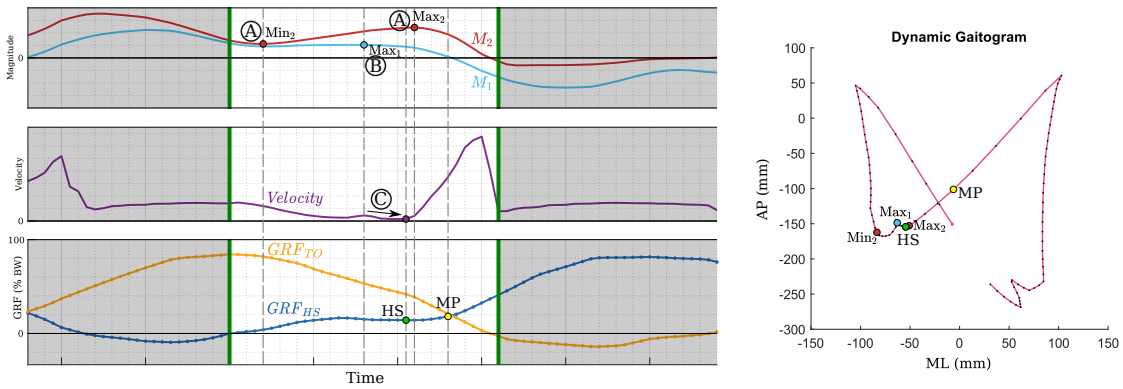

Figure 6.25: The gait event algorithm, illustrated.

Algorithm 6.1: Find a subject's heel strike event

Input: Midpoint MP; Measures M_1, M_2; Magnitude of CoP_d's velocity V
Output: The heel strike event HS

1 $\text{Max}_2 = findMaximumBeforePoint(\text{MP}, M_2)$;
2 $\text{Min}_2 = findMinimumBeforePoint(\text{Max}_2, M_2)$;
3 $\text{Max}_1 = findMaximumBetween(\text{Min}_2, \text{Max}_2, M_1)$;
4 $\text{HS} = findMinimumFollowingGradientFromPoint(\text{Max}_1, V)$;
5 **return** HS;

Implementation Notes and Modifications

Some data is smoothed using a uniform (mean) filter in order to remove small disturbances in the data, possibly caused by jerky movement. The filter is applied to the velocity's magnitude $V(t)$, measure $M_2(t)$, and the CoP's ML trajectory CoP_{ML} (Section 6.4.2). It spans 5% GC, which is approximately 150 ms in the recorded test data. Filtering is used to remove insignificant turns in CoP_{ML}, spurious maxima in $M_2(t)$, and small fluctuations in $V(t)$.

Measure $M_2(t)$ (Equation 6.11) does not depend on $GRF_{HS}(t)$. As mentioned in Section 6.4.3, relying on the change of a single GRF might be insufficient for GED. To account for the change in both GRFs, we propose a modification to $M_2(t)$. Tests have shown that the usage of a modified version of $M_2(t)$ provides slightly better results. This modified version effectively dampens non-relevant maxima while emphasizing points where both GRFs change. It is defined as:

$$M_2^*(t) = \frac{GRF_{TO}(t)}{GRF_{HS}(t) + GRF_{TO}(t)} \cdot D(t) \tag{6.12}$$

Furthermore, we propose a second modification to the CoP's calculation. A foot's movement leads to a slight change in its pressure point P, even if the magnitude of

Die approbierte gedruckte Originalversion dieser Diplomarbeit ist an der TU Wien Bibliothek verfügbar.
The approved original version of this thesis is available in print at TU Wien Bibliothek.
TU Bibliothek Your knowledge hub WIEN

pressure stays constant. This change in P leads to a subsequent change in the CoP and therefore influences the velocity measurements. Furthermore, a change in P influences the distance $D(t)$.

We are only interested in the interaction of forces between both feet. For our GED algorithm, the precise pressure point underneath the foot is irrelevant and, as mentioned before, might influence the calculations. Each foot's position is constant with respect to the pressure plate, since the foot straps hold the foot in place.

It is therefore sufficient to use a representative and fixed pressure point $P^*_{\{L,R\}}$ on each pressure plate to represent the respective foot. This removes the influence of any change in the foot's pressure point, while leaving the force measurements intact. For each foot, the ML component of P^* corresponds approximately to the foot's midline (i.e. the position in ML direction where the middle of the foot is arrested on the plate). Whereas the AP component is the respective pressure plate's offset in AP direction. These substitute coordinates remove distortions from $M_1(t), M_2(t), M_2^*(t)$, and $V(t)$, improving the detection of gait events.

6.5.3 Validation

Schepp's PerPedes is a novel system, with our work being the first approach at extracting user performance data. Since gait patterns can be vastly different than expected from literature, there is also no gold standard available for identifying the beginning and end of a weight transfer. In order to validate the algorithm, the first step was to manually annotate the test data and mark start and end of each weight transfer. It turned out that this process is inherently biased, since it depends on how the data is preprocessed, which data is used, and how it is presented. The static and dynamic gaitogram present information differently than velocity, M_1, M_2, or GRFs. Furthermore, the gait event might be ambiguous or not clearly identifiable by manual inspection.

The validation of our GED algorithm is twofold. First, one can expect that healthy participants are able to repeat similar movements over time. This consistency in movement should lead to a time-consistency in the occurrence of gait events. This means that events should occur at approximately the same time as in adjacent gait cycles if the movement is about the same. Secondly, we expect that the detected event is in accordance with literature for standard gait patterns. This means that if standard algorithms agree on a specific event location, our algorithm should agree as well. The first requirement relates to the precision of our algorithm, while the second one defines its accuracy. Figure 6.26 illustrates the difference between those two terms.

Die approbierte gedruckte Originalversion dieser Diplomarbeit ist an der TU Wien Bibliothek verfügbar.
The approved original version of this thesis is available in print at TU Wien Bibliothek.
TU Bibliothek Your knowledge hub WIEN

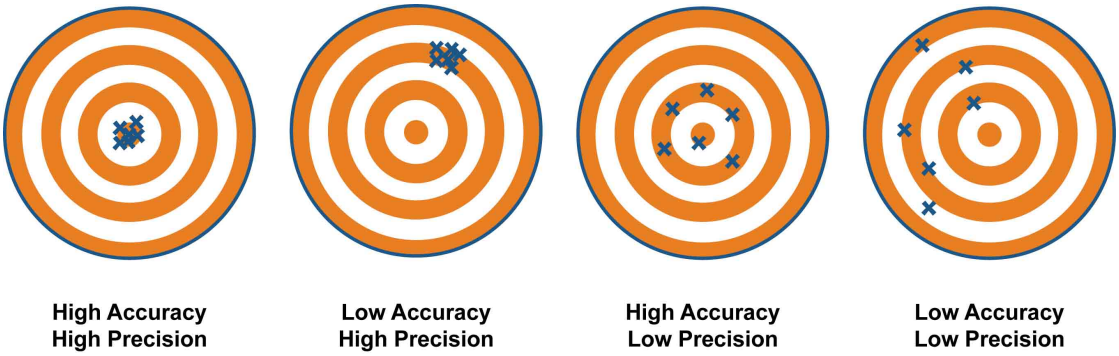

Figure 6.26: Accuracy vs. Precision. Image taken from Keller [Kel19].

The following algorithms are chosen for validation. Figure 6.27 shows the locations of all identified gait events in one representative example.

- HS1 - Point before the midpoint with zero AP velocity in static gaitogram
- HS2 - Point before the midpoint with zero AP velocity in dynamic gaitogram
- HS3 - Most posterior point in dynamic gaitogram
- HS4 - Start of largest positive CoP acceleration
- HS5 - Start of largest change in GRF_{HS}
- TO1 - Point after the midpoint with zero AP velocity in static gaitogram
- TO2 - Point after the midpoint with zero AP velocity in dynamic gaitogram
- TO3 - Most anterior point in dynamic gaitogram
- TO4 - Most anterior pressure point of the lifting foot

Algorithms from the Literature

Verkerke et al. [VHZ+05] defines heel strikes to occur when the dynamic CoP's velocity in AP direction crosses the zero level (HS2). This is typically equivalent to the point in time when the CoP reaches its most posterior position (HS3), but does not need to be (see Figure 6.28). Equivalently, toe off can be determined analogously through the zero-crossing of the velocity of the dynamic CoP's trajectory in AP direction after the midpoint (TO2) or the dynamic CoP's most anterior position (TO3). Both, HS3 and TO3 have been proposed in different publications [RCC+08], [RCS+14], [TCvDR19] in the context of gaitography, as well as with marker-based kinematics [ZJRH08]. In the following, we reason about standard gait patterns, what to expect, and how to derive the remaining algorithms for detection.

Die approbierte gedruckte Originalversion dieser Diplomarbeit ist an der TU Wien Bibliothek verfügbar.
The approved original version of this thesis is available in print at TU Wien Bibliothek.
TU Bibliothek Your knowledge hub WIEN

Algorithms per Foot

During normal gait, the initial contact is with the heel, followed by moving the pressure along the foot and ending contact at the toes. Keeping this in mind, the static CoP's trajectory can be examined as well. The point where the static CoP's AP direction changes (i.e. AP velocity is zero), can be identified as heel strike (HS1) and toe off (TO1), respectively. In case the pressure point moves from heel to toe, the TO event can be defined as the most anterior pressure point of the lifting foot (TO4) after the midpoint. Analogously, heel strike could be defined as the most posterior point of the striking foot before the midpoint, but test data has shown that this assumption rarely holds in PerPedes. Heel strikes appear to occur often midfoot, followed by the pressure point moving backwards during the weight transfer. The reasons for this are unknown, but could be connected to tightly fastened foot straps. Since this classification is unreliable for heel strikes, no corresponding algorithm has been used.

Velocity and Acceleration-based Algorithms

In general, detecting heel strikes is more challenging than toe offs, since the forces typically change gradually before the actual heel strike, but stop abruptly after the weight transfer is completed. In order to compensate for this difficulty in detection, we propose two additional heels strike algorithms. A weight transfer is typically accompanied by a spike in acceleration of the CoP's movement and a peak in the derivative of GRF_{HS}. We introduce two heuristics, identifying the beginning of the largest CoP acceleration (HS4) and the start of the largest change in GRF_{HS} (HS5). HS4 is found by searching for the start of the largest positive CoP acceleration before the midpoint. The acceleration's start is defined as the first point before the maximum where the acceleration is smaller or equal to zero. HS5 searches for the maximum in the derivative of GRF_{HS} within the standard search boundaries (Section 6.4.2) and a local minimum before this maximum marks the event's location.

With these standard GED algorithms, it is possible to visualize the range of fluctuation (i.e. the accuracy) and consistency in time (i.e. the precision) of our GED algorithm (see Section 8.6). We introduce a metric to measure the range of fluctuation in Section 7.1.3 and present examples based on test data in Chapter 9.

Die approbierte gedruckte Originalversion dieser Diplomarbeit ist an der TU Wien Bibliothek verfügbar.
The approved original version of this thesis is available in print at TU Wien Bibliothek.
TU Bibliothek Your knowledge hub WIEN

Die approbierte gedruckte Originalversion dieser Diplomarbeit ist an der TU Wien Bibliothek verfügbar.
The approved original version of this thesis is available in print at TU Wien Bibliothek.

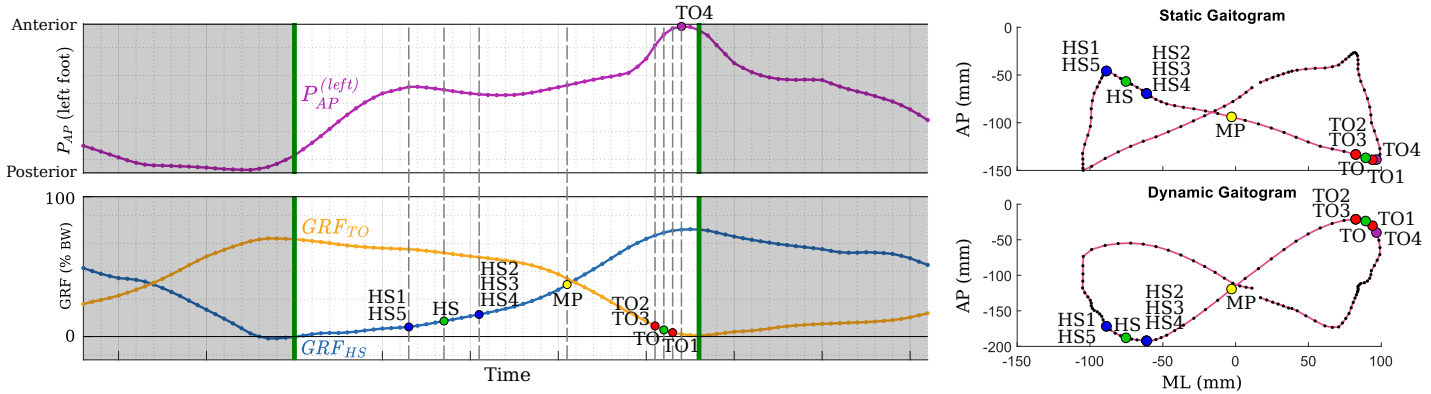

Figure 6.27: Different GED results. Pressure point's AP component of the lifting (left) foot $P_{AP}^{(left)}$ in purple. Our proposed gait events (HS, TO) are highlighted in green.

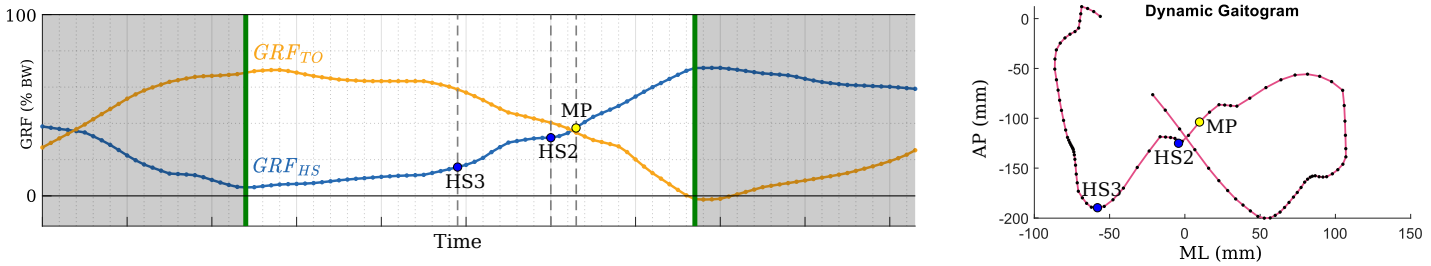

Figure 6.28: HS2 vs. HS3. The most posterior point in the gaitogram (HS3) might be different to the first point where the AP direction is reversed (HS2).

CHAPTER 7

Spatiotemporal Measures

Now that gait events have been identified, the framework for measuring the subject's performance has been established. This chapter shows how to derive the previously defined spatiotemporal parameters (Section 2.5) in the context of our system. Furthermore, we introduce metrics to interpret possible discrepancies between the subject's and the machine's gait cycle. Later on, the focus switches to symmetry measures, an important instrument for performance, especially with stroke patients.

7.1 Measures in PerPedes

The spatiotemporal parameters step length, stride length, swing time, stance time, and double support time can be directly inferred from the gait events. Swing time refers to the elapsed time (seconds) between the subject's TO and HS events for each leg respectively. Stance time is measured between HS and TO. Double support time corresponds to the duration of both double support phases, i.e. between HSL and TOR and between HSR and TOL events.

The parameter step length is usually measured as the distance between two similar contact points on both feet. Typically between two consecutive HS or TO locations. Both events, HS and TO occur with a minimal amount of contact area on the respective pressure plate, since the foot is either in the process of being lifted or just hit the ground. Because of this small contact area and PerPedes' low resolution of six pressure sensors, the pressure point at the moment of heel strike or toe off might only correspond to the reading of exactly one pressure sensor. This essentially means that the pressure point is imprecise and/or misleading and therefore cannot be used. Instead, a reliable measurement is the distance between both heels during the HS event. Since the feet are strapped in and fixed on the pressure plates and both feet can be assumed to be approximately of the same size, the distance between both heels is equal to the offset of one pressure plate to the other (compare with Figure 2.7). Essentially, in the context of

Die approbierte gedruckte Originalversion dieser Diplomarbeit ist an der TU Wien Bibliothek verfügbar.
The approved original version of this thesis is available in print at TU Wien Bibliothek.
TU Bibliothek Your knowledge hub WIEN

our system, the left step length SLL is equal to the offset of the left pressure plate in comparison the right pressure plate at the moment of the left HS event. The right step length SLR is calculated analogously. Stride length is derived from both step lengths as SLL + SLR.

7.1.1 Timing in PerPedes

The PerPedes platform with its predefined movements can act as a ground truth in regard to the optimal timing of gait events. We discussed in Section 6.2 that a subject's gait events might not coincide with the machine's gait events. It is useful to measure the discrepancy between the subject's behavior and the machine's movement. A simple measure is the timing difference between the subject's and machine's gait events (compare with δ in Figure 6.7 and Figure 6.8). These differences in timing are extensively used to generate patient instructions in order to improve the patient's timings and are discussed in Section 8.4.1.

7.1.2 System-specific Metrics

In the following, we introduce metrics, specific to PerPedes, derived from force measurements. These metrics are used to evaluate the balance or differences in strength between the left and the right leg. Furthermore, it is important to measure how well the subject is lifting his/her leg during swing phase.

In order to measure how much contact with the pressure plate occurs during the respective swing phase, we introduce a new metric, called the *swing ratio*:

$$R_{\text{swing},\{L,R\}} = 100\% \cdot \frac{1}{\int_0^{100} GRF^+_{\{L,R\}}(t)\mathrm{d}t} \int_{\text{swing phase,\{L,R\}}} GRF^+_{\{L,R\}}(t)\mathrm{d}t \tag{7.1}$$

This corresponds to the ratio of positive forces (GRF^+) applied in the machine's swing phase in relation to the whole gait cycle. Under ideal circumstances, the swing ratio is zero, meaning the foot is completely lifted off the ground and exerts no positive forces. The swing ratio is undefined, if there are no positive forces in the whole gait cycle (i.e. $\int_0^{100} GRF^+_{\{L,R\}}(t)\mathrm{d}t = 0$), which only occurs if the respective foot never touches its pressure plate during a whole gait cycle of the machine.

Three additional metrics are introduced, in order to evaluate the difference in strength between left and right leg during different intervals (stance phase, swing phase and whole gait cycle) of the machine's gait cycle:

$$\begin{aligned}
I &= \max(GRF^+_L(t), GRF^+_R(t)) - \min(GRF^+_L(t), GRF^+_R(t)), \forall t \in [0, 100] \\
D_{\text{stance}} &= 100\% \cdot \frac{1}{60I} \int_0^{60} GRF^+_R((t+50) \bmod 100) - GRF^+_L(t)\ \mathrm{d}t \\
D_{\text{swing}} &= 100\% \cdot \frac{1}{40I} \int_{60}^{100} GRF^+_R((t+50) \bmod 100) - GRF^+_L(t)\ \mathrm{d}t \\
D_{\text{total}} &= 100\% \cdot \frac{1}{100I} \int_0^{100} GRF^+_R((t+50) \bmod 100) - GRF^+_L(t)\ \mathrm{d}t
\end{aligned} \tag{7.2}$$

Die approbierte gedruckte Originalversion dieser Diplomarbeit ist an der TU Wien Bibliothek verfügbar.
The approved original version of this thesis is available in print at TU Wien Bibliothek.
TU Bibliothek Your knowledge hub WIEN

The differences compare the left positive GRF to the right positive GRF. Optimally, left and right leg move precisely the same, but the movement is offset by 50% of the gait cycle. Shifting the data by 50% GC allows us to compare the forces between both sides. Each value represents the mean difference between left and right forces over the respective interval, normalized with regard to the maximum possible difference I of forces in the whole gait cycle. If left and shifted right forces are equal across their respective ranges, the difference is zero. Since positive GRFs are compared, existing negative forces are treated as zero. A difference of $\pm 100\%$, as the worst case, states that the average difference over the interval corresponds exactly to the maximum occurring difference in the gait cycle. Meaning that the largest difference is actually happening in the respective interval. If one limb is substantially weaker than the other one, then D_{total} is negative for a stronger left leg and positive for a stronger right leg. Similarly, D_{stance} and D_{swing} indicate whether the left or right leg is more active during swing or stance phase. Note that all metrics are measured with respect to the machine's gait cycle, since the machine's gait cycle is clearly defined with fixed interval lengths. The defined metrics are applied in the context of patient instructions in Section 8.4.1.

7.1.3 Gait Discrepancy

As mentioned in Section 6.5.3, the system calculates standard gait events in order to measure and then further visualize (Section 8.6) the accuracy of our GED algorithm. If all gait events agree on the same location, the events' range of fluctuation is low and the accuracy is high. On the other hand, if standard gait events are spread out and have a low agreement, the gait pattern does not follow the standard definitions. Therefore, the range of fluctuation can be used to measure the discrepancy between standard gait and observed gait.

For each gait event (HSL, HSR, TOL, TOR) in every gait cycle, the range of fluctuation is determined. This range is called gait discrepancy (GD), expressed in percent of the gait cycle and defined as follows:

$$\begin{aligned}
\text{HS}_{\text{all},\{L,R\}} &= \{\text{HS}, \text{HS1}, \text{HS2}, \text{HS3}, \text{HS4}, \text{HS5}\}_{\{L,R\}} && (7.3)\\
\text{TO}_{\text{all},\{L,R\}} &= \{\text{TO}, \text{TO1}, \text{TO2}, \text{TO3}, \text{TO4}\}_{\{L,R\}} && (7.4)\\
\text{GD}_{\text{HSL}} &= \max(\text{HS}_{\text{all},L}) - \min(\text{HS}_{\text{all},L}) && (7.5)\\
\text{GD}_{\text{HSR}} &= \max(\text{HS}_{\text{all},R}) - \min(\text{HS}_{\text{all},R}) && (7.6)\\
\text{GD}_{\text{TOL}} &= \max(\text{TO}_{\text{all},L}) - \min(\text{TO}_{\text{all},L}) && (7.7)\\
\text{GD}_{\text{TOR}} &= \max(\text{TO}_{\text{all},R}) - \min(\text{TO}_{\text{all},R}) && (7.8)
\end{aligned}$$

The set $\text{HS}_{\text{all},\{L,R\}}$ contains the time of occurrence within the machine's gait cycle of our algorithm's heel strike (HS), and the standard algorithms' heel strikes (HS1 to HS5), for left and right side respectively. The set $\text{TO}_{\text{all},\{L,R\}}$ is defined similarly for toe off events. Each GD measures the time span between earliest ($\min(\text{HS}_{\text{all},\{L,R\}})$) and latest ($\max(\text{HS}_{\text{all},\{L,R\}})$) occurrence of the respective event. The GD is zero if all respective gait events occur at the same time, otherwise GD is strictly positive. We make use of

Die approbierte gedruckte Originalversion dieser Diplomarbeit ist an der TU Wien Bibliothek verfügbar.
The approved original version of this thesis is available in print at TU Wien Bibliothek.
TU Bibliothek Your knowledge hub WIEN

GD in Chapter 9 to illustrate whether or not gait patterns follow the standard definition of walking.

7.2 Symmetry Measures

As discussed in Section 3.3, symmetry measures can help to evaluate a subject's performance, give an indication on existing disabilities, and document the therapy's progress. Our system provides all symmetry measures listed in Table 3.1 for the spatiotemporal parameters step length, swing time, and stance time. These parameters have been identified [PGB+10] to be most useful in the context of gait symmetry with stroke patients.

In the following, we discuss three symmetry parameters, derived from the subject's dynamic gaitogram (Sections 2.4, 5.4.2). These parameters are used in gait analysis [KF15], [KDFA13] and are based on the gaitogram's central intersection point. Its location is an indicator for gait symmetry. Symmetrical timing and movement of left and right limbs results in a symmetrical gaitogram with the intersection point exactly centered in ML and AP direction.

The Gaitogram's Central Intersection Point

The gaitogram's central intersection point is an intersection between the two CoP trajectories during the double support phases (highlighted in green in Figure 7.1) of one gait cycle. The intersection needs to be located between the HS event of one limb and the following TO event of the contralateral limb. Given the CoP's data points P_i and the connecting line segments $L_j = \overline{P_j P_{j-1}}$, we can find all intersections in the gaitogram by checking overlaps between every two non-adjacent line segments. An intersection point between two line segments can be calculated by expressing both segments in parameterized form and then solve for the two unknown parameters in a system of two linear equations (compare to Lamothe [Lam99]). A healthy subject's gaitogram, measured on a treadmill has exactly one intersection point (Figure 7.1a). In our setup, the gaitogram might have multiple intersections or none at all. Since the subject is stabilized by a support harness, the subject is able to lift one or both feet at arbitrary points in time during the gait cycle. Doing so leads to distortions in the gaitogram, resulting in no intersections (Figure 7.1b) or additional ones (Figures 7.1c, 7.1d).

A good heuristic for finding the intersection point without the need of gait events is to assume that the correct intersection point is the one closest to the central axis between both feet. The central axis is located exactly in the center of the gaitogram in ML direction. In general, this heuristic holds well for standard cases, but might fail in highly distorted gaitograms (Figure 7.1d). By introducing the additional constraint of restricting the search for a valid intersection point to the paths between HS and TO events, we can reliably identify the correct intersection in the gaitogram, if one exists.

The central intersection point must not be confused with the midpoint (Section 6.3.2). The midpoint exists for each weight transfer and marks the data point closest to the weight

Die approbierte gedruckte Originalversion dieser Diplomarbeit ist an der TU Wien Bibliothek verfügbar.
The approved original version of this thesis is available in print at TU Wien Bibliothek.
TU Bibliothek Your knowledge hub WIEN

transfer's geometric center. Contrarily, the central intersection point is the intersection between the trajectories of exactly two weight transfers in a gait cycle.

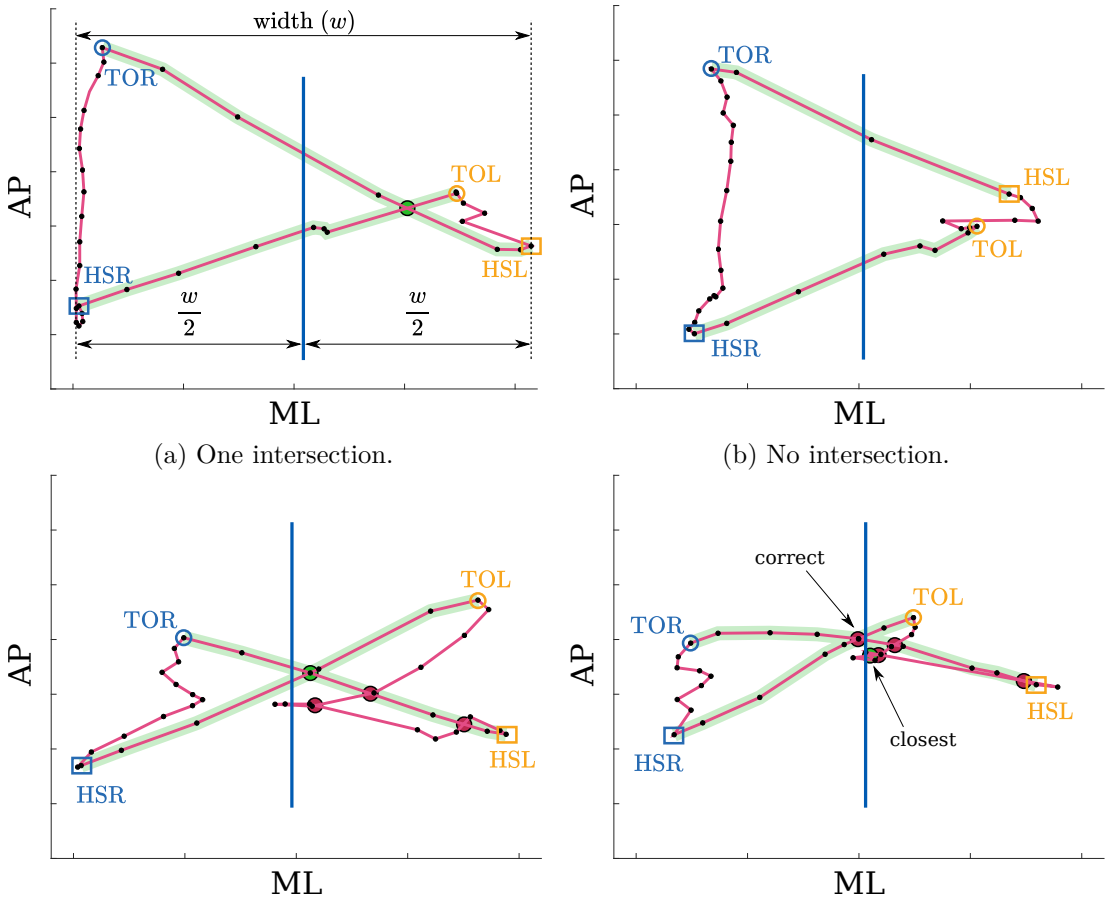

(a) One intersection.

(b) No intersection.

(c) Multiple intersections.

(d) Not closest intersection.

Figure 7.1: Intersection points in dynamic gaitograms. The images show the CoP's data points P_i (black dots), the central axis (vertical blue line), intersections of the gaitogram's line segments (red circles), and the closest intersection (green circle) to the central axis. If gait events are computable, the correct intersection point should be located at the closest crossing to the central axis of the two trajectories (highlighted in green) between HS and TO events.

Die approbierte gedruckte Originalversion dieser Diplomarbeit ist an der TU Wien Bibliothek verfügbar.
The approved original version of this thesis is available in print at TU Wien Bibliothek.

The Gaitogram's Symmetry Measures

The gaitogram's central intersection point allows us to extract three symmetry parameters [KF15], [KDFA13] over N gait cycles:

1. **AP variability** [mm]: The standard deviation of the N central intersection points along the AP axis.
2. **ML variability** [mm]: The standard deviation of the N central intersection points along the ML axis.
3. **ML symmetry** [%]: The mean normalized shift of the N central intersection points along the ML axis, away from the central axis.

Figure 7.2 shows two subjects with low and high variability in their respective central intersection points in both ML and AP direction. Low variability implies that the subject is able to perform repetitive movements throughout multiple gait cycles with higher precision. Although a large variability does not necessarily indicate a disability, Kalron and Frid [KF15] observed a correlation between cerebellar impairment and a gaitogram's variability, especially in AP direction. They found that variability can be used to estimate the severity of neurological impairment in the context of patients with multiple sclerosis.

ML symmetry relates to the offset of the central intersection point to the central axis. As demonstrated in Figure 7.3, the central intersection point can have a negative offset Δx to the left, no offset ($\Delta x = 0$), or a positive offset to the right of the central axis. The ML symmetry, as defined in the literature [KF15] corresponds to the offset Δx. In contrast, we normalize the ML symmetry to the range $\pm 100\%$ by calculating $\frac{\Delta x}{w/2}$. Here, w refers to the distance between outermost left and outermost right point of the CoP's trajectory of the corresponding gait cycle. By normalizing the offset Δx with respect to $w/2$, one can compare ML symmetry between different individuals. The original definition of ML symmetry does not take into account the different step widths per person or gait cycle and is given in mm.

Die approbierte gedruckte Originalversion dieser Diplomarbeit ist an der TU Wien Bibliothek verfügbar.
The approved original version of this thesis is available in print at TU Wien Bibliothek.
TU Bibliothek Your knowledge hub WIEN

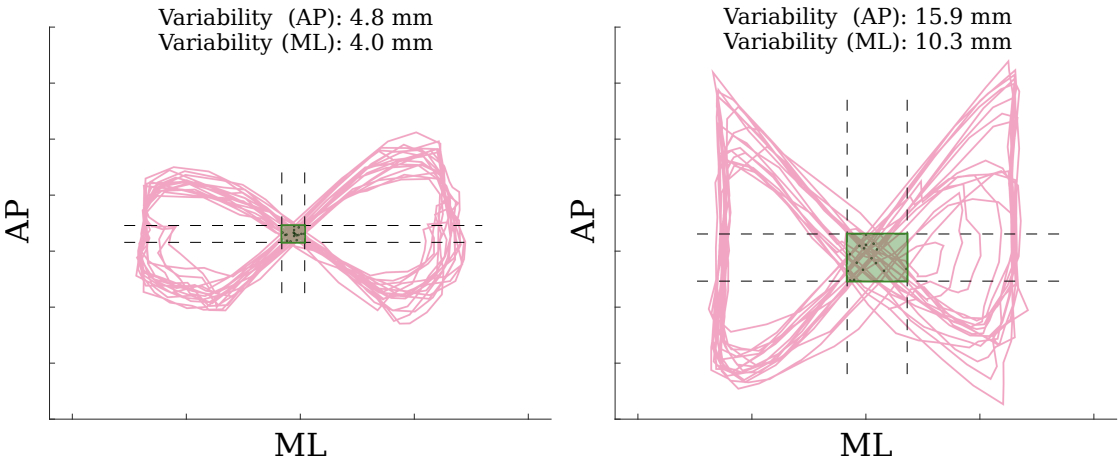

Figure 7.2: Central intersection point variability. Comparison between two test subjects with low (left) and high (right) variability with respect to their gaitogram's central intersection points (black dots). All intersections occur inside their respective green shaded area. The left subject was able to repeat the same movements over 17 gait cycles with higher precision, indicated by the lower AP and ML variabilities.

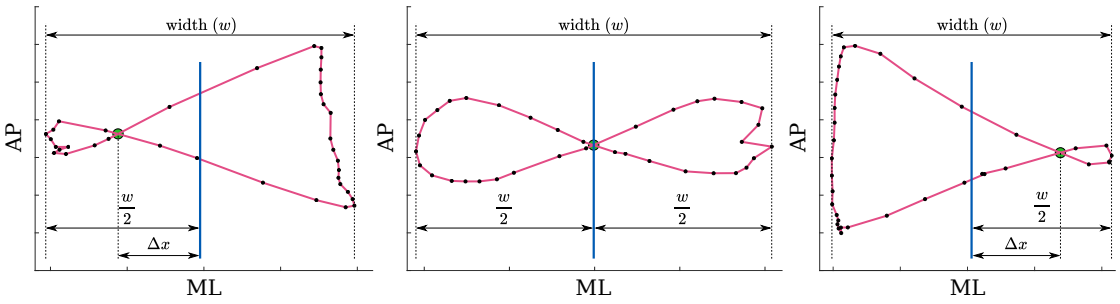

Figure 7.3: ML symmetry in gaitograms. The central intersection point's shift Δx in lateral direction, away from the central axis (vertical blue line), defines the ML symmetry. The example images from left to right show a left shift ($\Delta x < 0$), a perfect symmetry ($\Delta x = 0$), and a right shift ($\Delta x > 0$) respectively.

Die approbierte gedruckte Originalversion dieser Diplomarbeit ist an der TU Wien Bibliothek verfügbar.
The approved original version of this thesis is available in print at TU Wien Bibliothek.
TU Bibliothek Your knowledge hub WIEN

Die approbierte gedruckte Originalversion dieser Diplomarbeit ist an der TU Wien Bibliothek verfügbar.
The approved original version of this thesis is available in print at TU Wien Bibliothek.

CHAPTER 8

Visualization

This chapter introduces the user interface of our system. It can be used by therapists during rehabilitation training as well as medical experts for gait analysis. Known graphical elements, like the gaitogram and force visualizations have been integrated. Novel additions, particularly useful within the PerPedes system have been developed. The system is designed to support decision-making both during training with the patient, as well as after each training session by providing statistical data.

Die approbierte gedruckte Originalversion dieser Diplomarbeit ist an der TU Wien Bibliothek verfügbar.
The approved original version of this thesis is available in print at TU Wien Bibliothek.
TU Bibliothek Your knowledge hub WIEN

8.1 General Considerations

8.1.1 Colors and Themes

The user may choose to visualize the system with a light or dark theme. The light theme, using a positive polarity (dark text on white background) increases overall contrast. Hall and Hanna [HH04] compared different studies in the context of readability and contrast. They found conflicting results, but recommend black text on white background for improved readability. Buchner and Baumgartner [BB07] also found that proofreading performance is improved with dark text on light background in contrast to reading light text against dark background.

The dark theme uses negative polarity (light text on dark background). While a dark theme consumes less energy with some screen technologies (e.g. OLEDs), there are no other known advantages backed up by scientific studies. Nevertheless, in recent years "dark mode" has become a trend among users and designers [Cum19], allegedly reducing eye strain.

Throughout the whole application we follow a consistent color scheme. We use colors orange and blue opposing each other on the color wheel (Figure 8.1a) for the left and right leg respectively. The color magenta, located halfway between blue and orange is used as a visual representation for the CoP's trajectory. Indicators representing a rating (good/bad) are by common convention visualized with green/red colors (see Section 8.4.2). In general, the same colors are used for both light and dark themes, although the luminance of color blue has been increased when using the dark theme for better contrast (Figure 8.1b). We are aware that different research groups and medical personnel use different color schemes (e.g. red for the left leg and green for the right leg). Our system has been designed to easily change the colors to a familiar setting for the individual user.

Shieh and Lin [SL00] concluded in a study that blue-on-yellow text was the subjects' most preferred color combination and resulted in the best visual identification performance. This reaffirms our color choice of using high contrast colors for the left and right side of the body.

Die approbierte gedruckte Originalversion dieser Diplomarbeit ist an der TU Wien Bibliothek verfügbar.
The approved original version of this thesis is available in print at TU Wien Bibliothek.
TU Bibliothek Your knowledge hub WIEN

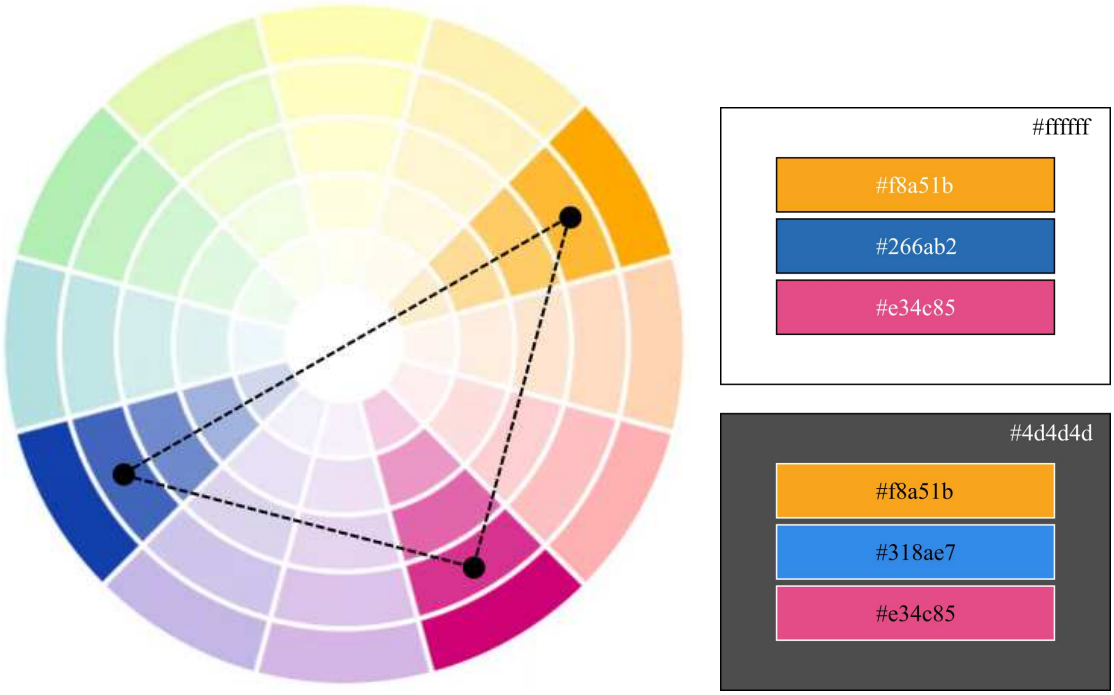

(a) Color wheel. Image adapted from Shutterstock [Shu19] (b) Hex color codes

Figure 8.1: Color scheme for the user interface. A color wheel with the positions of the main colors (a). The used colors with their hex color codes in the context of light and dark themes (b).

8.1.2 Live Perspective vs. Analysis Perspective

Our system is separated into two major areas, called *perspectives*. The live perspective presents current data streamed from the PerPedes machine during a therapy session and puts the live data into context of the past eight gait cycles. Contrarily, the analysis perspective allows the user to navigate the whole recorded data stream of the session and provide analytic tools for some chosen number of gait cycles.

While the subject is training in the PerPedes system, the therapist needs quick access to information regarding the subject's performance. The main focus of the live perspective is showing information through visualizations. Metrics and statistics are not presented with numbers, but using visuals and minimal textual information (e.g. patient instructions, Section 8.4.1). The therapist's attention is with the patient, while auxiliary information is provided by our system in an easy to grasp fashion.

In contrast, the analysis perspective provides aggregated data over multiple gait cycles. The focus is on gait events and statistics. It can be used to measure the overall performance of the subject, analyze repeatability of movements, and identify potential problems, like asymmetrical gait, foot placement, or timing of gait events. The analysis perspective is

Die approbierte gedruckte Originalversion dieser Diplomarbeit ist an der TU Wien Bibliothek verfügbar.
The approved original version of this thesis is available in print at TU Wien Bibliothek.
TU Bibliothek Your knowledge hub WIEN

expected to be used by the therapist or medical personnel (e.g. doctors) after a therapy session to obtain detail information about the subject's performance. Especially the generated statistical data is of interest for the comparison between different therapy sessions or subjects.

8.1.3 Panels

Each perspective is further subdivided into graphical elements, called *panels*. The live perspective (Figure 8.2a) contains:

- (A) The pressure distribution panel (Section 8.2) with
  - (A_1) gaitogram (Section 8.2.1) and
  - (A_2) pressure plates (Section 8.2.2)
- (B) The ground reaction force panel (Section 8.3)
- (C) The patient status information panel (Section 8.4) with
  - (C_1) patient instructions (Section 8.4.1) and
  - (C_2) visual indicators (Section 8.4.2)
- (D) The 3D representation panel (Section 8.5)

The analysis perspective (Figure 8.2b) contains four panels as well. Additionally to the pressure distribution and ground reaction force panels, it contains:

- (E) The gait event consistency panel (Section 8.6)
- (F) The statistics panel (Section 8.7)

While both perspectives share the pressure distribution and the ground reaction force panels, their respective content differs. The live perspective always displays the latest available data, streamed from the PerPedes machine, while the analysis perspective shows a user selected range of gait cycle data from the recorded data stream.

Die approbierte gedruckte Originalversion dieser Diplomarbeit ist an der TU Wien Bibliothek verfügbar.
The approved original version of this thesis is available in print at TU Wien Bibliothek.

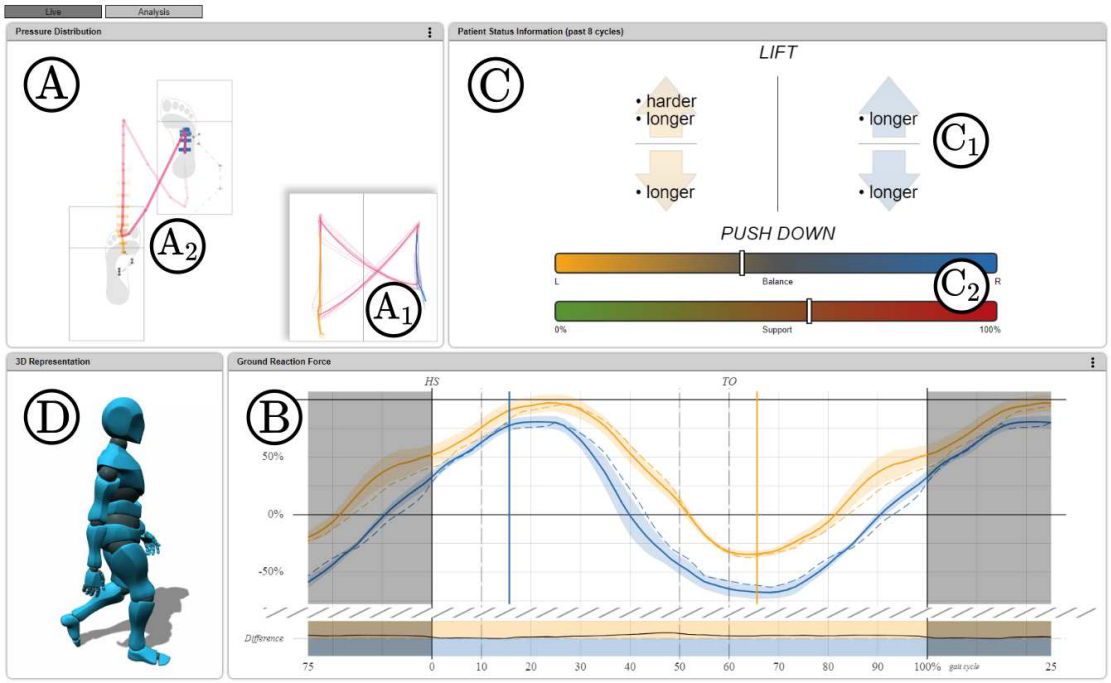

(a) Live perspective

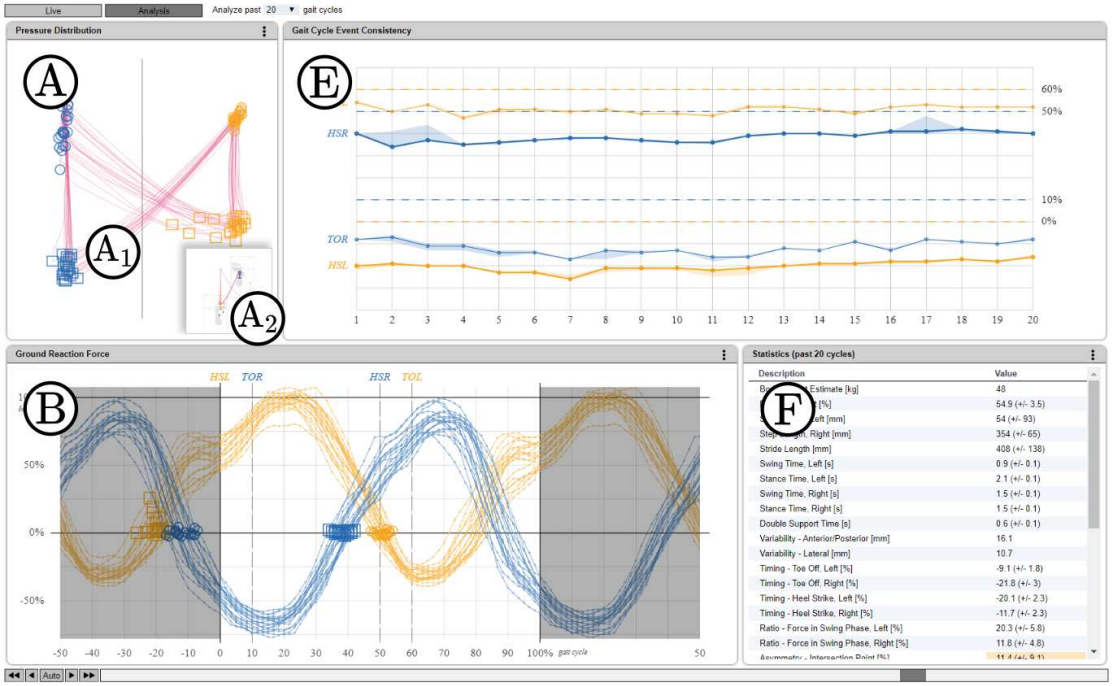

(b) Analysis perspective

Figure 8.2: *[Screenshots with annotations]* User interface using a light theme.

Die approbierte gedruckte Originalversion dieser Diplomarbeit ist an der TU Wien Bibliothek verfügbar.
The approved original version of this thesis is available in print at TU Wien Bibliothek.
TU Bibliothek Your knowledge hub WIEN

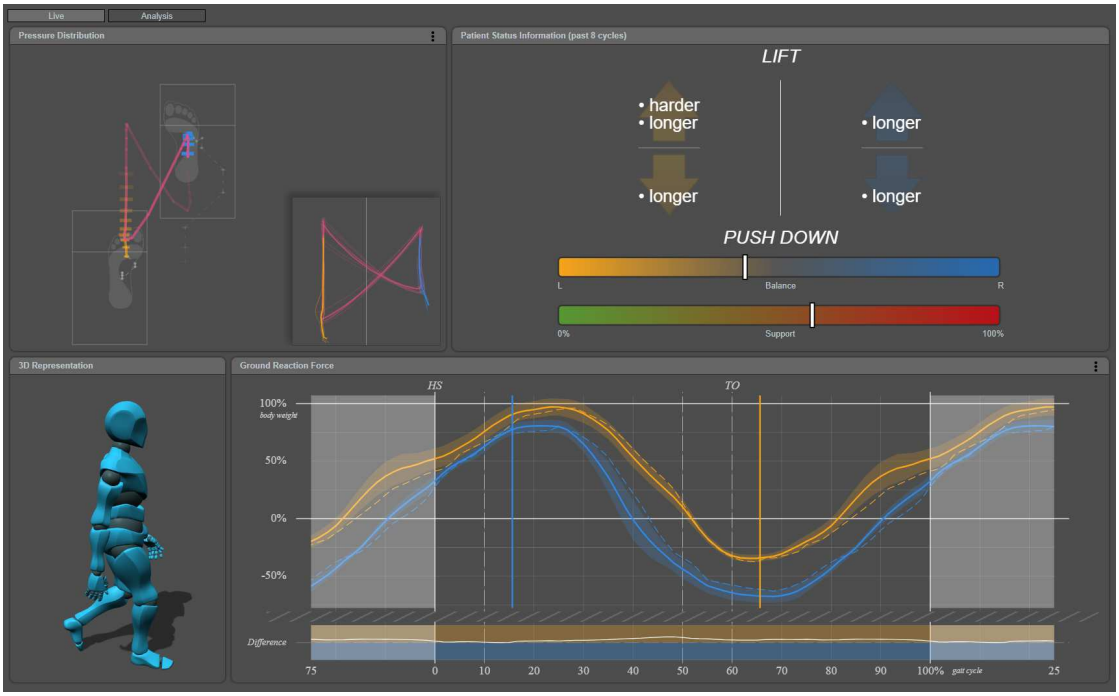

(a) Live perspective

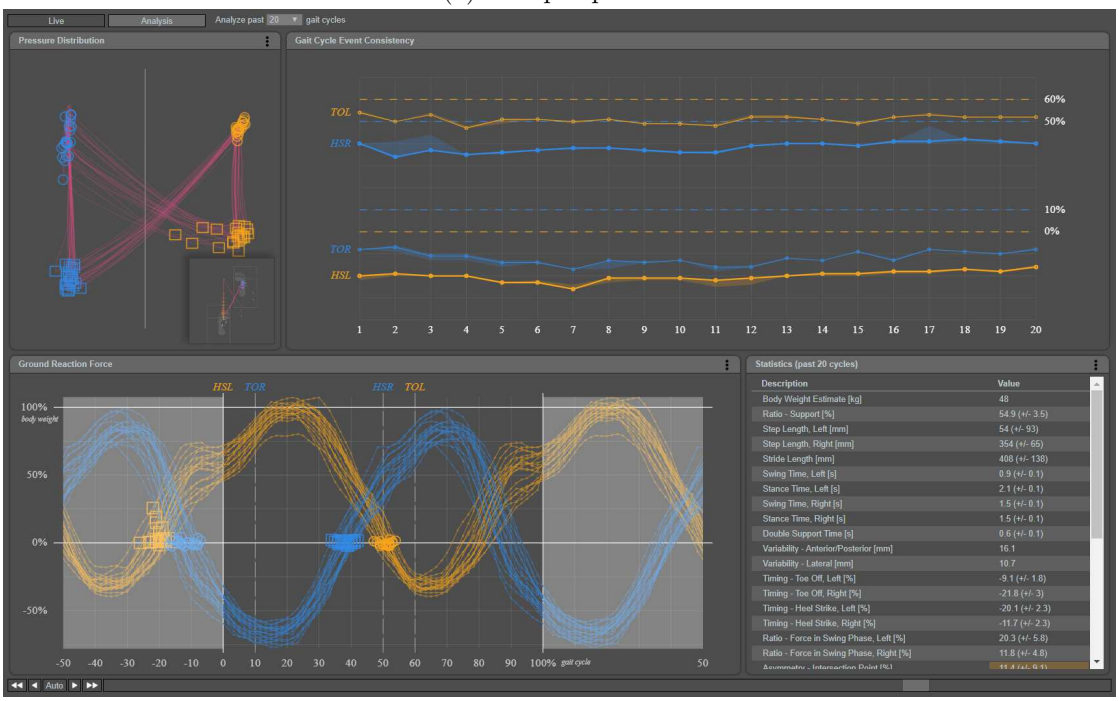

(b) Analysis perspective

Figure 8.3: *[Screenshots]* User interface using a dark theme. Same content as in Figure 8.2.

Die approbierte gedruckte Originalversion dieser Diplomarbeit ist an der TU Wien Bibliothek verfügbar.
The approved original version of this thesis is available in print at TU Wien Bibliothek.
TU Bibliothek Your knowledge hub WIEN

8.2 Pressure Distribution Panel

The pressure distribution panel contains two graphical elements displayed side by side. These elements are the gaitogram and the pressure plates. Both graphical elements are either shown in a static or dynamic frame of reference (FoR) (compare with Section 2.4 and Section 5.4.2). The dynamic FoR incorporates each pressure plate's movement, while the static FoR explicitly excludes the movement.

The static FoR is used to evaluate the utilization of each foot or analyze specific gait patterns, like tip toe or calcaneal gait [WCH+99]. More commonly used with treadmills [RCS+14], [RCC+08], [TCvDR19] is what we call dynamic FoR. It visualizes the pressure points including the machine's movements. Using the dynamic FoR, one can infer gait symmetry (Section 7.2) and how well the subject synchronizes his/her movement with the machine (Section 8.2.1). Figure 8.4 gives examples presenting the same data at the same time in different frames of reference. In both images the focus in on the pressure plates, while the gaitogram is presented in the lower right corner of the pressure distribution panel. The user can change the focus to be on the gaitogram instead with a simple click on the graphical element. This exchanges the graphical elements' positions, giving focus to the gaitogram and presenting the pressure plates in the lower right corner. Another click on the focused element will maximize its space while minimizing the other. The user can select which visualization is relevant to him/her in any given situation. Figure 8.5 shows all possible transitions between the graphical elements within the pressure distribution panel.

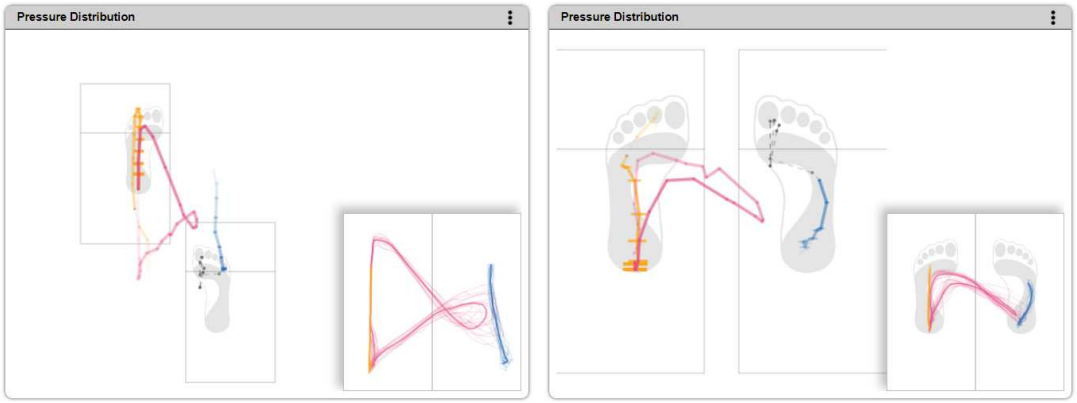

(a) Dynamic FoR (b) Static FoR

Figure 8.4: *[Screenshots]* Pressure Distribution Panel. Dynamic and static FoR. The user can choose to represent the data either with pressure plate movement (a) or with fixed pressure plates (b).

Die approbierte gedruckte Originalversion dieser Diplomarbeit ist an der TU Wien Bibliothek verfügbar.
The approved original version of this thesis is available in print at TU Wien Bibliothek.
TU Bibliothek Your knowledge hub WIEN

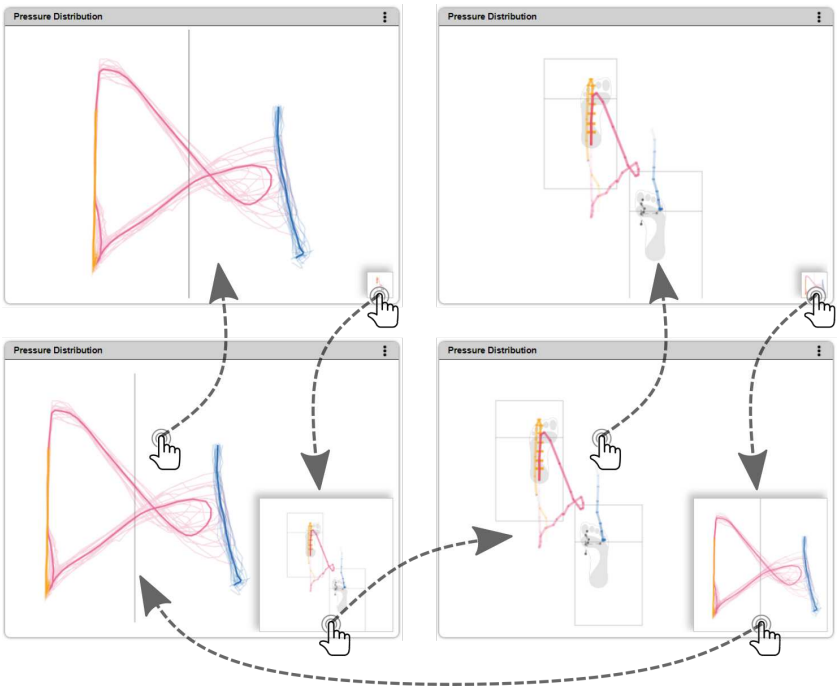

Figure 8.5: *[Screenshots with annotations]* Pressure Distribution Panel. UI transitions. The user can choose to focus on either the pressure plates or the gaitogram. Both elements are visible at the same time with clear priority for one while minimizing the other (top row) or shared space for both (bottom row).

8.2.1 The Gaitogram Visualization

The gaitogram shows the CoP's trajectory in either static or dynamic FoR for one or more gait cycles (Section 2.4). The gaitogram in a static FoR is shown with a depiction of footprints, while the gaitogram for a dynamic FoR is presented without footprints. This is consistently used in the graphical user interface to differentiate between both representations.

In the following, this section explains

- the gaitogram in the analysis perspective
- enhancements to the gaitogram in the live perspective
- interpretation of gaitograms in PerPedes

The Gaitogram in the Analysis Perspective

The gaitogram in the analysis perspective shows the CoP's trajectory in a static or dynamic FoR for a user-selected gait cycle count. This visualization depicts the variance

Die approbierte gedruckte Originalversion dieser Diplomarbeit ist an der TU Wien Bibliothek verfügbar.
The approved original version of this thesis is available in print at TU Wien Bibliothek.
TU Bibliothek Your knowledge hub WIEN

in movement and clustering of the gait events at specific locations. This demonstrates whether or not the subject is able to repeat the same movements throughout multiple gait cycles. With each gait cycle, four of the subject's gait events are depicted, i.e. HSL, HSR, TOL, and TOR. HS events are shown as squares, while TO events are shown as circles. The events are colored as usual (Section 8.1.1) for the respective left and right side. See Figure 8.6 for an example.

(a) Dynamic FoR (b) Static FoR

Figure 8.6: *[Screenshots]* Gaitograms in the analysis perspective. Shown are the CoP's trajectory (magenta), HSL (orange square), HSR (blue square), TOL (orange circle), TOR (blue circle), and the center of the PerPedes machine in ML direction (black line). Both gaitograms show the same data of 58 gait cycles in different FoRs.

Enhancements for the Gaitogram Visualization

The gaitogram in the literature only shows the CoP's trajectory, optionally with event visualization (e.g. in Roerdink et al. [RCS+14]). The PerPedes system defines an optimal gait cycle through its moving pressure plates. It is possible to show the subject's movement in relation to the machine's movement in an easy to grasp fashion within the gaitogram. We propose two enhancements for the gaitogram. The first enhancement is to visualize the trajectory of the left and right pressure points during the machine's single support stance phases. These trajectories are called *stance lines*. This will allow the visual inspection of the subject's timing with respect to the machine's optimal timing. Furthermore, one can evaluate if the subject correctly attempts to lift his/her feet or if the feet are being dragged. The second enhancement is to calculate and visualize the mean CoP's trajectory and mean stance lines across multiple gait cycles. In the live perspective, the gaitogram shows the past eight gait cycles while applying both enhancements.

Die approbierte gedruckte Originalversion dieser Diplomarbeit ist an der TU Wien Bibliothek verfügbar.
The approved original version of this thesis is available in print at TU Wien Bibliothek.
TU Bibliothek Your knowledge hub WIEN

Stance Line Visualization

The machine's single support stance phase is defined as the range $[10, 50)\%$ GC for the left foot and as the range $[60, 100)\%$ GC for the right foot. If the subject's timing is perfectly synchronized with the machine's movement, the subject's weight is entirely on the respective foot during the machine's single support stance phases and weight transfers only occur during the double support phases (i.e. $[0, 10)\%$ GC and $[50, 60)\%$ GC). By showing the left and the right pressure point's trajectories only during the machine's respective single support stance phase, stance lines are created.

Interpretation of the Dynamic Gaitogram

The CoP's trajectory (static or dynamic) will perfectly coincide with the stance lines if the full weight is on the respective foot during the machine's single support stance phase. More precisely, this means $CoP_{\{s,d\}} = P_L$ during $[10, 50)\%$ GC and $CoP_{\{s,d\}} = P_R$ during $[60, 100)\%$ GC (compare with Section 5.4). Under optimal circumstances, the CoP's trajectory will only diverge from the stance lines during the double support phases. Figure 8.7 shows a dynamic gaitogram for one gait cycle. In this optimal situation, the subject's gait cycle is perfectly synchronized with the machine's gait cycle. Weight is transferred exactly during the machine's double support phases.

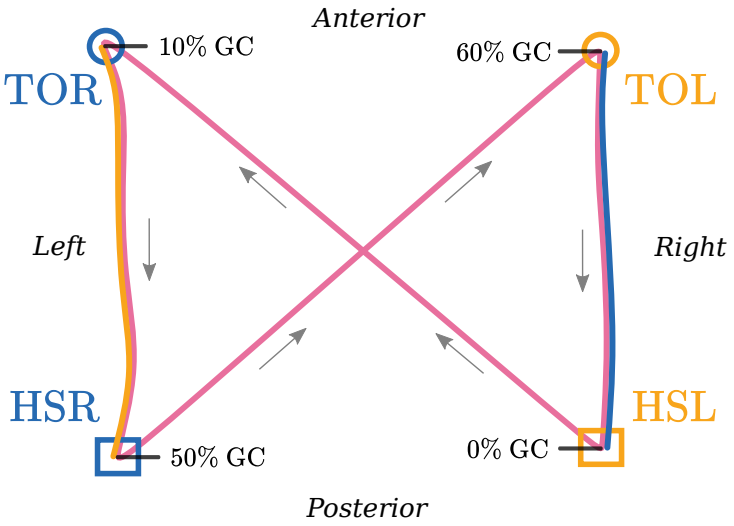

Figure 8.7: The perfect dynamic gaitogram from synthetic data. Machine and human subject move in unison.

Our recorded test data has shown that test subjects rarely move perfectly synchronized with the machine. Common issues are initiating the weight transfer too early or an incomplete weight transfer, i.e. dragging the feet during the swing phase. In the following, it is shown how to interpret the dynamic gaitogram in cases where the subject is not moving synchronized with the machine. Figure 8.8 provides an overview of common

Die approbierte gedruckte Originalversion dieser Diplomarbeit ist an der TU Wien Bibliothek verfügbar.
The approved original version of this thesis is available in print at TU Wien Bibliothek.
TU Bibliothek Your knowledge hub WIEN

phenomena occurring during training on PerPedes, encoded in the gaitogram. The right side shows that the full body weight is on the right foot during the machine's single support stance phase. This is shown by the CoP's trajectory (magenta) coinciding with the right stance line (blue). The stance line ends with the beginning of the machine's double support phase. During double support, the right pressure plate is still moving posterior (compare with Section 4.2). In case the subject's weight is still on the right foot and the weight transfer to the left starts (HSL) too late, it results in the visible offset Δa between the end of the stance line and the event location. Alternatively, the left heel strike might occur even later, after the right pressure plate moves forward again. This results in an additional non-zero offset Δb. During the weight transfer, the CoP moves to the left side and the weight transfer is completed with the right toe off event. In the given example, TOR occurs too late (during the machine's single stance support phase), resulting in the offset Δc. Furthermore, the right foot is not completely lifted off its pressure plate and exerts some force (i.e. foot dragging), resulting in an offset (hatched area) between CoP and left stance line. Subsequently, the weight transfer to the right (HSR) starts during the machine's single support stance phase and therefore too early, indicated by Δd. It also finishes too early (TOL), before the left single support stance phase starts (Δe). If in any case the weight transfer to the right finishes even earlier, while the right pressure plate is moving forward, the offset Δf will be non-zero.

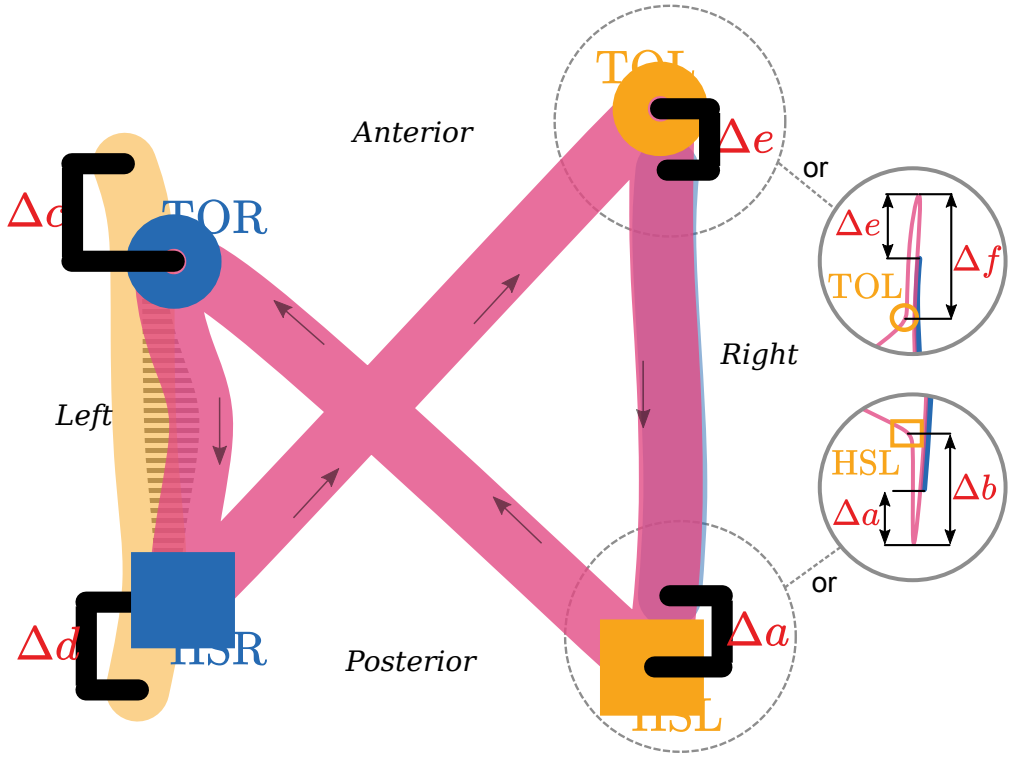

Figure 8.8: The dynamic gaitogram explained with synthetic data. Possible scenarios when training on PerPedes.

Die approbierte gedruckte Originalversion dieser Diplomarbeit ist an der TU Wien Bibliothek verfügbar.
The approved original version of this thesis is available in print at TU Wien Bibliothek.

Mean Trajectories

The second enhancement for the gaitogram is to create mean trajectories. Visualizing a gaitogram over multiple gait cycles results in multiple thin lines for the CoP's trajectory, as well as left and right stance lines. These thin lines might intersect or lay on top of each other. The resulting image can be hard to interpret, increasing in complexity with the amount of gait cycles. Especially the static gaitogram's readability might suffer, since movement happens on a smaller scale between feet than during gait (Figure 8.9).

As with statistical values, providing an average (mean) across trajectories can help identify tendencies in the subject's movements. The creation of mean trajectories is straightforward within in the PerPedes system. The machine's gait cycle has a well-defined start and end. A trajectory's coordinates can be sampled at regularly spaced points in time across one machine's gait cycle. For every gait cycle, this creates a set of samples of equal size. The mean trajectory is then an average across these sets. We create and visualize mean trajectories for the CoP, left, and right stance lines.

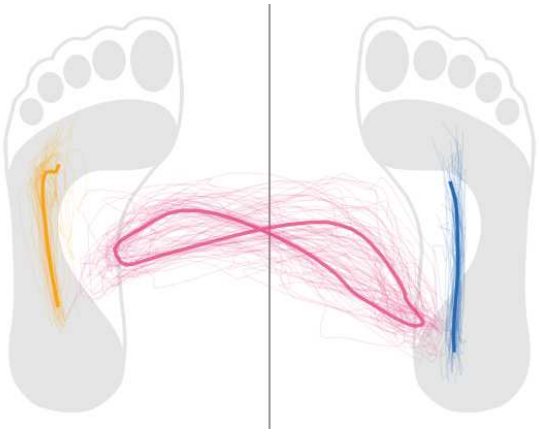

Figure 8.9: *[Screenshot]* Static gaitogram for 50 gait cycles with mean trajectories. The mean trajectories can improve identifying trends.

Gaitogram Examples

In Figure 8.10 participants are not moving perfectly synchronized with the machine. Offsets are marked in the images according to the notation introduced in Figure 8.8 and with respect to the mean trajectories. The following observations refer to the average behavior of each subject and do not necessarily apply to every gait cycle. The gait cycle events are not shown in these gaitograms. Therefore, a precise statement on how much the gait differs from an optimal one cannot be inferred from a visual inspection alone. Nonetheless, the average gait events are approximately located at the corners of the dynamic CoP's average trajectory, while straight lines between left and right side highlight the weight transfers.

Die approbierte gedruckte Originalversion dieser Diplomarbeit ist an der TU Wien Bibliothek verfügbar.
The approved original version of this thesis is available in print at TU Wien Bibliothek.
TU Bibliothek Your knowledge hub WIEN

Figure 8.10a shows symmetrical gait, although on average the weight is transferred too early ($\Delta d_1, \Delta d_2$), while finishing too late ($\Delta c_1, \Delta c_2$). This means that the subject is spending too much time in the double support phases.

In Figure 8.10b the right foot exerts pressure (hatched area ①) before the right heel strike starts the weight transfer. Additionally, the left foot is not fully lifted and exerts pressure during the right foot's stance phase. This results in a visible offset (hatched area ②) between the CoP's trajectory and the right stance line.

Figure 8.10c demonstrates a strong asymmetrical gait with minimal weight transfers to the right side. In this case, the CoP's mean trajectory barely crosses the center of the PerPedes machine (black line).

In Figure 8.10d the weight transfer to the left side starts too early (Δd_2) and subsequently finishes too early as well (Δe_1). Furthermore, the right heel strike occurs during the left single support gait phase and therefore too early (Δd_1).

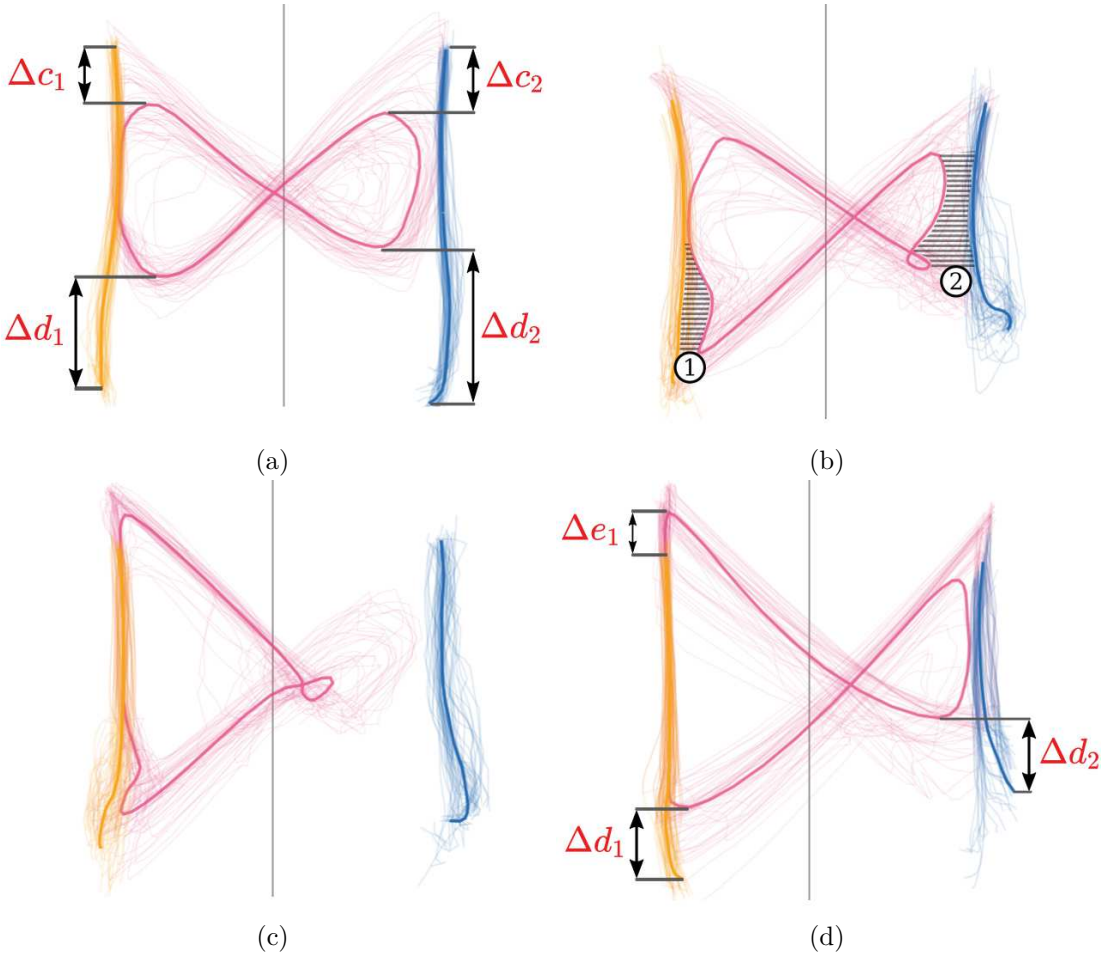

Figure 8.10: *[Screenshots with annotations]* Dynamic gaitograms with mean trajectories.

Die approbierte gedruckte Originalversion dieser Diplomarbeit ist an der TU Wien Bibliothek verfügbar.
The approved original version of this thesis is available in print at TU Wien Bibliothek.
TU Bibliothek Your knowledge hub WIEN

8.2.2 The Pressure Plate Visualization

As we have established in Section 5.4, our system calculates the pressure point for the left (P_L) and the right (P_R) foot plate as well as the CoP as a weighted average between those two. In order to visualize their respective trajectory, the locations of the last 1.5 seconds of each pressure point and the last 3 seconds of the CoP are shown in the pressure plate visualization. The locations are linearly connected and the alpha value is varied from fully opaque to fully transparent over the respective time spans. Additionally, for left and right pressure points the measured pressure's intensity is indicated by horizontal bars. Both thickness and length are varied according to the ratio of weight measured in relation to the total amount of weight on both pressure plates. More weight equals a longer and thicker bar. A pressure point measured with a weight below a threshold of four kilograms is deemed to be unreliable and visualized in gray.

In Figure 8.11, a comparison between the static and dynamic FoR is shown throughout the gait cycle. In both frames of reference one can see that the CoP is moving to the right side before the 40% mark of the machine's gait cycle. Ideally the start of the weight transfer with the right heel strike should occur at 50% GC. The weight transfer is completed with the left toe off at 60% GC, which is optimal. Although the whole length of the left foot is utilized (Figure 8.11a), the static gaitogram for the whole gait cycle (Figure 8.11b) reveals that the stance lines are located mostly at the heel. The dynamic gaitogram for the whole gait cycle (Figure 8.11d) reveals that both heel strikes occur too early ($\Delta d_1, \Delta d_2$), right toe off occurs too late (Δc_1), while left toe off is timed precisely. Notations according to Figure 8.8.

Die approbierte gedruckte Originalversion dieser Diplomarbeit ist an der TU Wien Bibliothek verfügbar.
The approved original version of this thesis is available in print at TU Wien Bibliothek.

Die approbierte gedruckte Originalversion dieser Diplomarbeit ist an der TU Wien Bibliothek verfügbar.
The approved original version of this thesis is available in print at TU Wien Bibliothek.

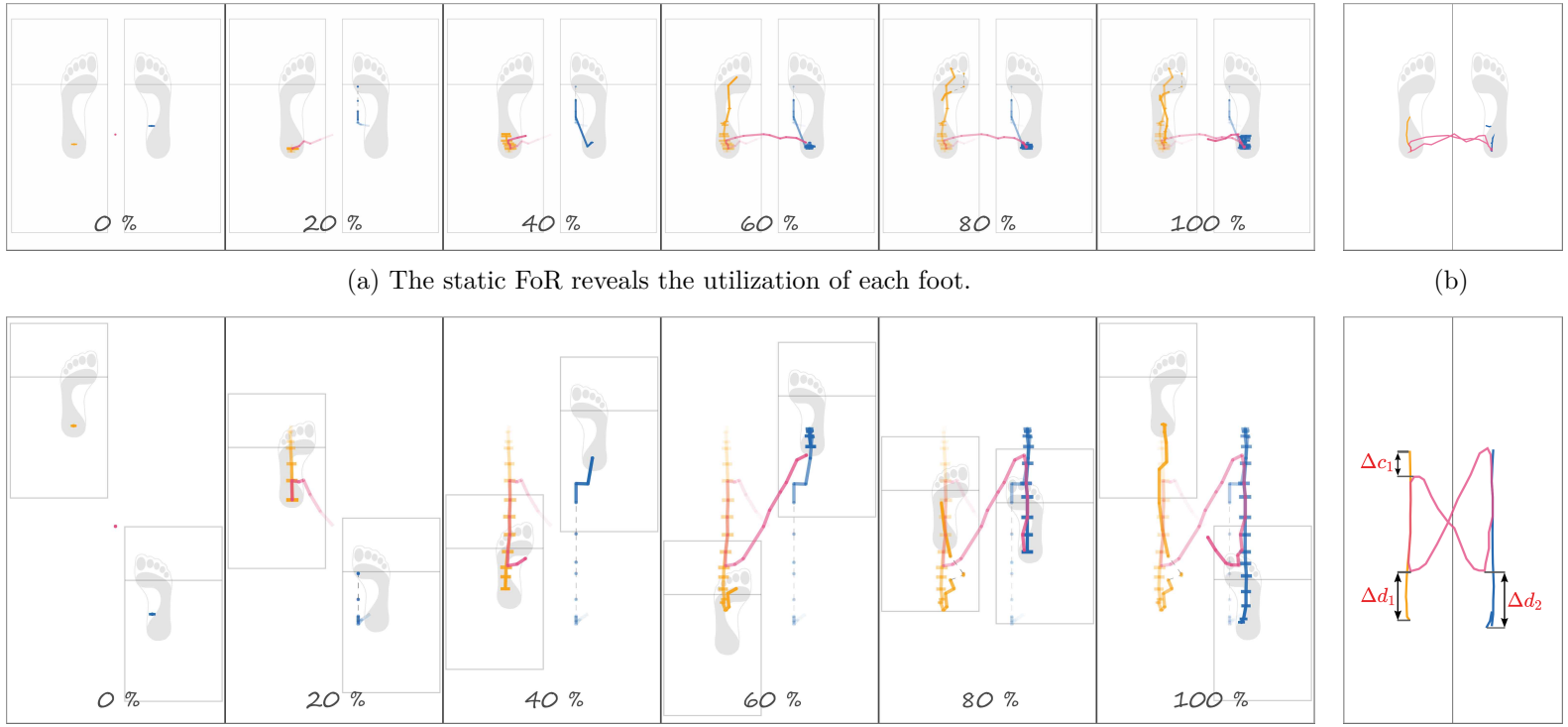

(a) The static FoR reveals the utilization of each foot.

(b)

(c) The dynamic FoR includes the pressure plates movement.

(d)

Figure 8.11: Pressure plate visualization throughout the gait cycle. Dynamic FoR vs. static FoR. One complete gait cycle (0% – 100%) is displayed in 20% increments. The resulting gaitograms are placed to the right. Pressure magnitude is shown with horizontal bars. Stronger pressure is mapped to a longer bar. Older contacts fade out over time. Gaitograms (b) and (d) show the single support stance lines and the CoP's progression over one gait cycle.

8.3 Ground Reaction Force Panel

The ground reaction force panel visualizes the left and right vertical GRFs for one complete gait cycle of the machine. The horizontal axis indicates the machine's gait cycle. The vertical axis, by common convention, is the vertical GRF normalized to the body weight in percent. While it is common during normal walking/running to measure forces above 100% body weight, this threshold is typically not exceeded in PerPedes. This is due to the fact that in a typical setup the subject is wearing a harness and part of the weight is supported by the equipment. Another distinctive feature is the possible occurrence of negative forces. These forces occur while trying to lift the feet and pulling on the foot straps, therefore creating negative readings at the force sensors.

The current position in the gait cycle is displayed with a progress indicator (vertical bar), moving from left to right, sweeping over old data while continuously updating the plot. In the live perspective the current force readings are plotted with dotted lines, the means (left/right) of the past eight gait cycles are shown with solid lines and surrounded by ± one standard deviation (colored areas). For context, the plot is extended beyond 0% GC and 100% GC by one quarter of a gait cycle (i.e. 25% GC). This is especially useful to analyze the behavior around the 0% GC / 100% GC mark, when the left heel strike is supposed to occur. Figure 8.12a gives an example with descriptive annotations. The machine's gait events at the top indicate the optimal occurrences of gait events in the machine's gait cycle. They are placed at 0% GC, 10% GC, 50% GC, and 60% GC, respectively.

The user can optionally choose to shift the force plot of the right side by 50% GC modulo 100% GC. This creates a visualization with synchronized left and right force readings (Figure 8.12b). The shift merges left and right gait events. The optimal occurrence for left and right heel strikes in the machine's gait cycle is then at 0% GC, while toe off events happen 60% GC afterwards. Synchronizing the forces splits the progress indicator into two indicators, separated by 50% GC. This occurs since the data is now progressing at two different locations for left and right forces within the visualization.

This synchronized visualization can be used for a direct comparison of left and right forces over time, in order to identify a one-sided weakness. Especially with patients suffering from hemiparesis after a stroke, comparing the difference in strength between both sides can be used to classify the severity of the disability. Furthermore, the change in this difference throughout therapy can be used to document the patient's progress.

Die approbierte gedruckte Originalversion dieser Diplomarbeit ist an der TU Wien Bibliothek verfügbar.
The approved original version of this thesis is available in print at TU Wien Bibliothek.

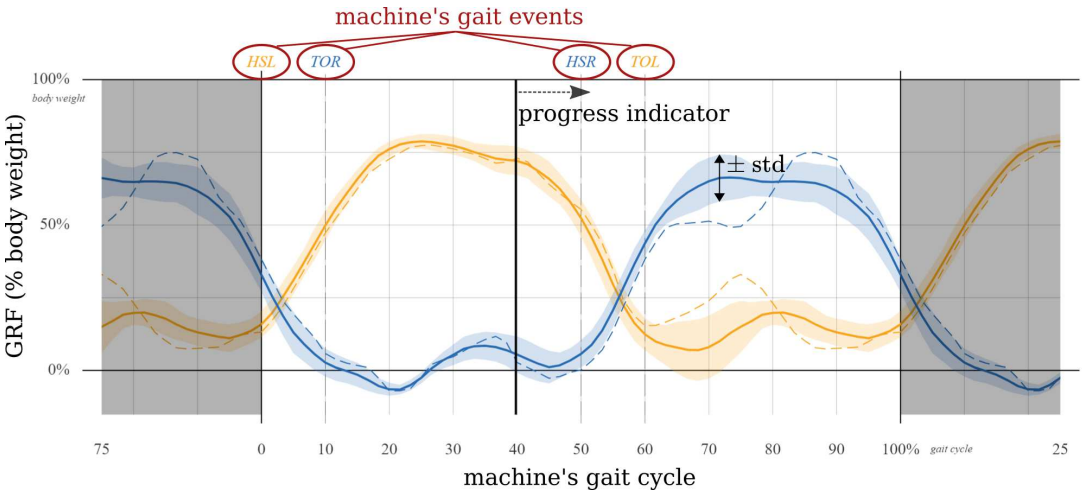

(a) Chronological

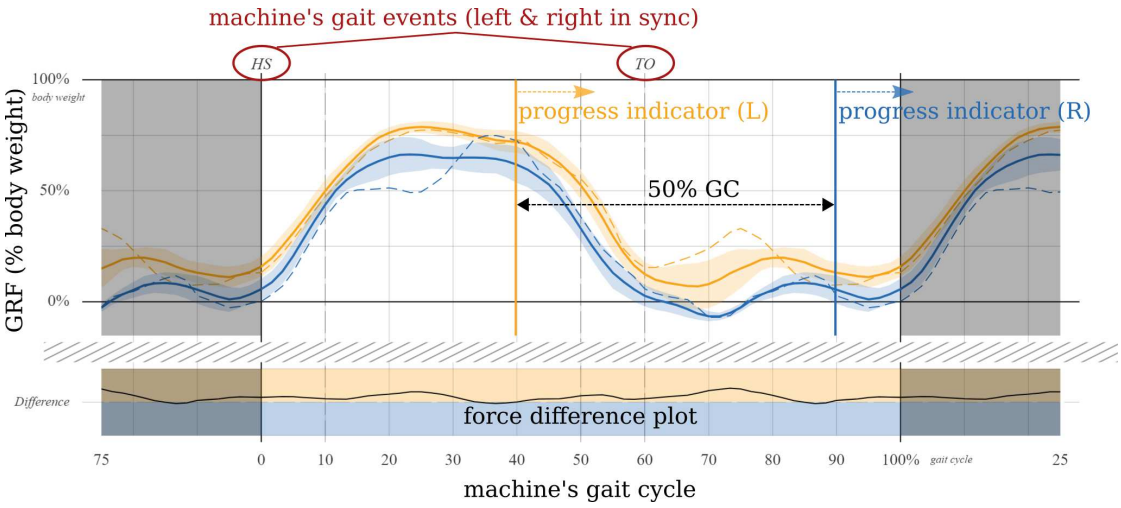

(b) Synchronized

Figure 8.12: *[Screenshots with annotations]* Vertical GRF visualization - chronological vs. synchronized. The current forces (dotted line), mean (solid line) and standard deviation (colored area) are plotted for left and right leg, respectively. Both (a) and (b) contain identical data, but (b) shifts the right GRF visualization by 50% GC.

8.3.1 Difference Plot

When synchronizing left and right forces, it is possible to highlight the force difference in a separate plot. This so created difference plot shows which side (left, right) is substantially stronger during the machine's gait cycle phases (double support, stance, or swing). The difference is created for the forces occurring in the current gait cycle. In order to have a meaningful visualization, the magnitude of the force difference needs to be normalized

Die approbierte gedruckte Originalversion dieser Diplomarbeit ist an der TU Wien Bibliothek verfügbar.
The approved original version of this thesis is available in print at TU Wien Bibliothek.
TU Bibliothek Your knowledge hub WIEN

to be within $[-100, 100]\%$. An obvious choice for normalization is using the largest occurring absolute difference Δd between left and right forces over the whole gait cycle:

$$\Delta d = \max(|GRF_L(t) - GRF_R(t)|), \forall t \in [0, 100) \tag{8.1}$$

$$\text{Diff}_A(t) = \frac{GRF_L(t) - GRF_R(t)}{\Delta d} \tag{8.2}$$

Although, this would disproportionately highlight small differences in otherwise equal force measurements (Figure 8.13, *Difference A*). Hence, we choose to normalize with respect to the maximally possible difference between left and right forces over the whole gait cycle:

$$s_1 = \max(GRF_L(t)) - \min(GRF_R(t)), \forall t \in [0, 100) \tag{8.3}$$

$$s_2 = \max(GRF_R(t)) - \min(GRF_L(t)), \forall t \in [0, 100) \tag{8.4}$$

$$\Delta max = \max(s_1, s_2) \tag{8.5}$$

$$\text{Diff}_B(t) = 100\% \cdot \frac{GRF_L(t) - GRF_R(t)}{\Delta max} \tag{8.6}$$

Doing so has the advantage of suppressing small fluctuations while highlighting severe differences between left and right forces (Figure 8.13, *Difference B*).

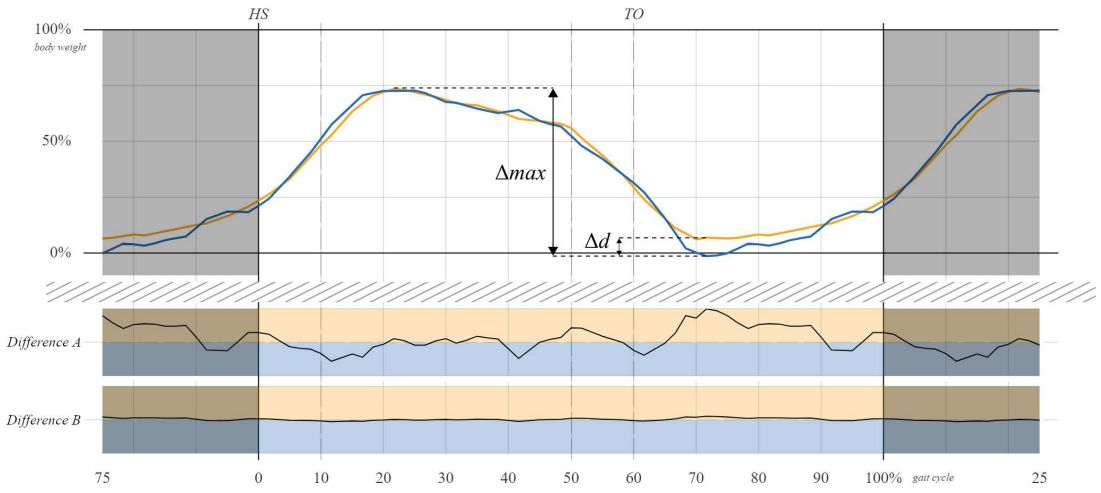

Figure 8.13: *[Screenshot with annotations]* Vertical GRF difference - Comparison between two variants. *Difference A*: The difference between left and right forces can be normalized with respect to the largest occurring absolute difference Δd. *Difference B*: Alternatively, normalization can be done with respect to the theoretical maximum difference Δmax.

8.3.2 Event Visualization with Ground Reaction Forces

The analysis perspective shows the subject's gait events in the context of vertical ground reaction forces. In contrast to the live perspective, it simultaneously shows multiple

Die approbierte gedruckte Originalversion dieser Diplomarbeit ist an der TU Wien Bibliothek verfügbar.
The approved original version of this thesis is available in print at TU Wien Bibliothek.
TU Bibliothek Your knowledge hub WIEN

gait cycles overlaid with the identified gait events. Furthermore, the graph shows up to −50% GC of the previous gait cycle as reference and is extended beyond 100% GC by half of the current gait cycle (i.e. 50% GC). This visualization can be used to analyze the subject's consistency in force application and timing.

In Figure 8.14, the subject shows consistent performance throughout the session with gait events clustered and clearly separated. On average, the subject's left heel strikes (orange squares) occur slightly before the expected machine event (marked with HSL). The subject's right heel strikes (blue squares) are clustered around the expected time of 50% GC (marked with HSR). Left and right toe off events (circles) are timed around the expected machine gait events (TOR, TOL) with only small variances.

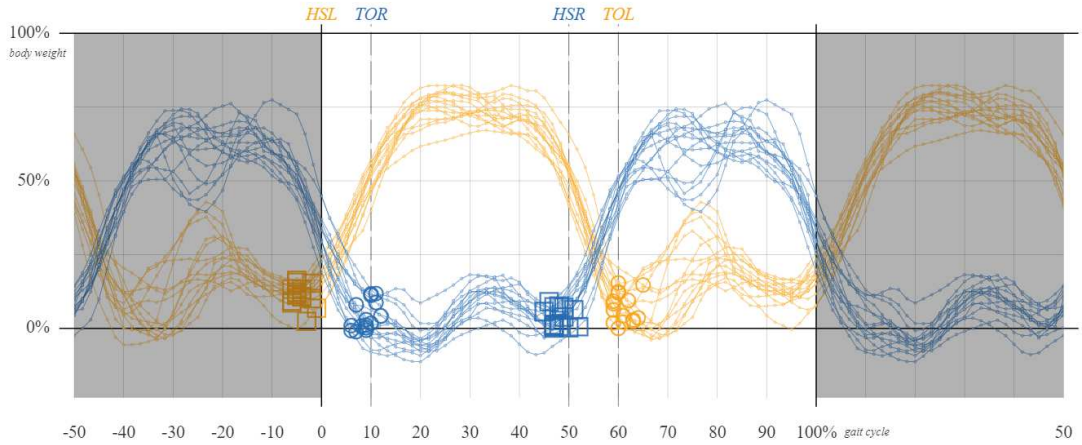

Figure 8.14: *[Screenshot]* Vertical GRF visualization with gait events. This example shows 15 gait cycles with the subject's identified gait events.

8.4 Patient Status Information Panel

The patient status information panel contains data related to the current performance of the patient in PerPedes. It consists of two parts. First of all, it contains a visualization with instructions to improve the patient's performance. Secondly, color-coded statistics are presented to the user, indicating the patient's current status.

8.4.1 Patient Instructions

During a live rehabilitation session, the therapist needs to be able to rate the patient's current performance. The question *»How is the patient doing?«* can be answered quickly with the vertical GRF and gaitogram visualizations. While these visualizations help in assessing whether or not problems exist, they cannot provide a quick answer to the question *»How could the patient improve?«*. Our system has knowledge about the patient's current movements as well as the ground truth, given by the machine's movements. Therefore, the difference in the timings between patient and machine can

Die approbierte gedruckte Originalversion dieser Diplomarbeit ist an der TU Wien Bibliothek verfügbar.
The approved original version of this thesis is available in print at TU Wien Bibliothek.
TU Bibliothek Your knowledge hub WIEN

be evaluated. Furthermore, patient-specific performance measures are generated by comparing data from the left and the right half of the body. By doing so, the system can spot individual differences between, e.g. paraplegic and non-paraplegic sides and provide personalized suggestions for improvement.

In the following section we introduce a novel visualization, which is targeted at therapists, and contains instructions for the patient to improve his or her performance. The aim of this visualization is to display easily comprehensible commands while being as detailed as possible. The visualization shows a total of six possible instructions per foot, without overwhelming the therapist. It is partitioned into a left and right side for each foot respectively. Furthermore, it is also partitioned into an upper half and lower half, dealing with the lifting up and pushing down of the respective foot. The generated commands are timing-based (i.e. *earlier, longer*) and force-based (i.e. *harder*). Timings are based on the difference between patient and machine movements, while forces are entirely patient-dependent. Force-based statistics compare left and right feet performances, while timings compare to the machine.

Figure 8.15 gives an example of generated patient instructions. The patient's left foot is not lifted properly. Both the timing, as well as the amount of force during lifting is insufficient. Therefore, the patient's first priority should be to concentrate on the left foot. Subsequently, the right foot should be pushed down stronger during the stance phase while lifting it for an extended period of time during the swing phase.

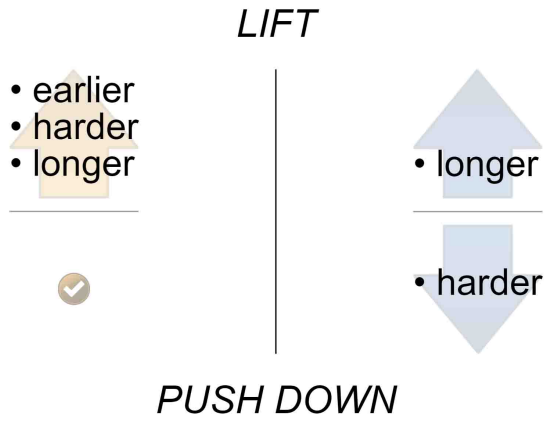

Figure 8.15: *[Screenshot]* System generated patient instructions. During a therapy session, the system generates suggestions for the therapist to quickly improve a patient's performance.

Timing-based Instructions

Each patient instruction is coupled to one or more criteria (see Table 8.1). Timing-based instructions are triggered as soon as the patient's event (e.g. HSR) occurs at a substantially different time than the machine's event. As an example, the patient's TOL

Die approbierte gedruckte Originalversion dieser Diplomarbeit ist an der TU Wien Bibliothek verfügbar.
The approved original version of this thesis is available in print at TU Wien Bibliothek.
TU Bibliothek Your knowledge hub WIEN

event should occur at around 60% GC. If the actual TOL event occurs substantially earlier, then the patient is instructed to lift the left foot later, or equivalently to push it down for a longer time.

Each patient has a certain variety in his or her gait, leading to imprecise timings of the patient's gait events. An issue is to determine how much discrepancy between machine and patient events is tolerable. In Section 6.2 we define the theoretical maximum discrepancy to be between $[-72, 28]$% GC. While these are reasonable bounds within which an event should be located, it does not specify which timing offset should trigger instructions for correction. We also established that an offset of -22% GC or $+28$% GC equals standing in one spot without progression. To narrow down the allowed discrepancy even more, we take a look at the gait cycle once more (Figure 2.1). The progression of events in the optimal gait cycle is rather quick. The HS event starts the double support subphase, ending only 10% GC later with the opposite foot's TO event. We assume that the event timings of healthy individuals are at least in the same subphase as the machine's gait cycle and therefore not more than 10% GC offset (10% GC is the length of the double support phase). Using these assumptions and the available test data, we set an empirically defined threshold of 8% GC as allowed discrepancy between patient and machine events. Hence, timing-based patient instructions are displayed only if a patient's event is off by more than ± 8% GC from the machine's event.

Force-based Instructions

In contrast to timings, force-based instructions are based on the comparison of the amount of force exerted by the patient in major gait cycle phases (i.e. swing and stance phase) and on the difference between the left and the right leg. The underlying assumption is that a healthy individual exerts the same amount of force on the left and on the right side. If there are measurable differences, then the patient can either improve with selective countermeasures or an existing disability prevents equal performance on both sides.

Whether or not a patient exerts enough force during the stance phase can be decided by comparing the difference between left and right limb. Patients with hemiparesis or other one-sided impairments are especially suitable for performance comparisons. The non-impaired side acts as a ground truth of achievable activity, while the other side can be put into relation accordingly. If one side is substantially weaker than the other one, instructions for improvement are triggered. Section 7.1.2 introduces metrics, summarized here for convenience:

- **Swing ratio** R_{swing} - The ratio of force applied in the swing phase in relation to the whole gait cycle.
- **Stance difference** D_{stance} - The force difference between left and right leg in the stance phase.
- **Swing difference** D_{swing} - The force difference between left and right leg in the swing phase.

Die approbierte gedruckte Originalversion dieser Diplomarbeit ist an der TU Wien Bibliothek verfügbar.
The approved original version of this thesis is available in print at TU Wien Bibliothek.
TU Bibliothek Your knowledge hub WIEN

In an optimal scenario, the swing ratio is zero, meaning the foot is lifted off the ground and exerts no positive forces during the swing phase. A patient might not be able to avoid exerting pressure during the swing phase, because of the foot straps or existing disabilities. Therefore, an empirical threshold of 10% for the swing ratio has been chosen, such that light pressure during the swing phase is permitted. In case this threshold is exceeded, the instruction to improve lifting of the corresponding foot is displayed.

A difference of zero in D_{stance} or D_{swing} relates to an equal amount of force applied during the respective stance or swing phase between left and right leg. If one of the differences is substantially large, instructions to increase pushing or lifting the weaker leg are presented to the user. Since our system is typically used for patients with one-sided impairments, the difference threshold is set to a rather large value of 20%. This results in instructions being triggered only when observing large force differences. They are therefore only displayed in cases of severe impairment.

Instruction	**Criterion**
Push longer	TO occurs too early
Lift earlier	TO occurs too late
Push earlier	HS occurs too late
Lift longer	HS occurs too early
Push harder	D_{stance} larger than 20%
Lift harder	R_{swing} larger than 10% *OR* D_{swing} larger than 20%

Table 8.1: Patient instructions and the corresponding criteria. Timing-based instructions are triggered if they occur 8% GC earlier or 8% GC later than the ground truth machine event. If the force difference during the stance phase between both legs exceeds 20%, more weight needs to be shifted onto the weaker leg. The patient is instructed to lift a leg more, if this leg is dragged (high swing ratio) or lifted less than the other leg (high swing difference).

8.4.2 Visual Indicators

Therapists during a training session must be able to quickly assess the patient's current performance. The gaitogram (Section 8.2.1) illustrates symmetry, timing, and utilization of each foot. The ground reaction force panel depicts the repeatability of force application and differences between left and right side throughout the gait cycle. The statistics table (Section 8.7) shows various measures in detail, but cannot be used for a quick assessment of the subject's status. Therefore, we visualize two selected measures to support the therapist in his/her evaluation of the current therapy.

Our system provides a balance indicator, visualizing if a subject exerts more force on the left or the right side. The underlying data is the D_{total} metric as introduced in Section 7.1.2, measuring the force distribution between both legs over a whole gait cycle. The balance indicator's presentation follows the system-wide applied color coding scheme.

Die approbierte gedruckte Originalversion dieser Diplomarbeit ist an der TU Wien Bibliothek verfügbar.
The approved original version of this thesis is available in print at TU Wien Bibliothek.
TU Bibliothek Your knowledge hub WIEN

The second indicator shows how much of the subject's weight is carried by the support harness. It is equal to the ratio of the support load, carried by the suspension system, in relation to the current body weight estimate (Section 5.2). Subjects unable to carry their own weight while walking will show a higher support ratio. Additionally, subjects who are unable to cope with the current therapy settings (e.g. speed, step length) will more likely rely on the suspension system to carry their weight. In situations when the support ratio is low, it is likely that the subject is comfortable with carrying his/her own weight during training.

Figure 8.16 gives an example for the visual indicators. The subject exerts slightly more force on the left side, represented by the indicator moving away from the central position to the left side of the bar. Furthermore, about 20% of the currently measured weight is carried by the suspension system.

Figure 8.16: *[Screenshot]* Visual indicators. This visualization allows a quick assessment of a subject's balance and current weight support.

8.5 3D Representation Panel

The live perspective offers a 3D rendering of a gender neutral character during walking. The character's movement is synchronized with the current machine's gait cycle by simply mapping the animation's keyframes to the current position in the gait cycle. Since the animation is strictly coupled with the displayed data in the live perspective, it helps the user to quickly understand which gait cycle phase is currently displayed. Furthermore, since the technical setup uses computer network connections and therefore introduces a possible latency, the animation helps to gauge the delay between real time and visualization time. The character is embedded in a fully functional 3D web framework (Section 1.5), therefore the user can choose to view the rendering from an arbitrary camera perspective.

Die approbierte gedruckte Originalversion dieser Diplomarbeit ist an der TU Wien Bibliothek verfügbar.
The approved original version of this thesis is available in print at TU Wien Bibliothek.
TU Bibliothek Your knowledge hub WIEN

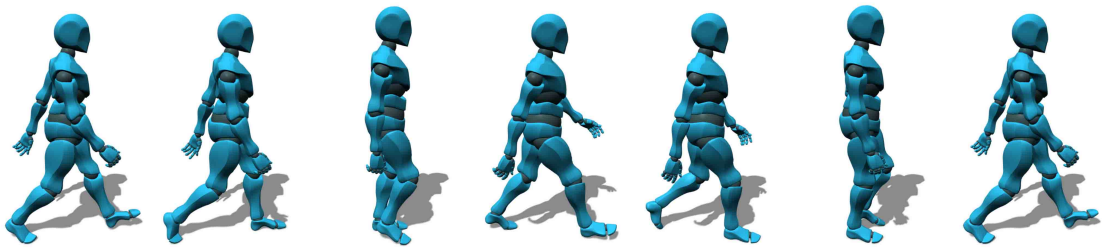

(a) 0% GC (b) 10% GC (c) 30% GC (d) 50% GC (e) 60% GC (f) 80% GC (g) 100% GC

Figure 8.17: *[Screenshots]* 3D character movement throughout one gait cycle.

8.6 Gait Event Consistency Panel

The gait event consistency panel contains a graph plotting for each gait cycle the time of occurrence of each gait event. Additionally, for each gait event and gait cycle, the range of fluctuation is visualized. The range of fluctuation is determined by the standard gait event definitions introduced in Section 6.5.3. If this range is small, algorithms agree on the position of the gait event, otherwise there is high variance and little agreement. Figure 8.18 shows an example, where gait cycles 11 and 12 are directly compared to each other. In gait cycle 12, the GED algorithms agree on the event location of HSL with little variance (small range of fluctuation). Contrary to this, in gait cycle 11, the algorithms do not agree on a common HSL event location, represented by a larger range of fluctuation. The dynamic gaitograms for both gait cycles are shown below the gait event consistency panel. Our proposed HSL event is marked in green, the standard gait events are marked in blue. On average over all gait cycles, the example shows that HSL events occur too early (before the 0% GC mark), HSR events are well timed (around the 50% GC mark), while both left and right toe off events occur too late (after the 10% GC and 60% GC mark respectively).

The gait event consistency panel can be used to verify our proposed GED algorithm. For consistent movements, the detected events should also be consistent in their timely occurrence. Additionally, the closer a participant's gait is to normal gait, the more agreement there should be between different gait algorithms, since these algorithms were designed for GED in standard gait. This agreement is then expressed in a small range of fluctuation, immediately visible to the user with this visualization.

Die approbierte gedruckte Originalversion dieser Diplomarbeit ist an der TU Wien Bibliothek verfügbar.
The approved original version of this thesis is available in print at TU Wien Bibliothek.
TU Bibliothek Your knowledge hub WIEN

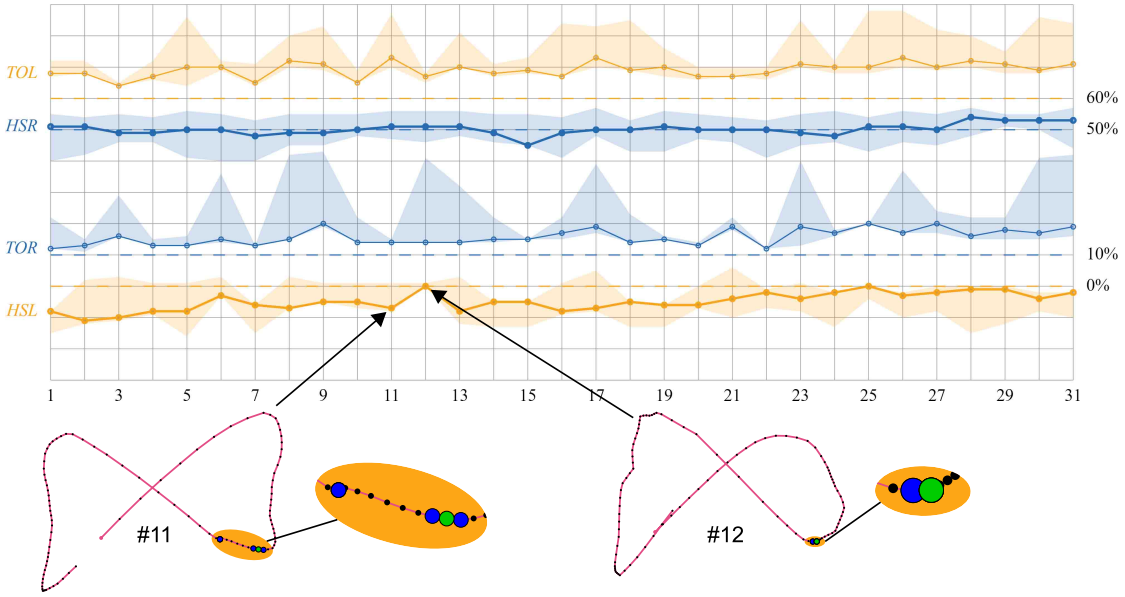

Figure 8.18: *[Screenshots with annotations]* The gait event consistency panel contains a line chart for each of the subject's gait events (TOL, HSR, TOR, HSL) with their respective range of fluctuations, determined by standard gait event definitions. The horizontal axis shows the gait cycles and the vertical axis depicts the time of occurrence.

8.7 Statistics Panel

The statistics panel in the analysis perspective presents multiple statistical values in tabular form. An overview of the collected measures is shown in Table 8.2. Additionally to this content, the symmetry index (SI), symmetry angle (SA), gait asymmetry (GA), and symmetry ratio (SR), as discussed in Section 7.2, are calculated for step length, swing time, and stance time parameters. For the sake of clarity, these symmetry measures have been omitted in Table 8.2. Generally, the values are shown as mean (± standard deviation). AP and ML variabilities are defined as standard deviations. The body weight estimate is an average value over all available data and is treated as a system-wide valid measure. Gait discrepancies show the range of fluctuation across all gait event definitions and are averaged over the selected gait cycles.

In contrast to Table 8.2, the statistics panel used in our system additionally provides a color coding for left/right statistical values. The color coding indicates the symmetry of the parameter, or in other words which side is more dominant. Figure 8.19 shows an example of the statistics panel for 49 gait cycles. For illustrative purposes, the dynamic gaitogram for this data is shown next to the panel. The asymmetry of the intersection point (20.2%) as well as the gaitogram indicate a strongly dominated left gait. The differences also show stronger activity on the left side in the gait cycle phases ($D_{\text{stance}} = -63.6\%, D_{\text{swing}} = -11.5\%$) and over the whole gait cycle ($D_{\text{total}} = -42.9\%$).

Die approbierte gedruckte Originalversion dieser Diplomarbeit ist an der TU Wien Bibliothek verfügbar.
The approved original version of this thesis is available in print at TU Wien Bibliothek.
TU Bibliothek Your knowledge hub WIEN

The subject starts the weight transfer to the left very early (Timing HSL = −15.6% GC and Δd_2 in the gaitogram). This results in a short left step length of 234 mm. The weight transfer also finished early (Timing TOR = −9.2% GC and Δe_1 in the gaitogram). Contrarily, the weight transfer to the right is well timed, only slightly before the optimal point in time (Timing HSR = −3.4% GC). This results in a larger step length on the right (524 mm) and an overall longer left stance phase (2.5 s). The weight transfer to the right is slow and finishes too late (Timing TOL = 7.1% GC and Δc_2 in the gaitogram). Stance time on the right is therefore comparatively short (1.6 s). Notations in the gaitogram are according to Figure 8.8 and with respect to the mean trajectories.

Measure	Value	Unit	Description
Body Weight Estimate	81	kg	Section 5.2
Ratio - Support	30.7 (±1.6)	%	①
Step Length, Left	537 (±24)	mm	Section 7.1
Step Length, Right	523 (±28)	mm	— » —
Stride Length	1060 (±28)	mm	— » —
Swing Time, Left	0.9 (±0.2)	s	— » —
Stance Time, Left	2.1 (±0.1)	s	— » —
Swing Time, Right	0.8 (±0.1)	s	— » —
Stance Time, Right	2.2 (±0.1)	s	— » —
Double Support Time	1.3 (±0.1)	s	— » —
ML Symmetry	14.5 (±8.8)	%	Section 7.2
AP Variability	10.4	mm	— » —
ML Variability	6	mm	— » —
Timing - Toe Off, Left (T_{TOL})	7 (±3.1)	% GC	②
Timing - Toe Off, Right (T_{TOR})	11.1 (±2.5)	% GC	— » —
Timing - Heel Strike, Left (T_{HSL})	-2.5 (±1.9)	% GC	— » —
Timing - Heel Strike, Right (T_{HSR})	-3.1 (±2.5)	% GC	— » —
Ratio - Force in Swing Phase, Left ($R_{\mathrm{swing},L}$)	13 (±4.1)	%	Section 7.1.2
Ratio - Force in Swing Phase, Right ($R_{\mathrm{swing},R}$)	9.5 (±3.8)	%	— » —
Difference - Stance phase (D_{stance})	-3.4 (±6.2)	%	— » —
Difference - Swing phase (D_{swing})	-4.9 (±6.3)	%	— » —
Difference - Gait cycle (D_{total})	-4.1 (±5.4)	%	— » —
Gait Discrepancy - Toe Off, Left	1.2	% GC	Section 7.1.3
Gait Discrepancy - Toe Off, Right	0.9	% GC	— » —
Gait Discrepancy - Heel Strike, Left	3.4	% GC	— » —
Gait Discrepancy - Heel Strike, Right	5.2	% GC	— » —

Table 8.2: Statistics table example. This table shows statistical values over eight gait cycles. ① The support ratio corresponds to the fraction of support load W_S to body weight W_B (Section 5.2). ② Timing is the offset of the subject's gait event to the machine's gait event, expressed in percentage of the gait cycle. A negative timing indicates the subject's event occurs before the machine's event (Section 7.1.1).

Die approbierte gedruckte Originalversion dieser Diplomarbeit ist an der TU Wien Bibliothek verfügbar.
The approved original version of this thesis is available in print at TU Wien Bibliothek.
TU Bibliothek Your knowledge hub WIEN

Statistics (past 49 cycles)

Description	Value
Body Weight Estimate [kg]	72
Ratio - Support [%]	52.8 (+/- 2.9)
Step Length, Left [mm]	234 (+/- 67)
Step Length, Right [mm]	524 (+/- 20)
Stride Length [mm]	758 (+/- 67)
Swing Time, Left [s]	0.5 (+/- 0.1)
Stance Time, Left [s]	2.5 (+/- 0.1)
Swing Time, Right [s]	1.4 (+/- 0.1)
Stance Time, Right [s]	1.6 (+/- 0.1)
Double Support Time [s]	1.1 (+/- 0.1)
Variability - Anterior/Posterior [mm]	15.2
Variability - Lateral [mm]	7.3
Timing - Toe Off, Left [%GC]	7.1 (+/- 3)
Timing - Toe Off, Right [%GC]	-9.2 (+/- 1.4)
Timing - Heel Strike, Left [%GC]	-15.6 (+/- 1.9)
Timing - Heel Strike, Right [%GC]	-3.4 (+/- 1.7)
Ratio - Force in Swing Phase, Left [%]	10.6 (+/- 2.8)
Ratio - Force in Swing Phase, Right [%]	9.6 (+/- 2.6)
Asymmetry - Intersection Point [%]	20.2 (+/- 12.4)
Difference - Stance Phase [%]	-63.6 (+/- 3.7)
Difference - Swing Phase [%]	-11.5 (+/- 4.7)
Difference - Gait Cycle [%]	-42.9 (+/- 3.6)
Symmetry Index (SI) - Step Length [%]	78.8
Symmetry Angle (SA) - Step Length [%]	23.6
Gait Asymmetry (GA) - Step Length [%]	86.1
Symmetry Ratio (SR) - Step Length [%]	55.3
Symmetry Index (SI) - Swing Time [%]	90.5
Symmetry Angle (SA) - Swing Time [%]	26.9
Gait Asymmetry (GA) - Swing Time [%]	99.3
Symmetry Ratio (SR) - Swing Time [%]	61.6
Symmetry Index (SI) - Stance Time [%]	-42.6
Symmetry Angle (SA) - Stance Time [%]	-13.4
Gait Asymmetry (GA) - Stance Time [%]	-43.4
Symmetry Ratio (SR) - Stance Time [%]	-35
Gait Discrepancy HS, Left [%GC]	6.3
Gait Discrepancy TO, Left [%GC]	2.9
Gait Discrepancy HS, Right [%GC]	10.2
Gait Discrepancy TO, Right [%GC]	5.3

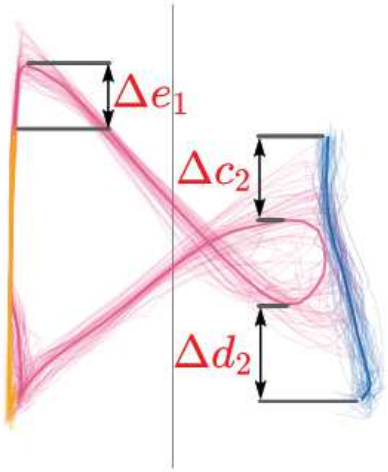

Figure 8.19: *[Screenshots with annotations]* Statistics panel example, additionally with the dynamic gaitogram for reference.

Die approbierte gedruckte Originalversion dieser Diplomarbeit ist an der TU Wien Bibliothek verfügbar.
The approved original version of this thesis is available in print at TU Wien Bibliothek.

Die approbierte gedruckte Originalversion dieser Diplomarbeit ist an der TU Wien Bibliothek verfügbar.
The approved original version of this thesis is available in print at TU Wien Bibliothek.

CHAPTER 9

Results

9.1 Test Data

The recording of test data has been done by the project partners on four different occasions with the following test scenarios and recordings:

- Normal (active) walking (17 x)
- Only actively walking on the right side (17 x)
- Only actively walking on the left side (17 x)
- Avoiding movement (passive walking) (20 x)
- Walking backwards (1 x)

With a few exceptions, each recording contains around 50 gait cycles worth of data. The predefined machine's step length SL_M (left/right) was set to 600 mm. The participant's resulting step length cannot exceed the range $[-\mathrm{SL}_M, \mathrm{SL}_M]$. The walking speed (cadence) was fixed and set to 40 steps per minute. Test data was recorded at a frequency of 10 Hz, i.e. a sampling rate of 100 ms. Walking backwards was performed with different settings, as is mentioned in Section 9.4.2.

The following participants were involved:

- Seven healthy participants
- One participant with multiple sclerosis (MS)

Die approbierte gedruckte Originalversion dieser Diplomarbeit ist an der TU Wien Bibliothek verfügbar.
The approved original version of this thesis is available in print at TU Wien Bibliothek.
TU Bibliothek Your knowledge hub WIEN

In the following sections we identify each recording with the participant's identification code ($A - H$) and a test number. For example, the second test recording of participant B would be labeled as B_2. The amount of recordings is different between participants:

- Participant A: 16 recordings (active 4, left 4, right 4, passive 3, backwards 1)
- Participant B: 8 recordings (active 2, left 2, right 2, passive 2)
- Participant C: 10 recordings (active 2, left 2, right 2, passive 4)
- Participant D: 10 recordings (active 2, left 2, right 2, passive 4)
- Participant E: 9 recordings (active 2, left 2, right 2, passive 3)
- Participant F: 4 recordings (active 1, left 1, right 1, passive 1)
- Participant G: 12 recordings (active 3, left 3, right 3, passive 2, therapy 1)
- Participant H: 4 recordings (active 1, left 1, right 1, passive 1)

Participant H with MS is discussed separately in Section 9.4.1. Walking backwards of participant A is shown in Section 9.4.2. The therapy training session of participant G can be found in Section 9.4.3.

9.2 Analysis

The analysis of the test data is split into two sections. Section 9.3 analyzes the test results of the healthy participants. It discusses normal walking, and actively walking on the left and right side, respectively. Section 9.4 concentrates on selected case studies. It highlights important and conspicuous test cases. Additionally, it discusses some recordings of passive walking to demonstrate the robustness of the GED algorithm. Passive walking was originally recorded in the context of EEG analysis. The test cases were used to train a classifier in order to differentiate the brain's activity during active and passive walking. Since we do not expect the results of passive walking to be meaningful in the context of gait analysis, we excluded the majority of them from this thesis. Walking backwards was chosen as a test case, since an earlier recording (D_1) showed behavior reminiscent of walking backwards. In order to verify this, the separate recording A_{16} was created as a reference (Section 9.4.2). As it turned out (Section 9.4.7), test recording D_1 indeed contained sections, where the participant was walking backwards.

Gait Discrepancy

As discussed in Section 7.1.3, the GD (i.e. $\mathrm{GD_{HSL}}, \mathrm{GD_{HSR}}, \mathrm{GD_{TOL}}, \mathrm{GD_{TOR}}$) for each gait event corresponds to the events' range of fluctuation. It indicates the timespan between the earliest and the latest occurring gait event of the respective kind. A large

Die approbierte gedruckte Originalversion dieser Diplomarbeit ist an der TU Wien Bibliothek verfügbar.
The approved original version of this thesis is available in print at TU Wien Bibliothek.
TU Bibliothek Your knowledge hub WIEN

GD indicates that the algorithms do not agree on the same place of occurrence for an event and this might indicate a non-standard gait pattern.

In the following results, we will, where appropriate, show the average gait discrepancy over N gait cycles

$$\mathrm{GD}_{\mathrm{avg}} = \frac{1}{N}\sum_{i=1}^{N}(\mathrm{GD}_{\mathrm{HSL}} + \mathrm{GD}_{\mathrm{HSR}} + \mathrm{GD}_{\mathrm{TOL}} + \mathrm{GD}_{\mathrm{TOR}}) \tag{9.1}$$

instead of the individual ones. This retains clarity and serves as a single indicator for the agreement between different algorithms.

Sensitivity to Outliers

Gait discrepancy is the range defined by the earliest and latest occurrence of standard gait events. It is therefore also susceptible to only one event definition being out of place. Figure 9.1 shows an example where event TO4 has a large influence on the gait discrepancy. As a reminder, TO4 is defined as the most anterior pressure point of the lifting foot after the midpoint. In case there is no clear heel to toe pressure movement along one foot, TO4 might be different from the actual TO event. To conclude, gait discrepancy might indicate that a gait pattern differs from standard definitions, but does not clearly indicate which behavior is responsible for the large deviations.

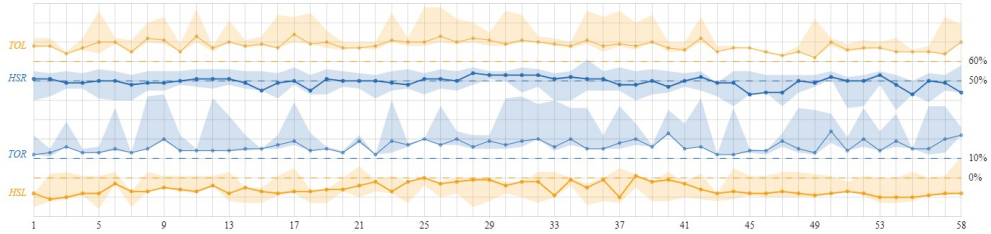

(a) Including TO4. $\mathrm{GD}_{\mathrm{TOL}} = 8.6\%$ GC, $\mathrm{GD}_{\mathrm{TOR}} = 12.3\%$ GC.

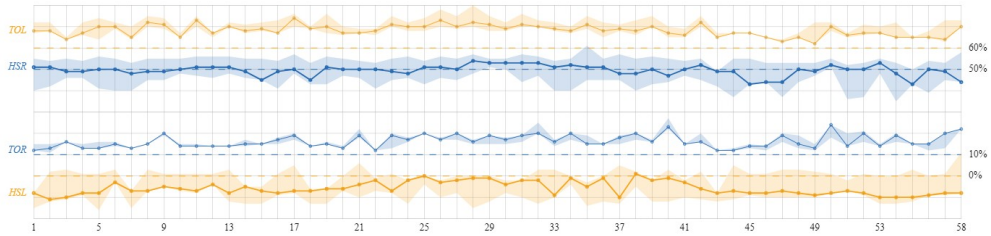

(b) Excluding TO4. $\mathrm{GD}_{\mathrm{TOL}} = 4.4\%$ GC, $\mathrm{GD}_{\mathrm{TOR}} = 2.4\%$ GC.

Figure 9.1: *[Screenshots]* Influence of one standard gait event on gait discrepancy. Test recording G_3. In this recording, TO4 differs from the other TO event definitions. This nearly doubles the range of fluctuation for TOL and increases the range for TOR by more than a factor of five. Shown are the average GD values over all gait cycles.

Die approbierte gedruckte Originalversion dieser Diplomarbeit ist an der TU Wien Bibliothek verfügbar.
The approved original version of this thesis is available in print at TU Wien Bibliothek.
TU Bibliothek Your knowledge hub WIEN

9.3 Healthy Participants

9.3.1 Normal Walking

Participants were not given specific instructions, but to walk normally within the PerPedes system. Both the dynamic gaitograms (Figure 9.2) as well as the statistics (Table 9.1) show that participants tend to start the weight transfer too early (i.e. heel strikes occur ahead of the machine's optimal time). One notable exception is test recording G_2, where on average HSR is happening slightly too late (3.4% GC). Gaitograms can expose different gaits. Sharp corners in the CoP's trajectory indicate quick weight transfers (e.g. B_2). Round corners show gradual weight transfers (e.g. A_3, E_1). Dragging the foot during swing phase leads to gaps between single support stance lines and CoP trajectory (e.g. A_3, C_1). Furthermore, test recordings D_1 and D_2 both show unusual behavior, which is also clearly visible as outliers in Figure 9.3. Both recordings are examined separately in Section 9.4.5 and Section 9.4.7.

Step Length Variability

Table 9.1 shows that the standard deviation of both SLL and SLR can be remarkably large. In the following, it is highlighted why this variability in step length occurred within the recorded test data.

Step length variability is analyzed with the coefficient of variation (CV). It is defined as the ratio between the standard deviation to the (absolute value of the) mean, often expressed as a percentage:

$$\mathrm{CV} = 100\% \cdot \frac{\mathrm{std}}{|\mathrm{mean}|} \tag{9.2}$$

Table 9.2 lists the CV for the left and right step lengths, as well as the stride length. It can be observed that the CV values are large, especially in comparison with the literature. Collins and Kuo [CK13] report a CV for step lengths during overground walking of 2.0%. Sekiya et al. [SNIF97] determined mean step lengths and mean standard deviation of step lengths over all participants for different walking speeds. The CV for the step length can be extracted from their data and shows a minimum of 2.5% at the subjects' preferred walking speed and a maximum of 7.2% during the "slowest walking" test scenario.

Generally speaking, the CV is larger, the closer the mean value is to zero (and it is undefined at zero). Therefore, the smaller the subject's achieved mean step length is, the smaller the respective CV can become. Additionally, the CV depends on the standard deviation. As mentioned before, the participants' heel strikes generally occur too early in comparison to the optimal time given by the machine's movements. The step length is solely dependent on the timing of the corresponding heel strike (Section 7.1). An earlier heel strike leads to a shorter step length and in turn leads to a higher CV. Furthermore, an earlier heel strike typically occurs during a time when the pressure plates are still moving. This means that small variations in the timing of the heel strike across multiple

Die approbierte gedruckte Originalversion dieser Diplomarbeit ist an der TU Wien Bibliothek verfügbar.
The approved original version of this thesis is available in print at TU Wien Bibliothek.
TU Bibliothek Your knowledge hub WIEN

gait cycles can lead to a large variation in the pressure plate's position and therefore to a large standard deviation in the resulting step length.

Test recording B_2 is selected as a demonstrating example. The HSL is timed well (T_{HSL} in Table 9.1) with a low standard deviation of 4% GC. Nonetheless, the SLL's standard deviation is 149 mm. This, in relation to the already small SLL (mean: 161 mm), caused by the very early HSL (mean: −17.1% GC), leads to a large CV_{SLL} of 92.6% (Table 9.2). Figure 9.4 shows the graphical analysis of test recording B_2. Standard algorithms agree on the location of the gait events. This can be seen with the low average gait discrepancy of $\text{GD}_{\text{avg}} = 7\%$ GC as well as visually in Figure 9.4a. The GRF visualization in Figure 9.4b shows occurring negative forces, which indicate that the feet are pulling on the foot straps. The gait events are rather ordinarily located at or near the GRF's zero crossings. However, it can also be seen that the left heel strikes are clustered and occur too early between −25% GC and −10% GC before the optimal timing. This corresponds to the time when the pressure plate of the striking foot is in full motion. The plate is in full motion around −20% GC before the machine's heel strike event. In Figure 4.4, this relates to the inflection point at 80% GC for the left pressure plate's position and to the inflection point at 30% GC for the right pressure plate. These inflection points represent the maxima of the respective pressure plate's velocity function (i.e. the first derivative of the pressure plate's position).

From a technical point of view, the large variability in step length is plausible and can be explained with the heel strikes occurring too early. Nonetheless, the reasons for this early timing are speculative. Our assumption is that the participants started transferring their weight earlier because of the machine settings used during the tests. Recordings have been performed with a cadence of 40 steps per minute and a machine's step length of 600 mm. This corresponds to a slow walking speed of just 0.4 m/s, or equivalently 1.44 km/h. Collins and Kuo [CK13] state that there is a tendency in human gait for the step length to increase with walking speed. This could also mean that the step length shortens with slower walking speeds. As a consequence of the used settings, while the striking foot was slowly being moved forward by the machine over a large distance, the participants might have involuntarily shortened their steps. In turn, this might have lead to earlier heel strikes, shorter step lengths, and higher variability.

Die approbierte gedruckte Originalversion dieser Diplomarbeit ist an der TU Wien Bibliothek verfügbar.
The approved original version of this thesis is available in print at TU Wien Bibliothek.
TU Bibliothek Your knowledge hub WIEN

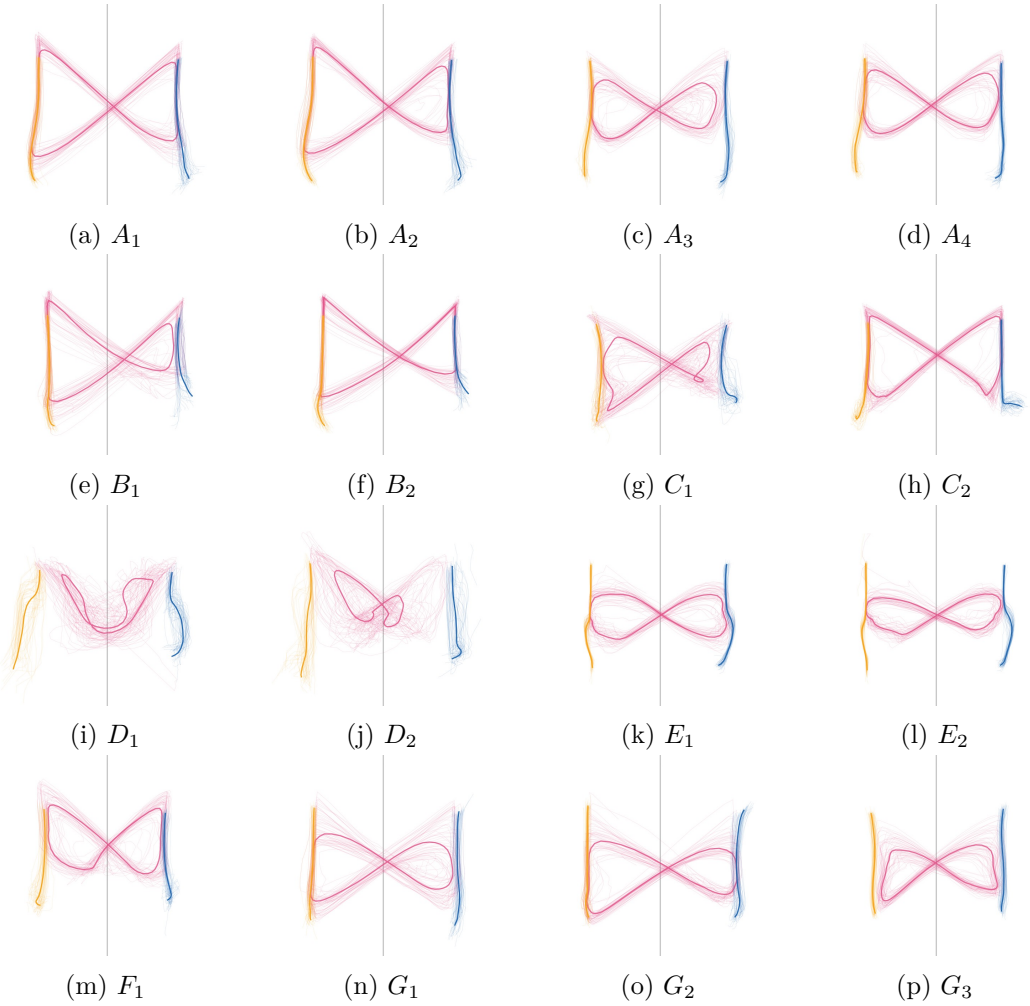

(a) A_1 (b) A_2 (c) A_3 (d) A_4

(e) B_1 (f) B_2 (g) C_1 (h) C_2

(i) D_1 (j) D_2 (k) E_1 (l) E_2

(m) F_1 (n) G_1 (o) G_2 (p) G_3

Figure 9.2: *[Screenshots]* Normal (active) walking. Dynamic gaitograms.

Die approbierte gedruckte Originalversion dieser Diplomarbeit ist an der TU Wien Bibliothek verfügbar.
The approved original version of this thesis is available in print at TU Wien Bibliothek.

ID	Gait	SLL (mm)	SLR (mm)	T_{HSL} (% GC)	T_{HSR} (% GC)	T_{TOL} (% GC)	T_{TOR} (% GC)	D_{total} (%)	GD_{avg} (% GC)
A_1		301 ± 92	418 ± 68	−13.1 ± 3	−9.1 ± 3	−2.9 ± 4	−6.8 ± 3	−8.0 ± 7	15
A_2		205 ± 81	396 ± 55	−16.1 ± 2	−10.0 ± 2	−2.2 ± 4	−7.2 ± 3	−13.8 ± 6	13
A_3		292 ± 115	325 ± 78	−13.2 ± 4	−12.4 ± 3	0.9 ± 4	1.9 ± 3	−3.7 ± 9	35
A_4		262 ± 74	273 ± 68	−14.4 ± 2	−14.2 ± 3	−0.3 ± 3	1.0 ± 3	1.6 ± 4	31
B_1		121 ± 227	421 ± 84	−18.0 ± 7	−8.6 ± 4	−5.0 ± 5	−16.6 ± 6	−19.6 ± 7	10
B_2		161 ± 149	364 ± 61	−17.1 ± 4	−11.3 ± 2	−8.4 ± 2	−17.4 ± 4	−11.9 ± 4	7
C_1		466 ± 118	518 ± 69	−6.0 ± 5	−3.1 ± 4	1.3 ± 3	−0.3 ± 6	−11.5 ± 7	17
C_2		406 ± 88	458 ± 66	−9.4 ± 3	−7.1 ± 3	−3.7 ± 2	−6.0 ± 2	−1.0 ± 4	18
D_1		−398 ± 312	−375 ± 352	−37.3 ± 12	−37.3 ± 20	−28.7 ± 18	−29.8 ± 12	−0.4 ± 11	49
D_2		110 ± 362	−32 ± 443	−19.0 ± 15	−22.0 ± 22	−13.5 ± 19	−12.1 ± 17	−10.8 ± 18	33
E_1		437 ± 29	492 ± 49	−8.4 ± 1	−5.1 ± 3	7.2 ± 2	5.0 ± 3	−3.4 ± 4	33
E_2		456 ± 42	470 ± 55	−7.4 ± 2	−6.4 ± 3	6.3 ± 1	7.7 ± 2	0.4 ± 4	34
F_1		268 ± 113	226 ± 165	−13.7 ± 4	−15.0 ± 5	−4.5 ± 4	−5.0 ± 3	7.3 ± 9	25
G_1		435 ± 112	477 ± 95	−7.5 ± 5	−5.1 ± 6	4.2 ± 6	3.7 ± 4	−7.4 ± 7	22
G_2		536 ± 57	573 ± 13	−1.2 ± 5	3.4 ± 3	8.6 ± 3	6.4 ± 3	−9.9 ± 6	16
G_3		467 ± 52	544 ± 28	−5.8 ± 3	−0.5 ± 3	8.2 ± 3	6.3 ± 3	−4.9 ± 5	42

Table 9.1: Normal (active) walking. Statistical data (1). Step lengths SLL and SLR, gait event timings T, gait cycle force difference (i.e. balance) D_{total}, and average gait discrepancy GD_{avg}. Balance highlighted if $|D_{total}| \geq 10\%$.

Die approbierte gedruckte Originalversion dieser Diplomarbeit ist an der TU Wien Bibliothek verfügbar.
The approved original version of this thesis is available in print at TU Wien Bibliothek.
TU Bibliothek Your knowledge hub WIEN

ID	SLL (mm)	CV_{SLL} (%)	SLR (mm)	CV_{SLR} (%)	Stride (mm)	CV_{Stride} (%)	Var_{AP} (mm)	Var_{ML} (mm)
A_1	301 ± 92	30.5	418 ± 68	16.3	719 ± 130	18.1	13.6	5.1
A_2	205 ± 81	39.4	396 ± 55	13.9	601 ± 105	17.4	11.5	5.4
A_3	292 ± 115	39.3	325 ± 78	24.0	617 ± 128	20.8	14.3	9.0
A_4	262 ± 74	28.4	273 ± 68	25.1	534 ± 104	19.4	10.7	4.3
B_1	121 ± 227	187.9	421 ± 84	19.9	542 ± 284	52.5	25.2	8.9
B_2	161 ± 149	92.6	364 ± 61	16.8	525 ± 195	37.1	8.9	6.4
C_1	466 ± 118	25.2	518 ± 69	13.3	983 ± 166	16.8	17.8	8.0
C_2	406 ± 88	21.7	458 ± 66	14.4	864 ± 120	13.9	8.7	3.9
D_1	−398 ± 312	78.3	−375 ± 352	94.0	−773 ± 619	80.0	48.1	20.8
D_2	110 ± 362	328.7	−32 ± 443	1378.5	78 ± 731	935.2	41.9	18.4
E_1	437 ± 29	6.7	492 ± 49	9.9	930 ± 50	5.4	7.7	5.2
E_2	456 ± 42	9.1	470 ± 55	11.7	927 ± 69	7.4	10.1	4.8
F_1	268 ± 113	42.1	226 ± 165	72.9	494 ± 246	49.7	19.6	8.0
G_1	435 ± 112	25.8	477 ± 95	19.9	913 ± 198	21.7	18.6	8.4
G_2	536 ± 57	10.7	573 ± 13	2.3	1109 ± 59	5.3	9.6	6.6
G_3	467 ± 52	11.2	544 ± 28	5.1	1011 ± 66	6.5	12.3	4.5

Table 9.2: Normal (active) walking. Statistical data (2). Mean ± standard deviation for step length left SLL, step length right SLR, and stride length Stride. Coefficient of variation for SLL CV_{SLL}, for SLR CV_{SLL}, and for the stride length CV_{Stride}. Coefficients of variation above 40% are highlighted in red. Variability in AP direction is given by Var_{AP} and in ML direction by Var_{ML}.

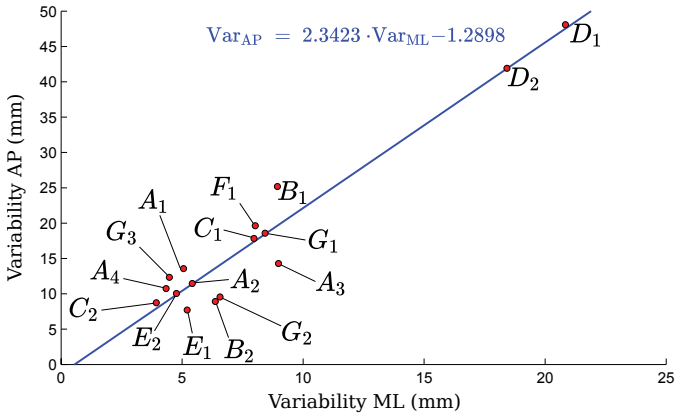

Figure 9.3: Normal (active) walking. Variability of the intersection point in AP direction plotted against the variability in ML direction. A linear correlation between both variabilities exists. Regression line in a least squares sense shown in blue. The corresponding data is listed in Table 9.2.

Die approbierte gedruckte Originalversion dieser Diplomarbeit ist an der TU Wien Bibliothek verfügbar.
The approved original version of this thesis is available in print at TU Wien Bibliothek.
TU Bibliothek Your knowledge hub WIEN

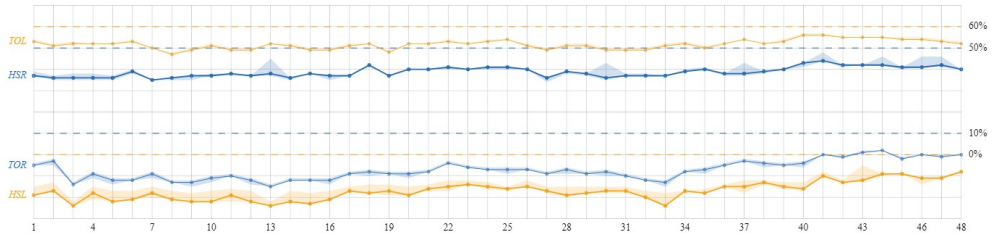

(a) Gait event consistency graph

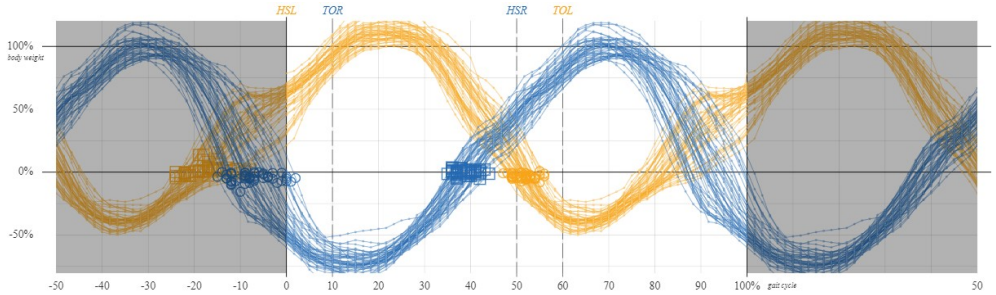

(b) GRF event visualization

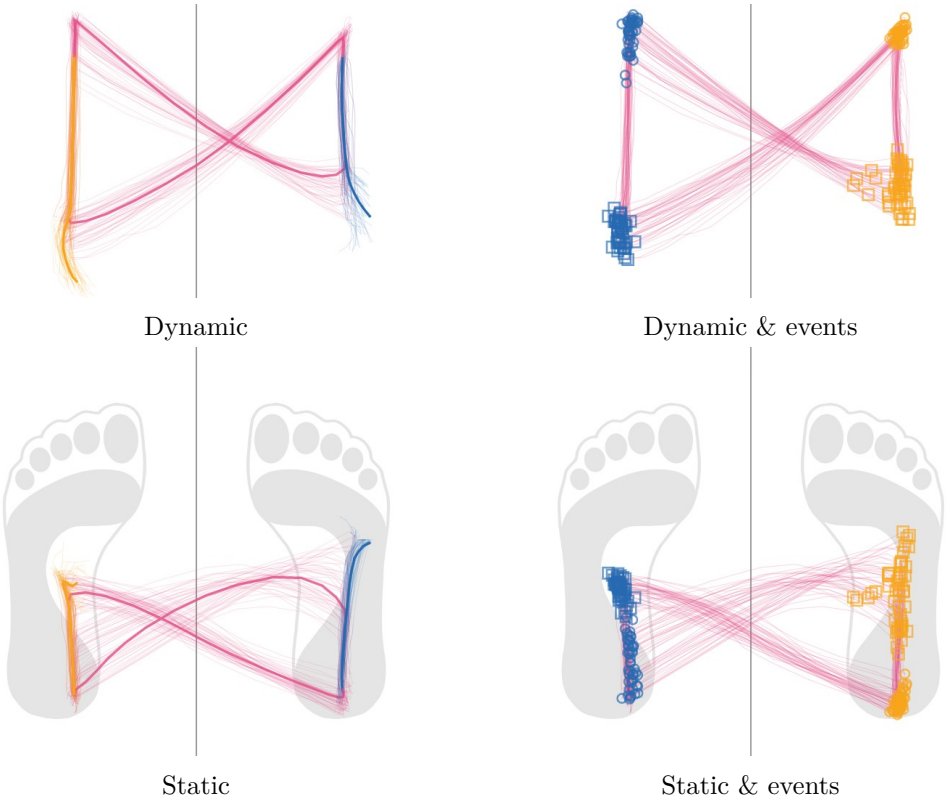

(c) Gaitogram visualizations

Figure 9.4: *[Screenshots]* Normal (active) walking. Test recording B_2.

Die approbierte gedruckte Originalversion dieser Diplomarbeit ist an der TU Wien Bibliothek verfügbar.
The approved original version of this thesis is available in print at TU Wien Bibliothek.

9.3.2 Walking on the Left

Participants were instructed to only actively walk on the left side. Since instructions were up for interpretation, participants showed different behavior. Dynamic gaitograms are given in Figure 9.5 and corresponding statistics in Table 9.3. The results ranged from avoiding contact (C_4, D_3, D_4) to reducing weight on the right side. In general, test data shows that the right step length is larger than the left step length (Table 9.3). Noteworthy exceptions are test recordings D_3 and D_4 which additionally show exceptionally high variance readings. This discrepancy in the step length can be explained by examining the gait event timings. Generally speaking, weight transfers to the left occur as early as possible, in order to avoid putting weight on the right side. Simultaneously, a weight transfer to the right occurs around the time it becomes inevitable, i.e. the time when the right pressure plate is most frontal. Weight is then transferred back to the left at the next appropriate moment. Additionally, as expected, we observe that the force difference D_{total}, averaged over all gait cycles, consistently shows more applied force on the left side for all test recordings.

Die approbierte gedruckte Originalversion dieser Diplomarbeit ist an der TU Wien Bibliothek verfügbar.
The approved original version of this thesis is available in print at TU Wien Bibliothek.

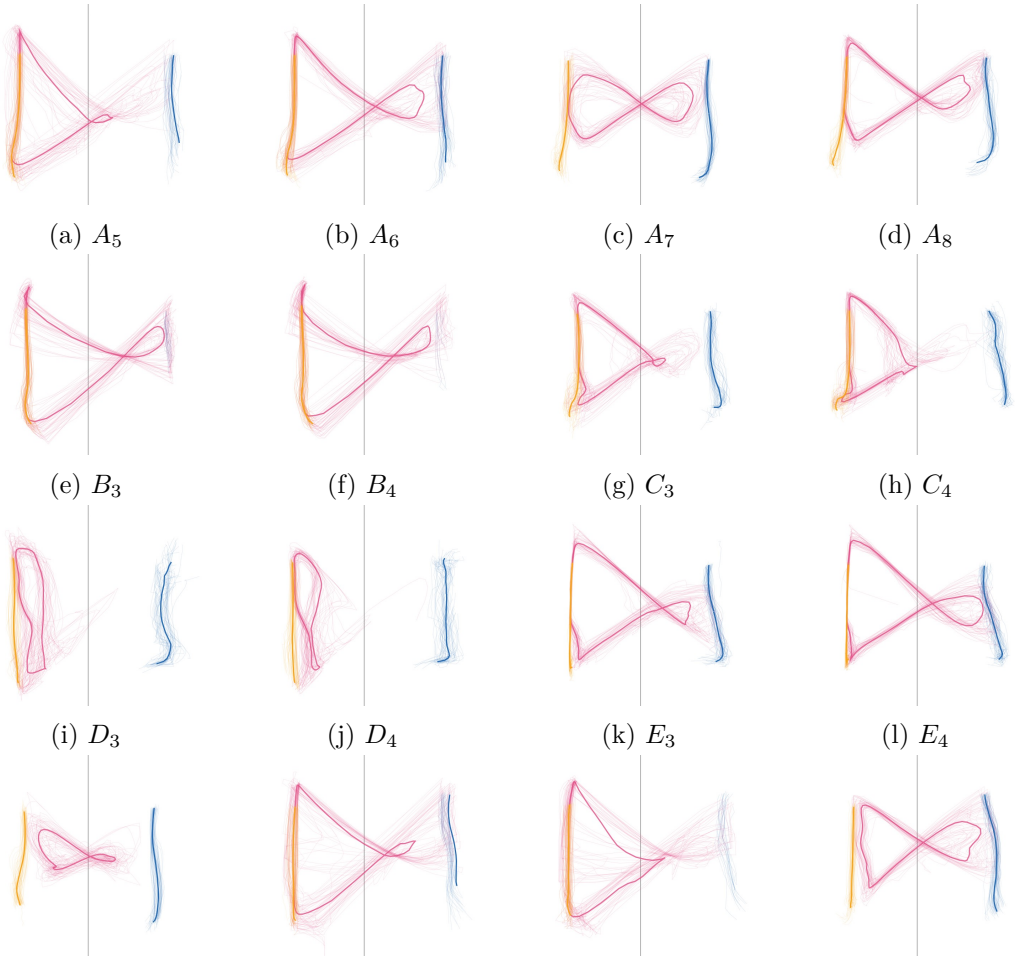

(a) A_5 (b) A_6 (c) A_7 (d) A_8

(e) B_3 (f) B_4 (g) C_3 (h) C_4

(i) D_3 (j) D_4 (k) E_3 (l) E_4

(m) F_2 (n) G_4 (o) G_5 (p) G_6

Figure 9.5: *[Screenshots]* Actively walking on the left. Dynamic gaitograms.

Die approbierte gedruckte Originalversion dieser Diplomarbeit ist an der TU Wien Bibliothek verfügbar.
The approved original version of this thesis is available in print at TU Wien Bibliothek.

ID	Gait	SLL (mm)	SLR (mm)	T_{HSL} (% GC)	T_{HSR} (% GC)	T_{TOL} (% GC)	T_{TOR} (% GC)	D_{total} (%)	GD_{avg} (% GC)
A_5		−199 ± 259	531 ± 48	−26.9 ± 8	−1.6 ± 5	1.6 ± 4	−21.3 ± 10	−49.4 ± 10	19
A_6		28 ± 168	512 ± 49	−20.8 ± 4	−3.9 ± 3	1.1 ± 5	−12.5 ± 4	−39.0 ± 7	16
A_7		153 ± 83	353 ± 66	−17.8 ± 2	−11.4 ± 3	1.6 ± 3	−0.1 ± 3	−19.3 ± 8	38
A_8		120 ± 71	421 ± 51	−18.7 ± 2	−8.9 ± 2	0.6 ± 4	−7.4 ± 2	−34.4 ± 6	24
B_3		20 ± 209	568 ± 14	−20.9 ± 6	0.9 ± 2	−0.9 ± 4	−23.7 ± 3	−39.5 ± 4	8
B_4		−173 ± 156	569 ± 18	−25.8 ± 4	1.6 ± 2	−3.4 ± 4	−24.3 ± 2	−41.8 ± 4	11
C_3		245 ± 129	536 ± 24	−14.9 ± 4	−2.4 ± 2	4.6 ± 5	−7.0 ± 3	−38.5 ± 6	18
C_4		181 ± 164	534 ± 21	−16.7 ± 5	−2.7 ± 2	0.9 ± 5	−8.8 ± 4	−47.7 ± 4	19
D_3		417 ± 235	389 ± 368	−4.7 ± 11	−3.4 ± 15	0.0 ± 14	−5.4 ± 10	−65.9 ± 9	20
D_4		448 ± 221	197 ± 268	−6.6 ± 8	9.4 ± 20	10.5 ± 18	−7.8 ± 2	−72.1 ± 8	21
E_3		262 ± 99	519 ± 28	−14.6 ± 3	−3.7 ± 2	7.7 ± 4	−7.9 ± 2	−41.4 ± 5	26
E_4		219 ± 75	524 ± 20	−15.9 ± 2	−3.4 ± 2	7.3 ± 3	−9.0 ± 1	−42.9 ± 4	25
F_2		314 ± 104	488 ± 64	−12.2 ± 4	−4.5 ± 4	6.6 ± 4	−0.5 ± 3	−21.5 ± 7	30
G_4		22 ± 240	552 ± 45	−20.9 ± 6	2.9 ± 5	1.4 ± 5	−20.9 ± 11	−45.8 ± 5	11
G_5		−90 ± 238	525 ± 131	−23.8 ± 6	7.7 ± 7	6.3 ± 7	−26.5 ± 10	−49.0 ± 5	11
G_6		284 ± 91	508 ± 33	−13.3 ± 3	−3.9 ± 2	3.8 ± 4	−3.8 ± 2	−34.1 ± 4	22

Table 9.3: Actively walking on the left. Statistical data. Step lengths SLL and SLR, gait event timings T, gait cycle force difference (i.e. balance) D_{total}, and average gait discrepancy GD_{avg}. Balance highlighted if $|D_{total}| \geq 10\%$.

Die approbierte gedruckte Originalversion dieser Diplomarbeit ist an der TU Wien Bibliothek verfügbar.
The approved original version of this thesis is available in print at TU Wien Bibliothek.
TU Bibliothek Your knowledge hub WIEN

9.3.3 Walking on the Right

Walking on the right produces analogous data to walking on the left side. Dynamic gaitograms are given in Figure 9.6 and corresponding statistics in Table 9.4. The step length on the left is generally larger than on the right, except for test recordings B_5, B_6, D_6. D_{total} shows more applied force on the right side for all test recordings.

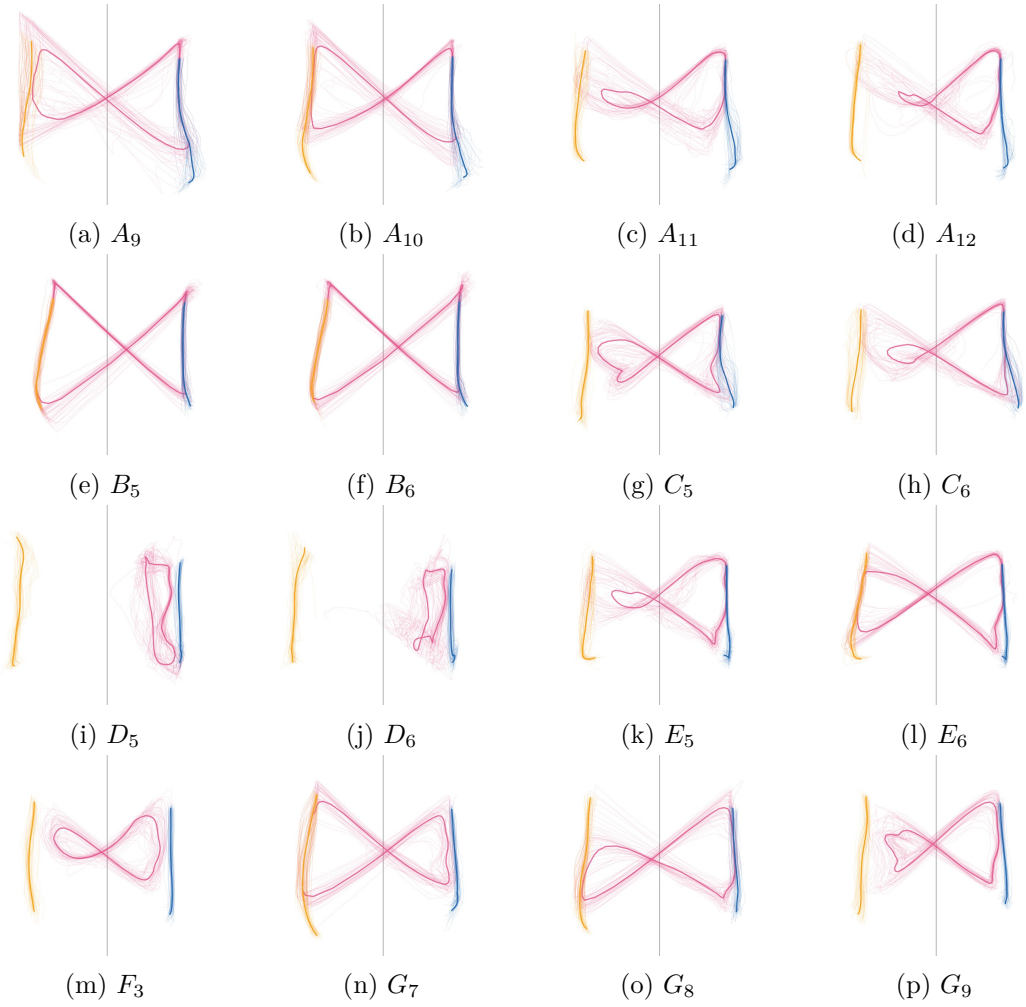

(a) A_9 (b) A_{10} (c) A_{11} (d) A_{12}

(e) B_5 (f) B_6 (g) C_5 (h) C_6

(i) D_5 (j) D_6 (k) E_5 (l) E_6

(m) F_3 (n) G_7 (o) G_8 (p) G_9

Figure 9.6: *[Screenshots]* Actively walking on the right. Dynamic gaitograms.

Die approbierte gedruckte Originalversion dieser Diplomarbeit ist an der TU Wien Bibliothek verfügbar.
The approved original version of this thesis is available in print at TU Wien Bibliothek.

ID	Gait	SLL (mm)	SLR (mm)	T_{HSL} (% GC)	T_{HSR} (% GC)	T_{TOL} (% GC)	T_{TOR} (% GC)	D_{total} (%)	GD_{avg} (% GC)
A_9		411 ± 78	239 ± 177	−9.1 ± 4	−15.0 ± 5	−12.7 ± 5	−3.6 ± 6	25.5 ± 10	11
A_{10}		348 ± 85	229 ± 133	−11.6 ± 3	−15.6 ± 4	−7.7 ± 4	−6.4 ± 5	20.2 ± 12	10
A_{11}		450 ± 77	137 ± 78	−7.1 ± 4	−18.2 ± 2	−5.9 ± 2	2.4 ± 5	33.9 ± 9	27
A_{12}		468 ± 69	48 ± 196	−6.4 ± 3	−20.8 ± 6	−6.8 ± 2	1.4 ± 5	38.9 ± 7	33
B_5		450 ± 46	520 ± 33	−7.8 ± 2	−3.9 ± 2	−11.2 ± 2	−12.1 ± 2	21.9 ± 4	5
B_6		431 ± 54	486 ± 31	−8.7 ± 2	−6.2 ± 2	−13.8 ± 2	−12.6 ± 2	22.4 ± 5	5
C_5		528 ± 22	451 ± 48	−3.2 ± 2	−7.7 ± 2	−2.0 ± 2	4.7 ± 3	24.2 ± 4	14
C_6		522 ± 43	284 ± 125	−3.5 ± 3	−13.7 ± 4	−4.9 ± 1	4.4 ± 5	34.5 ± 7	18
D_5		456 ± 233	272 ± 364	4.5 ± 15	11.7 ± 17	12.5 ± 19	9.8 ± 16	60.5 ± 5	25
D_6		341 ± 273	429 ± 287	−0.3 ± 16	−6.2 ± 11	−6.7 ± 10	−1.2 ± 15	61.0 ± 11	24
E_5		500 ± 25	138 ± 177	−5.2 ± 2	−17.8 ± 5	−5.6 ± 5	3.5 ± 5	39.5 ± 7	30
E_6		506 ± 27	354 ± 79	−4.8 ± 2	−11.5 ± 3	−5.5 ± 2	2.4 ± 4	33.7 ± 3	22
F_3		427 ± 65	51 ± 232	−7.9 ± 3	−19.9 ± 7	−7.6 ± 6	0.7 ± 3	34.0 ± 6	34
G_7		465 ± 39	405 ± 45	−7.2 ± 2	−9.7 ± 2	−3.1 ± 2	−1.2 ± 3	28.4 ± 5	18
G_8		558 ± 21	432 ± 45	0.0 ± 3	−8.6 ± 2	−2.7 ± 3	10.9 ± 4	36.8 ± 6	20
G_9		463 ± 46	387 ± 110	−6.2 ± 2	−9.8 ± 3	−2.6 ± 2	1.9 ± 3	29.9 ± 5	26

Table 9.4: Actively walking on the right. Statistical data. Step lengths SLL and SLR, gait event timings T, gait cycle force difference (i.e. balance) D_{total}, and average gait discrepancy GD_{avg}. Balance highlighted if $|D_{total}| \geq 10\%$.

Die approbierte gedruckte Originalversion dieser Diplomarbeit ist an der TU Wien Bibliothek verfügbar.
The approved original version of this thesis is available in print at TU Wien Bibliothek.
TU Bibliothek Your knowledge hub WIEN

9.4 Noteworthy Case Studies

9.4.1 Multiple Sclerosis Participant

The only non-healthy participant with MS (EDSS score of 4.0) shows signs of monoparesis in the left leg with a weakness in dorsiflexion leading to foot drop. As we have established in Section 2.6, literature suggests that hemiplegic stroke patients show gait asymmetry, leading to a longer step length, longer swing phase, and shorter stance phase with the paretic leg. Although we could not identify studies regarding MS patients, this gait asymmetry might also hold for monoparesis in general. Statistics are summarized in Table 9.5, while visualizations can be found in Figure 9.7.

In accordance with the aforementioned studies, the examination of the recorded test data shows the following distinctive features. Step length on the paretic (left) side is larger than on the nonparetic side (489 mm vs. 454 mm) with similar variances on both sides. Furthermore, swing time ($T_{\text{swing},L}$ vs. $T_{\text{swing},R}$) is longer, while stance time ($T_{\text{stance},L}$ vs. $T_{\text{stance},R}$) is shorter for the paretic side. Comparing gait event timings, one can observe that the average length of double support when transferring weight from left to right (i.e. HSR $\rightarrow$ TOL) is $6.8 + 10 - 1.2 = 15.6\%$ GC[1], while the weight transfer to the paretic leg (i.e. HSL $\rightarrow$ TOR) lasts $4.3 + 10 + 5.4 = 19.7\%$ GC. In other words, the weight transfer to the paretic leg starts later and takes longer than to the contralateral side. The nonparetic leg exerts more force during both stance (D_{stance}) and swing phase (D_{swing}). Furthermore, since HSR occurs earlier than HSL, the force ratio in the swing phase ($R_{\text{swing},R}$) for the nonparetic leg is also larger than for the paretic side.

The GRF visualization (Figure 9.7b) shows more variance in the amplitude on both sides during the left stance phase (i.e. between HSL and TOL) in contrast to the right stance phase. This suggests that forces can be controlled more precisely during the nonparetic leg's stance phase. In addition to the statistical parameters, one can observe in both dynamic gaitograms (Figure 9.7c) that the variance of the CoP's trajectory is higher on the paretic side. Furthermore, the static gaitogram shows that utilization of the left foot on average (mean trajectory of the CoP) starts more frontal than on the right. This could be an indication of the subject's foot drop, leading to initial contacts located at the middle of the foot rather than the heel.

[1] $6.8 + 10 - 1.2 = 15.6\%$ GC: 6.8% GC before the machine's HSR event, 10% GC is the machine's double support phase between HSR and TOL, and 1.2% GC before the machine's TOL event.

Die approbierte gedruckte Originalversion dieser Diplomarbeit ist an der TU Wien Bibliothek verfügbar.
The approved original version of this thesis is available in print at TU Wien Bibliothek.
TU Bibliothek Your knowledge hub WIEN

SLL (mm)	SLR (mm)	T_{HSL} (% GC)	T_{HSR} (% GC)	T_{TOL} (% GC)	T_{TOR} (% GC)	D_{total} (%)	GD_{avg} (% GC)
489 ± 61	454 ± 69	−4.3 ± 3	−6.8 ± 3	−1.2 ± 2	5.4 ± 5	11.8 ± 7	15

$T_{\text{swing},L}$ (s)	$T_{\text{swing},R}$ (s)	$T_{\text{stance},L}$ (s)	$T_{\text{stance},R}$ (s)	D_{swing} (%)	D_{stance} (%)	$R_{\text{swing},L}$ (%)	$R_{\text{swing},R}$ (%)
1.1 ± 0.1	0.8 ± 0.2	1.9 ± 0.1	2.2 ± 0.2	6.6 ± 4.4	15.5 ± 9.2	2.7	7.3

Table 9.5: Participant with MS. Statistical data for test recording H_1. Step lengths SLL and SLR, gait event timings $T_{\text{HSL}}, T_{\text{HSR}}, T_{\text{TOL}}, T_{\text{TOR}}$, average gait discrepancy GD_{avg}, swing times T_{swing}, stance times T_{stance}, force difference during swing phase D_{swing}, stance phase D_{stance} and the whole gait cycle D_{total}, as well as force ratios during swing phase R_{swing}.

Die approbierte gedruckte Originalversion dieser Diplomarbeit ist an der TU Wien Bibliothek verfügbar.
The approved original version of this thesis is available in print at TU Wien Bibliothek.

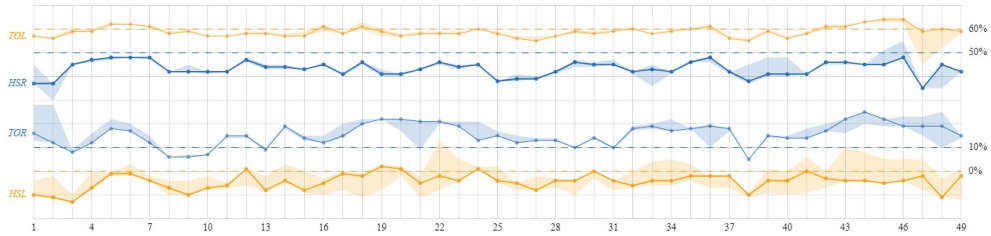

(a) Gait event consistency graph

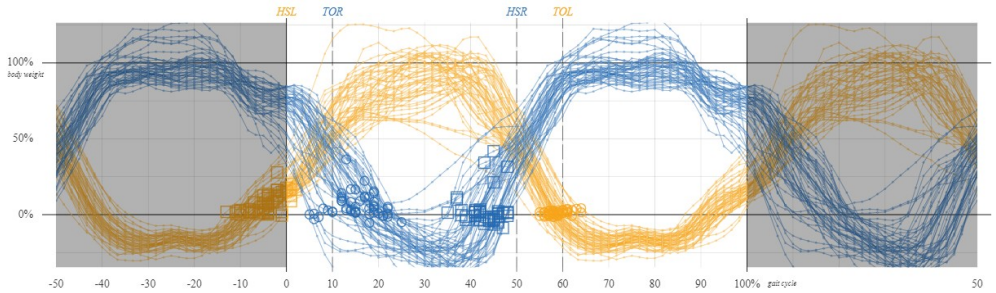

(b) GRF event visualization

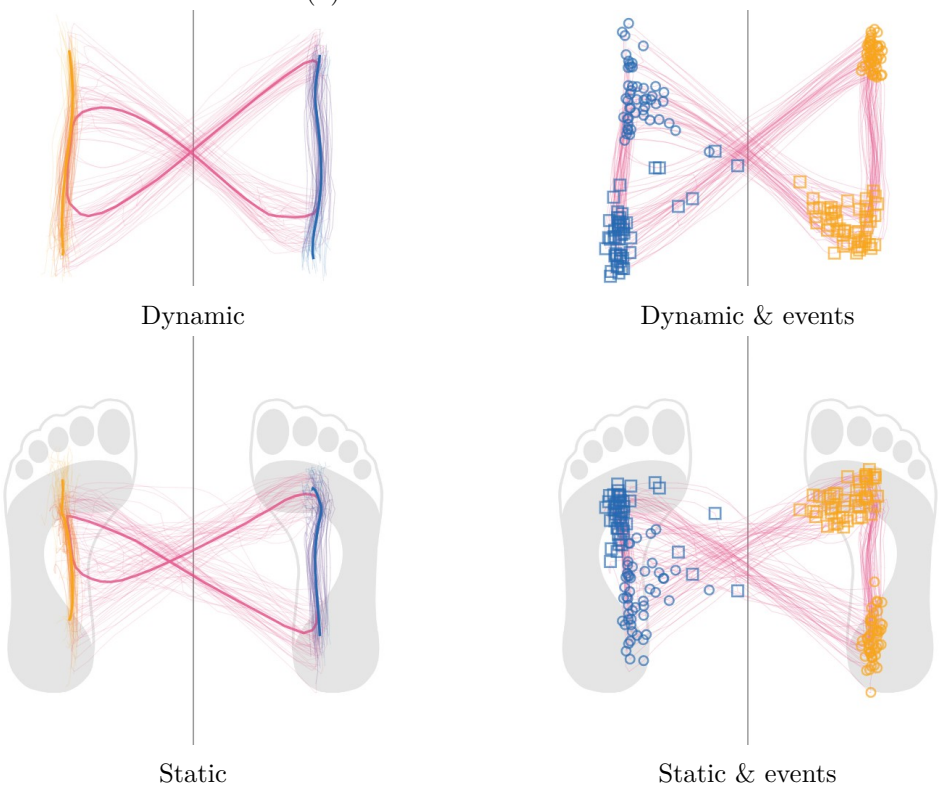

(c) Gaitogram visualizations

Figure 9.7: *[Screenshots]* Case study - participant with MS. Test recording H_1.

Die approbierte gedruckte Originalversion dieser Diplomarbeit ist an der TU Wien Bibliothek verfügbar.
The approved original version of this thesis is available in print at TU Wien Bibliothek.
TU Bibliothek Your knowledge hub WIEN

9.4.2 Walking Backwards

Walking backwards was done with a predefined machine's step length of 460 mm, a cadence of 30 steps per minute, and a sampling rate of 50 Hz. In total, 18 gait cycles have been recorded.

As we have established in Section 6.2, we would expect an event offset of −43% GC to the machine's gait event for an optimal backwards movement with −100% step length. The statistics in Table 9.6 show that both HSL and HSR occur around this expected offset, while the TO events occur around 5% GC too late. The timings also show that weight shifts to the left (HSL → TOR) happen with less variance than vice versa (HSR → TOL). This can also be extracted from Figure 9.8b, with HSL and TOR events being more clustered than HSR and TOL events. The GRF curves also show less variance around HSL and TOR than with the other events. Figure 9.8a also shows what appears to be a behavioral change in HSR and TOL, beginning with gait cycle 11, where both events occur later than in previous cycles. This contributes to the higher variance observed in the statistics regarding these events. The average gait discrepancy is rather high ($GD_{avg} = 36\%$ GC), which is to be expected, since walking backwards does not follow a standard gait pattern.

ID	SLL (mm)	SLR (mm)	T_{HSL} (% GC)	T_{HSR} (% GC)	T_{TOL} (% GC)	T_{TOR} (% GC)	D_{total} (%)	GD_{avg} (% GC)
A_{16}	−418 ± 54	−328 ± 111	−43.0 ± 6	−41.4 ± 12	−36.6 ± 14	−37.0 ± 5	7.6 ± 11	36

Table 9.6: Walking backwards. Statistical data. Step lengths SLL and SLR, gait event timings T, gait cycle force difference (i.e. balance) D_{total}, and average gait discrepancy GD_{avg}.

Die approbierte gedruckte Originalversion dieser Diplomarbeit ist an der TU Wien Bibliothek verfügbar.
The approved original version of this thesis is available in print at TU Wien Bibliothek.
TU Bibliothek Your knowledge hub WIEN

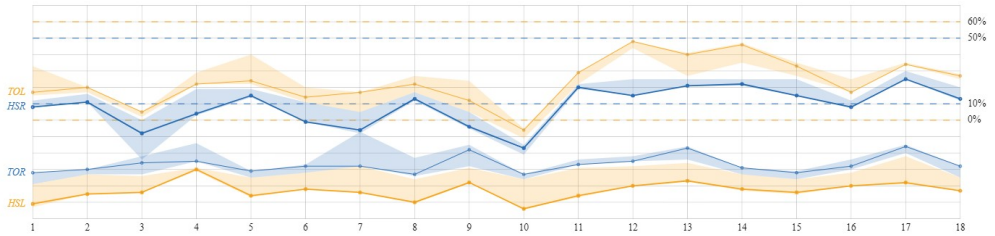

(a) Gait event consistency graph

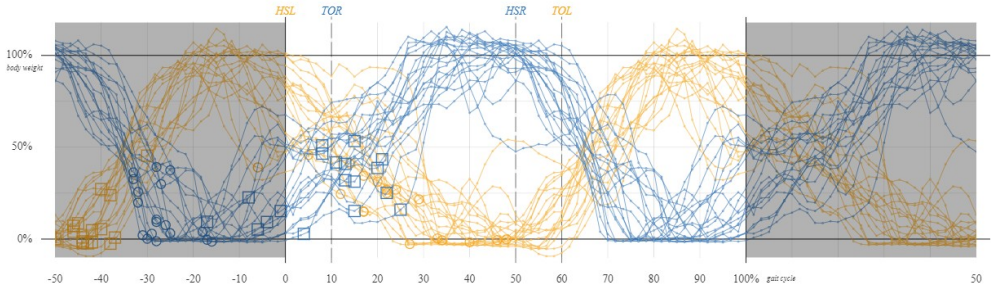

(b) GRF event visualization

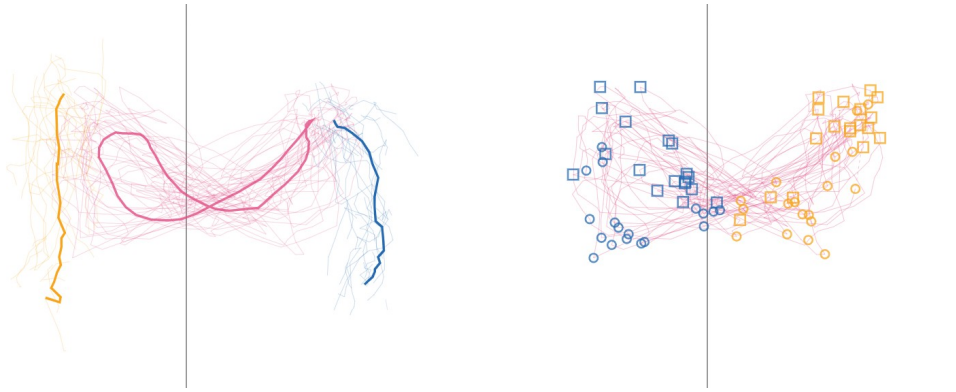

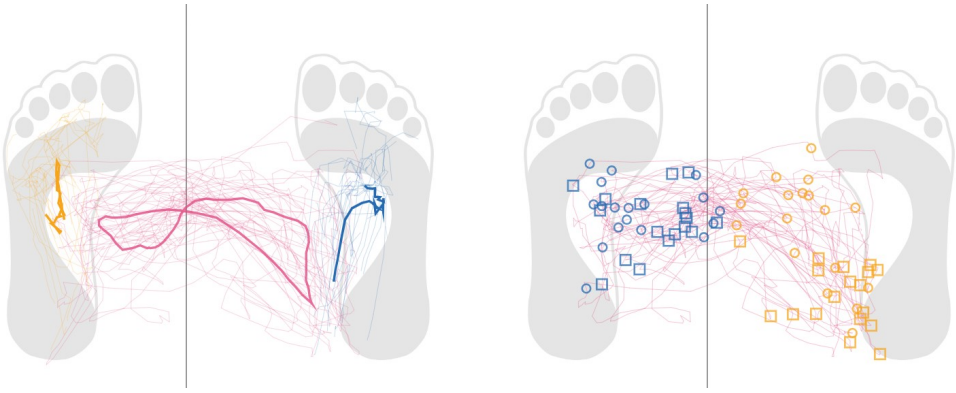

(c) Gaitogram visualizations

Figure 9.8: *[Screenshots]* Case study - participant walking backwards. Test recording A_{16}.

Die approbierte gedruckte Originalversion dieser Diplomarbeit ist an der TU Wien Bibliothek verfügbar.
The approved original version of this thesis is available in print at TU Wien Bibliothek.
TU Bibliothek Your knowledge hub WIEN

9.4.3 Testing Patient Instructions

Participant G took part in testing the system's generated patient instructions (Section 8.4.1). The goal of this test has been to trigger an autonomous self-correction of the participant by providing these instructions. The test recording was then evaluated if there is a change in the participant's gait pattern. Unfortunately, only seven gait cycles were recorded before the instructions were issued, followed by fifteen gait cycles afterwards.

As can be seen in Figure 9.9, Figure 9.10, and with the statistical results in Table 9.7, before the instructions were issued, the participant did not fully lift the feet during the swing phases. This lead to a high swing ratio (R_{swing}) on both sides. Additionally, gait events were not timed precisely with the machine's gait cycle. Heel strikes on both sides occurred too early, while TOL occurred too late.

Overall, after patient instructions were communicated to the participant, the step length on each side increased, the swing ratio (amount of force during swing phase) decreased significantly, the event timings improved, and the gait discrepancy of all events was cut in half, indicating a more standard gait pattern. The sum over all absolute gait event timings $T_{\text{total}} = |T_{\text{HSL}}| + |T_{\text{HSR}}| + |T_{\text{TOL}}| + |T_{\text{TOR}}|$) was drastically reduced after instructions were given (Table 9.7). T_{total} measures the total deviation between subject and machine. In other words, it reflects how precisely the participant coordinated heel strike and toe off with the movement of the machine.

	gait cycle count	SLL (mm)	SLR (mm)	$R_{\text{swing},L}$ (%)	$R_{\text{swing},R}$ (%)	T_{total} (% GC)	GD_{avg} (% GC)
Before	7	474 ± 38	518 ± 31	9.6 ± 3.2	11.6 ± 2.1	13.1	20
After	15	508 ± 59	539 ± 29	1.1 ± 1.4	2.2 ± 1.3	4.0	10

Table 9.7: Participant receives patient instructions. Statistical data. Step lengths SLL and SLR, swing ratios R_{swing}, average gait discrepancy GD_{avg}, and T_{total} as the sum over all absolute gait event timings.

Die approbierte gedruckte Originalversion dieser Diplomarbeit ist an der TU Wien Bibliothek verfügbar.
The approved original version of this thesis is available in print at TU Wien Bibliothek.
TU Bibliothek Your knowledge hub WIEN

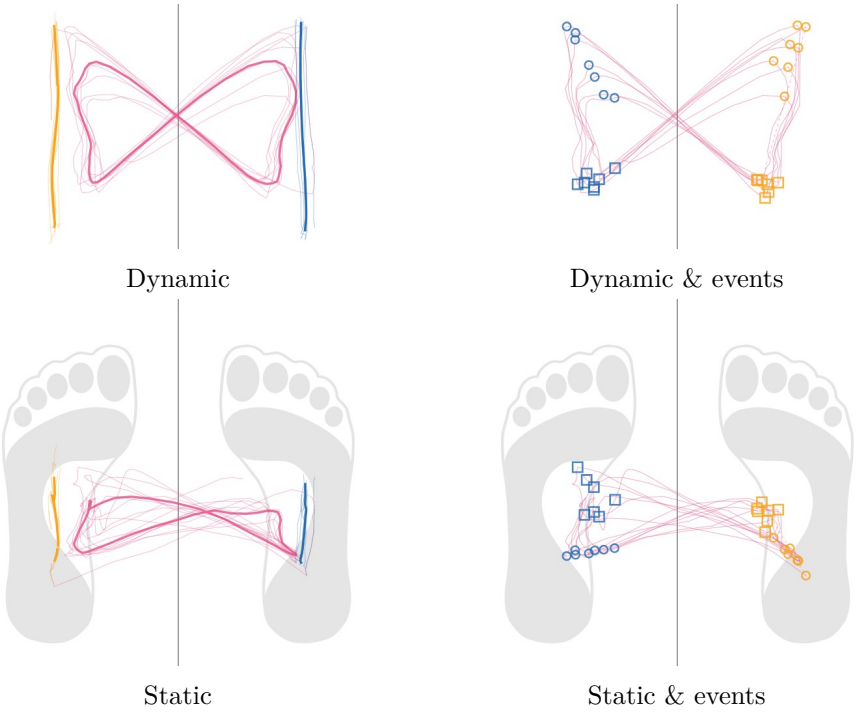

(a) Gaitogram visualizations, before instructions

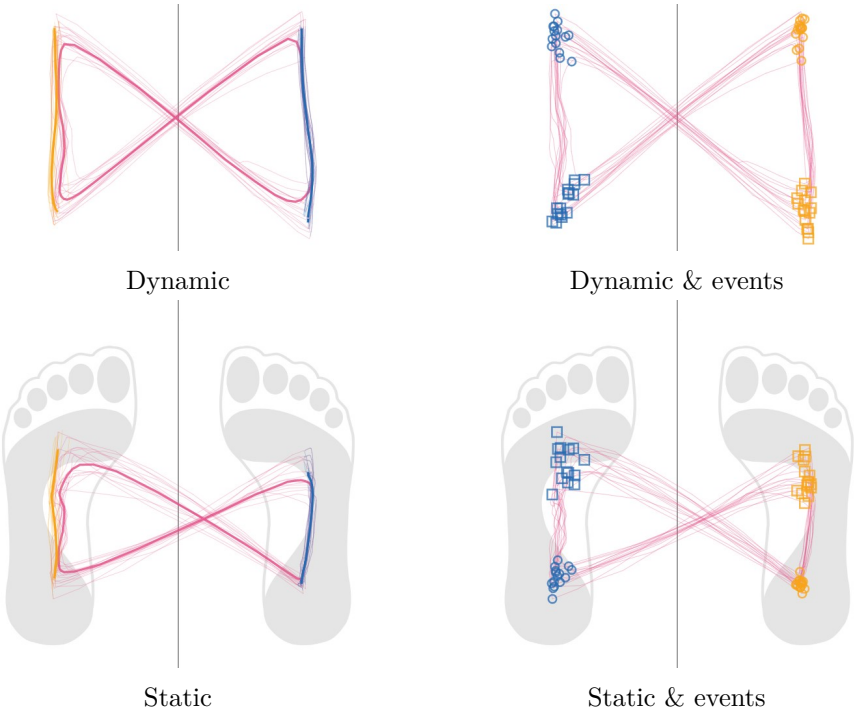

(b) Gaitogram visualizations, after instructions

Figure 9.9: *[Screenshots]* Case study - participant receiving patient instructions (1). Test recording G_{10}.

Die approbierte gedruckte Originalversion dieser Diplomarbeit ist an der TU Wien Bibliothek verfügbar.
The approved original version of this thesis is available in print at TU Wien Bibliothek.
TU Bibliothek Your knowledge hub WIEN

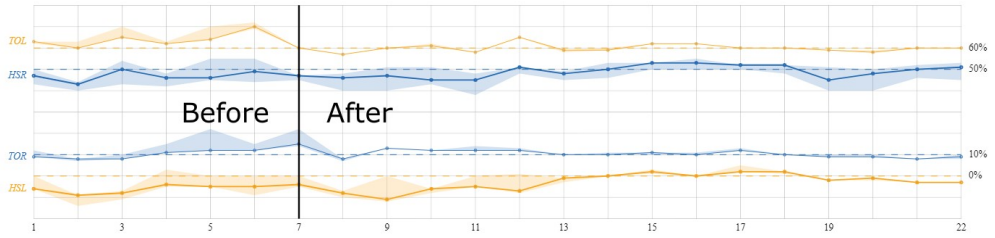

(a) Gait event consistency graph, before and after instructions

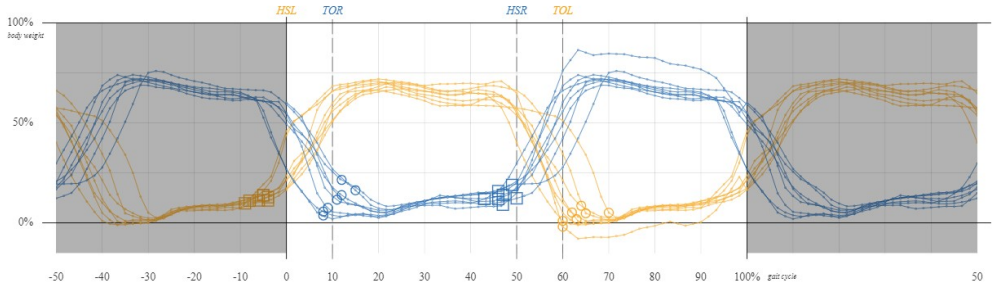

(b) GRF event visualization, before instructions

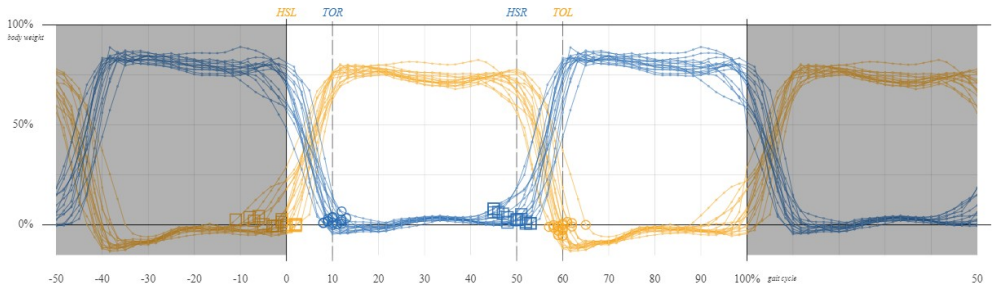

(c) GRF event visualization, after instructions

Figure 9.10: *[Screenshots with annotations]* Case study - participant receiving patient instructions (2). Test recording G_{10}.

9.4.4 Timing - Smallest Variance

Test recording E_2 exhibited the smallest sum of standard deviations in gait event timings ($T_{\text{HSL}}, T_{\text{HSR}}, T_{\text{TOL}}, T_{\text{TOR}}$). In other words, the participant was able to perform weight transfers across all gait cycles uniformly and most precisely among all candidates. However, this does not mean that the participant showed the best synchronization with the machine's movement. This would be so, if the sum of all absolute event timings T_{total} is minimal. Figure 9.11 shows little variance, both in the GRF curves as well as the CoP's trajectories. The participant was able to repeat the same movements with the same amount of force over multiple gait cycles. The dynamic gaitogram shows heel strikes occur too early, while TO events occur too late. This is also backed up by the test recording's statistics (Table 9.1). Gait discrepancy is high, especially for heel strike

Die approbierte gedruckte Originalversion dieser Diplomarbeit ist an der TU Wien Bibliothek verfügbar.
The approved original version of this thesis is available in print at TU Wien Bibliothek.
TU Bibliothek Your knowledge hub WIEN

events. This is caused by the initial dragging of each foot prior to the start of each weight transfer (Figure 9.11b, compare with Figure 6.8a), which diverges from a standard gait pattern.

9.4.5 Timing - Largest Variance

The largest sum of standard deviations in gait event timings was observed with test recording D_2. The participant showed highly unusual and inconsistent gait patterns. Variance in all determined parameters (e.g. timing, symmetry) is exceptionally high (compare with Table 9.1). Overall, analysis of this test recording is inconclusive - it is unclear why the participant showed this behavior. Another test recording D_1 with the same participant (Section 9.4.7) showed signs of walking backwards. An inquiry of the participant did not yield any insights, since the participant was not aware of any abnormal behavior during training.

9.4.6 Smallest Gait Discrepancy

Test recording B_5 exhibited the smallest average gait discrepancy. In order words, it shows the best agreement among all standard gait detection algorithms. Surprisingly, B_5 shows the smallest $\mathrm{GD}_{\mathrm{avg}}$ of 5% GC although the gait is asymmetric, since the objective was to walk actively on the right side only. As can be appreciated in Figure 9.13, the gait events are located in the corners of both the static and the dynamic gaitogram, therefore fulfilling standard event criteria. Statistics are shown in Table 9.4.

9.4.7 Largest Gait Discrepancy

The largest average gait discrepancy is given in test recording D_1. According to the statistical data (Table 9.1), the participant was walking backwards, while also showing high variances in all parameters. Figure 9.14a shows consistent timings in the gait events in the beginning, but a change in the participant's behavior, starting around gait cycle 40. The gait changes from backwards movement to standard forward movement over the course of ten gait cycles. The large average gait discrepancy ($\mathrm{GD}_{\mathrm{avg}} = 49\%$ GC) is not surprising, since walking backwards does not follow standard gait definitions. Overall this test recording is especially challenging for our GED algorithm, because of spurious and non-existing WTPs, indicating non-relevant weight transfers.

Die approbierte gedruckte Originalversion dieser Diplomarbeit ist an der TU Wien Bibliothek verfügbar.
The approved original version of this thesis is available in print at TU Wien Bibliothek.
TU Bibliothek Your knowledge hub WIEN

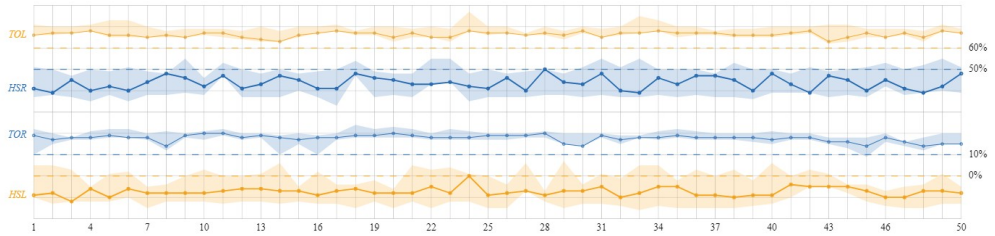

(a) Gait event consistency graph

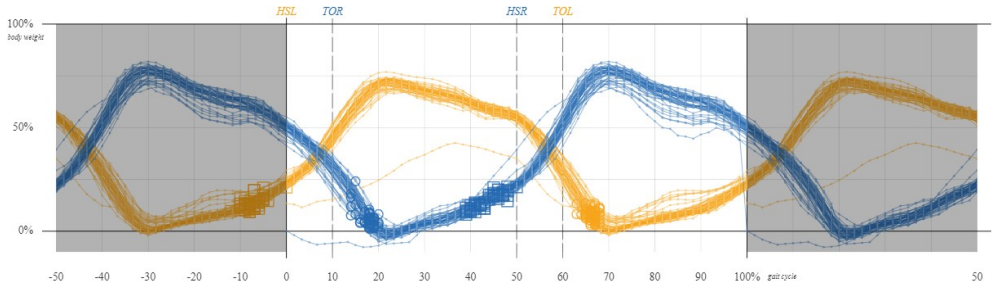

(b) GRF event visualization

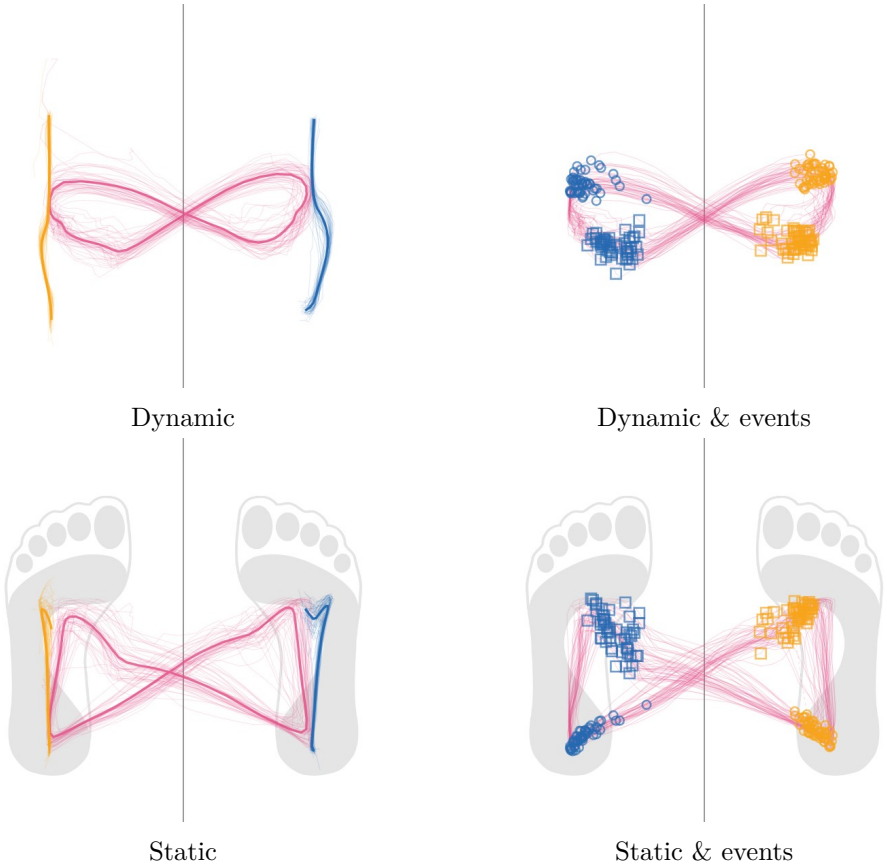

(c) Gaitogram visualizations

Figure 9.11: *[Screenshots]* Case study - smallest variance in timing. Test recording E_2 shows the smallest sum of standard deviations in gait event timings.

Die approbierte gedruckte Originalversion dieser Diplomarbeit ist an der TU Wien Bibliothek verfügbar.
The approved original version of this thesis is available in print at TU Wien Bibliothek.
TU Bibliothek Your knowledge hub WIEN

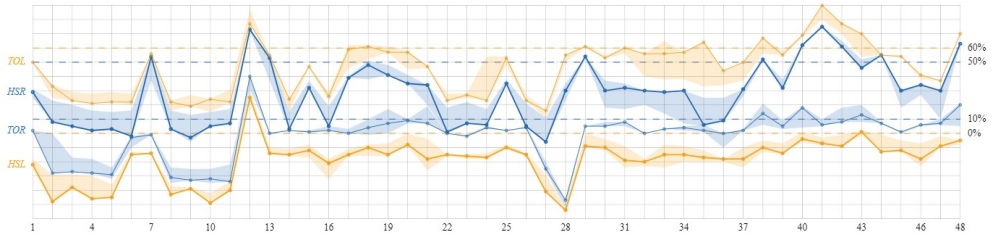

(a) Gait event consistency graph

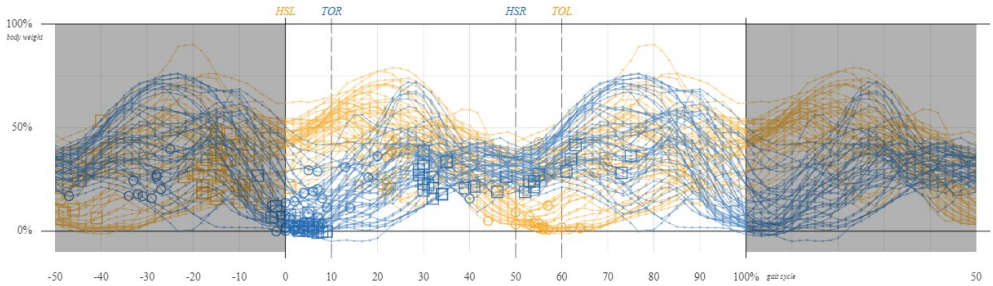

(b) GRF event visualization

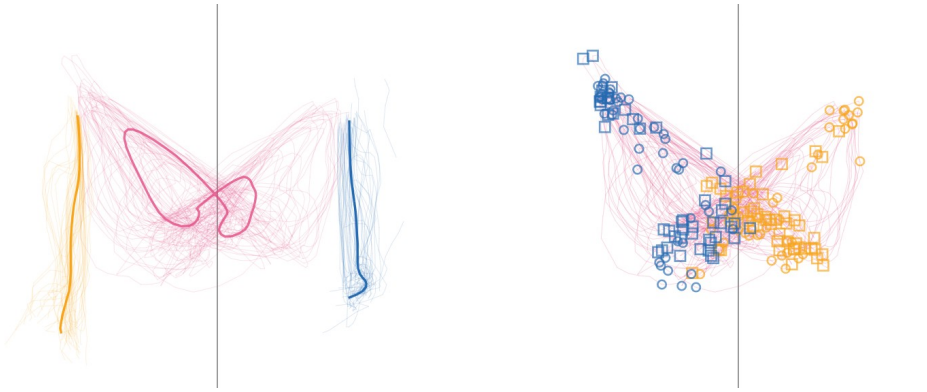

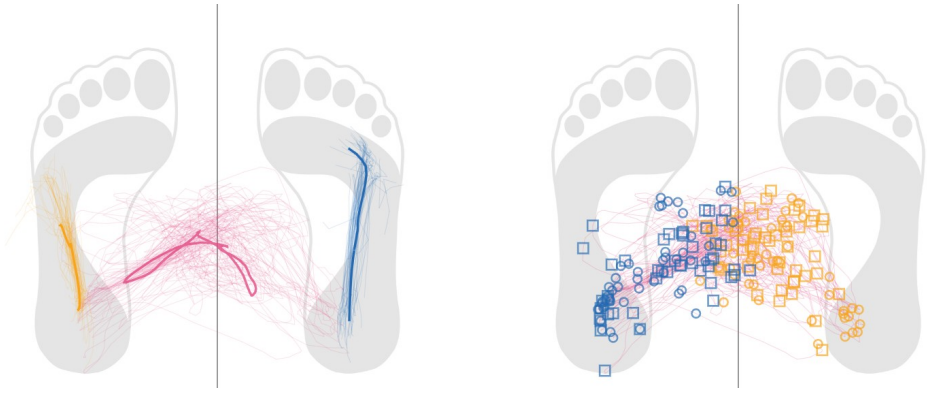

(c) Gaitogram visualizations

Figure 9.12: *[Screenshots]* Case study - largest variance in timing. Test recording D_2 shows the largest sum of standard deviations in gait event timings.

Die approbierte gedruckte Originalversion dieser Diplomarbeit ist an der TU Wien Bibliothek verfügbar.
The approved original version of this thesis is available in print at TU Wien Bibliothek.
TU Bibliothek Your knowledge hub WIEN

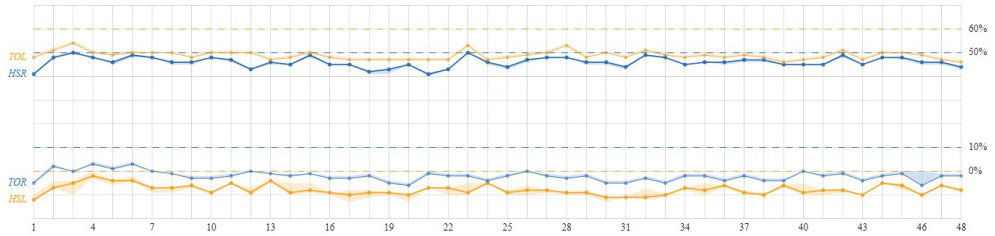

(a) Gait event consistency graph

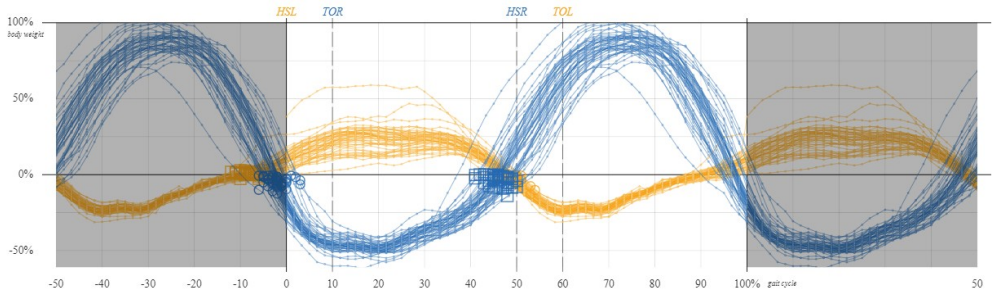

(b) GRF event visualization

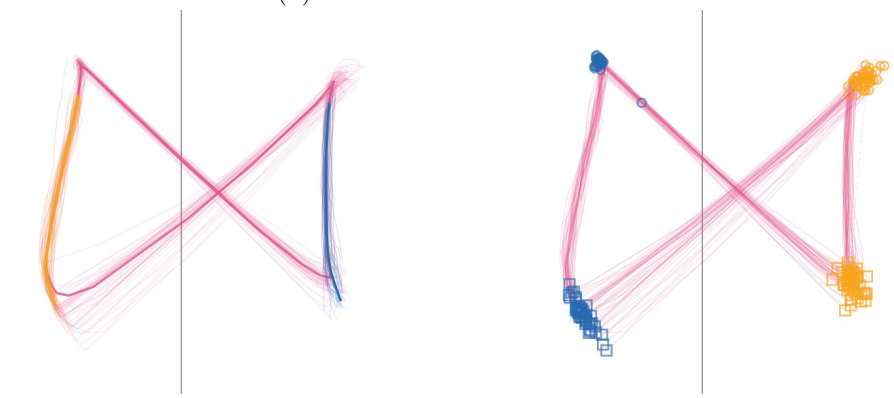

Dynamic

Dynamic & events

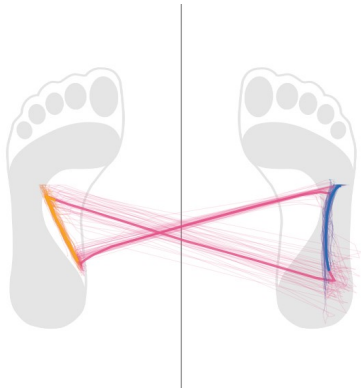

Static

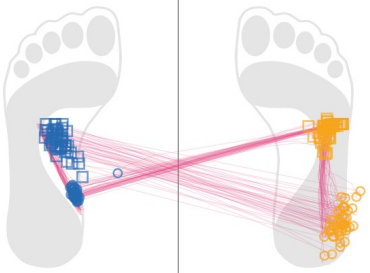

Static & events

(c) Gaitogram visualizations

Figure 9.13: *[Screenshots]* Case study - smallest GD_{avg}. Test recording B_5 exhibits the smallest average gait discrepancy.

Die approbierte gedruckte Originalversion dieser Diplomarbeit ist an der TU Wien Bibliothek verfügbar.
The approved original version of this thesis is available in print at TU Wien Bibliothek.
TU Bibliothek Your knowledge hub WIEN

(a) Gait event consistency graph

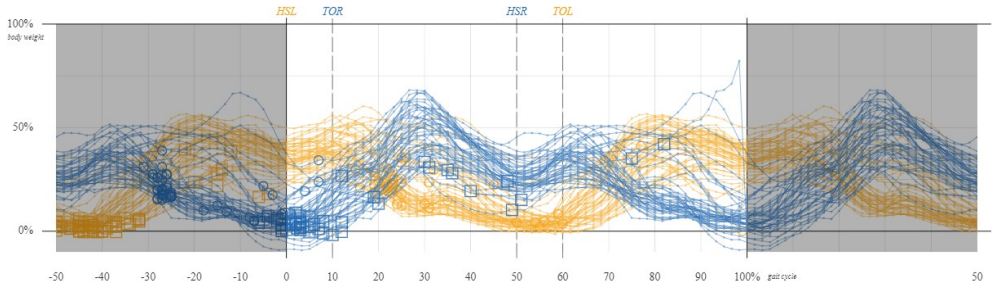

(b) GRF event visualization

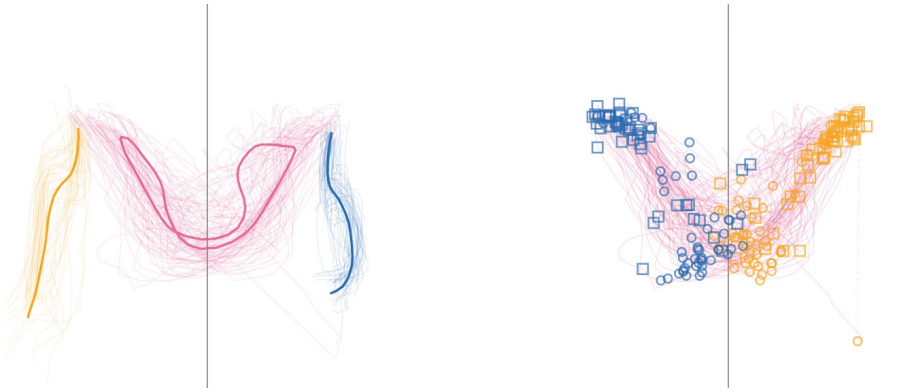

Dynamic

Dynamic & events

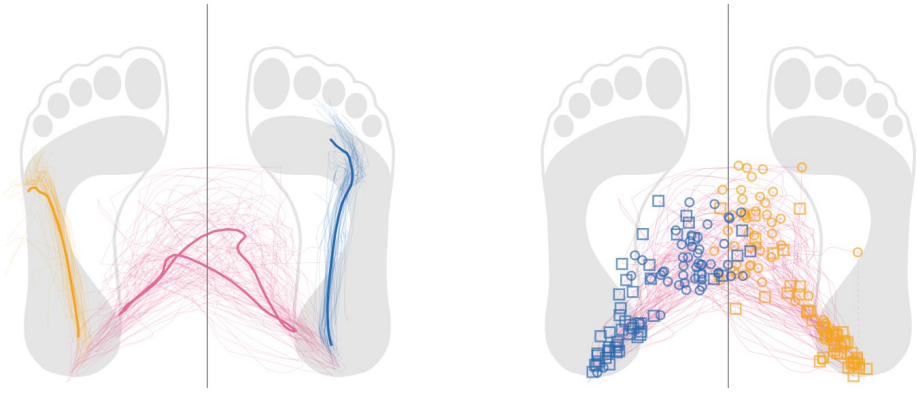

Static

Static & events

(c) Gaitogram visualizations

Figure 9.14: *[Screenshots]* Case study - largest GD_{avg}. Test recording D_1 exhibits the largest average gait discrepancy.

Die approbierte gedruckte Originalversion dieser Diplomarbeit ist an der TU Wien Bibliothek verfügbar.
The approved original version of this thesis is available in print at TU Wien Bibliothek.
TU Bibliothek Your knowledge hub WIEN

9.4.8 Passive Walking

We selected two test recordings regarding passive walking to demonstrate that our GED algorithm can also handle severe cases with minimal activity. The first recording E_8 (Figure 9.15) shows minimal contact with the force plates while around 90% of the participant's body weight is being carried by the support system. The second recording B_7 (Figure 9.16), on average, actually has more than 100% of the body weight carried by the support system, since the participant is additionally pulling on the foot straps. Peaks in negative GRF reach up to −50% body weight. Weight transfers are detected during times when left and right GRFs are both negative. Even under these extreme conditions, we can observe periodicity in the GRF visualizations and consistent GED in both recordings. However, it is unclear under these circumstances whether or not the subject's movements are measured or if the machine's periodic movement dominates the results.

ID	Gait	SLL (mm)	SLR (mm)	T_{HSL} (% GC)	T_{HSR} (% GC)	T_{TOL} (% GC)	T_{TOR} (% GC)	D_{total} (%)	GD_{avg} (% GC)
E_8		270 ± 115	274 ± 99	−14.3 ± 4	−14.1 ± 3	−3.8 ± 2	−10.4 ± 2	−9.1 ± 5	18
B_7		−397 ± 83	508 ± 33	−32.6 ± 3	−4.8 ± 2	−6.1 ± 3	−25.1 ± 3	−19.5 ± 7	24

Table 9.8: Passive walking. Statistical data. Step lengths SLL and SLR, gait event timings T, gait cycle force difference (i.e. balance) D_{total}, and average gait discrepancy GD_{avg}. Balance highlighted if $|D_{\text{total}}| \geq 10\%$.

Die approbierte gedruckte Originalversion dieser Diplomarbeit ist an der TU Wien Bibliothek verfügbar.
The approved original version of this thesis is available in print at TU Wien Bibliothek.
TU Bibliothek Your knowledge hub WIEN

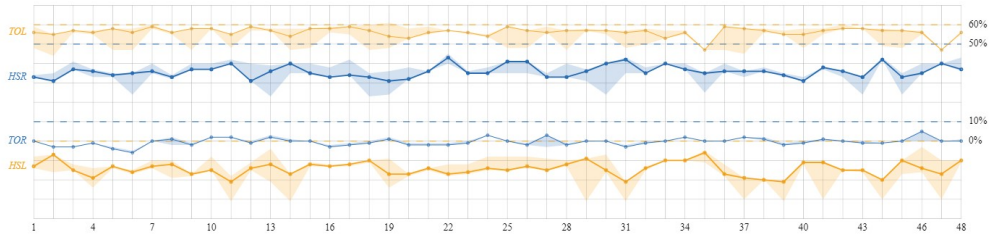

(a) Gait event consistency graph

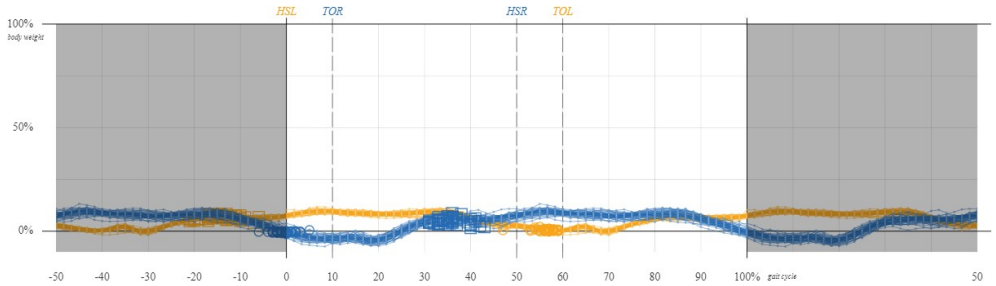

(b) GRF event visualization

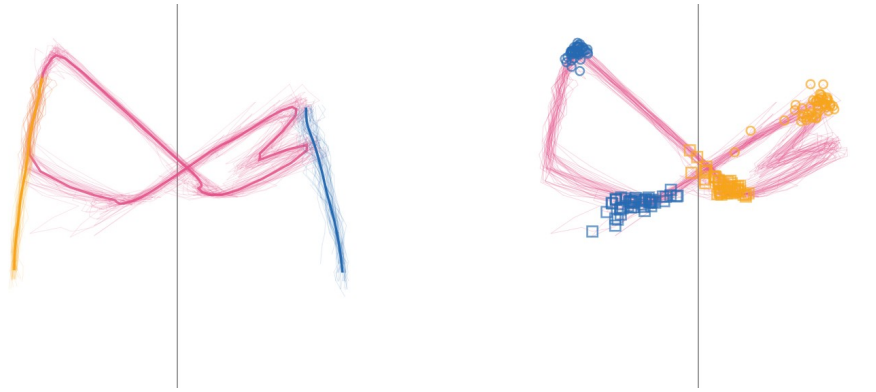

Dynamic

Dynamic & events

Static

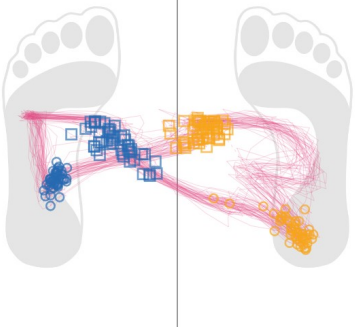

Static & events

(c) Gaitogram visualizations

Figure 9.15: *[Screenshots]* Case study - passive walking (1). Test recording E_8.

Die approbierte gedruckte Originalversion dieser Diplomarbeit ist an der TU Wien Bibliothek verfügbar.
The approved original version of this thesis is available in print at TU Wien Bibliothek.
TU Bibliothek Your knowledge hub WIEN

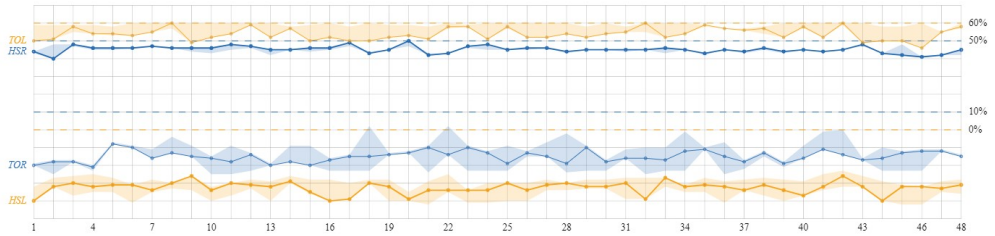

(a) Gait event consistency graph

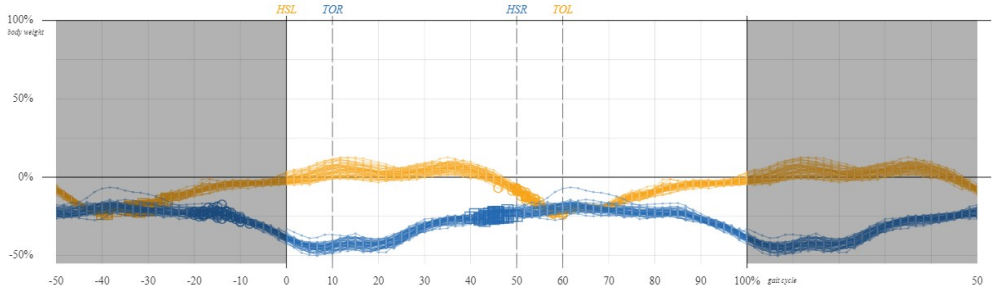

(b) GRF event visualization

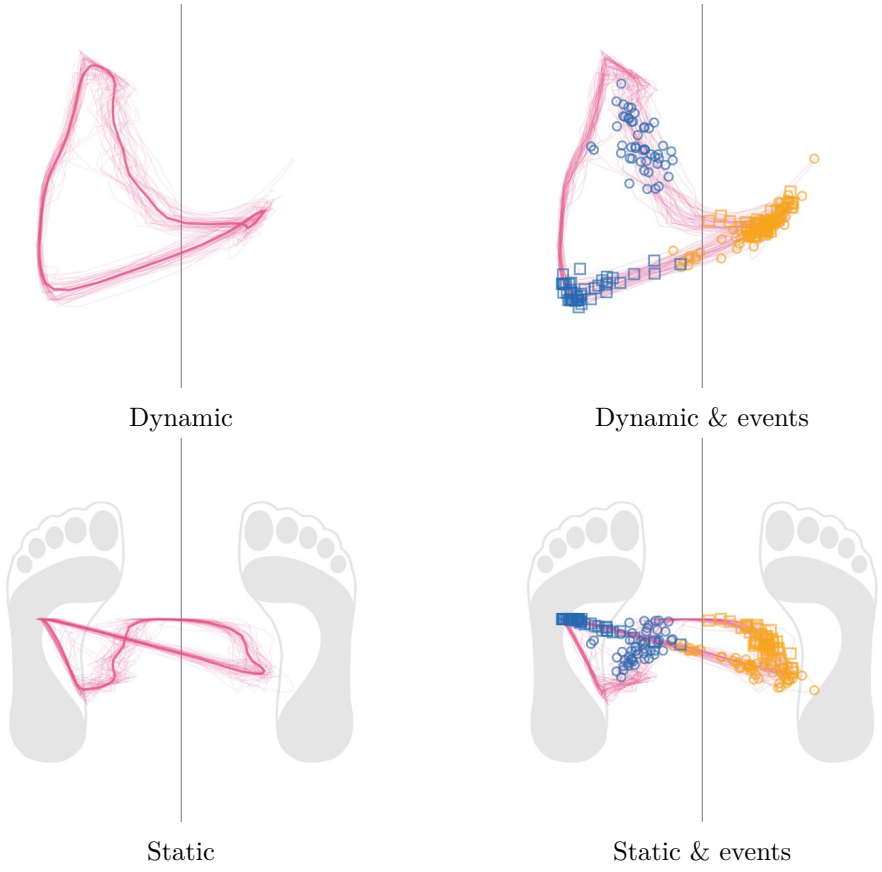

(c) Gaitogram visualizations

Figure 9.16: *[Screenshots]* Case study - passive walking (2). Test recording B_7.

Die approbierte gedruckte Originalversion dieser Diplomarbeit ist an der TU Wien Bibliothek verfügbar.
The approved original version of this thesis is available in print at TU Wien Bibliothek.
TU Bibliothek Your knowledge hub WIEN

CHAPTER 10

Conclusion

10.1 Summary

We present a novel GED algorithm in the context of a new robotic gait rehabilitation device, i.e. the PerPedes system. Furthermore, we demonstrate that standard GED algorithms will likely fail with PerPedes, since initial and last contact with the ground are not considered meaningful anymore. With our new GED algorithm, it is possible to robustly identify gait events, even under severe circumstances, like minimal gait activity, dragging the feet, or walking backwards. The algorithm is designed in such a way that it could potentially be used outside the PerPedes ecosystem, with other force-based systems. It might be applicable in the analysis of distorted gait patterns or certain motor impairments, observed in patients with hemiplegia, Multiple Sclerosis, or Parkison's disease.

Our developed software provides standard visualizations used in gait analysis. The vertical GRF visualization is further improved to highlight gait asymmetries with the introduction of a synchronized (left/right) view and a difference plot. The gaitogram has been extended with the visualization of stance lines for the use in PerPedes and provides a multitude of information regarding timing, weight transfers, and symmetry. During training, the physiotherapist is presented with easy to grasp information about the patient's performance. The system automatically generates possible instructions to improve the patient's gait and we have demonstrated its applicability to correct timing, lifting, and symmetry during therapy.

Furthermore, the system collects statistics during each therapy session. These values can be used to analyze the patient's current performance and overall therapy progress. Additionally, normalized measures allow inter-patient comparison for medical experts. This thesis gives an overview of commonly used spatiotemporal measures. Special attention has been paid to determine and analyze symmetry. In the context of the

Die approbierte gedruckte Originalversion dieser Diplomarbeit ist an der TU Wien Bibliothek verfügbar.
The approved original version of this thesis is available in print at TU Wien Bibliothek.
TU Bibliothek Your knowledge hub WIEN

PerPedes system, new measures have been developed. These are used for the patient instructions and the balance indicator. The results show that the balance of the patient (left/right leaning) can be reliably identified (via D_{total}).

10.2 Discussion

This work presents the first scientific evaluation of the PerPedes system, but is by no means complete. Although we analyzed 72 test recordings and approximately 3600 gait cycles, only eight participants were involved. The proposed target group of stroke survivors was not represented in the dataset. Furthermore, test data was recorded with the same machine settings (cadence, step length, sampling rate) with a few exceptions. The sample size is insufficient, healthy participants are not representative for gait disabilities and different machine settings (e.g. the sampling rate) might influence the outcome of the GED.

The GED has been performed after manually annotating representative test data samples. The gait patterns recorded in PerPedes can be vastly different from the ones reported in the literature. There was no gold standard available to identify the gait events. Since manual annotation was done by only one investigator, the identified events could be inherently biased. But, as Mansfield and Lyons [ML03] state:

> *"The concept of the precise detection of heel contact events is somewhat misleading. The transitions between the phases of the gait cycle are gradual and very often two different and equally experienced investigators may disagree on the exact moment of, for example, heel contact based on video recordings."*

Because of these circumstances, we decided to introduce the gait discrepancy metric. Test data has shown that our GED algorithm agrees on the location of the events with comparative algorithms, if the gait follows a standard pattern. A standard gait demonstrates the actual lifting of the feet, quick weight transfers, and the pressure moving across each foot from heel to toe. In such cases, we can indeed see that our algorithm finds the gait events, expressed by a small GD_{avg} value. In case this gait discrepancy is large, i.e. the comparative algorithms do not agree on a specific location, results show that our algorithm's detection of gait events is consistent in time for test data with small variances in movement. Temporal consistency is not enforced between gait cycles. Therefore, if the same gait event is found at the same relative time in multiple adjacent gait cycles, one can assume that there is a significance to this specific point. The pressure plates' movement does influence the GED, since we analyze the velocity of the CoP's trajectories. However, we did not find a clear distortion caused by this movement. This is likely because the start and end of a weight transfer is categorized by a quick movement of the CoP, basically eliminating the influence of pressure plate movement. With increased walking speeds, the plates move quicker, but the weight transfers must happen proportionally even faster, suppressing the influence of the plate movement accordingly.

Die approbierte gedruckte Originalversion dieser Diplomarbeit ist an der TU Wien Bibliothek verfügbar.
The approved original version of this thesis is available in print at TU Wien Bibliothek.
TU Bibliothek Your knowledge hub WIEN

As an alternative gait event definition, one could use the median event among all possible candidates. We decided against this, because of three reasons. First, the median event can be driven to a wrong position of occurrence, depending on the used event definitions, introducing a bias. Second, it increases complexity of the detection, making it harder to reason about why an event is found at a specific location. Third, there is no reason to assume that the median event is correct.

10.3 Future Work

10.3.1 Gait Event Detection

The proposed GED algorithm is used to identify events after a machine's gait cycle is completed. This is insufficient for real-time GED. In order to allow prompt identification of heel strikes, one could search for the event as soon as a WTP is detected. Since a WTP does not necessarily exist or might not identify a weight transfer in non-standard gait patterns, the heel strike might be misidentified. Toe off events could be found as soon as negative forces are detected or within a specific time-window after a WTP. Overall, precision will be traded for speed in the detection.

In order to further validate the algorithm, more test data needs to be collected on the PerPedes platform. First and foremost, a larger variety in healthy participants' data needs to be collected. The parameter space of the machine, especially step length and cadence, needs to be explored. This means that for each participant, test data with different machine settings needs to be recorded. Afterwards, this data needs to be annotated by experienced investigators, marking the gait events. Alternatively, the events could be detected with a kinematic approach. Using a camera one could identify heel strikes as the minimal vertical displacement of a heel marker. This approach might fail, since the foot straps prevent clear movement of the feet. If the gait events can be successfully identified, they can be used for validation and PerPedes specific statistics can be inferred, for example the average duration of stance and swing times. The influence of the machine's parameters on the subject's gait variability can be determined. We would expect that gait variability is at its lowest with each subject's preferred speed and step length settings. The generated statistics should be compared to free walking and/or treadmill walking, as reported in the standard literature. Once this norm data of healthy participants has been collected and analyzed, groups of participants with certain gait disabilities can be tested.

Recently, Fukuchi et al. [FFD18] made a public dataset available, including both kinematic and kinetic data of healthy individuals. The provided (vertical) GRF data can be used to validate whether or not our GED is suitable for standard gait data not recorded on the PerPedes device.

Die approbierte gedruckte Originalversion dieser Diplomarbeit ist an der TU Wien Bibliothek verfügbar.
The approved original version of this thesis is available in print at TU Wien Bibliothek.
TU Bibliothek Your knowledge hub WIEN

10.3.2 Gait Report

Currently, statistical data is collected and presented in the analysis perspective of the user interface. In the future, it will be necessary to present statistics over multiple therapy sessions of the same patient to the medical practitioner. The gaitogram visualization provides a good overview of the patient's performance for one therapy session. Additionally, detailed information is available with the statistical measures. Change throughout the therapies could be visualized for selected measures as a function over time, similar to the gait event consistency panel.

Wagner et al. [WSH+18] state that a clinician focuses on symmetry measures between both feet, but also on the deviations from the norm. They developed an interactive user interface, especially suited for inter-patient comparison. In comparison, our system does not offer a visual tool to compare different patients yet.

In order to present deviations from the norm without interactivity, one can use a radar plot as proposed by Mc Ardle et al. [MAGD+19] (Figure 10.1a). This visualization shows the z-score (positive/negative) for selected spatiotemporal parameters. The z-score is the distance from the mean, expressed in standard deviations. Alternatively, a simple line chart can be used instead of a radar plot (Figure 10.1b). There is no significant advantage of one visualization over the other, therefore the choice is merely a stylistic one. In order to create any of these plots, one must first collect a fairly large amount of norm data. In their paper they used a control group size of 29 participants.

Die approbierte gedruckte Originalversion dieser Diplomarbeit ist an der TU Wien Bibliothek verfügbar.
The approved original version of this thesis is available in print at TU Wien Bibliothek.

Die approbierte gedruckte Originalversion dieser Diplomarbeit ist an der TU Wien Bibliothek verfügbar.
The approved original version of this thesis is available in print at TU Wien Bibliothek.

(a) Radar plot. Image taken from Mc Ardle et al. [MAGD+19]

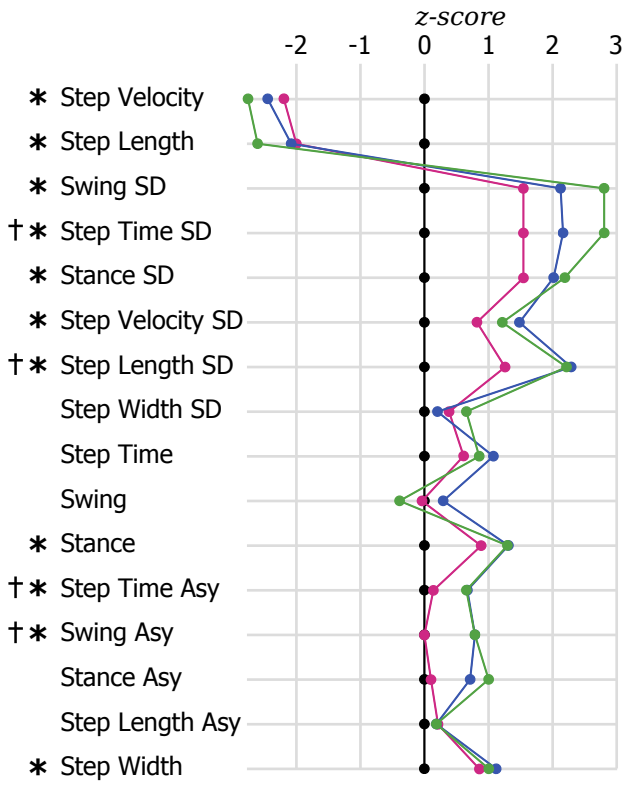

(b) Reproduction of (a) as a line chart

Figure 10.1: Plots for spatiotemporal parameters. Multivariate data for different groups of impairment (AD, DLB, PDD) is visualized. For each group/parameter combination, the z-score is shown. Abbreviations: SD, standard deviation; Asy, asymmetry; AD, Alzheimer's disease; DLB, dementia with Lewy bodies; PDD, Parkinson's disease dementia; LBD, Lewy body dementia. * = differences between controls and disease groups, †= differences between AD and LBD.

Die approbierte gedruckte Originalversion dieser Diplomarbeit ist an der TU Wien Bibliothek verfügbar.
The approved original version of this thesis is available in print at TU Wien Bibliothek.

APPENDIX A

Relevant Source Code

A.1 Validation of McCamley et al. [MDGM12]

```
% Evaluation of McCamley et al. 2012 - An enhanced estimate of initial
    contact and final contact instants of time using lower trunk inertial
    sensor data.
% Goals:
% 1. Verify results
% 2. Compare continuous wavelet transformation with Gaussian smoothing
%
% Necessary functions:
% - gaussfilt - https://www.mathworks.com/matlabcentral/fileexchange
    /43182-gaussfilt-t-z-sigma
% - derivative_cwt - https://www.mathworks.com/matlabcentral/fileexchange
    /13948-numerical-differentiation-based-on-wavelet-transforms
% - cwt - from Matlab Wavelet toolbox

% Acceleration data from McCamley et al. Figure 1
% (points extracted via http://www.graphreader.com/)
x = [-0.019,0.116,0.385,0.655,1.001,1.348,1.502,1.81,2.272,2.58,2.927,...
    3.389,3.582,3.736,4.005,4.39,4.698,4.852,5.16,5.777,6.123,6.778,...
    7.664,8.126,8.703,9.166,9.474,9.705,10.167,10.398,10.591,11.014,...
    11.322,11.515,11.669,11.977,12.246,12.593,12.901,13.286,13.71,...
    14.288,14.942,15.404,16.021,16.829,16.945,17.214,17.368,17.831,...
    18.37,18.639,18.909,19.255,19.679,20.103,20.834,21.605,22.259,...
    22.991,23.376,23.838,24.454,25.071,25.456,25.841,26.226,26.804,...
    27.227,27.766,28.306,29.384,29.904];
y = [6.639,6.286,5.63,5.109,4.824,4.874,4.807,4.269,3.412,2.319,1.227,...
```


Die approbierte gedruckte Originalversion dieser Diplomarbeit ist an der TU Wien Bibliothek verfügbar.
The approved original version of this thesis is available in print at TU Wien Bibliothek.
TU Bibliothek Your knowledge hub WIEN

```
    0.37,1.261,3.664,6.084,7.294,5.647,4,2.723,4.739,6.605,7.899,7.042,...
    6.555,5.277,3.916,3.63,3.496,2.773,1.378,0.924,2.924,4.471,5.244,...
    5.983,5.176,4.185,3.866,4.504,5.832,7.143,7.933,7.277,5.882,4.689,...
    3.63,3.563,3.664,3.513,2.067,0.605,2.353,4.857,6.874,5.361,3.109,...
    5.445,7.866,7.126,5.899,5.697,5.059,3.697,2.824,1.613,0.739,3.294,...
    6.42,5.261,3.496,5.765,7.933,7.412];

% Scale x (time axis) to the range [0,2]
xscale = 2/max(x);
x = (x - min(x)) / (max(x) - min(x)) * 2;
% Scale y (acceleration) to the range [-1,1]
y = (y - min(y)) / (max(y) - min(y)) * 2 - 1;

% Uniform spacing and spline interpolation
dx = 0.005; % 5 ms signal sampling, since original resolution is 10 ms
xx = 0:dx:2;
y = spline(x,y,xx);
x = xx;

% Parameters to closely match paper results
scaleCWT = 2.5 * xscale / dx;   % ~ 33.4
sigma = 1.75 * xscale;          % ~ 0.12 on [0,2] domain

% ------------------------------
% CALCULATIONS
% ------------------------------

% 1. Gaussian filtering with boundary == mean of signal
resFilt = gaussfilt(-2:dx:4,[ones(size(y)) * mean(y) y ones(size(y)) *
    mean(y)],sigma);
resFilt = resFilt(length(y)+1:end-length(y));

% 2. Use CWT
yInt = cumsum(y) .* dx; % integrate signal
resCWT = derivative_cwt(yInt,'gaus1',scaleCWT,dx,1);

% Calculate the 'jerk' with another differentiation
resJerk = derivative_cwt(resCWT,'gaus1',scaleCWT,dx,1);
% Scale accordingly to match the paper
resJerk = resJerk * 20 * xscale;

% Find minima/maxima
[~,idxMin] = findpeaks(-resCWT);
```


Die approbierte gedruckte Originalversion dieser Diplomarbeit ist an der TU Wien Bibliothek verfügbar.
The approved original version of this thesis is available in print at TU Wien Bibliothek.
TU Bibliothek Your knowledge hub WIEN

```
64  [~,idxMax] = findpeaks(resJerk);
65
66  % ---------------------------------
67  % DISPLAY
68  % ---------------------------------
69
70  set(0,'DefaultFigureWindowStyle','docked');
71
72  figure; % first figure
73  hold on;
74  plot(xx,y,'-','LineWidth',1,'Color',[0.8 0.2 0.2]); % signal
75  plot(x,resCWT,'--','LineWidth',1,'Color',[0.2 0.2 0.8]); % CWT
76  plot(x,resJerk,':k','LineWidth',1); % jerk
77
78  % Plot minima
79  xmin = x(idxMin);
80  plot(xmin,resCWT(idxMin),'ok','MarkerSize',10,'LineWidth',2);
81  for xm = xmin
82      plot([xm xm], [-1.5 1.75], '--k','LineWidth',1);
83  end
84
85  % Plot maxima
86  xmax = x(idxMax);
87  plot(xmax,resJerk(idxMax),'xk','MarkerSize',12,'LineWidth',2);
88  for xm = xmax
89      plot([xm xm], [-1.5 1.75], ':k','LineWidth',1);
90  end
91
92  ylim([-1.5 1.75]);
93  xlabel('Time [s]', 'FontSize', 12);
94  ylabel('[m/s^2]', 'FontSize', 12);
95
96  %---------------------
97
98  figure; % second figure
99  hold on;
100 plot(xx,y,'-','LineWidth',1,'Color',[0.8 0.2 0.2]); % signal
101 plot(x,resCWT,'--','LineWidth',1,'Color',[0.2 0.2 0.8]); % CWT
102 plot(x,resFilt,':g','LineWidth',1,'Color',[0.2 0.8 0.2]); % filter
103
104 ylim([-1.1 1.1]);
105 xlabel('Time [s]', 'FontSize', 12);
106 ylabel('[m/s^2]', 'FontSize', 12);
```


Die approbierte gedruckte Originalversion dieser Diplomarbeit ist an der TU Wien Bibliothek verfügbar.
The approved original version of this thesis is available in print at TU Wien Bibliothek.
TU Bibliothek Your knowledge hub WIEN

A.2 1D Gaussian and Derivative of Gaussian

```
% Gaussian and Gaussian derivative
x = -4:0.01:4;
sigma = 1;

G  = 1/(sigma * sqrt(2*pi)) * exp(-x.^2 / (2 * sigma^2));
dG2 = -x/sigma .* G;

figure;
hold on;
plot(x,G,'LineWidth',2,'Color',[0.8 0.2 0.2]);
plot(x,dG2,'--','LineWidth',2,'Color',[0.2 0.2 0.8]);
xlabel('x');
ylabel('Amplitude');
```

A.3 Uniform Filtering

```
function data = filterUniform(data,filtersize)
% filter data uniformly with the given filter size
if filtersize > 0
    kernel = ones(1,filtersize)/filtersize;
    fHalf = round(filtersize / 2);

    data_start = data(1) * ones(1,filtersize);
    data_end = data(end) * ones(1,filtersize);
    data_ext = [data_start data data_end];
    data_ext = filter(kernel,1,data_ext);
    data_ext = [data_ext(fHalf:end) zeros(1,fHalf-1)];

    data = data_ext(filtersize+1:end-filtersize);
end
end
```

A.4 Find the Mediolateral Midpoint

```
function mp = findCopMidpoint(copML,grfDiff,idxMachineWTP)
% searches for the nearest midpoint to the machine's WTP
% copML         ... CoP in ML direction. high values are for the heel
    striking limb's side.
% grfDiff       ... Difference (grf_HS - grf_TO)
```


Die approbierte gedruckte Originalversion dieser Diplomarbeit ist an der TU Wien Bibliothek verfügbar.
The approved original version of this thesis is available in print at TU Wien Bibliothek.
TU Bibliothek Your knowledge hub WIEN

```
% idxMachineWTP ... the index of the machine's WTP (halfway between HS and
    TO)

[idxMinmax,isMinimum] = findMinMax(grfDiff,17);
if all(isMinimum)
    % try again without smoothing
    [idxMinmax,isMinimum] = findMinMax(grfDiff,0);
end

% split according to maxima in grfDiff and look in each section for
   midpoints
midpoints = [];
idxLast = 1;
for ii = 1:length(idxMinmax)
    if isMinimum(ii)
        continue; % we are interested in maxima
    end
    i1 = idxLast;
    i2 = idxMinmax(ii);
    idxLast = i2;

    [~,idxMin] = min(copML(i1:i2));
    idxMin = idxMin + i1 - 1;

    [~,idxMax] = max(copML(idxMin:i2));
    idxMax = idxMax + idxMin - 1;

    center = (copML(idxMax) + copML(idxMin)) / 2;
    mp = findCrossing(copML,center,idxMin,idxMax);
    midpoints = [midpoints mp];
end

if isempty(midpoints)
    warning('no midpoints');
    mp = idxMachineWTP;
else
    % take the closest to the machine's WTP
    dist = abs(idxMachineWTP - midpoints);
    mp = midpoints(min(dist) == dist);
    mp = mp(end); % in case there are more than one points with equal
       distance
end

```

Die approbierte gedruckte Originalversion dieser Diplomarbeit ist an der TU Wien Bibliothek verfügbar.
The approved original version of this thesis is available in print at TU Wien Bibliothek.
TU Bibliothek Your knowledge hub WIEN

```
45  end
46
47  function idxCrossing = findCrossing(data,toCross,iMin,iMax)
48  % finds the crossing 'toCross' between [iMax,iMin]
49  idxCrossing = [];
50  for jj = iMax-1:-1:iMin
51      if data(jj) <= toCross && data(jj+1) >= toCross
52          if abs(data(jj) - toCross) < abs(data(jj+1) - toCross)
53              idxCrossing = jj;
54          else
55              idxCrossing = jj+1;
56          end
57          break;
58      end
59  end
60  end
61
62  function [idxMinmax,isMinimum] = findMinMax(data,filter)
63  % find indices of minima and maxima in data
64  data_smooth = filterUniform(data,filter);
65  minData = min(data_smooth);
66  maxData = max(data_smooth);
67  center = (minData + maxData) / 2;
68
69  idxMin = 1;
70  idxMax = 1;
71  idxMinmax = [];
72  searchMin = -1; % -1 = not started, 0 = search max, 1 = search min
73  for ii = 1:length(data)
74      if data(ii) < data(idxMin)
75          idxMin = ii;
76      end
77      if data(ii) > data(idxMax)
78          idxMax = ii;
79      end
80
81      if data_smooth(ii) <= center && searchMin ~= 1
82          if ii > 1
83              idxMinmax = [idxMinmax idxMax];
84          end
85          idxMin = ii;
86          searchMin = 1;
87      elseif data_smooth(ii) >= center && searchMin ~= 0
```


Die approbierte gedruckte Originalversion dieser Diplomarbeit ist an der TU Wien Bibliothek verfügbar.
The approved original version of this thesis is available in print at TU Wien Bibliothek.
TU Bibliothek Your knowledge hub WIEN

```
        if ii > 1
            idxMinmax = [idxMinmax idxMin];
        end
        idxMax = ii;
        searchMin = 0;
    end
end

if searchMin == 0
    idxMinmax = [idxMinmax idxMax];
elseif searchMin == 1
    idxMinmax = [idxMinmax idxMin];
end

isMinimum = data(idxMinmax) < center;
end
```

A.5 Find the Gait Event

```
function eventResult = findEvent(midpoint,grf1,grf2,plate1AP,plate2AP)
% finds a gait cycle event (HS or TO)
% Parameters:
% - midpoint        ... ML midpoint (or the weight transfer point)
% - grf1            ... The increasing GRF
% - grf2            ... The other GRF
% - plate1AP        ... Pressure plate 1. Position in AP direction
% - plate2AP        ... Pressure plate 2. Position in AP direction

%--------------------------------
% Data preparation
%--------------------------------

filtersize = 5;

% ------ calculate CoP and velocity (excluding feet)
grf1_pos = max(0,grf1);
grf2_pos = max(0,grf2);
grf_total = grf1_pos + grf2_pos;

copAP = (plate1AP .* grf1_pos + plate2AP .* grf2_pos) ./ grf_total;
copML = ((100) * grf1_pos + (-100) * grf2_pos) ./ grf_total;

```

Die approbierte gedruckte Originalversion dieser Diplomarbeit ist an der TU Wien Bibliothek verfügbar.
The approved original version of this thesis is available in print at TU Wien Bibliothek.
TU Bibliothek Your knowledge hub WIEN

```
velAP = [0 diff(copAP)];
velML = [0 diff(copML)];

velCoP = [velAP ; velML];
velCoP = sqrt(sum(velCoP .* velCoP,1));

% ------ calculate distance (excluding feet)
dx = plate1AP - plate2AP;
dy = 200 * ones(size(grf1)); % feet are 200 mm apart
distance = sqrt((dx .* dx) + (dy .* dy));

% ------ calculate measures
Measure1 = (grf2 - grf1) .* distance;
dtMeasure1 = [0 diff(Measure1)];

g2Rel = 100 * grf2 ./ max(0.1, grf1 + grf2);
Measure2 = g2Rel .* distance; % better results with relative GRF
dtMeasure2 = [0 diff(Measure2)];

% ------ smoothing
dtMeasure2_smooth = filterUniform(dtMeasure2,filtersize);
copML_smooth = filterUniform(copML,filtersize);
velCoP_smooth = filterUniform(velCoP,filtersize);

%---------------------------------
% Defining search boundaries
%---------------------------------

idxFrom = max(1, midpoint-50);
idxTo = min(length(grf1), midpoint+50);

[~,idxMaxCopML] = max(copML(midpoint:idxTo));
idxMaxCopML = idxMaxCopML + midpoint - 1;

[~,idxMinCopML] = min(copML(idxFrom:midpoint));
idxMinCopML = idxMinCopML + idxFrom - 1;

[~,idxMaxGRF] = max(grf1(midpoint:idxTo));
idxMaxGRF = idxMaxGRF + midpoint - 1;

[~,idxMinGRF] = min(grf1(idxFrom:midpoint));
idxMinGRF = idxMinGRF + idxFrom - 1;

```


Die approbierte gedruckte Originalversion dieser Diplomarbeit ist an der TU Wien Bibliothek verfügbar.
The approved original version of this thesis is available in print at TU Wien Bibliothek.
TU Bibliothek Your knowledge hub WIEN

```
idxFrom = max([idxMinGRF idxMinCopML]);
idxTo = min([idxMaxGRF idxMaxCopML]);

% find (if it exists) grf1 <= 0 (backward search)
idxFromGRF = [];
for ii = midpoint:-1:idxFrom
    if grf1(ii) <= 0 && grf2(ii) > 0
        idxFromGRF = ii;
        break;
    end
end
idxFrom = max([idxFromGRF idxFrom]);

% find (if it exists) grf2 <= 0 (forward search)
idxToGRF = [];
for ii = midpoint:idxTo
    if grf2(ii) <= 0 && grf1(ii) > 0
        idxToGRF = ii;
        break;
    end
end
idxTo = min([idxToGRF idxTo]);

%--------------------------------
% Searching...
%--------------------------------

% find local maximum in measure2 (backward search)
idxMax2_smooth = max([idxFrom find(dtMeasure2_smooth(idxFrom:midpoint) >=
    0,1,'last') + idxFrom - 1]);

% find local minimum in measure2 (backward search)
idxMin2_smooth = max([idxFrom find(dtMeasure2_smooth(idxFrom:
    idxMax2_smooth-1) <= 0,1,'last') + idxFrom - 1]);

% find points in original data:
f = max(idxFrom, idxMax2_smooth-(filtersize-1)/2);
t = min(midpoint, idxMax2_smooth+(filtersize-1)/2);
[~,idxMax2] = max(Measure2(f:t));
idxMax2 = idxMax2 + f - 1;

f = max(idxFrom, idxMin2_smooth-(filtersize-1)/2);
[~,idxMin2] = min(Measure2(f:idxMax2));
```

Die approbierte gedruckte Originalversion dieser Diplomarbeit ist an der TU Wien Bibliothek verfügbar.
The approved original version of this thesis is available in print at TU Wien Bibliothek.

```
idxMin2 = idxMin2 + f - 1;

% find local maximum in measure1 (backward search)
idxMax1 = max([idxMin2 find(dtMeasure1(idxMin2:idxMax2) >= 0,1,'last') +
    idxMin2 - 1]);

% find local minimum in velocity
idxMinVel_smooth = idxMax1;
for ii = idxMinVel_smooth+1:idxTo % forward
    if velCoP_smooth(ii) > velCoP_smooth(ii-1)
        idxMinVel_smooth = ii-1;
        break;
    end
end
for ii = idxMinVel_smooth-1:-1:idxMin2 % backward
    if velCoP_smooth(ii) >= velCoP_smooth(ii+1)
        idxMinVel_smooth = ii+1;
        break;
    end
end

% find minimum in original data
f = max(idxMinVel_smooth-(filtersize-1)/2,idxMin2);
t = min(idxMinVel_smooth+(filtersize-1)/2,idxTo);
[~,idxMinVel] = min(velCoP(f:t));
idxMinVel = idxMinVel + f - 1;

eventResult = idxMinVel;

%--------------------------------
% Event should not be before a major turn in CoP_ML
%--------------------------------

idxFirstGood = idxFrom;
down = false;
for ii = (midpoint-1):-1:idxFrom
    if copML_smooth(ii) < copML_smooth(ii+1)
        down = true;
    end
    if down && copML_smooth(ii) > copML_smooth(ii+1)
        [~,idxFirstGood] = min(copML(ii-1:ii+3));
        idxFirstGood = idxFirstGood + ii-1 - 1;
        break;
```


Die approbierte gedruckte Originalversion dieser Diplomarbeit ist an der TU Wien Bibliothek verfügbar.
The approved original version of this thesis is available in print at TU Wien Bibliothek.
TU Bibliothek Your knowledge hub WIEN

```
150     end
151 end
152
153 eventResult = max(eventResult,idxFirstGood);
154 end
```

Die approbierte gedruckte Originalversion dieser Diplomarbeit ist an der TU Wien Bibliothek verfügbar.
The approved original version of this thesis is available in print at TU Wien Bibliothek.

Die approbierte gedruckte Originalversion dieser Diplomarbeit ist an der TU Wien Bibliothek verfügbar.
The approved original version of this thesis is available in print at TU Wien Bibliothek.

List of Figures

Die approbierte gedruckte Originalversion dieser Diplomarbeit ist an der TU Wien Bibliothek verfügbar.
The approved original version of this thesis is available in print at TU Wien Bibliothek.
TU Bibliothek Your knowledge hub WIEN

Die approbierte gedruckte Originalversion dieser Diplomarbeit ist an der TU Wien Bibliothek verfügbar.
The approved original version of this thesis is available in print at TU Wien Bibliothek.
TU Bibliothek Your knowledge hub WIEN

Die approbierte gedruckte Originalversion dieser Diplomarbeit ist an der TU Wien Bibliothek verfügbar.
The approved original version of this thesis is available in print at TU Wien Bibliothek.

Die approbierte gedruckte Originalversion dieser Diplomarbeit ist an der TU Wien Bibliothek verfügbar.
The approved original version of this thesis is available in print at TU Wien Bibliothek.

List of Tables

Die approbierte gedruckte Originalversion dieser Diplomarbeit ist an der TU Wien Bibliothek verfügbar.
The approved original version of this thesis is available in print at TU Wien Bibliothek.
TU Bibliothek Your knowledge hub WIEN

Die approbierte gedruckte Originalversion dieser Diplomarbeit ist an der TU Wien Bibliothek verfügbar.
The approved original version of this thesis is available in print at TU Wien Bibliothek.

List of Algorithms

Die approbierte gedruckte Originalversion dieser Diplomarbeit ist an der TU Wien Bibliothek verfügbar.
The approved original version of this thesis is available in print at TU Wien Bibliothek.

Die approbierte gedruckte Originalversion dieser Diplomarbeit ist an der TU Wien Bibliothek verfügbar.
The approved original version of this thesis is available in print at TU Wien Bibliothek.

Glossary

Anterior-posterior (AP) The back (*posterior*) to front (*anterior*) axis of a subject. 8, 9, 163

Cadence The rate at which a person walks, expressed in steps per minute. 28, 31, 105, 109, 122, 136, 137

Calcaneal gait A gait disturbance, characterized by walking on the heel, due to paralysis of the calf muscles, seen following poliomyelitis and in some other neurologic diseases (Sources: Farlex [Far20], Government of Canada[Pub20]). 53, 83

Contralateral Adjective. Referring to something (e.g. event, body part) on the opposite side of the body. 6, 11, 36, 53, 61, 72

Dorsiflexion (DF) Dorsiflexion is the movement, which brings the toes closer to the shin; it reduces the angle between leg and foot. 28, 119, 163

Electroencephalography (EEG) The measurement and recording of electrical activity in the brain. 2, 163

Electromyography (EMG) The measurement and recording of the electrical activity of muscles. 2, 163

Foot drop A gait abnormality caused by weakness or disruption in the nerve pathway between brain and foot. Subjects suffering from foot drop have difficulties lifting the front of the foot, showing a weakened dorsiflexion. 17, 119

Functional electrical stimulation (FES) The application of small electrical charges to stimulate muscles. 2, 163

Gait cycle (GC) The sequence of foot contact events during normal walking. One gait cycle starts with the initial contact of one foot and ends with the next similar contact of the same foot. 36, 163

Hemiparesis The weakness of one entire half of the body. 92

Die approbierte gedruckte Originalversion dieser Diplomarbeit ist an der TU Wien Bibliothek verfügbar.
The approved original version of this thesis is available in print at TU Wien Bibliothek.
TU Bibliothek Your knowledge hub WIEN

Hemiplegia One-sided paralysis. 1, 135, 162

Hemiplegic Adjective. See hemiplegia. 17

Ipsilateral Adjective. Referring to something (e.g. event, body part) on the same side of the body. 6

Knee flexion Knee flexion is the bending of the knee, bringing the foot towards the back of the thigh. 6

Loading rate The speed at which forces are applied. The derivative of the GRF. 24

Mediolateral (ML) The side to side axis of a subject. 8, 9, 39, 40, 50, 164

Monoparesis Paresis in one leg. 119

Orthosis The correction of disorders of the limbs or spine by use of braces and other devices to correct alignment or provide support (Source: Lexico [Lex20]). 15

Paralysis Complete loss or weakness of muscle function in one or more muscles. 1, 162

Plantar flexion (PF) Plantar flexion is the movement in which the foot points down and away from the leg. 28, 164

Stance phase The stance phase starts with the heel strike and ends with the toe off event for each foot respectively. It accounts for about 60 % of the whole gait cycle. 5

Step length The distance between one foot's position of contact with the ground and the other foot's previous similar position of contact during gait. For example, the distance between the positions of the current left heel strike and the previous right heel strike results in the left foot's step length. 13, 14, 69, 153

Stride length The distance between two successive similar positions of contact of the same foot. For example, the distance between two successive positions of the left heel strike results in the stride length. 13, 14, 69, 108, 112, 153

Swing phase The swing phase starts with the toe off and ends with the heel strike event for each foot respectively. It accounts for about 40 % of the whole gait cycle. 5

Tibia The shinbone. The frontal bone in the lower leg. 6, 24, 28

Weight transfer point (WTP) The point of equal forces (force equilibrium) between left and right vertical ground reaction force. (Source: Nolan and Yarossi [NY11]). 9, 164

Die approbierte gedruckte Originalversion dieser Diplomarbeit ist an der TU Wien Bibliothek verfügbar.
The approved original version of this thesis is available in print at TU Wien Bibliothek.
TU Bibliothek Your knowledge hub WIEN

Acronyms

AP anterior-posterior. 8, 17, 18, 33, 34, 36, 37, 53–55, 58–60, 65–68, 72, 74, 75, 101, 112, 161

CoM center of mass. 9, 10, 28

CoP center of pressure. 11, 12, 17, 26, 38–40, 43, 44, 46, 50, 53–55, 59–67, 72–74, 78, 84–91, 108, 119, 126, 136, 153, 154

CV coefficient of variation. 108, 109, 112

CWT continuous wavelet transform. 20–24

DF dorsiflexion. 28, 29, 161

DoG derivative of Gaussian. 20–22

EEG electroencephalography. 2, 161

EMG electromyography. 2, 161

FES functional electrical stimulation. 2, 161

FoR frame of reference. 83–85, 90, 91, 154

GC gait cycle. 36–38, 40, 41, 43, 50, 55, 57, 59, 64, 71, 86, 90, 92, 93, 95, 97, 98, 100, 102, 107–109, 111, 116, 118–120, 122, 124, 127, 132, 161

GD gait discrepancy. 71, 72, 106, 107

GED gait event detection. 3, 4, 17, 18, 21, 24, 25, 35, 36, 47, 51, 57, 58, 63–65, 67, 68, 71, 100, 106, 127, 132, 135–137, 153, 154

GRF ground reaction force. 8–11, 17, 18, 24, 25, 27, 36, 38, 41, 43, 45, 48–54, 57, 58, 60, 63–65, 71, 92–95, 109, 113, 119, 121–123, 126, 128–135, 137, 153, 154, 162

HIS hospital information system. 2, 3

Die approbierte gedruckte Originalversion dieser Diplomarbeit ist an der TU Wien Bibliothek verfügbar.
The approved original version of this thesis is available in print at TU Wien Bibliothek.
TU Bibliothek Your knowledge hub WIEN

HS heel strike. 8, 11, 13, 16–18, 21–23, 36–38, 40, 47, 50, 53, 54, 57, 58, 61–63, 68–73, 85, 97, 98, 153

HSL heel strike, left. 8, 11, 14, 38, 40, 69, 71, 85, 87, 95, 100–102, 109, 119, 122

HSR heel strike, right. 8, 11, 14, 38, 69, 71, 85, 87, 95, 96, 100–102, 108, 119, 122

IMU inertial measurement unit. 17, 21, 22

ML mediolateral. 8, 28, 33, 36, 38–40, 43, 53, 64, 65, 72, 74, 75, 85, 101, 112, 153, 154, 162

MS multiple sclerosis. 105, 106, 119–121, 155, 157

PF plantar flexion. 28, 29, 162

RLA Rancho Los Amigos. 6–8

SLL step length, left. 13, 14, 70, 108, 109, 111, 112, 116, 118, 120, 122, 124, 132

SLR step length, right. 13, 14, 70, 108, 111, 112, 116, 118, 120, 122, 124, 132

TO toe off. 8, 11, 13, 16, 17, 21–23, 36–38, 40, 47, 51, 57, 58, 61, 67–69, 72, 73, 85, 97, 98, 107, 122, 126

TOL toe off, left. 8, 11, 69, 71, 85, 87, 95–97, 101, 102, 107, 119, 122, 124

TOR toe off, right. 8, 11, 40, 69, 71, 85, 87, 95, 101, 102, 107, 119, 122

WTP weight transfer point. 9, 10, 36, 38–40, 43–48, 50, 51, 127, 137, 153, 162

Die approbierte gedruckte Originalversion dieser Diplomarbeit ist an der TU Wien Bibliothek verfügbar.
The approved original version of this thesis is available in print at TU Wien Bibliothek.
TU Bibliothek Your knowledge hub WIEN

Bibliography

[Ado20] Adobe Systems Incorporated. Mixamo. https://www.mixamo.com, 2020. [Online; accessed 09-January-2020].

[AWG09] Paul S Addison, James Walker, and Rodrigo C Guido. Time–frequency analysis of biosignals. *IEEE engineering in medicine and biology magazine*, 28(5):14–29, 2009.

[BB07] Axel Buchner and Nina Baumgartner. Text–background polarity affects performance irrespective of ambient illumination and colour contrast. *Ergonomics*, 50(7):1036–1063, 2007.

[BBNK07] Chitralakshmi K Balasubramanian, Mark G Bowden, Richard R Neptune, and Steven A Kautz. Relationship between step length asymmetry and walking performance in subjects with chronic hemiparesis. *Archives of physical medicine and rehabilitation*, 88(1):43–49, 2007.

[BCW+19] Lauren C Benson, Christian A Clermont, Ricky Watari, Tessa Exley, and Reed Ferber. Automated accelerometer-based gait event detection during multiple running conditions. *Sensors*, 19(7):1483, 2019.

[BR14] Dustin A Bruening and Sarah Trager Ridge. Automated event detection algorithms in pathological gait. *Gait & posture*, 39(1):472–477, 2014.

[BWW14] Michalina Błażkiewicz, Ida Wiszomirska, and Andrzej Wit. Comparison of four methods of calculating the symmetry of spatial-temporal parameters of gait. *Acta of bioengineering and biomechanics*, 16(1), 2014.

[CIR20] CIR Systems, Inc. GAITRite. https://www.gaitrite.com, 2020. [Online; accessed 09-January-2020].

[CK13] Steven H Collins and Arthur D Kuo. Two independent contributions to step variability during over-ground human walking. *PloS one*, 8(8), 2013.

[Con13] Connexions. Dorsiflexion and plantar flexion. https://en.wikipedia.org/wiki/File:Dorsiplantar.jpg, 2013. [Online; accessed 09-January-2020].

Die approbierte gedruckte Originalversion dieser Diplomarbeit ist an der TU Wien Bibliothek verfügbar.
The approved original version of this thesis is available in print at TU Wien Bibliothek.
TU Bibliothek Your knowledge hub WIEN

[CRR20] David Catuhe, David Rousset, and Michel Rousseau. Babylon.js. http://babylonjs.com, 2020. [Online; accessed 09-January-2020].

[Cum19] Eleanor Cummins. Dark mode is easier on your eyes–and battery. https://www.popsci.com/night-dark-mode-design/, 2019. [Online; accessed 09-January-2020].

[DDGR15] Silvia Del Din, Alan Godfrey, and Lynn Rochester. Validation of an accelerometer to quantify a comprehensive battery of gait characteristics in healthy older adults and Parkinson's disease: toward clinical and at home use. *IEEE journal of biomedical and health informatics*, 20(3):838–847, 2015.

[Ecl20a] Eclipse Foundation, Inc. Eclipse Equinox. https://www.eclipse.org/equinox, 2020. [Online; accessed 09-January-2020].

[Ecl20b] Eclipse Foundation, Inc. Eclipse Jetty. https://www.eclipse.org/jetty, 2020. [Online; accessed 09-January-2020].

[EEA07] Niell G Elvin, Alex A Elvin, and Steven P Arnoczky. Correlation between ground reaction force and tibial acceleration in vertical jumping. *Journal of applied biomechanics*, 23(3):180–189, 2007.

[Eur11] Eurostat. Statistics explained - disability statistics. https://ec.europa.eu/eurostat/statistics-explained/index.php/Disability_statistics, 2011. [Online; accessed 09-January-2020].

[Far20] Farlex, Inc. Definition of calcaneal gait. https://medical-dictionary.thefreedictionary.com/calcaneus+gait, 2020. [Online; accessed 10-April-2020].

[FFD18] Claudiane A Fukuchi, Reginaldo K Fukuchi, and Marcos Duarte. A public dataset of overground and treadmill walking kinematics and kinetics in healthy individuals. *PeerJ*, 6:e4640, 2018.

[FMK14] Emma Fortune, Melissa MB Morrow, and Kenton R Kaufman. Assessment of gait kinetics using triaxial accelerometers. *Journal of applied biomechanics*, 30(5):668–674, 2014.

[FOL19] Matthew William Flood, Ben O'Callaghan, and Madeleine Lowery. Gait event detection from accelerometry using the Teager-Kaiser energy operator. *IEEE transactions on biomedical engineering*, 2019.

[For20] FFG Die Österreichische Forschungsförderungsgesellschaft. BrainGait. https://projekte.ffg.at/projekt/2808447, 2020. [Online; accessed 09-January-2020].

Die approbierte gedruckte Originalversion dieser Diplomarbeit ist an der TU Wien Bibliothek verfügbar.
The approved original version of this thesis is available in print at TU Wien Bibliothek.
TU Bibliothek Your knowledge hub WIEN

[Goo20] Google, Inc. Google Web Toolkit (GWT). http://www.gwtproject.org, 2020. [Online; accessed 09-January-2020].

[GSDE04] Salim Ghoussayni, Christopher Stevens, Sally Durham, and David Ewins. Assessment and validation of a simple automated method for the detection of gait events and intervals. *Gait & posture*, 20(3):266–272, 2004.

[HA09] Michael Hanlon and Ross Anderson. Real-time gait event detection using wearable sensors. *Gait & posture*, 30(4):523–527, 2009.

[HB12] Caroline Hodt-Billington. Measures of symmetry in gait. *Methodological principles and clinical choices [dissertation].[Bergen (Norway)]: University of Bergen*, 2012.

[HH04] Richard H Hall and Patrick Hanna. The impact of web page text-background colour combinations on readability, retention, aesthetics and behavioural intention. *Behaviour & information technology*, 23(3):183–195, 2004.

[HHH+13] Sandra R Hundza, William R Hook, Christopher R Harris, Sunny V Mahajan, Paul A Leslie, Carl A Spani, Leonhard G Spalteholz, Benjamin J Birch, Drew T Commandeur, and Nigel J Livingston. Accurate and reliable gait cycle detection in Parkinson's disease. *IEEE transactions on neural systems and rehabilitation engineering*, 22(1):127–137, 2013.

[HM00] Alan Hreljac and Robert N Marshall. Algorithms to determine event timing during normal walking using kinematic data. *Journal of biomechanics*, 33(6):783–786, 2000.

[Hoc20a] Hocoma. Hocoma Andago. https://www.hocoma.com/us/solutions/andago, 2020. [Online; accessed 09-January-2020].

[Hoc20b] Hocoma. Hocoma Locomat. https://www.hocoma.com/solutions/lokomat, 2020. [Online; accessed 09-January-2020].

[HRJ+97] Stefan Hesse, Frank Reiter, Matthias Jahnke, Michael Dawson, Thompson Sarkodie-Gyan, and Karl-Heinz Mauritz. Asymmetry of gait initiation in hemiparetic stroke subjects. *Archives of physical medicine and rehabilitation*, 78(7):719–724, 1997.

[KDFA13] Alon Kalron, Zeevi Dvir, Lior Frid, and Anat Achiron. Quantifying gait impairment using an instrumented treadmill in people with multiple sclerosis. *ISRN neurology*, 2013.

[KDS19] Łukasz Kidziński, Scott Delp, and Michael Schwartz. Automatic real-time gait event detection in children using deep neural networks. *PloS one*, 14(1):e0211466, 2019.

Die approbierte gedruckte Originalversion dieser Diplomarbeit ist an der TU Wien Bibliothek verfügbar.
The approved original version of this thesis is available in print at TU Wien Bibliothek.
TU Bibliothek Your knowledge hub WIEN

[Kel19] Aaron Keller. Precision vs. accuracy. http://kaffee.50webs.com/Science/labs/Lab-Precision.vs.Accuracy.html, 2019. [Online; accessed 09-January-2020].

[KF15] Alon Kalron and Lior Frid. The butterfly diagram: a gait marker for neurological and cerebellar impairment in people with multiple sclerosis. *Journal of the neurological sciences*, 358(1-2):92–100, 2015.

[KW16] Siddhartha Khandelwal and Nicholas Wickström. Gait event detection in real-world environment for long-term applications: Incorporating domain knowledge into time-frequency analysis. *IEEE transactions on neural systems and rehabilitation engineering*, 24(12):1363–1372, 2016.

[KYB16] Sibel Kibar, Ferdi Yavuz, and Birol Balaban. An accelerated multi-modality rehabilitation protocol combined with botulinum toxin-a injection in adult idiopathic toe walking: Case report. *Journal of clinical and diagnostic research: JCDR*, 10(6):YD01, 2016.

[Lam99] André Lamothe. *Tricks of the Windows Game Programming Gurus Fundamentals of 2D and 3D Game Programming*. Sams publishing, 1999.

[LBAN14] Selena Lauziere, Martina Betschart, Rachid Aissaoui, and Sylvie Nadeau. Understanding spatial and temporal gait asymmetries in individuals post stroke. *International journal of physical medicine & rehabilitation*, 2(3):201, 2014.

[LBS06] Jianwen Luo, Jing Bai, and Jinhua Shao. Application of the wavelet transforms on axial strain calculation in ultrasound elastography. *Progress in natural science*, 16(9):942–947, 2006.

[Lex20] Lexico. Definition of orthosis in English. https://www.lexico.com/en/definition/orthosis, 2020. [Online; accessed 10-April-2020].

[Lin20] Motekforce Link. Motek GRAIL. https://www.motekmedical.com/product/grail, 2020. [Online; accessed 09-January-2020].

[LN05] Pamela K Levangie and Cynthia C Norkin. *Joint structure and function: a comprehensive analysis*. FA Davis, 4th edition, 2005.

[Luo07] Jianwen Luo. Numerical differentiation based on wavelet transforms. https://www.mathworks.com/matlabcentral/fileexchange/13948-numerical-differentiation-based-on-wavelet-transforms, 2007. [Online; accessed 09-January-2020].

[MAGD+19] Ríona Mc Ardle, Brook Galna, Paul Donaghy, Alan Thomas, and Lynn Rochester. Do Alzheimer's and Lewy body disease have discrete pathological signatures of gait? *Alzheimer's & dementia*, 2019.

Die approbierte gedruckte Originalversion dieser Diplomarbeit ist an der TU Wien Bibliothek verfügbar.
The approved original version of this thesis is available in print at TU Wien Bibliothek.
TU Bibliothek Your knowledge hub WIEN

[MDGM12] John McCamley, Marco Donati, Eleni Grimpampi, and Claudia Mazza. An enhanced estimate of initial contact and final contact instants of time using lower trunk inertial sensor data. *Gait & posture*, 36(2):316–318, 2012.

[Med15] Schepp Medtech. PerPedes. `http://www.schepp.at/en/`, 2015. [Online; accessed 09-January-2020].

[Mer19] Merriam-Webster, Incorporated. Definition of buzzword. `https://www.merriam-webster.com/dictionary/buzzword`, 2019. [Online; accessed 09-January-2020].

[MHBHK13] Firas Mawase, Tamar Haizler, Simona Bar-Haim, and Amir Karniel. Kinetic adaptation during locomotion on a split-belt treadmill. *Journal of neurophysiology*, 109(8):2216–2227, 2013.

[Mil09] Adam Miller. Gait event detection using a multilayer neural network. *Gait & posture*, 29(4):542–545, 2009.

[ML03] Avril Mansfield and Gerard M Lyons. The use of accelerometry to detect heel contact events for use as a sensor in FES assisted walking. *Medical engineering & physics*, 25(10):879–885, 2003.

[Moo09] Jean Mooney. *Illustrated dictionary of podiatry and foot science*. Elsevier Health Sciences, 1st edition, 2009.

[MPC+17] Giovanni Morone, Stefano Paolucci, Andrea Cherubini, Domenico De Angelis, Vincenzo Venturiero, Paola Coiro, and Marco Iosa. Robot-assisted gait training for stroke patients: current state of the art and perspectives of robotics. *Neuropsychiatric disease and treatment*, 13:1303, 2017.

[Neu10] Donald A Neumann. Kinesiology of the musculoskeletal system; foundation for rehabilitation. *Mosby & Elsevier*, 2010.

[NHB12] Jennifer M Neugebauer, David A Hawkins, and Laurel Beckett. Estimating youth locomotion ground reaction forces using an accelerometer-based activity monitor. *PloS one*, 7(10):e48182, 2012.

[NWL+02] Lei Nie, Shouguo Wu, Xiangqin Lin, Longzhen Zheng, and Lei Rui. Approximate derivative calculated by using continuous wavelet transform. *Journal of chemical information and computer sciences*, 42(2):274–283, 2002.

[NY11] Karen J Nolan and Mathew Yarossi. Weight transfer analysis in adults with hemiplegia using ankle foot orthosis. *Prosthetics and orthotics international*, 35(1):45–53, 2011.

[OHCGB18] Catherine A Okoro, NaTasha D Hollis, Alissa C Cyrus, and Shannon Griffin-Blake. Prevalence of disabilities and health care access by disability status and type among adults–United States, 2016. *Morbidity and mortality weekly report*, 67(32):882, 2018.

Die approbierte gedruckte Originalversion dieser Diplomarbeit ist an der TU Wien Bibliothek verfügbar.
The approved original version of this thesis is available in print at TU Wien Bibliothek.
TU Bibliothek Your knowledge hub WIEN

[Pat10] Kara K Patterson. *Gait asymmetry post-stroke*. PhD thesis, University of Toronto, 2010.

[PBvD04] Mirjam Pijnappels, Maarten F Bobbert, and Jaap H van Dieën. Contribution of the support limb in control of angular momentum after tripping. *Journal of biomechanics*, 37(12):1811–1818, 2004.

[Pea19] Janet Pearl. What causes metatarsophalangeal (MTP) joint pain? `https://www.mortonsneuroma.com/blog/causes-metatarsophalangeal-mtp-joint-pain/`, 2019. [Online; accessed 09-January-2020].

[Per08] Jacquelin Perry. Normal and pathologic gait. *AAOS atlas of orthoses and assistive devices E-Book*, page 63, 2008.

[PGB+10] Kara K Patterson, William H Gage, Dina Brooks, Sandra E Black, and William E McIlroy. Evaluation of gait symmetry after stroke: a comparison of current methods and recommendations for standardization. *Gait & posture*, 31(2):241–246, 2010.

[PLVRL14] Annie Pouliot-Laforte, Louis-Nicolas Veilleux, Frank Rauch, and Martin Lemay. Validity of an accelerometer as a vertical ground reaction force measuring device in healthy children and adolescents and in children and adolescents with osteogenesis imperfecta type I. *Journal of musculoskeletal and neuronal interactions*, 14(2):155–161, 2014.

[PPK+01] Ion PI Pappas, Milos R Popovic, Thierry Keller, Volker Dietz, and Manfred Morari. A reliable gait phase detection system. *IEEE transactions on neural systems and rehabilitation engineering*, 9(2):113–125, 2001.

[Pub20] Public Works and Government Services Canada. Definition of calcaneal gait. `https://www.btb.termiumplus.gc.ca/tpv2alpha/alpha-eng.html?lang=eng&i=1&index=alt&srchtxt=calcaneal%20gait`, 2020. [Online; accessed 10-April-2020].

[PVS17] Lucia Pepa, Federica Verdini, and Luca Spalazzi. Gait parameter and event estimation using smartphones. *Gait & posture*, 57:217–223, 2017.

[RB11] Melvyn Roerdink and Peter J Beek. Understanding inconsistent step-length asymmetries across hemiplegic stroke patients: impairments and compensatory gait. *Neurorehabilitation and neural repair*, 25(3):253–258, 2011.

[RCC+08] Melvyn Roerdink, Bert H Coolen, Bert (H)E Clairbois, Claudine JC Lamoth, and Peter J Beek. Online gait event detection using a large force platform embedded in a treadmill. *Journal of biomechanics*, 41(12):2628–2632, 2008.

Die approbierte gedruckte Originalversion dieser Diplomarbeit ist an der TU Wien Bibliothek verfügbar.
The approved original version of this thesis is available in print at TU Wien Bibliothek.
TU Bibliothek Your knowledge hub WIEN

[RCS+14] Melvyn Roerdink, Andrea G Cutti, Aurora Summa, Davide Monari, Davide Veronesi, Mariëlle W van Ooijen, and Peter J Beek. Gaitography applied to prosthetic walking. *Medical and biological engineering and computing*, 52(11):963–969, 2014.

[Red20] Red Hat, Inc. WildFly. `https://wildfly.org`, 2020. [Online; accessed 09-January-2020].

[Reh20] Reha Technology AG. Reha Technology G-EO1. `https://www.rehatechnology.com/en/g-eo1`, 2020. [Online; accessed 09-January-2020].

[RS12] Alex V Rowlands and Victoria H Stiles. Accelerometer counts and raw acceleration output in relation to mechanical loading. *Journal of biomechanics*, 45(3):448–454, 2012.

[RSLA10] Jan Rueterbories, Erika G Spaich, Birgit Larsen, and Ole K Andersen. Methods for gait event detection and analysis in ambulatory systems. *Medical engineering & physics*, 32(6):545–552, 2010.

[SBM16] Fabio A Storm, Christopher J Buckley, and Claudia Mazzà. Gait event detection in laboratory and real life settings: Accuracy of ankle and waist sensor based methods. *Gait & posture*, 50:42–46, 2016.

[SFB+05] Ruud W Selles, Margriet AG Formanoy, Johannes BJ Bussmann, Peter J Janssens, and Henk J Stam. Automated estimation of initial and terminal contact timing using accelerometers; development and validation in transtibial amputees and controls. *IEEE transactions on neural systems and rehabilitation engineering*, 13(1):81–88, 2005.

[Sha49] Claude E Shannon. Communication in the presence of noise. *Proceedings of the IRE*, 37(1):10–21, 1949.

[Shu19] Shutterstock. What is a color scheme: Definitions, types, and examples. `https://www.shutterstock.com/blog/color-scheme-definitions-types-examples`, 2019. [Online; accessed 09-January-2020].

[SL00] Kong-King Shieh and Chin-Chiuan Lin. Effects of screen type, ambient illumination, and color combination on VDT visual performance and subjective preference. *International journal of industrial ergonomics*, 26(5):527–536, 2000.

[SM03] Xueguang Shao and Chaoxiong Ma. A general approach to derivative calculation using wavelet transform. *Chemometrics and intelligent laboratory systems*, 69(1-2):157–165, 2003.

Die approbierte gedruckte Originalversion dieser Diplomarbeit ist an der TU Wien Bibliothek verfügbar.
The approved original version of this thesis is available in print at TU Wien Bibliothek.
TU Bibliothek Your knowledge hub WIEN

[SMS+14] Amira Skopljak, Mirsad Muftic, Aziz Sukalo, Izet Masic, and Lejla Zunic. Pedobarography in diagnosis and clinical application. *Acta informatica medica*, 22(6):374, 2014.

[SNIF97] Noboru Sekiya, Hiroshi Nagasaki, Hajime Ito, and Taketo Furuna. Optimal walking in terms of variability in step length. *Journal of Orthopaedic & Sports Physical Therapy*, 26(5):266–272, 1997.

[Ste17] Steirische Wirtschaftsförderungsgesellschaft mbH (SFG). Roboter statt Rollstuhl. `https://www.sfg.at/cms/3540/8426/Roboter-statt-Rollstuhl//`, 2017. [Online; accessed 28-November-2018].

[TCDC14] Diana Trojaniello, Andrea Cereatti, and Ugo Della Croce. Accuracy, sensitivity and robustness of five different methods for the estimation of gait temporal parameters using a single inertial sensor mounted on the lower trunk. *Gait & posture*, 40(4):487–492, 2014.

[TCvDR19] Celine Timmermans, Andrea G Cutti, Hester van Donkersgoed, and Melvyn Roerdink. Gaitography on lower-limb amputees: Repeatability and between-methods agreement. *Prosthetics and orthotics international*, 43(1):71–79, 2019.

[The18] The MathWorks, Inc. Matlab R2018a. `https://www.mathworks.com/products/new_products/release2018a.html`, 2018. [Online; accessed 09-January-2020].

[TLR+07] Michael H Thaut, Anne Kathrin Leins, Ruth R Rice, Heike Argstatter, Gary P Kenyon, Gerald C McIntosh, Hans Volker Bolay, and Michael Fetter. Rhythmic auditory stimulation improves gait more than NDT/Bobath training in near-ambulatory patients early poststroke: a single-blind, randomized trial. *Neurorehabilitation and neural repair*, 21(5):455–459, 2007.

[TMR97] Michael H Thaut, Gerald C McIntosh, and Ruth R Rice. Rhythmic facilitation of gait training in hemiparetic stroke rehabilitation. *Journal of the neurological sciences*, 151(2):207–212, 1997.

[Tol17] Jan Tolar. Zebris gait report example. `https://is.cuni.cz/webapps/zzp/download/130241995`, 2017. [Online; accessed 09-January-2020].

[TRHC15] Diana Trojaniello, Andrea Ravaschio, Jeffrey M Hausdorff, and Andrea Cereatti. Comparative assessment of different methods for the estimation of gait temporal parameters using a single inertial sensor: application to elderly, post-stroke, Parkinson's disease and Huntington's disease subjects. *Gait & posture*, 42(3):310–316, 2015.

Die approbierte gedruckte Originalversion dieser Diplomarbeit ist an der TU Wien Bibliothek verfügbar.
The approved original version of this thesis is available in print at TU Wien Bibliothek.
TU Bibliothek Your knowledge hub WIEN

[TW10] Anthony Tongen and Roshna E Wunderlich. Biomechanics of running and walking. *Mathematics and sports*, 43:1–12, 2010.

[VAA+17] Theo Vos, Amanuel Alemu Abajobir, Kalkidan Hassen Abate, Cristiana Abbafati, Kaja M Abbas, Foad Abd-Allah, Rizwan Suliankatchi Abdulkader, Abdishakur M Abdulle, Teshome Abuka Abebo, Semaw Ferede Abera, and 717 others. Global, regional, and national incidence, prevalence, and years lived with disability for 328 diseases and injuries for 195 countries, 1990–2016: a systematic analysis for the global burden of disease study 2016. *The Lancet*, 390(10100):1211–1259, 2017.

[vdVHBH18] Susanne M van der Veen, Ulrike Hammerbeck, Richard J Baker, and Kristen L Hollands. Validation of gait event detection by centre of pressure during target stepping in healthy and paretic gait. *Journal of biomechanics*, 79:218–222, 2018.

[VHZ+05] Gijsbertus Jacob Verkerke, At L Hof, Wiebren Zijlstra, Wim Ament, and Gerhard Rakhorst. Determining the centre of pressure during walking and running using an instrumented treadmill. *Journal of biomechanics*, 38(9):1881–1885, 2005.

[VvWvP+14] Janne Marieke Veerbeek, Erwin van Wegen, Roland van Peppen, Philip Jan van der Wees, Erik Hendriks, Marc Rietberg, and Gert Kwakkel. What is the evidence for physical therapy poststroke? a systematic review and meta-analysis. *PloS one*, 9(2):e87987, 2014.

[WC96] James C Wall and Jack Crosbie. Accuracy and reliability of temporal gait measurement. *Gait & posture*, 4(4):293–296, 1996.

[WCH+99] Alice MK Wong, Chia-Ling Chen, Wei-Hsien Hong, Wen-Ko Chiou, Hsieh-Ching Chen, and Fuk-Tan Tang. Gait analysis through foot pattern recognition for children with cerebral palsy. *Journal of musculoskeletal research*, 3(01):71–81, 1999.

[Wel62] B.P. Welford. Note on a method for calculating corrected sums of squares and products. *Technometrics*, 4(3):419–420, 1962.

[WNA+16] Haidong Wang, Mohsen Naghavi, Christine Allen, Ryan M Barber, Zulfiqar A Bhutta, Austin Carter, Daniel C Casey, Fiona J Charlson, Alan Zian Chen, Matthew M Coates, and 762 others. Global, regional, and national life expectancy, all-cause mortality, and cause-specific mortality for 249 causes of death, 1980–2015: a systematic analysis for the global burden of disease study 2015. *The Lancet*, 388(10053):1459–1544, 2016.

[Wor11] World Health Organization. *World report on disability 2011*. World Health Organization, 2011.

Die approbierte gedruckte Originalversion dieser Diplomarbeit ist an der TU Wien Bibliothek verfügbar.
The approved original version of this thesis is available in print at TU Wien Bibliothek.
TU Bibliothek Your knowledge hub WIEN

[WPH+04] Alice M Wong, Yu-Cheng Pei, Wei-Hsien Hong, Chia-Yin Chung, Yiu-Chung Lau, and Carl P Chen. Foot contact pattern analysis in hemiplegic stroke patients: An implication for neurologic status determination. *Archives of physical medicine and rehabilitation*, 85(10):1625–1630, 2004.

[WSEG+12] Johanna Wagner, Teodoro Solis-Escalante, Peter Grieshofer, Christa Neuper, Gernot Müller-Putz, and Reinhold Scherer. Level of participation in robotic-assisted treadmill walking modulates midline sensorimotor EEG rhythms in able-bodied subjects. *Neuroimage*, 63(3):1203–1211, 2012.

[WSH+18] Markus Wagner, Djordje Slijepcevic, Brian Horsak, Alexander Rind, Matthias Zeppelzauer, and Wolfgang Aigner. KAVAGait: Knowledge-assisted visual analytics for clinical gait analysis. *IEEE transactions on visualization and computer graphics*, 25(3):1528–1542, 2018.

[Zeb20a] Zebris Medical GmbH. Zebris FDM-T evaluation software. `https://www.zebris.de/en/medical/products-solutions/gait-analysis-fdm-t/`, 2020. [Online; accessed 09-January-2020].

[Zeb20b] Zebris Medical GmbH. Zebris Rehawalk. `https://www.zebris.de/en/medical/products-solutions/gait-analysis-and-gait-training`, 2020. [Online; accessed 09-January-2020].

[ZH03] Wiebren Zijlstra and At L Hof. Assessment of spatio-temporal gait parameters from trunk accelerations during human walking. *Gait & posture*, 18(2):1–10, 2003.

[ZJRH08] Joseph Zeni Jr, James G Richards, and Jill Higginson. Two simple methods for determining gait events during treadmill and overground walking using kinematic data. *Gait & posture*, 27(4):710–714, 2008.

Die approbierte gedruckte Originalversion dieser Diplomarbeit ist an der TU Wien Bibliothek verfügbar.
The approved original version of this thesis is available in print at TU Wien Bibliothek.
TU Bibliothek Your knowledge hub WIEN